Development of Non-Fullerene-Based Electron Acceptors for Solar Cell Applications

Wael Hamed K Alsaedi

A thesis submitted to
The University of Sheffield
As partial fulfilment for the degree of Doctor of Philosophy

Department of Chemistry

May 2020

Declaration

This thesis submitted for the degree of Doctor of Philosophy (PhD) at the University of Sheffield, having been submitted for no other degree. It records the research carried out at the University of Sheffield from October 2016 to April 2019. It is entirely my original work, unless where referenced

Signed …………………………..

Date ……………………………..

Acknowledgments

Firstly, I believe that all honour and thanks belongs to God Almighty as it is through Him that I have acquired the intelligence, capability, stamina and opportunity to persevere through this thesis. This achievement would be impossible without His blessings.

During my journey towards this PhD degree, I have to acknowledge some people who have been an inspiration and a pillar of support in my journey. First of all, I would like to express the deepest sense of appreciation to my supervisor Dr, Ahmed Iraqi for continually providing heartfelt advice, invaluable guidance and support. He has given me directions, suggestion and critical reviews of several aspects of this project. In addition, he has allowed me to pursue my research with full of freedom. I am sure this research would not be accomplished without his assistance. I am extremely grateful to him.

I have great appreciation in acknowledging my gratitude to my colleagues Dr. Bakhet, Dr.Bader, Dr. Omer, Dr. Majeed and Osama for their motivation, guidance and assistance both in lab and in collecting data for my research. Their support, encouragement and credible ideas have been magnificent contributors to the completion of the thesis.

In addition, I would like to thank several faculty members in the chemistry department such as Sandra for NMR, Rob for the TGA measurements, Steven for the elemental analysis, Simon and Sharon for the mass spectroscopy, Nick and his colleagues in store, Kith for the dry solvent and Richard for safety in laboratory. Furthermore, it is worth acknowledging the contribution of Dr David Ladidzy and Emma from the physics department as they assembled the solar cell devices. I would also like to thank my sponsor Tabiah University for their financial support for the PhD program. In addition, I am thankful to the Royal Embassy of Saudi Arabian cultural Bureau.

I would like to take this opportunity to thank the biggest source of my success, which is my family. I am extremely grateful to my brothers Waleed, Abedrheem and Zyid as well as the love and care of my only sister Rawan. It is their consistent support that has enabled me to fulfil my aspirations of obtaining a doctorate certificate. This would be impossible without their unwavering and unselfish love as well as continual encourangement when I need it most.

I would take this opportunity to acknowledge my mother who has made this all achievable. She has been a permanent source of encouragement, support and inspiration and has made an untold number of sacrifices for the whole family, and especially for me to continue with my PhD degree. She is a great inspiration to me. Your prayers for me sustained me. Thus, she is due a considerable amount of appreciation and I owe my achievements to her as without her support, I am certain that I would not have achieved this feat.

Last but not least, I would like to express my deepest gratitude to my wife, Reem Aloufi, for her patience and tolerance regarding the PhD work. Undoubtedly, I would not have been able to complete this work without her support. Thank you for staying by my side, I appreciate your sacrifices.

Abstract

The challenge of an increasing global energy demand and environmental consequences lead researchers to explore new alternative sources to conventional fossil or nuclear fuel sources. Photovoltaic devices exhibit one of the most promising approaches to generate electricity in a clean way. As an emerging technology in photovoltaic devices, organic solar cells (OSCs) have gained considerable attention due to their low-cost, flexibility, lightweight, and solution processability. Despite the fact that power conversion efficiencies (PCEs) of OSCs have exceeded 13%, significant effort is being implemented to design new materials with improved PCEs as well as to address device durability.

Amongst solution-processed OPVs, fullerenes and their derivatives have been widely used as the highest performing electron acceptor component in solar cell devices. However, their low absorption in the solar spectrum, high-cost of synthesis and difficulties in their purification has lead researchers to look for alternative electron acceptors. Thus, non-fullerene acceptors can be alternative materials in solar cell devices for low-cost synthesis, tunable energy levels and providing complementary absorption to electron-donor polymer components, improving the photocurrent in devices.

The main objective of this dissertation is to design and synthesise non-fullerene acceptor based conjugated small molecules using the core of **IDTT** and **IDT** as donor units and **TPD** and **DPP** as electron deficient moieties and explore their use as electron acceptor components in OSCs applications.

The present study utilises numerous non-fullerene acceptor families obtained from direct arylation reactions, Stille cross-coupling and the Knoevenagel condensation reaction. The structure and elemental composition of the non-fullerene acceptors have been characterised by ^{1}H NMR, elemental analysis and mass spectroscopy. The non-fullerene acceptors' optical, thermal and electrochemical properties in solid state have been investigated to evaluate their suitability for organic photovoltaic devices application. The properties of the non – fullerene acceptors were found to be strongly dependent upon the use of TPD and DPP electron withdrawing moieties, as well as electron donating and other electron-deficient end capping moities.

Table of content

List of Figures

List of Schemes

List of Tables

List of abbre*via*tions

Acetone-d_6	Deuterated Acetone
BHJ	Bulk Heterojunction
br	Broad peak (NMR)
a.u.	Arbitrary Units
CV	Cyclic Voltammetry
$CDCl_3$	Deuterated Chloroform
DCM	Dichloromethane
s	Singlet (NMR)
dd	Doublet of Doublets (NMR)
d	Doublet (NMR)
t	Triplet (NMR)
m	Multiplet (NMR)
NMR	Nuclear Magnetic Resonance
DMF	N,N-Dimethylformamide
E	Energy
Eg (elec)	Electrochemical Band Gap
UV-vis	Ultraviolet-Visible Spectrscopy
Eg (opt)	Optical Band Gap
eV	Electron Volt
J-V	Current-Voltage
Voc	Open Circuit Voltage
FF	Fill Factor
Jsc	Short Circuit Current
ITO	Indium Tin
HOMO	Highest Occupied Molecular Orbital
LUMO	Lowest Unoccupied Molecular Orbital
λmax	Maximum Absorption Wavelength
PCE	Power Conversion Efficiency
PC70BM	Phenyl-C70-Butyric Acid Methyl Ester
PC60BM	Phenyl-C60-Butyric Acid Methyl Ester
PEDOT:PSS	Poly(3,4-ethylenedioxythiophene):Polystyrene Sulfonate
P(*o*-tol)$_3$	Tri-*ortho*-tolyl Phosphine

PPh_3	Triphenylphosphine
$Pd(PPh_3)_2Cl_2$	Bis(triphenylphosphine)palladium(II)dichloride
NBS	N-Bromosuccinimide
$Pd(OAc)_2$	Palladium (II) Acetate
TLC	Thin Layer Chromatography
Td	Onset of Decomposition
TGA	Thermogravimetric Analysis
THF	Tetrahydrofuran

Chapter I: Introduction

1.1 Introduction

1.1.1 Organic semiconductors

Once the electrical conductivity of polyacetylene had been determined (Shirakawa, Heeger and MacDiarmird, 1977), a substantial number of researchers have sought to identify potential conjugated polymers and their significance in the global market. [1] Electrical conducting polymers can be employed as photoactive parts in organic electronic devices, such as light-emitting diodes (LED), photovoltaic solar cells, field effect transistors, thin film transistors and, electrochromic devices. The electrical properties of these polymers support the area of organic conjugated materials, thus, organic electronics were studied and incredible progress occured. The combination of any suitable materials offers a possibility of obtaining multifunctional molecules that afford an opportunity for desired applications. [2-4]

Therefore, an amalgamation of the properties of organic polymers with that of the semiconductors has provided a foundation for notable attention in the solar industry. **Figure 1.1** shows electronically conducting polymers such as polyaniline (PANI), poly(para-phenylene ethylene) (PPE), polythiophene (PT), poly(para-phenylene vinylene) (PPV), polypyrrole (PPY), poly(para-phenylene) (PPP) to be a group of organic semiconductors or "synthetic metals." with various potential domains of application.

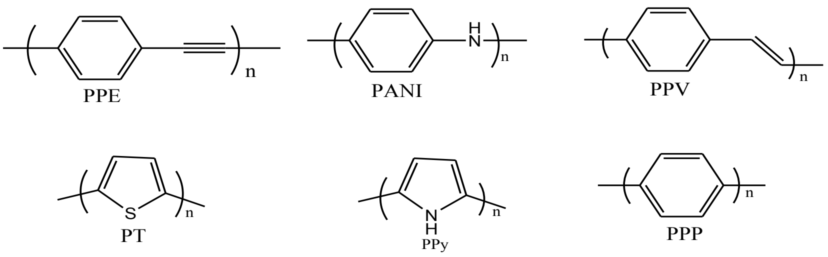

Figure 1. 1: The chemical structure of common semiconductors

The electrical properties of CPs are maintained by electron movement through the conjugated backbone. Most of the CPs experience one general structural characteristic, namely a rigid nature initiated by the sp^2 hybridisation of the polymer backbone. The use of a conjugated structure provides polymer chains with extended π-electron delocalisation along the molecule backbone, and this unique feature distinguishes the CPs from their other polymeric counterparts.

The overlpping of atomic pZ orbital with adjcent atomic p^Z orbtials results in molecular π-orbitals, which are devided into π-bonding orbitals and π*-antibonding orbitals. The π-bonding orbitals refers to occupied molecular orbitals (HOMO) has low energy and the π*-antibonding orbitals refers to the lowest unoccupied molecular orbitals (LUMO) has high energy. The energy difference between the top of the valence band and bottom of the conduction refers to the band gap (Eg). The large band gap in small molecule is due to lower overlapping of π-orbitals. However, the increase of the conjugated system leads to the more overlapping and reduction in the band gap **Figure 1.2**. The electronic structure is an imperative factor in the electrical properties of any material. The CPs produces bands through a large overlap of the molecular orbital.

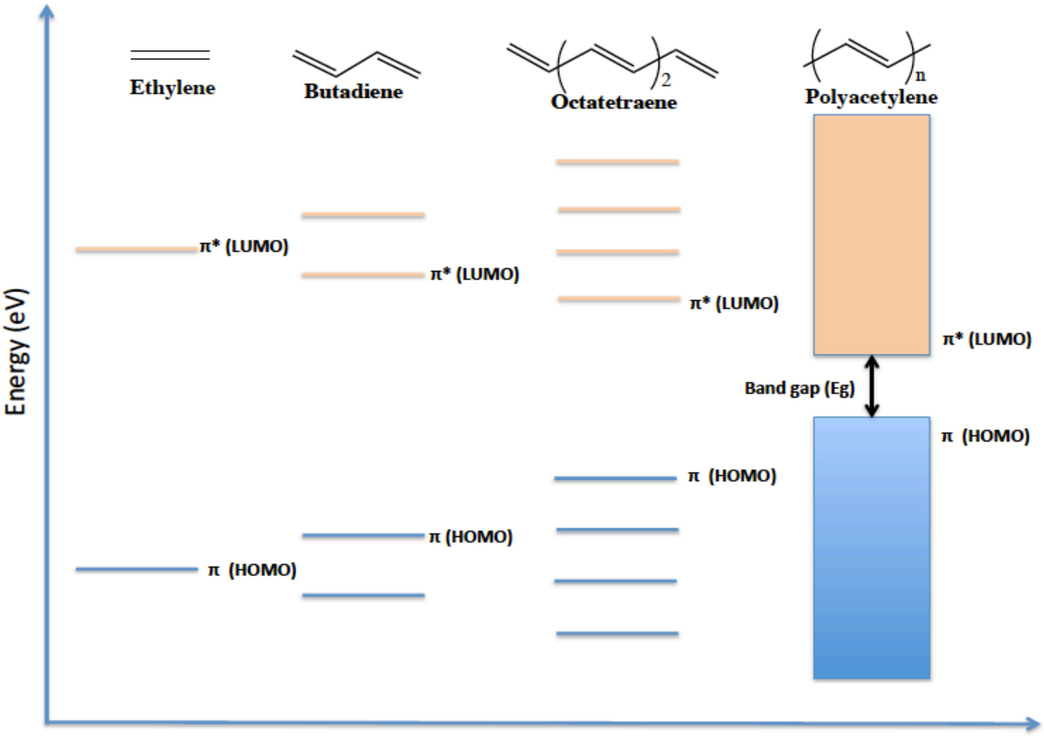

Figure 1. 2: The Molecular Orbital (MO) diagram**.**

According to the band theory, [5-8] materials are categorized into three groups, namely: insulators, semiconductors, and conductors as shown in **Figure 1.3**. The high conductivity of metals is due to the absence of a band gap, which can be as a result of overlapping bands or a partially filled band. However, insulator materials exhibit a lack of conductivity, which is attributed to the large band gap. Semiconductor materials possess a smaller band gap compared to insulators, thus electrons can be promoted thermally or photon via excitation from the valence band to the conduction band.

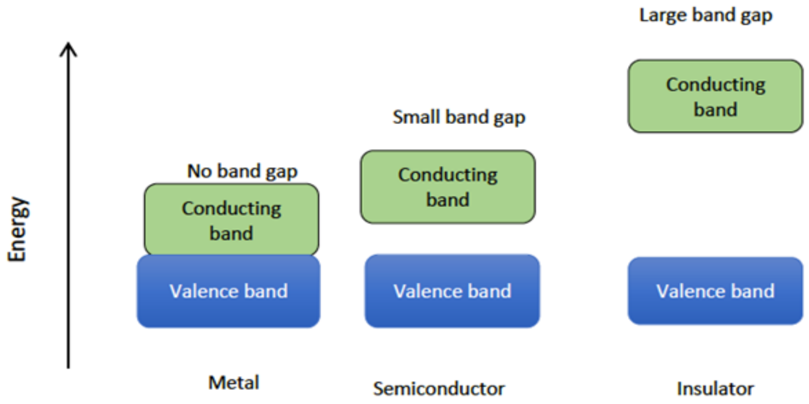

Figure 1. 3: The difference in band gap for Metals, Semiconductors and Insulators.

1.1.2 Doping

The doping of silicon-based semiconductors can occur through a substitution of a Si atom by another atom in a crystal lattice. This tolerates the energy states within the band gap subject on either type of the dopant, which produces excess of electrons (n-type) or holes (p-type) charge carriers. [9] In contrast, in the case of the conjugated polymer, substitution doping does not demonstrate new energy states because of the bonding interactions. Rather, new bands are created primarily due to an amalgamation of atomic orbitals. Thus, the HOMO/LUMO states are modified by the introduction of heteroatoms, also affecting the solid-sate structure. [10]

The doping of CPs can be performed by either a chemical or electrochemical reaction through an incorporation of oxidants (p-type) or reductants (n type). In addition, free charge carriers can be generated thermally or photochemically. The doping of CPs causes the electrical, electronic structural, magnetic, and optical properties of the polymer to alter noticeably. Upon doping of the polymer, there are two elements that must be considered, namely the excited electronic states within the band gap area and the physical rearrangement of the structure using resonance to accommodate the new energy states. [11-14]

The impact of doping on the electronic structure depends the degeneracy of the ground state. For example, doping poly (acetylene) results in two distinct resonance forms (A and B), which are of equal energy. The convergence of phases A and B produce a radical referred to as a soliton. A neutral soliton is an excited state, which works as the boundary between the two degenerate resonances between these phases. The location of soliton is directly in-between the CB and VB and it has an unpaired spin. The formation of solitons can be positive (oxidative doping) or negative (reductive doping). [15] The formations are responsible for generating a new subgap energy level in the center, resulting in the flow of electrons and the conductivity. With regards to the degeneracy of polyacetylene, three forms of solitons and their spin are demonstrated in **Figure 1.4.**

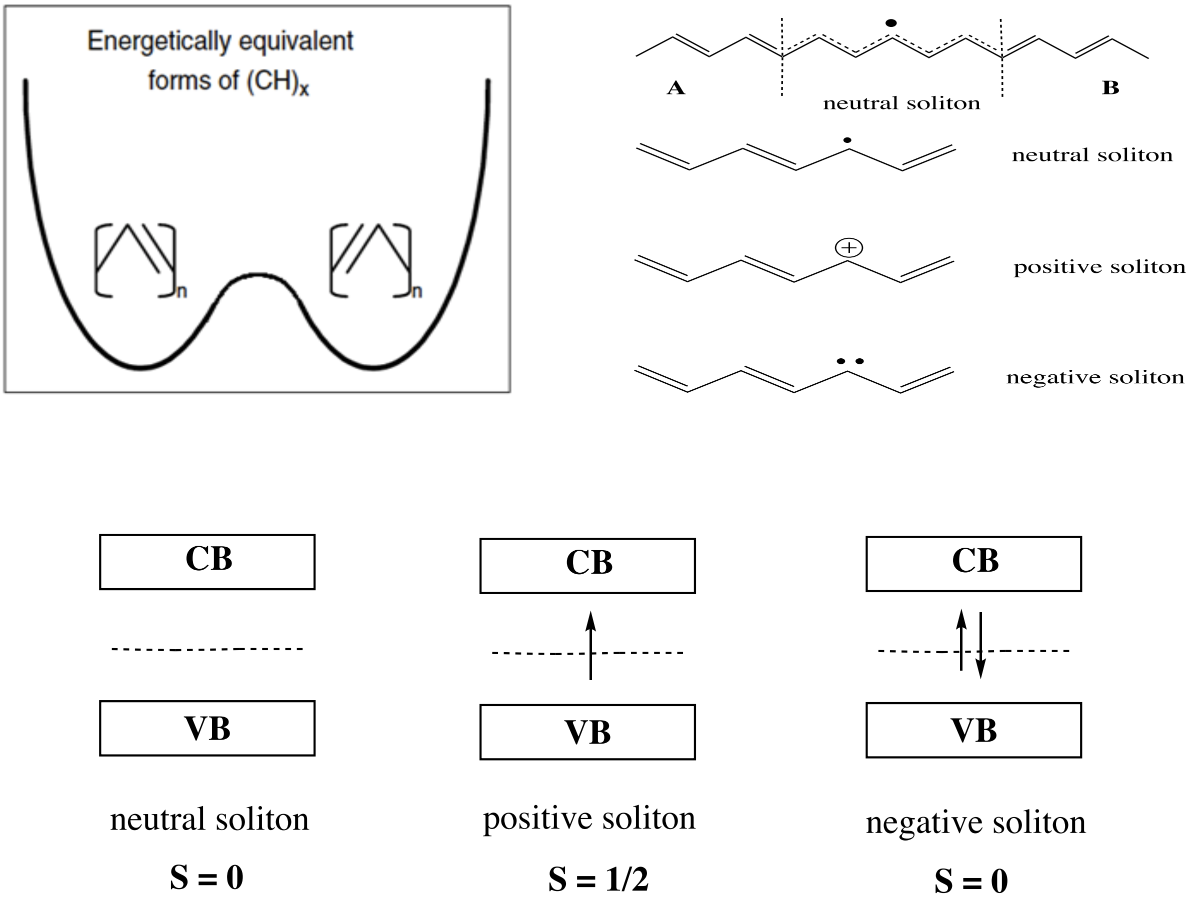

Figure 1. 4: The degeneracy of polyacetylene, three forms of solitons and their energy level.

Conversely, the majority of CPs do not exhibit a degenerate ground state. Typically, they have two forms of resonance strucutres, namely benzenoid (which has a low energy level and aromatic properties) and, quinoid (which has a high energy level and broken aromaticity). Typically, the doping of CPs is represented by polaron or bipolaron states. [11,16] The oxidation of CPs (p-doping) leads to a removal of an electron from the VB, creating a cation, which is referred to as polaron. The cation has higher energy than that of energy the CB and delocalises only over several monomeric units with a paramagnetic spin property. Upon further oxidation on the polaron, the unpaired electron will be extracted, resuling in special dication known as bipolaron, which is not independent. The bipolaron has a spinless property. Moreover, a high degree of doping leads to gerenration of a many bipolaron levels and eventually causing a formation of a bipolaron band **Figure 1.5**. [17-20]

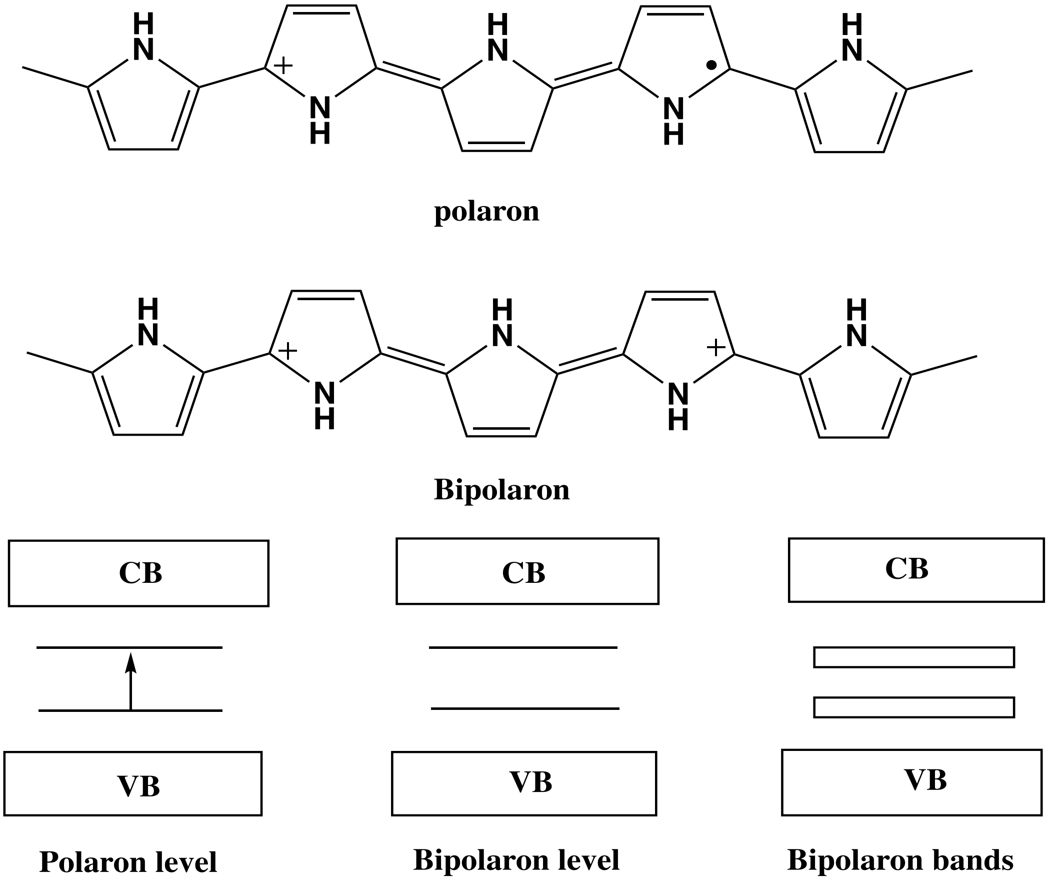

Figure 1. 5: The polaron, bipolaron and bipolaron band.

1.1.3 Application of conjugated polymers

The fundamental notion in optoelectronic applications is the converse exchange between light and electricity. This type of application primarily depends on the natural interaction of light and electrons within semiconducting materials. The band gap of the semiconductors is a significant aspect in the desired application and the semiconductors band gap can be tuned, thus, their properties can be altered from insulator state to conducting state materials. The semiconductors can be classified into organic and inorganic materials. From the early 20th century, inorganic semiconductors have been employed in electronic devices. However, the emergence of new semiconductors in the last three decades has been dependent on organic materials. Since that time, a substantial amount of effort has been applied to develop the performance of these devices. One of the efficient ways is the use of conjugated polymers. The presence of a π electron along the CPs chain can faciliate the reversible (oxidation and reduction) reactions, which can be carried out through electrochemical or chemical processes. This characteristic creates an invaluable chance to employ CPs for different modern applications such as the Light Emitting Diode (LED), Electrochromic devices (ECDs) and organic solar cells, etc. [21]

In LED applications, a polymer is a thin light source in which a polymer is utilised as a function of the emissive material. LEDs facilitate a broad range of devices to manufacture cheaper devices. The polymer LED is used as an active layer in LED application. In 1963, Pope *et al.* reported the first discovery of electroluminescence in organic materials. [22] In 1990, Burroughes *et al.* made the first electroluminescence from conjugated polymers based on polyphenylene vinylene (PPV). [23] The implementation of conjugated polymers in electroluminescence brought tremendous attention to other types of organic electronic devices, such as FETs, OLEDs and solar cells. The operation concept of LED devices is based on the presence of an electric field on conjugated polymers. Thus, the conjugated polymer is injected by holes and electrons from anode and cathode respectively. Following this, the positive and negative charges associated with the massive layer generate an exciton which decays, resulting in the emission of energy in photons. This process is known as photoluminescence (PL) and the band gap of the polymer controls the colour of the emission light. The LED can be built in two forms, namely a single and multi-layer. Essentially, a thin film of a polymer is inserted between Indium Tin Oxide (ITO) as an anode electrode, and metals such as aluminium (Al) and calcium (Ca) as a cathode electrode. [24]

In addition, CPs can be used in electrochromic devices. For example, in electrochromic devices, there must be a transparent electrode for observation of the colour changes. In the basic performance of electrochromic windows, the doped and undoped state of CPs will take a place electrical potential from sunlight. Thus, a positive potential is applied causing p-doping leading to the colour changes to be visible. Several CPs have been investigated such as polypyrrole, polyaniline, and polythiophene for potential imploy in electrochromic devices application. [21]

Finally, polymer solar cells (PSC) have earned a tremendous amount of attention in the research community due to the potential benefits of PSC such as low cost, light weight, fast and affordable roll-to-roll. Basically, a photoactive layer is made of CPs to build up solar cell devices. CPs play a significant role in the development of the power conversion efficiency of solar cells.

1.2 Organic solar cells

1.2.1 Introduction

Energy consumption has increased considerably in the last century. Traditionally, energy is produced from fossil fuels and nuclear power. It is highly probable that these unrenewable energy sources will ultimately have to be replaced in the near future by an efficient source that will be less harmful to the environment. At present, renewable energy sources such as wind, biomass, solar, and geothermal energy tends to be the clear alternative sources for supplying electricity to future generations. Each day, the earth acquires a tremendous amount of energy, which is higher than the world's energy needs, but an extremely low amount of energy has been used for the world's energy requirement.

Despite other sources of energy, solar energy is the most abundant sustainable power source. Solar thermal electricity, heating and photovoltaic (PV) are the significant technologies for the conversion of incident light into heat and electricity. It is worth acknowledging that the advent of PV devices provides ample opportunity for ecological energy consumption. In addition, this approach to energy conversion has environmental advantages.

However, the efficiency of the conversion of energy based on photovoltaic cells is a significant challenge due to its low efficiency. Commonly, the inorganic materials have been utilised in the solar cell application. For example, the inorganic semiconductor materials such as silicon and CdTe were used to produce the inorganic solar cell, which has reached efficiencies of 25%.[25] Meanwhile, the exorbtant cost of fabricating silicon solar cells has caused the researcher to investigate cheaper photovoltaic materials and devices.

Over the years, numerous developments have been employed and new substances for solar cells have been investigated. The past two decades have observed the replacement of solar cells comprised of inorganic materials with organic polymer semiconductors. Some features such as low cost, flexibility, large scale production, and easy manipulation of characteristics are the principles of designing organic solar cells as an alternative to the high cost of inorganic solar cells. In contrast, organic solar cells typically exhibit a significantly lower performance than that of the Si solar cells. Moreover, organic polymers degrade in the environment with prolonged exposure. Some critical factors, such as the cost-efficiency, reduced damage, large space, scalable electrodes deposition techniques on organic materials are also unexplored. Overcoming the shortcomings of these problems has inspired vigorous efforts in organic photovoltaic devices. [26] Organic solar cells have revealed substantial enhancement in device features. The recent introduction of organic materials into solar cells is a novel solution for the previous instability and inefficiency when inorganic materials were utilised. Organic solar cells have attained rapid progress due to their light-weight, low-cost and flexibility advantages. There has been a dramatic enhancement in power conversion (PCEs) as well as in the stability of the devices within the atmosphere. It is predicted that such devices will provide a marketable advantage within the solar energy industry.

1.2.2 Photovoltaic effect

Photovoltaic cells produce electrical power from incident sunlight through several stages of energy conversion processes. Light is constructed from packets of energy, known as photons, whose energy relies on the frequency or colour of the photon. The solar spectrum overlays from ultraviolet (UV) to infrared wavelength ranges **Figure 1.6**. There is only 30% of incoming light absorbed in the visible region. However, over 50% is absorbed in the infrared region. The photons in UV and the visible region have sufficient energy to promote electrons in the organic semiconducting materials, and this can be effectively utilised for charge production. The infrared waves, on the other hand, are not able to generate electrical energy using conventional PV technology.

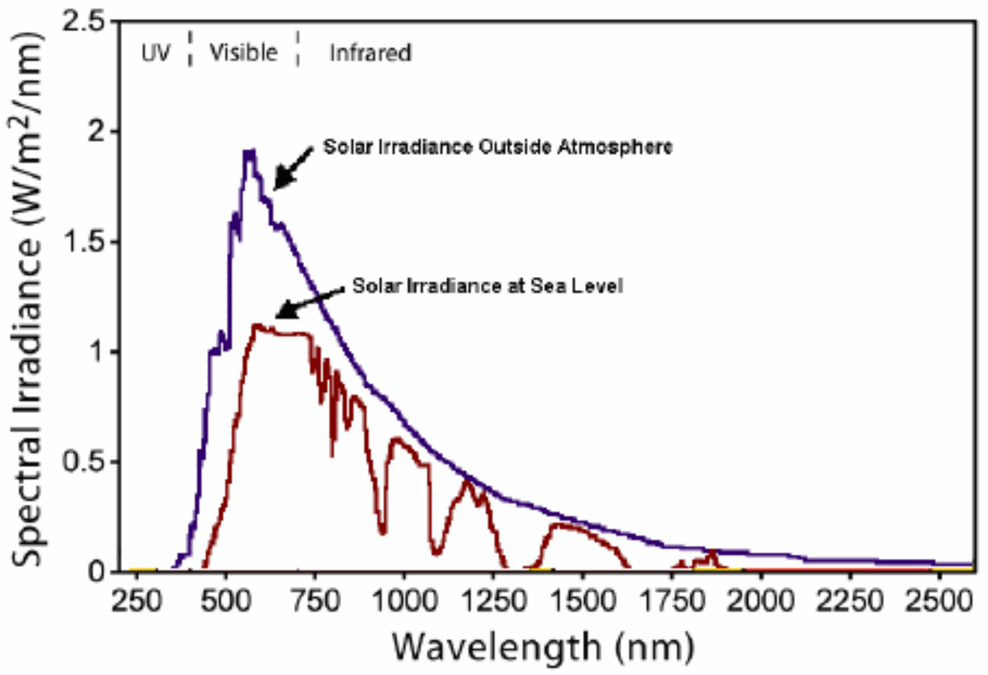

Figure 1. 6: The solar spectrum.[27]

1.2.3 Solar cell working principle

Photovoltaic solar cells are constituted to convert solar energy into electric energy. The principal working of the photovoltaic solar cells depends on several stages including light absorption, charge generation, transport, and collection **Figure 1.7**.[28]

A solar cell is a photodiode comprised of two different materials, namely p-type and n-type semiconductors materials. When these two types of semiconductors converge, results in the formation of a depletion region. Excitons (electron-hole pair) emerge when the photoactive conjugated molecule absorbs the incident light. An incoming photon promotes an electron from the top level of the valence band to a higher energy level (the bottom of the conduction band) and produces a Coulomb-attracted electron-hole pair. This phenomenon occurs when the energy of a photon is equal or higher than the energy of the material's bandgap. The exciton is a charge-neutral pair and has high binding energy approximately 0.5 to 1 eV**.**[29] As a result, an external field is applied to make an effective dissociation of the exciton to deliver a current. The production and separation of excitons are key steps occurring in organic solar cells. Typically, the devices are presented as excitonic solar cells.

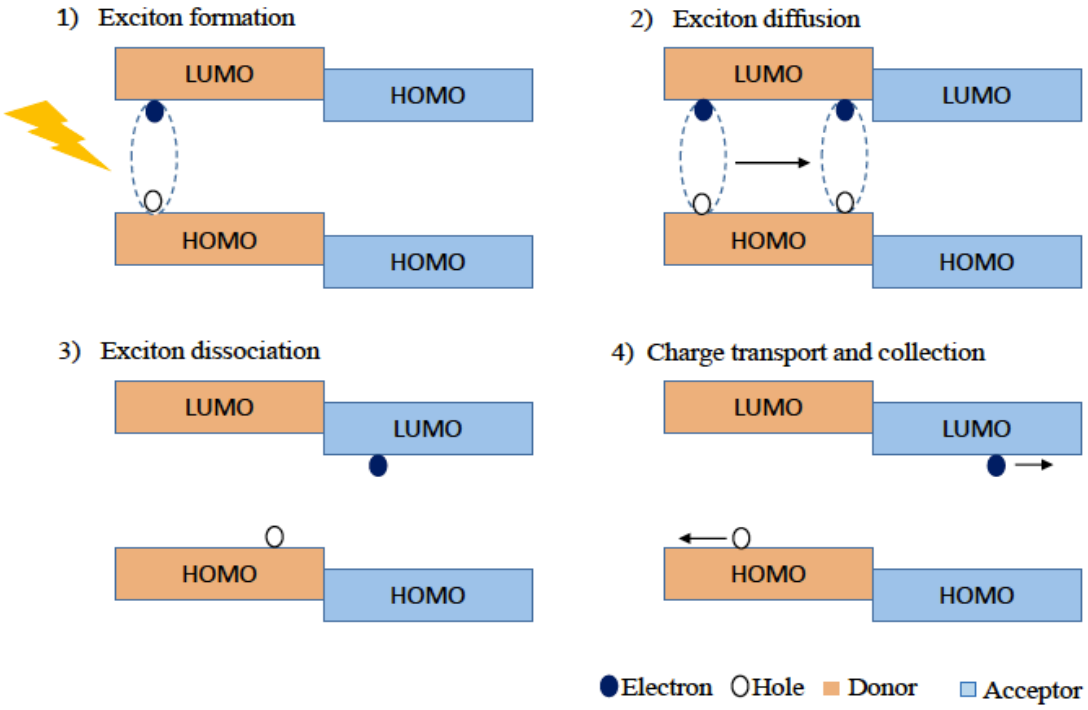

Figure 1. 7: The principle working of solar cell.

The separation of excitons into the positive and negative charge is a significant step in converting the energy of photons into electrical power. The implementation of an external electric field can help to accomplish the dissociation of the excitons. The different potentials between the two electrodes in the photovoltaic cell is, however, not adequate to dissociate the exciton. The exciton alternatively transfers back to the material - electrode interface where it is separated. In the majority of cases, the free charge will recombine as a result of the exciton's reduced diffusion duration. This process of the exciton reconnection is referred to as geminate, monomolecular or trap-assisted recombination. [30] Nevertheless, the junction of the n-type (donor) and p-type (acceptor) materials has sufficient potential to generate an electrical field tolerating the separation of the exciton. [31] This phenomenon transpires in the event that the difference in energy exceeds the binding energy of the exciton. Hence, the organic photovoltaic strongly depends on the interfacial design of the acceptor and the donor materials.

When the excitons are dissociated, they transition to the respective electrodes due to the effect of different potentials between the electrodes. This leads to passing the current to the external circuit. The recombination of the free charges may occur anywhere at the interface of the donor and acceptor before they arrive at the electrodes. This process is termed non-geminate. [32]

1.2.4 Generation of the photovoltaic solar cell

There are three categories of solar cells. Currently, the first generation of the solar cell is referred to in commercial productions. The first generation of the solar cell utilises a high quality, large area and single junction silicon device. It is extremely expensive and time-consuming to manufacture this device and it expends a substantial amount of energy. Regardless of the high construction costs, silicon solar cells dominate commercially because of its high efficiency in comparison to other generation devices.

Thin film solar cell is the second generation of the solar cell, which is significantly more affordable than the first generation solar cells. However, it exhibits lower efficiencies. The predominant features of thin film solar cells are their flexibility and lightweight compared to silicon solar cells. The most effective materials for the second-generation cells are copper indium gallium selenide (CIGS), micro-amorphous silicon, cadmium telluride (CdTe) and amorphous silicon. Thus, this type of solar cell has potential for future use.

The third generation of solar cells is comprised of an extensive range of innovations such as polymer solar cells, dye-sensitised and nano-crystalline solar cells. This type of solar cell has been investigated extensively to improve the weak efficiency of thin film solar cells and lower production costs. In addition, these solar cells are considered to be a breakthrough in technology. Although the organic solar cells show efficiencies with approximately 13%, it is still an interesting field for research to attain higher efficiencies.

1.2.5 Organic solar cell architectures

1.2.5.1 Single layer devices

Single layer organic solar cells are the first type of organic material solar cells, and it was discovered in 1959 based on anthracene crystals in a single layer device. [33] **Figure 1.8** illustrates the basic structure of this device. An organic active layer is sandwiched between two dissimilar electrodes. Typically, a high work function electrode such as Indium Tin Oxide (ITO) and a low work function electrode such as Al, Mg or Ca are commonly utilised in the single layer devices. The performance of a single solar cell device is entirely dependent on the features of the electrodes. The primary purpose of using two different electrodes in work function is to generate an electric field, which is responsible for the dissociation of the excitons. excitons. The primary concern for this device is the weak diffusion and dissociation of the excitons, which significantly reduces its conversion efficiency. The low efficiency contributes to the generation of insufficient energy to perform an effective separation. Therefore, holes and electrons tend to recombine rather than transferring the electrodes to deliver the current.

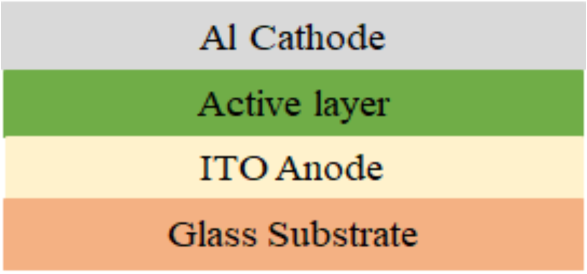

Figure 1. 8: The structure of single layer device

1.2.5.2 Bilayer devices

The structure of bilayer solar cell devices involves producing an extra layer (electron transporting layer) in comparison to the construction of single layer devices. Tang et al. were the first group that designed bilayer solar cell devices in 1986. [34] Two photoactive layers of CuPc (copper phthalocyanine) as a donor and PTCBI as acceptors were utilised to construct this device. The bilayer solar cell devices demonstrated in the conversion efficiency was approximately 1%.[34] Sariciftci et al. first employed this bilayer solar cell device structure into polymer photovoltaic cells in 1993. [35] In the architecture of bilayer devices, donor and acceptor semiconductors materials are deposited on a glass electrode such as ITO. The last component is a metallic electrode (cathode), which is deposited above the acceptor layer. The architecture of the bilayer device is depicted in **Figure 1.9.**

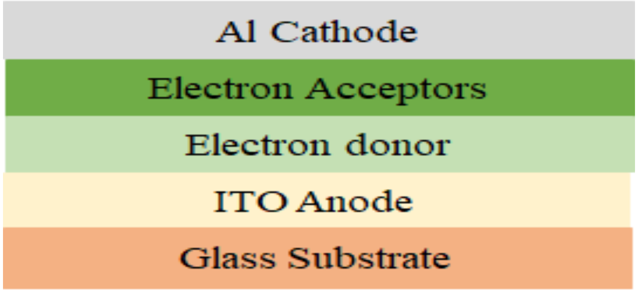

Figure 1. 9: The architecture of bilayer device.

The incorporation of the donor and acceptor interface into this system is to promote the efficient charge dissociation into electrons and holes. Therefore, the presence of the electric field facilitates the free charges transported to their respective electrodes and eventually produces the output voltage. Bilayer devices are significantly influenced by the characteristics of donor and acceptor semiconductors. These two organic semiconductors must have high different ionisation potentials and electron affinities to increase the efficiency of the charge movement. [36]

1.2.5.3 Bulk hetrojunction devices

In such a bulk heterojunction structure, the electron acceptor and donor are blended to produce an interpenetrating network and to develop the interfacial interaction between the donor and the acceptor. As a result, the traveling distance between the location of excitons and the interface should be in the exciton diffusion length range. **Figure 1.11** depicts the bulk heterojunction device. [37-39]

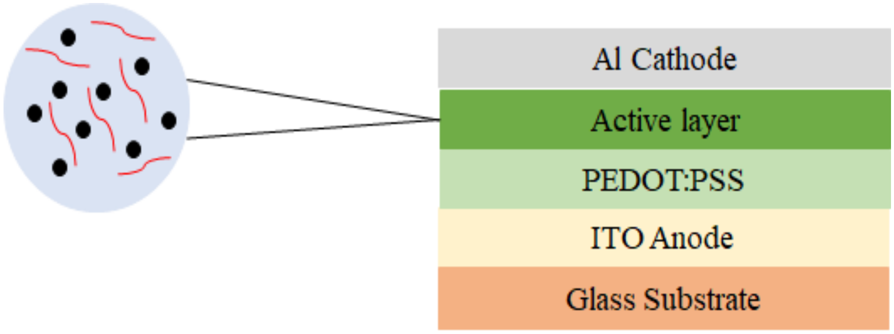

Figure 1. 10: The structure of bulk hetrojunction devices.

In the bulk heterojunction structure, considering bicontinuous blend interfaces are associated with the two metallic electrodes and produce an efficient charge transport route, the charge formation could be established in the whole organic active layer, and then effectively spread over the high density of the heterojunction interface in the device. Ultimately, the separation electron and hole can migrate to the electrodes through the efficient interpenetrating network trails and produce the output voltage.

1.2.6 Parameters in solar cells

Figure 1.11 demonstrates the photovoltaic performance in current-voltage (J-V). It is a measure of generated current across an applied voltage. Some critical parameters such as open-circuit voltage (Voc), short-circuit current density (Jsc), fill factor (FF) and power conversion efficiency (η) can be extracted from a J-V curve. In the J–V curve, the measurement is taken in dark conditions and compared to conditions with illumination at 100 mW cm^{-2} with AM1.5 radiation.

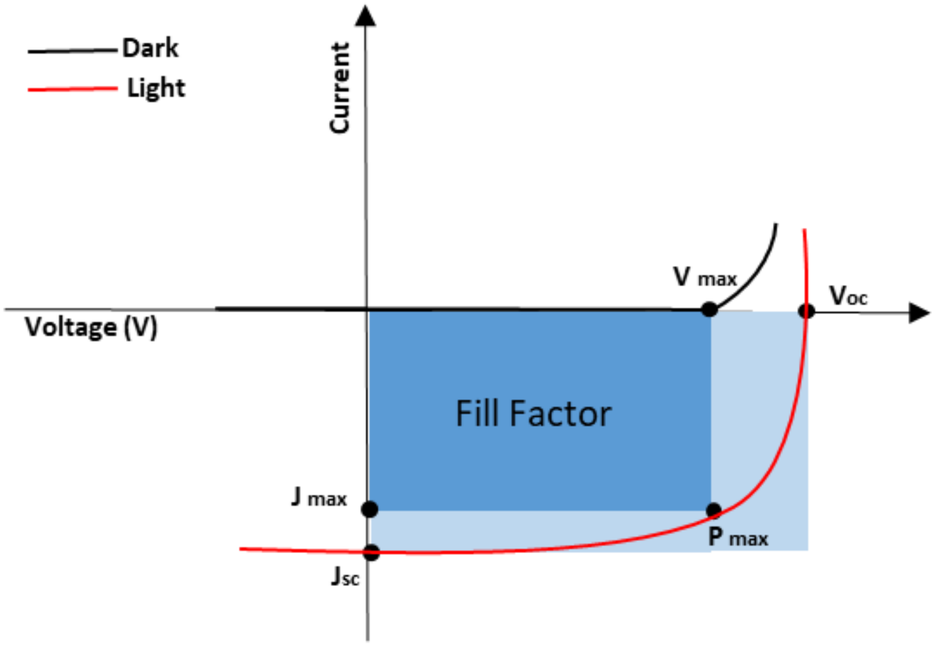

Figure 1. 11: Current – voltage curves of typical PV in the dark and under illumination

1.2.6.1 Power Conversion Efficiency (PCE)

This parameter is principally evaluated by its solar electrical power conversion efficiency (PCE). The PCE of solar cell devices can be defined as the ratio between power output from the solar cell device to power input from the incident light (P_{inc}); hence, the PCE can be deduced from the J–V curve as described in the equation 1.1.

$$\eta = \frac{J_{max}\, V_{max}}{P_{inc}} = FF = \frac{J_{sc}\, V_{oc}}{P_{inc}}$$

Jsc: short circuit current.

Voc: open circuit voltage.

J max: short circuit current at the maximum power point

Vmax= open circuit voltage at the maximum power point

FF: Fill Factor.

P_{inc}: power input from the incident light.

η: power conversion efficiency.

1.2.6.2 Open circuit voltage V_{oc}

The open circuit voltage (Voc) is defined as the maximum voltage obtained from the solar cell in the absence of a net current and is a significant calculation in solar cell devices. Voc is the difference between the HOMO level of the donor materials and the LUMO of the acceptor material level. Thus, a low-lying of donor HOMO level would result in a high Voc. In addtition, the minimum energy distance between the LUMO level of the donor and acceptor is ~ 0.3 eV to perform an effective dissociation of excitons. Furthermore, the nature of organic materials and its architecture can affect the Voc as well as the charge recombination, which leads to a lower Voc. [40,41]

1.2.6.3 Short circuit current J_{sc}

The short circuit current (Jsc) is defined as the maximum current expended from the solar cell device in the absence of applied voltage between both electrodes. In addition, different factors can determine the Jsc including the morphology of the active layer, an effective charge separation, collection and the optical properties of the organic materials. Jsc is associated with the number of charge carriers, hence, the efficient organic materials should possess an expanded absorption area within wavelengths 380 to 900 nm[42] and a high absorption coefficient in order to produce more excitons. [43-45]

1.2.6.4 Fill Factor (FF)

The Fill Factor (FF) parameter indicates the quality performance of PV devices. FF is the maximum power output from the solar cell device. Moreover, FF is mainly influenced by several components such as the thickness and morphology of the active layer and interfacial effects. These factors are associated with charge carrier transportation. [46] In order to maximise the FF, the morphology of the active layer requires optimisation to facilitate the charge separation and the transportation to their corresponding electrodes. FF is computed from the ratio between theoretical power output (V_{MPP} J_{MPP}) at the maximum power point to the absolute power (Voc and Jsc) **Equation 1.1**.

$$FF = \frac{PMax}{J_{sc}\, V_{oc}} = \frac{J_{max}\, V_{max}}{J_{sc}\, V_{oc}}$$

Jsc: short circuit current.

Voc: open circuit voltage.
J max: short circuit current at the maximum power point
Vmax= open circuit voltage at the maximum power point
FF: Fill Factor.
P max: theoretical power output at the maximum power point

1.3 Synthetic Aspects

1.3.1 Direct arylation reaction

The formation of new **C-C** bonds can be accomplished by coupling reactions. Generally, the Stille and Suzuki cross-couplings are utilised to synthesise polymers or small molecules. These two approaches require aoganostannanes or organoborons to couple with halides. However, the direct arylation method (DA) has been innovated, and it is a powerful approach to form a biaryls product. There are a number of benefits offered by the DA method, namely, cost-effectiveness, high yield, rapid process, eco-friendliness and it avoids the use of noxious organometallic precursors and ligands. [47-51] This approach involves coupling an aryl unit at a carbon with a hydrogen substituent with aryl halide using palladium catalysts, a base such as caesium carbonate (Cs_2CO_3) and a carboxylate source such as pivalic acid (trimethyl acetic acid). [50,52,53]

Research on DA coupling is still required in order to fully elucidate the mechanism. However, the common mechanism of the DA, particularly for heterocycles materials is described by the concerted metalation-deprotonation (CMD) mechanism as shown in **Scheme 1.1**. [54] The initial step of the reaction mechanism involves oxidative addition of the aryl halide (Ar_1– Br) to the Pd(0) complex with ligands (L) to produce an aryl-halo complex (1). Subsequently, a carboxylate ion reacts with complex (1) to deprotonate Ar_2, resulting in the generation of Ar_2–Pd and accordingly yielding the transition state. Following this, the deprotonation step of Ar-H occurs through concerted metalation – deprotonation (CMD). Finally, the reductive elimination is accomplished to render biaryls compound from palladium.

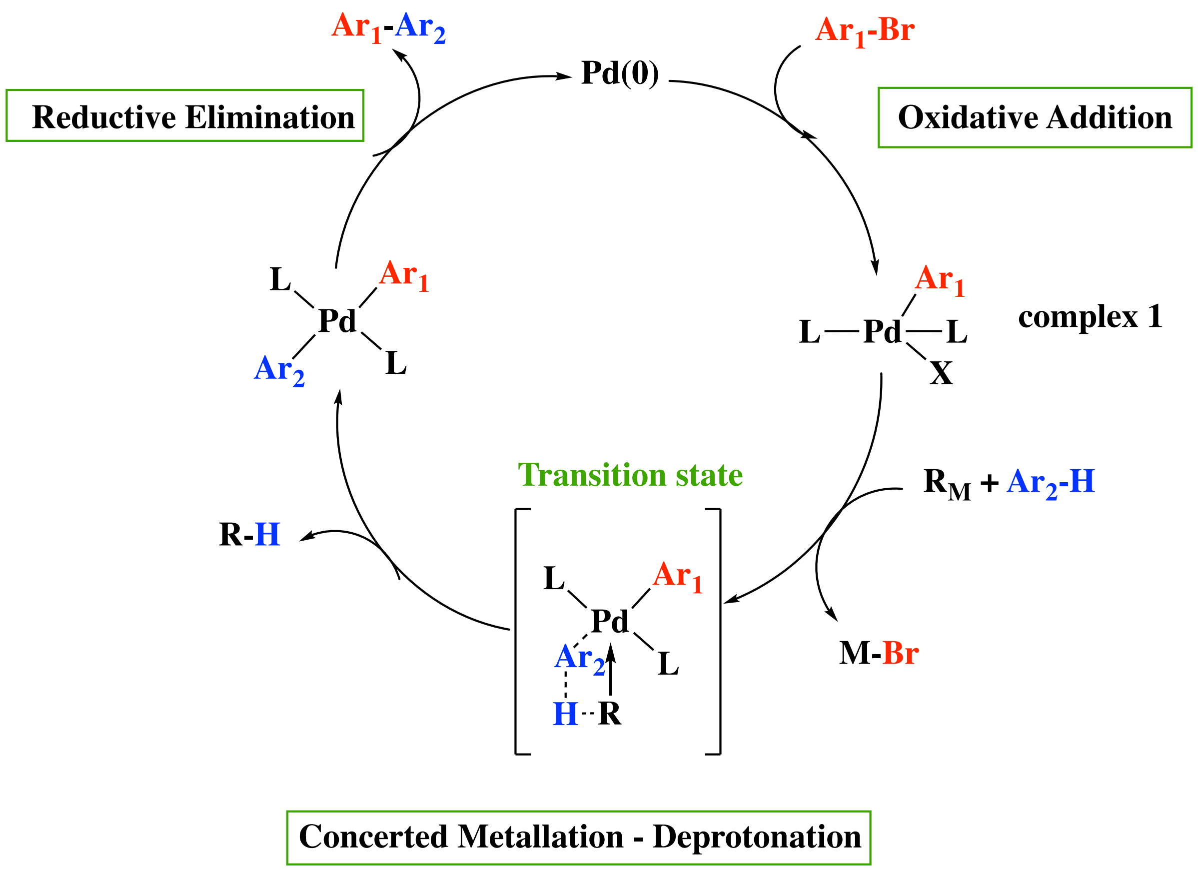

Ar$_1$, Ar$_2$ = Arene
L = Ligand
R$_M$ = Metal carboxylate
M-Br = Metal bromide
R-H Carboxylate

Scheme1. 1: The proposed schematic route of the direct arylation mechanism *via* the concert metalation - deprotonation (CMD).

1.3.2 Stille coupling reaction

The Stille reaction[55-58] involves coupling of an organostannane with an organic halide or pseudo-halide using palladium as a catalyst.[55-58] The catalytic cycle of the Stille reaction is almost the same as the Suzuki reaction apart from the utilisation of a base in the Stille reaction **Scheme 1.2**. [59-61] The Stille reaction allows an exceptional tolerance for functional groups, which for example, can be sensitive to bases. The step-growth of the Stille reaction is comprised of electron-donating stannyl and electron-accepting halide monomers. [62]

Unfortunately, the Stille coupling reaction requires extremely harmful organostannane compounds in order to function.[63]

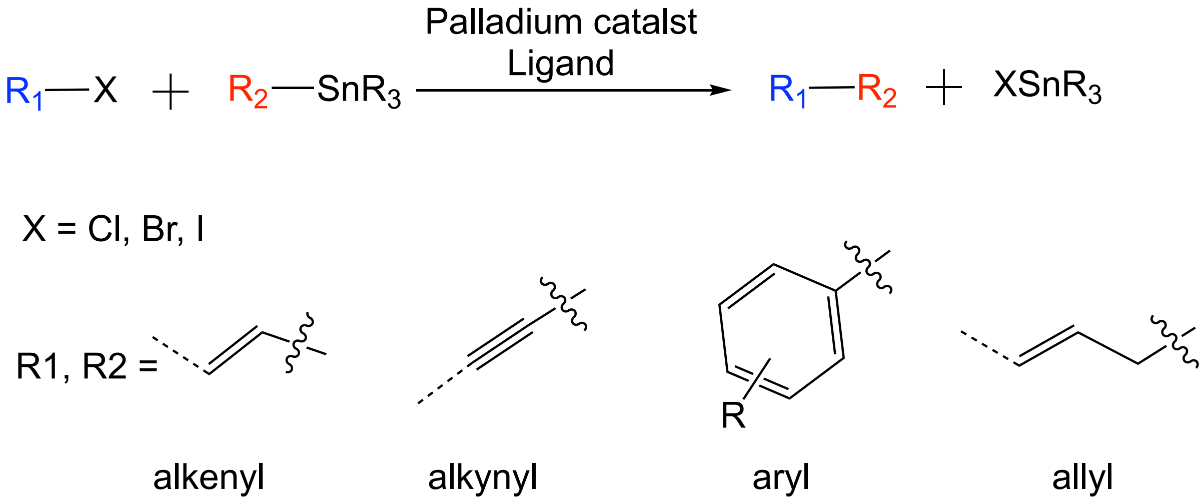

Scheme1. 2: The Stille cross - coupling of reaction.

1.3.3 Suzuki coupling reaction

The Suzuki reaction[64-67] is a palladium-catalysed cross-coupling reaction between an organoboron and an aryl boronic ester or acid derivatives in the presence of a base.[68,69] The Suzuki reaction does not require toxic compounds, it is relatively inexpensive and can initiate step growth polymerisation using tetrakis(triphenylphosphine) palladium(0) $Pd(PPh_3)_4$ as a catalyst.[70,71]

The Suzuki reaction mechanism commences from the oxidative addition of an aryl halide or pseudo-halide to produce a palladium (II) intermediate, which undergoes transmetalation in the presence of base – activated organoboron compound to yield an organopalladium intermediate. The reductive elimination of the organopalladium intermediate will take place to produce the coupled product and the palladium (0) catalyst**.** **Scheme 1.3** shows the schematic route of the Suzuki reaction mechanism**.**

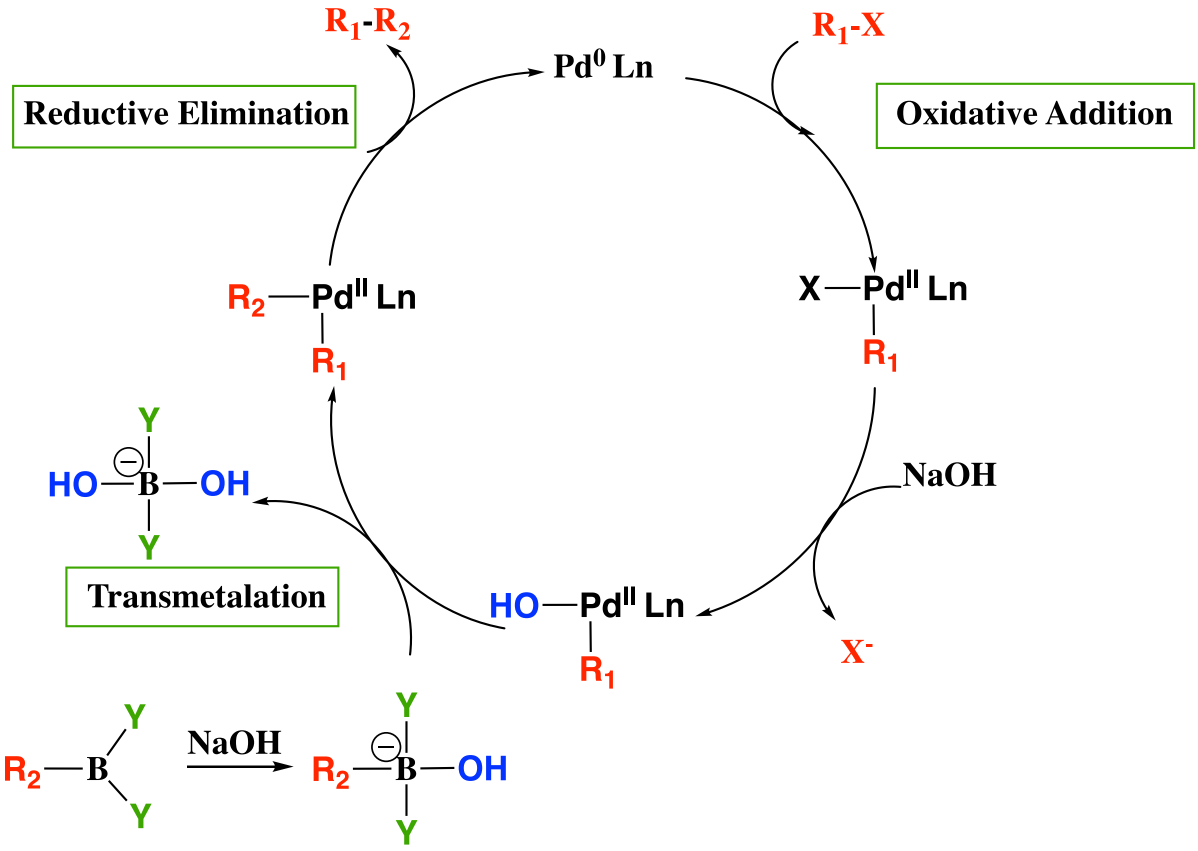

Scheme1. 3: The schematic route of the Suzuki reaction mechanism.

1.4 Rqiured properties of donor materials for organic solar cells.

The solar radiation spectrum extends from ~315 to1400 nm, which indicates that this region of photon flux is supposed to be covered and efficiently absorbed for better solar cell performance. The required band gap of conjugated polymers is from 1.0 to 2.0 eV to improve the absorption of the organic solar cell. Generally, a conventional organic electron donor material is supposed to confer a broad spectral to cover the light absorption range with a high absorption coefficient. [72] Moreover, the proper molecular orbital energy levels of the donor should match the energy level orbitals of the acceptor materials to enhance power generation, [73] Furthermore, the suitable solution processability plays a significant role in the formation of a thin film and the nano construction ability, preparing the desired morphology to use in the active layer when blended with acceptors with nano segregated and bicontinuous interpenetrating donor, namely acceptor regions and long term stability. However, the difficulty arises from a combination of multiple properties into one individual compound, thus, conjugated polymers with a perfect match of HOMO and LUMO levels are introduced for effective use in photovoltaic solar cells and absorption, covering the significant region of the solar cell spectra, which can be prepared to as a starting strategy of choice. However, Notwithstanding, additional mechanical alterations can ensure that the device operates appropriately. [73-78]

1.5 Band gap engineering

The most effective approach to decreasing the band gap of the conjugated polymer was reported by Havinga et al., [79] who demonstrated that incorporating an alternative electron conjugated donor (D) and electron conjugated acceptor (A) moieties in the polymer backbone. The formation of D-A copolymer can merge the valance and conduction bands resulting in organic conducting polymers. The resulting D-A polymer owns an intramolecular charge transfer between electron donor and acceptor moieties thus, lowering the band gap. [80,81] The alternating strong donors and acceptor groups can tolerate increased electron delocalisation along the polymer backbone since the donor and acceptor groups can accommodate the charges associated with a mesomerism (D-A↔ $D^+ = A^-$). Therefore, the band gap can be reduced in the event that the donor and acceptor units in the primary polymer chain are selected adequately.

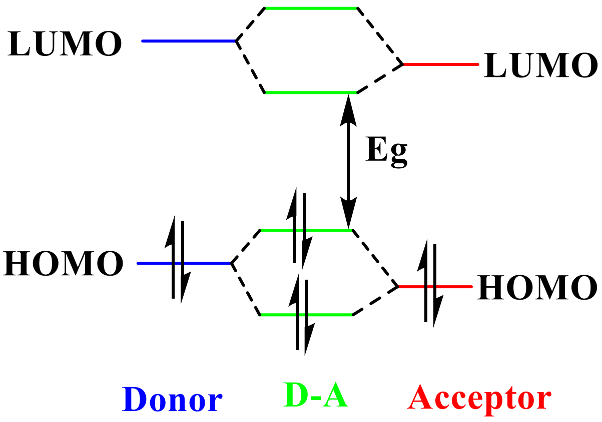

Figure 1. 12: The reduction of the band gap through the way of D-A hybridization orbitals of the donor and acceptor moieties

The D-A architecture of the conjugated polymer is also beneficial to energy level manipulation and can be demonstrated by molecular orbital theory as depicted in **Figure**

1.12. The interaction between the HOMO energy level of the donor with that of the acceptor through molecular orbital (MO) hybridisation can create two new occupied MOs. Moreover, the two new LUMO energy levels are formed through the hybridisation of the donor and acceptor groups. As a result, the redistribution of new generated energy levels leads to higher lying HOMO and a lowering lying LUMO, consequently lower the band gap. [82-84] **Scheme 1.4** depictes the common chemical structures of donor and acceptor groups used in D-A copolymerztion.

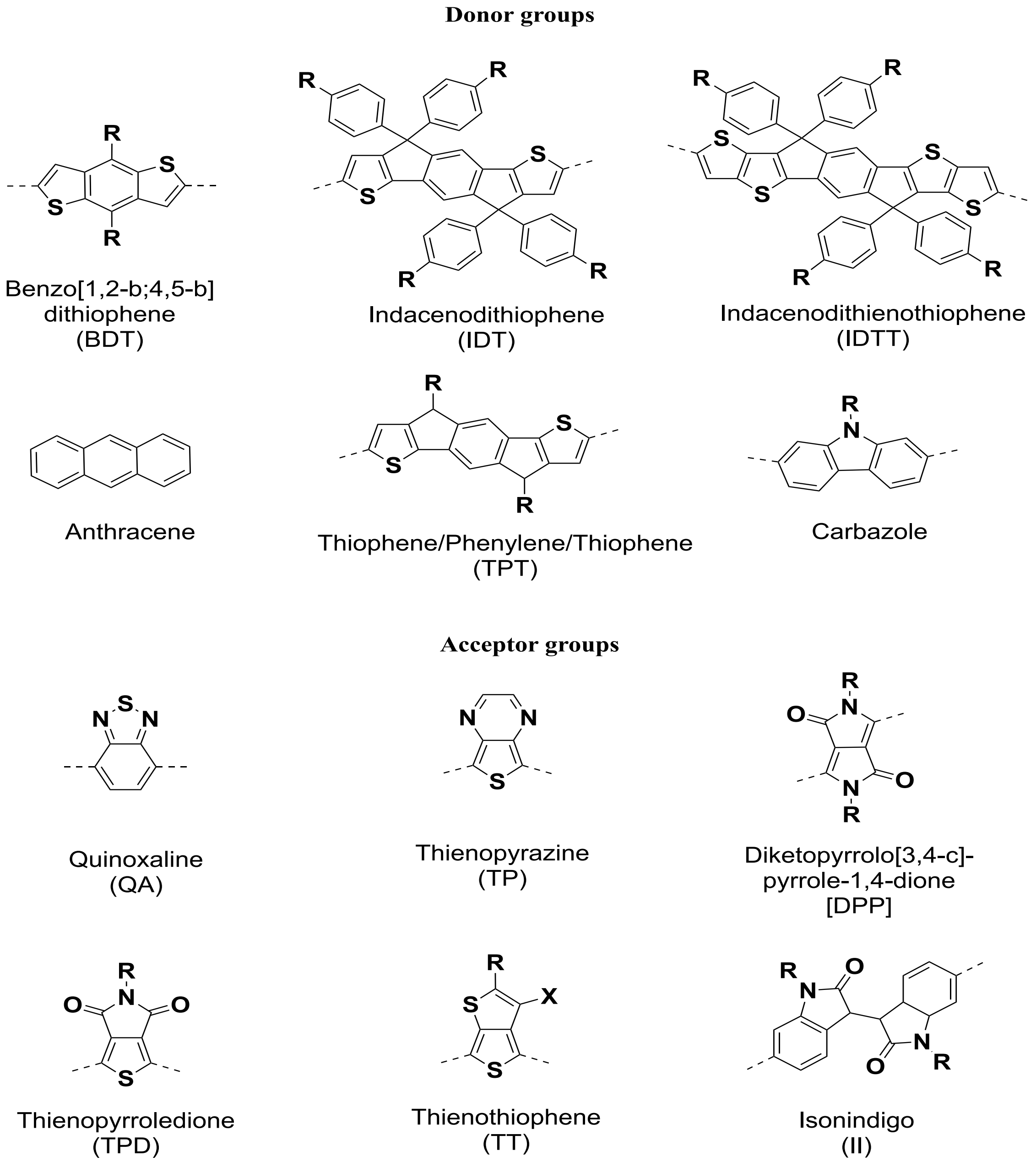

Scheme1. 4: The common chemical structures of donor and acceptor groups used in D-A copolymerztion.

Furthermore, the quinoidal effect reduces the band gap when the single-double alternation on the polymer chain is reversed. The conjugated polymer has two resonance forms; aromatic and quinoidal forms as illustrated in **Scheme 1.5**. The electrons in the aromatic resonance localise in the aromatic ring whilst the electrons delocalise along the polymer chain in the quinoidal resonance. The energy of the quinoidal resonance is higher than the aromatic structure, leading to the interruption of the aromatic system and energetically less stable relative to the aromatic resonance. Consequently, the quinoid structure possesses a smaller band gap compared to that of aromatic structure.

It is worth acknowledging that the band gap of a polymer is lowered most effectively by enhancing the quinoid effect of the polymer backbone. For example, poly(phenylene) (PP), poly(phenylenevinylene) (PPV), polythiophene (PT), and polyisothianaphthene (PITN) can demonstrate the strength of the quinoidal effect. The poly (phenylene) is comprised of highly aromatic phenyl rings, thus, having the highest band gap of 3.2 eV. In the case of PPV polymer, the induction of the vinyl link between the aromatic phenyl rings assists in decreasing the aromatic effect leading to the reduction of the band gap to 2.5 eV. The aromaticity of the thiophene ring is lower than that of the phenyl ring; polythiophene has a higher quinoidal effect where the band gap is 2 eV. The greatest quinoidal effect of PINT displays a noticeable reduction in the band gap to 1 eV. The chemical polymeric structures are depicted in **Scheme 1.5**. [85]

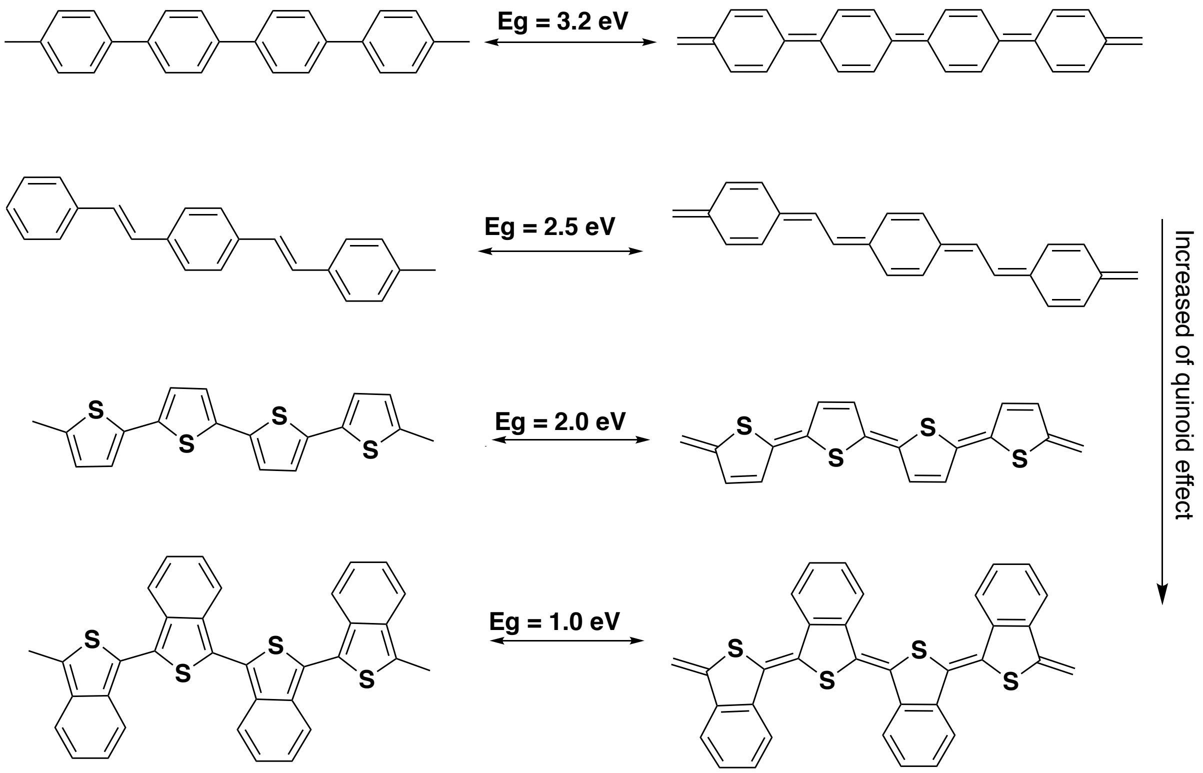

Scheme1.5: The aromatic and quinoid resonances of poly(phenylene) (PP), poly(phenylenevinylene) (PPV), polythiophene (PT), and polyisothianaphthene (PITN).

The side chains is an extremely significant component for developing some required properties of conjugated polymers such as molecular weight, solubility and processability. However, the incorrect attachment of side chains may present a steric hindrance to the resulting polymer from the formation of the planarity and twist the conjugated polymer chain. If the side chain is short, the torsion angle of the polymer chain will be small and the solubility will be decreased and thus, restricting the solution processability of the polymer. However, if the side chain is large, the solubility and processability of the polymer will be increased. Additionally, the distance of π-π stacking will enlarge, resulting in a low absorption ability of the polymer. This will result in an enlarged band gap and a reduced charge carrier mobility. [86] The introduction of an appropriate side chain is a crucial factor for not only improving the solubility and processability of the polymer but also for the morphology of the polymer for developing the performance of the organic solar cell device. Evidently, the solar cell functions according to the physical characteristics of the side chain, namely its length and shape.

Finally, the substituents are usually attached to specify the electronic properties of a conjugated polymer, such as the band gap, charge mobility and energy levels. The introduction of an electron-donor unit such as alkyl, alkoxy and alkylsulfanyl groups and electron-acceptor units such as fluorine, ester, ketone or cyano groups can modify the band gap through the influence on the HOMO and LUMO level band gap. The introduction of strong donors and acceptors on the polymer backbone is an effective technique to reduce the HOMO and LUMO level to produce a polymer with a low band gap. [79,87]

1.6 Materials used as organic solar cell Acceptors

Recently, there has been significant enhancement in fundamental knowledge, device structure, processing of the photoactive layer, and synthesis of novel materials. [88,89] Considerable investigations have been directed at creating better conjugated polymers as donors, and this enhancement has demonstrated a tremendous improvement of organic solar cell performance in the past few years. In contrast, fullerene and its derivatives were rapidly observed as the most effective acceptors, but the devotion on different types of n-type acceptors is very limited. Typically, organic materials used as acceptors in the organic solar cell can be divided into two categories, namely fullerene-based acceptors[90,91] and non-fullerene materials. [92,93]

1.6.1 Fullerenes acceptors for organic solar cells

The electron acceptor unit assumes an integral role in BHJ devices and is central to its function. The most well-known material utilised for this has commonly been the soluble derivatives fullerene C_{60} of phenylC_{61}-butyric acid-methyl ester ($PC_{60}BM$) in the 1990s. [94] Thereafter, various fullerene derivatives of C_{60} and larger compounds (C_{70}, C_{80}) have been produced with slightly adjusted properties. [95,96] **Figure 1.13** reveals the chemical structures of $PC_{60}BM$ and phenyl-C_{71}-butyric acid-methyl ester ($PC_{70}BM$), which has demonstrated a development in light absorption properties, and indene-C_{60} bisadduct (ICBA), which is proffered due to a lower electron affinity and thus increases the Voc in comparison to $PC_{60}BM$.

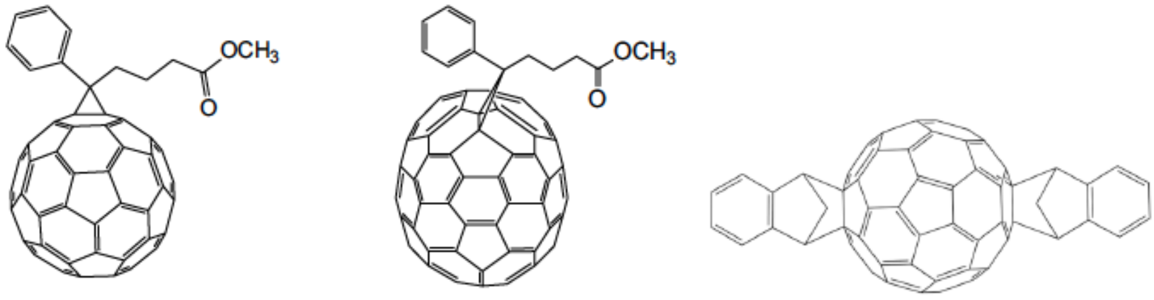

PC$_{60}$BM PC$_{70}$BM ICBA

Figure 1. 13: The common chemical structures of fullerene acceptors.

Several elements determine the application of fullerene derivatives as electron acceptors in OSC. As such, research has focused predominantly on novel donor polymers. Firstly, the high electron affinity of PC$_{60}$BM can lower the LUMO energy level, which was recorded between 3.7 and 4.3 eV, and generates a strong driving force for electron transfer from the donor. [95] In addition, the fullerene derivatives possess high electron mobility and isotropic charge transport properties, and this may contribute to the LUMO level delocalising over the outer surface of the fullerenes. Furthermore, the electrochemical properties of fullerene derivatives demonstrate multiple reversible reductions resulting in the stabilisation of reduced analogues, and it has been expected that the low-lying excited states adjacent to the LUMO improve disassociation of charges in polymer-fullerene blends. [97] Finally, in the solution processing of BHJ devices, fullerenes as acceptors exhibit the ability to aggregate and produce an appropriate morphology with a wide range of the polymer donors, which promotes the charge separation. [98,99] The PCE performance of OSCs based fullerenes as acceptors has attained 10% in a single junction and exceeds 11% in a tandem cell. [100,101]

Although fullerenes and their derivatives (acceptor) have demonstrated a dramatic improvement in the solar cell applications, they exhibit significant shortcomings which limit OSC performance. The fullerenes suffer from their relatively weak light absorption in the visible and NIR regions of the solar spectrum resulting in reduced the harvesting of photons and thus limiting the performance of PV. [102]

Therefore, most of the previous BHJ devices have been devoted to enhancing the light absorption of the donor polymer. Despite this, fullerene acceptors have become the primary source of electron acceptors and transport charges. Evidently, OSC function can be significantly enhanced by augmenting the optical absorption for donors and acceptors as it is applicable to the solar spectrum. In addition, morphological instability is another hindrance of fullerene acceptors, which tend to produce aggregation domains in BHJ devices over time. [103] Moreover, it is relatively challenging to tune the electronic and optical properties of fullerenes using chemical modification. Furthermore, the synthesis and purification of fullerenes acceptors is a high cost issue.

1.6.2 Non-fullerene acceptors for organic solar cells

It is evident that all the aforementioned disadvantages of fullerene acceptors must be taken into consideration to improve novel materials. This coincides with the ability to harvest more photons resulting in the generation of higher photocurrents and a larger open circuit value, which leads to higher PCE of the organic solar cell to overcome these shortcomings. Recently, substantial effort has been attributed on the design and synthesis of a NFA acceptor to replace fullerene acceptors and develop the performance of the solar cell. [104-106] The design of an alternative electron acceptor provides an excellent opportunity to make n-type materials with desired properties whilst maintaining the features of fullerenes. In particular, these properties such as a tunable energy level, high optical absorption in the visible and near infra-red (NIR) regions and charge transporting are the prerequisite requirements for developing the PCE in photovoltaic solar cells. [93,105,107,108] In addition, NFAs are simply prepared, purified and inexpensive to make, which make NFAs a proficient candidate for OSCs application.

Tang reported the first heterojunction organic solar cell based on NFA using a 3,4,9,10-perylene tetracarboxylic bisbenzimidazole (PTCBI) as the acceptor and copper phthalocyanine (CuPc) as the donor where the PCE of the producing bilayer device was 0.95% **Figure 1.14.** [34] The same materials were utilised to construct a different device structure, and the PCE increased over 2%.[109,110] The dawning of 2013 has observed the sudden emergence of NFA development.

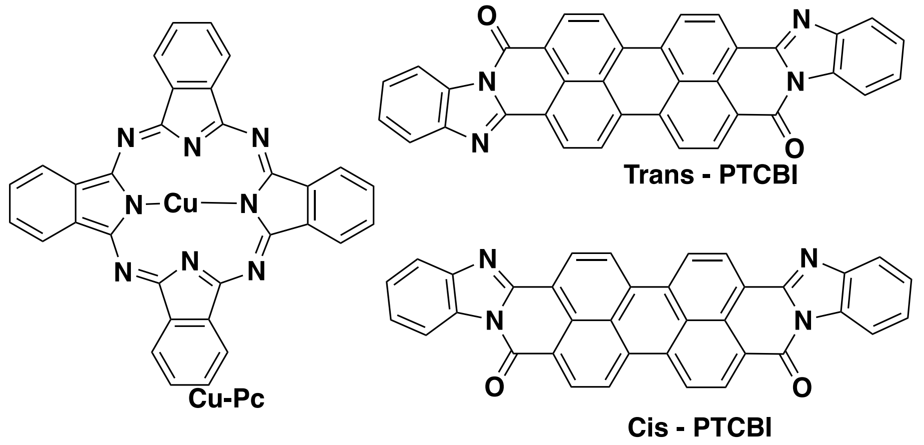

Figure 1. 14: The chemical structure of **Cu-Pc** as donor and **PTCBI** as acceptor

Perylene-3,4:9,10-bis(dicarboximide) (PBI) derivatives are another example of non-fullerene acceptor **Figure 1.15**. At present, PBI derivatives are regarded as the ideal n-type organic semiconductors available [111,112] due to their outstanding optical, stability, redox properties, charge mobility, and low cost. PBI dyes afford important opportunities for studies in solar cell devices. [113]

Organic solar cells have utilised a number of alternative acceptors. One of these is the diketopyrrolopyrrole (DPP) moiety **Figure 1.15**. Recently, DPP based polymers have gained extensive attention due to their unique performance as donor materials in the BHJ device with an efficiency of 4.7% in incorporation with a fullerene derivative. [114] Interestingly, the incorporation of high electron negative groups such as fluoro or fluoroalkyl groups developed the DPP electron affinity to be as acceptor materials. For example, trifluoromethylphenyl groups have been attached to the DPP core, which then blended in a BHJ solar cell with the poly(3- hexylthiophene) (P3HT) as a donor. The PCE of this BHJ was about 1%. [115]

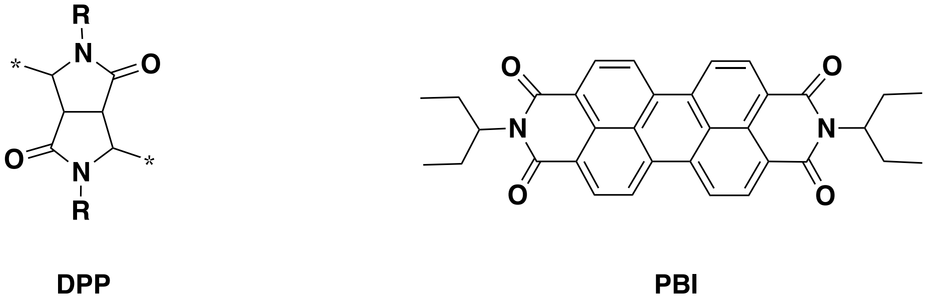

Figure 1. 15: The molecular structure of the **DPP** and **PBI**

Recently, a new fused ring electron acceptor (ITIC) with terminal INCN units has been synthesised, and it demonstrated optimum absorption in the visible and NIR areas with a maximum absorption of 700 nm and coefficient absorption of 1.10×10^{5} cm^{-1}. The HOMO and LUMO energy levels were located at -5.50 and 3.89 eV, respectively. In addition, the blended of (ITIC) as a acceptor with PTB7-TH illustrated an efficiency of 6.80% **Figure 1.16**. [116] It is worth noting that the blended PBDB with (ITIC) showed remarkable performance in the solar cell with a PCE exceeding 11% based on the non fullerene. [117]

In 2017, Zhao and his co-workers reported a new NFA IT-4F, which was synthesised by a modification of ITIC and the insertion of four fluorine atoms at the end capping INIC. In comparsion to the nonfluorinated ITIC, IT-4F showed higher maximum absorption by 17 nm with a coefficient absorption of 1.16×10^{5} cm^{-1}. Moreover, the HOMO and LUMO were observed to be lower than the energy level of the ITIC with -5.66 and -4.14 eV, respectively. Thus, the reduced IT-4F energy level is due to the integration of fluorine atoms. The BHJ device of IT-4F as NFA with PBDB-T-SF as a polymer donor was fabricated and showed a high PCF of 13%.[118] It is worth elaborating that this value of PCE PBDB-T-SF with IT-4F is the highest recorded based on fullerene or any other type of solar cell device **Figure 1.16.**

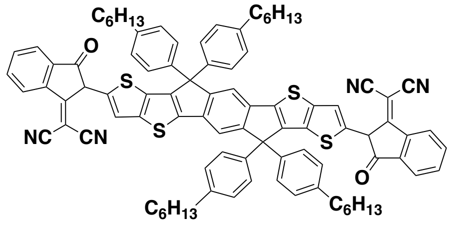

ITIC

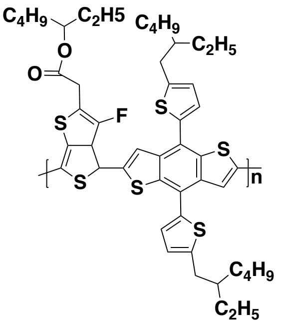

PTB7-TH

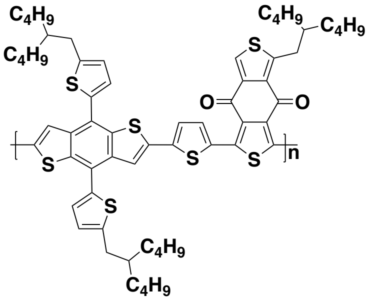

PBDB

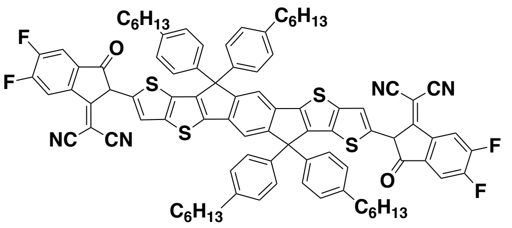

IT-4F

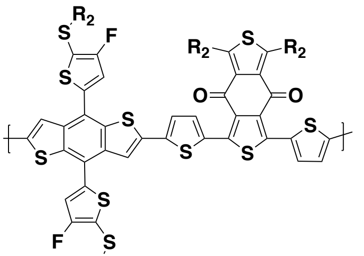

PBDB-T-SF

Figure 1. 16: The chemical structures of **(ITIC), (IT-4F) (PTB7-TH), (PBDB)** and **(PBDB-T-4F).**

1.7 Aims.

Solar cell devices based on inorganic materials have shown excellent power conversion efficiencies up to 29%. In spite of this, the exorbitant cost of construction, limits the implementation of solar cell devices with inorganic materials on a wider scale. Alternatively, the emergence of polymer organic solar cells has acquired considerable attention due to their promising features such as lightweight building upon a large-area scale at affordable cost. In organic solar cells devices, the derivatives of fullerene, such as $PC_{60}BM$, $PC_{71}BM$ ([6,6]-phenylC_{71}butyric acid methyl ester), and ICBA (indene-C_{60} bisadduct) have been extensively employed as acceptors due to their remarkable properties such as high electron mobility, high electron affinity and several reversible reductions. However, fullerene derivatives have several intrinsic drawbacks including, weak absorption in the region of the solar spectrum resulting in a low capability of fullerene derivatives to harvest light energy resulting in low photocurrents, the limited tunability of their energy levels, high cost of synthesis and difficulty of purification.

The primary aim of this project is to design and synthesise new small molecule non-fullerene acceptors with a structure of Acceptor-Donor-Acceptor (A-D-A) for use in BHJ OPVs. The manufacture of novel NFAs enables researchers to ascertain optimum characteristics that the fullerene derivatives could not provide. Moreover, there are some essential criteria that must be taken into consideration when preparing new NFAs such as strong absorption in the visible regain and NIR to cover the solar spectrum, high electron mobility, tunable energy levels, high electron affinity, electrochemical and thermal stabilities. These factors can improve the solar cell parameters including open-circuit, short-circuit, and FF, which leads to the enhancement of solar cell performance to obtain a high PCE.

The present study has formulated and assembled a number of NFAs, categorised into three aspects. These target acceptors were synthesised by directed arylation reaction, Stille coupling reaction and Knoevenagel condensation reaction. **Chapter 2** addresses the synthetic route of three NFAs using a spiro molecule indacenodithienothiophene (**IDTT**) as a central donor core with three different withdrawing units of thieno[3,4-c]pyrrole-4,6(5H)-dione (**TPD**). The aim of employing the ladder-fused ring such as **IDTT** and **IDT** is stemmed from its rigidity and coplanar structure, which facilities π-π interactions through the backbone and enhancement of the absorption, particularly in the visible and NIR area. Recently, the fused ring materials such as **IDTT** and **IDT** have shown significant progress based on NFAs and contribute vastly to the improvement of OSCs performance with the highest PCE of approximately 13%. Moreover, the purpose of attaching various high electron deficient **TPD** moieties at the distal end is to investigate the influence on electrochemical, optical and physical properties. Furthermore, the OPV devices for the new acceptor will be fabricated with different donor polymers to measure their PCE performance. The results and discussion of the NFAs will be presented in this chapter.

In **Chapter 3**, the **TPD** electron deficient groups will be replaced by diketopyrrolopyrrole (**DPP**), which has stronger withdrawing units and the same central spiro **IDTT** were utilised as a donor in order to make a comparsion. Four different withdrawing **DPP** monomers flanked to **IDTT** will be synthesised. The present study also aims to compare and evaluate the characteristics of optoelectronics with the OPV performance. However, in **Chapter 4,** the **IDTT** will be replaced by **IDT** whilst, maintaining the same four different withdrawing **DPP** units, which were connected to the **IDT** to prepare four NFAs**.** The impact of changing the core donor with **IDT** on the basic optoelectronic properties and evolution of OPV performance results will be discussed.

Chapter II:

Preparation of Non-fullerene Electron Acceptors for Organic Solar Cells Based on indacenodithieno[3,2-b]thiophene (IDTT) and thieno[3,4-c]pyrrole-4,6(5H)-dione (TPD)

Abstract

Three novel non-fullerene acceptors (NFA), were synthesised *via* direct arylation reaction and Knoevenagel condensation reaction, and investigated as electron acceptors in Bulk-Heterojunction (BHJ) devices. The **IDTT-TPD-PHT, IDTT-TPD-CN** and **IDTT-TPD-INIC** molecules had a donor core of extended fused-ring indacenodithienothiophene (**IDTT**) and three different electron withdrawing moieties based on thieno[3,4-c]pyrrole-4,6(5H)-dione (**TPD**) including **TPD-PHT**, **TPD-PHT**, **TPD-CN** and **TPD-INIC** as the end-capping group. The **IDTT-TPD-PHT** was soluble in common organic solvents. However, the **IDTT-TPD-INIC** possessed poor solubility in organic solvents, which may be ascribed to having not enough solubilising substituents on the **TPD** monomer moiety. **IDTT-TPD-CN** exhibited better solubility in organic solvents compared to **IDTT-TPD-INIC**. The three NFA showed strong and broad absorption from ~ 320 to 800 nm, with an optical band gap of 2.03, 1.75, and 1.55 eV respectively. The small optical bandgap was a result of the insertion of more electron deficient units, which affected the LUMO and HOMO energy for these **IDTT-TPD-PHT, IDTT-TPD-CN**, and **IDTT-TPD-INIC** acceptors, located at -3.22, -3.64, -3.89 eV and -5.36 to -5.30, -5.26 eV respectively. **IDTT-TPD-PHT, IDTT-TPD-CN** and **IDTT-TPD-INIC** exhibit strong absorption capability in chloroform ranging from around 350 nm to 750 nm with a molar extinction coefficient of 1.3×10^5 M^{-1} cm^{-1}, 7.6×10^4 M^{-1} cm^{-1} and 9.7×10^4 M^{-1} cm^{-1} respectively. All three NFAs developed exhibited excellent thermal stability with onset decomposition occurring above 350°C. The melting point for these materials was not observed at over 380°C.

2.1 Introduction

In the past two decades, bulk-heterojunction (BHJ) organic solar cells (OSCs) have gained considerable attention in relations solar cell devices due to their properties of being light weight, flexible, and low-cost. [125-128] Basically, the structure of BHJ has the active layer sandwiched between donor and acceptor materials, which generate the electricity from the incident sunlight. [129,130] Characteristics such as high electron withdrawing properties, high electron mobility, and isotropic charge transport ability, favor the use of fullerenes and their derivatives, including $PC_{61}BM$ and $PC_{71}BM$, as acceptors units for OSCs devices. [131-133] The PCE for fullerenes-based OSCs has reached over 11%.[134-139]

The weak optical absorptivity of fullerenes, poor tunability of their energy levels, and difficulty of purification have restricted further development in the performance of OSCs. [140-142] As a result, the recent emergence of non-fullerene acceptors as an alternative class of material provides the opportunity to synthesise NFAs with desired properties and overcome the intrinsic drawback properties of fullerenes; eventually, photovoltaic performance may be improved. Several attempts have been reported as employing NFA moieties such as benzothiadiazole, [143-146] diketopyrrolopyrrole, [147-150] rylene diimide, [151-159] and other electron withdrawing acceptors [160-165] in OSCs devices, exhibiting a PCE exceeding 6%.

Recently, the A-D-A structure of NFA was found to be the most effective design for acceptor units in OSCs where the PCE reached 13.2%; this exceeds the PCE of fullerene derivatives in OSCs. [118] From the point of view of chemical structure, the ladder-type forms, such as indacenodithiophene (**IDT**) and indacenodithienothiophene (**IDTT**), are among the most attractive electron rich units **Figure 2.1**. [166-169] The rigid backbone of fused rings plays an essential role in promoting π-electron delocalisation and inhibits the rotational disorder, decreasing the reorganisation energy, which leads to high charge-carrier mobility. The covalent bond of 4-hexylphenyl groups on the backbone of **IDTT** or **IDT** prevents large crystalline domains forming and restricts self-aggregation within the BHJ film. Moreover, the energy level can be adjusted by flanking various electron-withdrawing units as end capping units.

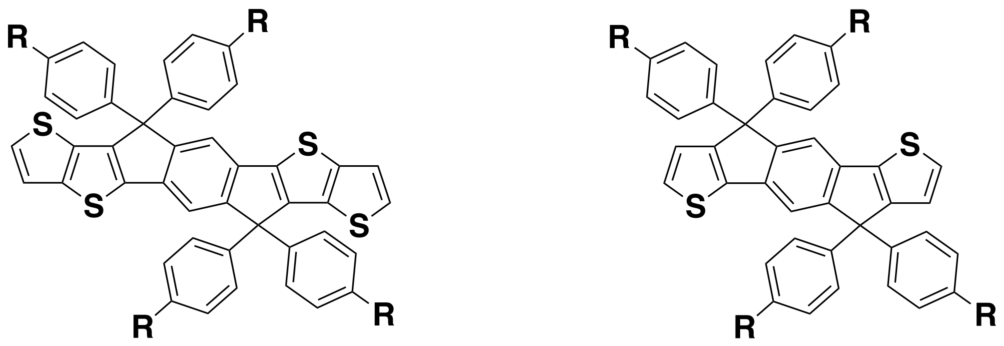

Indacenodithienothiophene
(IDTT)

Indacenodithiophene
(IDT)

R = 4-hexylphenyl

Figure 2. 1: The chemical structure of **IDTT** and **IDT** .

There is a wide range of acceptor moieties that withdraw electrons such as benzothiadiazole (BT), and diketopyrrolopyrrole (DPP) that have been applied in designing NFA materials for OSCs. In recent years, thieno[3,4-c]pyrrole-4,6(5H)-dione (**TPD**) derivatives have been extensively employed as acceptor materials; their promising properties include ease of synthesis, symmetry, rigidly fused and coplanar structure. Moreover, the high electron affinity of the TPD is attributed to the presence of imide, which can deepen the HOMO level energy, while maintaining or lowering the bandgap. [170,171] Also, the imide group can be subjected to alkylation, which enhances the solubility of the compounds. The **TPD** acceptor units have been commonly used in polymers, which exhibited a PCE above 8%. [172] However, unlike benzothiadiazole (BT), isoindigo (iI) and diketopyrrolopyrrole (**DPP**), there is limited research into applying **TPD** moieties to fabricate small acceptor molecules. [173,174] In 2011, Lin et al. synthesised the first small molecule for OSC with a D-A-D structure using the **TPD** as the acceptor and TPA as a donor, where the PCE was around 2.9%.[175]

In this chapter, we design and prepare three novel NFAs using the fused ring (**IDTT**) as donor units. However, three different **TPD** monomers were prepared and flanked on the **IDTT** to extend the planar backbone. These were 5-(3,7-dimethyloctyl)-1-(5-phenylthiophen-2-yl)-4H-thieno[3,4-c]pyrrole-4,6(5H)-dione **(TPD-PHT)**, 2-((5'-(5-(3,7-dimethyloctyl)-4,6-dioxo-5,6-dihydro-4H-thieno[3,4-c]pyrrol-1-yl)-[2,2'-bithiophen]-5-yl) methylene)malononitrile **(TPD-CN)** and 2-(2-((5'-(5-(3,7-dimethyloctyl)-4,6-dioxo-5,6-dihydro-4H-thieno[3,4-c]pyrrol-1-yl)-[2,2'-bithiophen]-5-yl)methylene)-3-oxooctahydro-1Hinden-1-ylidene)malononitrile **(TPD-INIC)**. The extended planar backbone is beneficial to promoting strong π-π interaction, leading to a lower bandgap and broader intramolecular charge transfer ICT absorption **Figure 2.2**. Furthermore, the incorporation of an electron-withdrawing unit into the **IDTT** can lower the energy level of these NFAs, leading to broadening red-shifted absorption, decreasing the optical bandgap, and enhancing the Jsc. The purpose of introducing different electron withdrawing units as end capping is to regulate the electronic and optical properties.

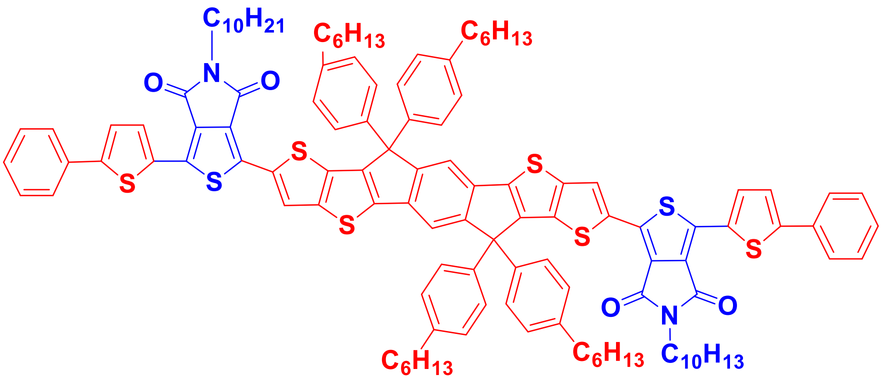

IDTT-TPD-PHT

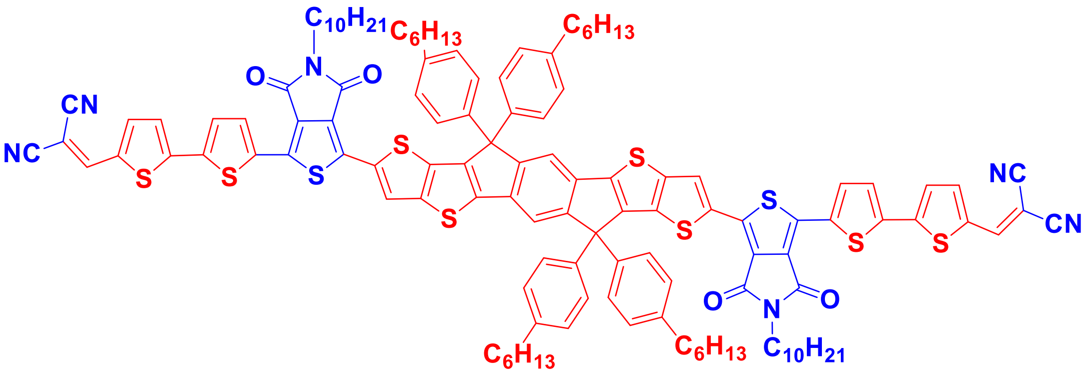

IDTT-TPD-CN

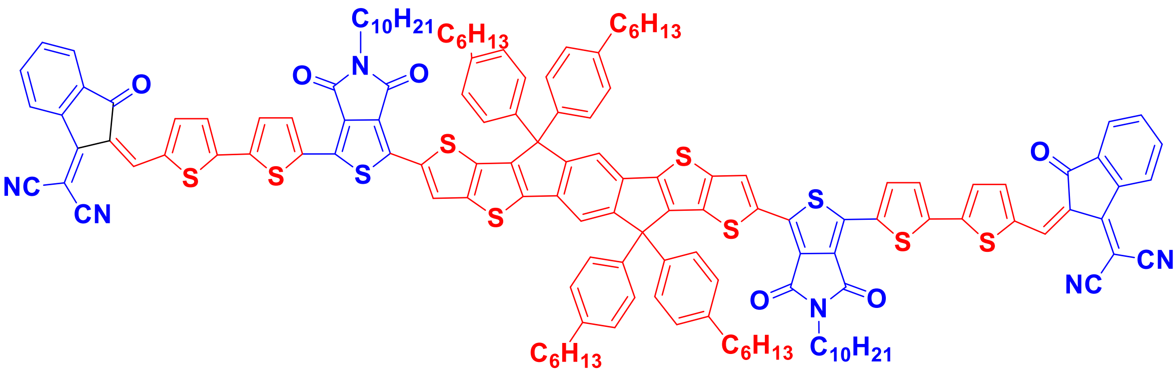

IDTT-TPD-INIC

Figure 2. 2: The chemical structures of **IDTT-TPD-PHT, IDTT-TPD-CN** and **IDTT-TPD-INIC** (red: donor unit and blue: acceptor unit)**.**

2.2 Result and discussion

2.2.1 Synthesis of the monomers

The synthetic route for the **IDTT-Br$_2$ (M1)** donor molecule is depicted in **Scheme 2.1**. The 2-bis (2,2-diethoxyethyl) disulfide **(1)** was obtained with a good yield of (88%) *via* reduction of 2-bromo-1,1-diethoxyethane in the presence of sodium sulfide, potassium iodide (catalyst), and ethanol as a solvent. Then t-BuLi (two equivalents) was used to lithate 3-bromothiophene, which was then quenched 2-bis(2,2-diethoxyethyl) disulfide **(1).** The crude product was purified *via* column chromatography to furnish 3-(2,2-diethoxy-ethylsulfanyl) thiophene **(2)** in yield 70%**.**

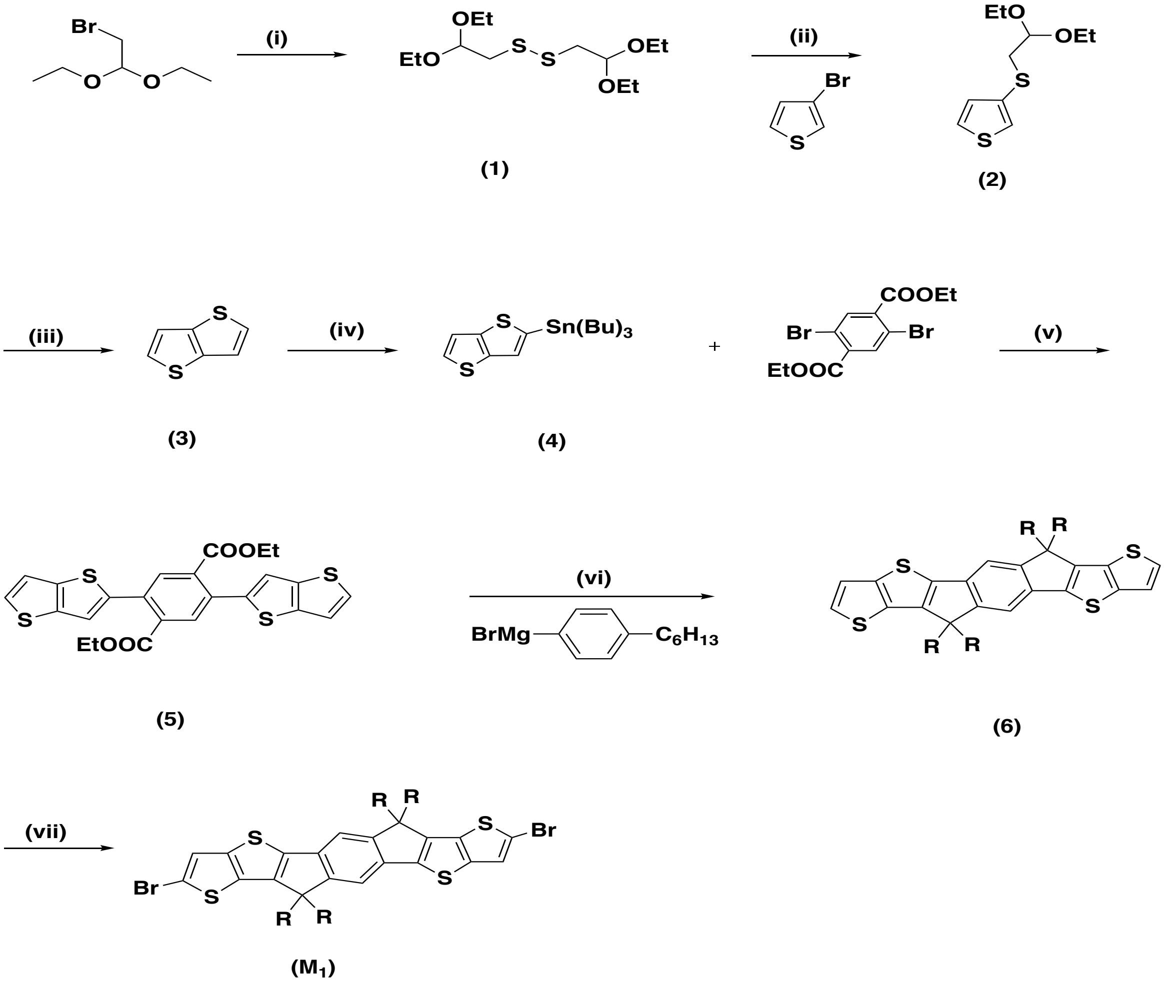

Scheme 2. 1: The synthetic route of **IDTT-Br$_2$ M1.**

Reaction condition: (i) Na_2S, S, KI, EtOH, reflux 24 h; (ii) t-BuLi, ether, -78 ^{O}C, 24 h; (iii) amberlyst 15 resin, ether, reflux, 24 h ;(iv) n-BuLi, -78^{O}C, $(Bu)_3SnCl$, THF; (v) $Pd(PPh_3)_4$, toluene, 110 ^{O}C; (vi) Mg, THF, acetic acid, conc H_2SO_4; (vii) $CHCl_3$, DMF,NBS.

Compound **(2)** was then subjected to sulfonic acid resin and refluxed in ether to achieve the ring closure reaction and afford yield of 71% of thieno [3,2-b] thiophene **(3)**. Compound **(3)** was then lithated by n-BuLi (one equivalent) and quenched by dropwise addition of tributylthin chloride to produce 2-(tributylstannyl) thieno [3,2-b] thiophene compound **(4)** with a yield of 93%, which was used in the next step without further purification. **Scheme 2.2** displays the proposed mechanism reaction of compound **(4).**

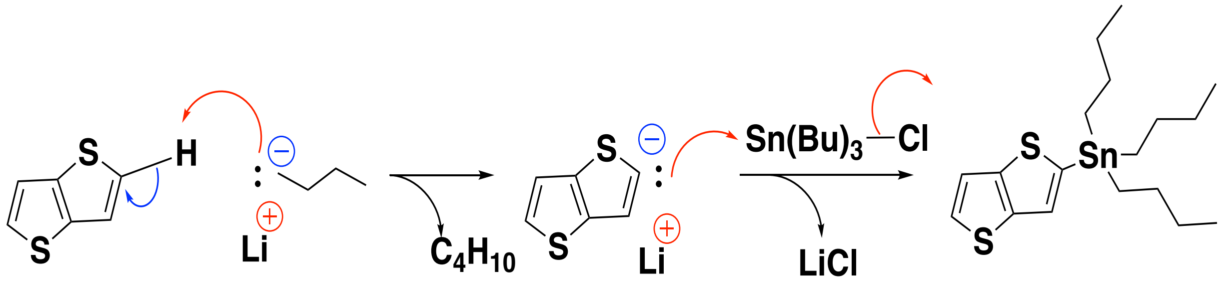

Scheme 2. 2: The mechanism of synthesis comound **4.**

In the initial step, n-BuLi was used to deprotonate the thieno[3,2-b] thiophene **(3)** to form a nucleophile, which then attacks the tributyltin chloride *via* the bimolecular nucleophilic substitution S_N2 reaction, resulting in the corresponding monostannyled thieno[3,2-b]thiophene **(4)**. Compound 1,4-benzendicarboxylic acid, 2,5 dithieno[3,2-b]thien-2-yl,1,4 diethyl ester **(5)** was prepared using the Stille coupling reaction of diethyl 2,5-dibromoterephthalate and an excess of compound **(4)** in the presence of a palladium catalyst. The crude was purified *via* column chromatography and compound **(5)** was obtained in 73% yield. The double nucleophilic of freshly prepared of (4-hexyl) phenyl magnesium bromide occurs to the diester group to produce benzylic alcohol, which is converted to compound **(6)** indacenodithieno [3,2-b] thiophene **(IDTT)** by intramolecular Friedel-Craft cyclisation in acidic condition. The crude product was purified *via* column chromatography, using a mixture of petroleum ether and DCM. The target product was obtained in a low yield of 37%. The expected mechanism of this reaction comprises several steps as shown in **Scheme 2.3.**

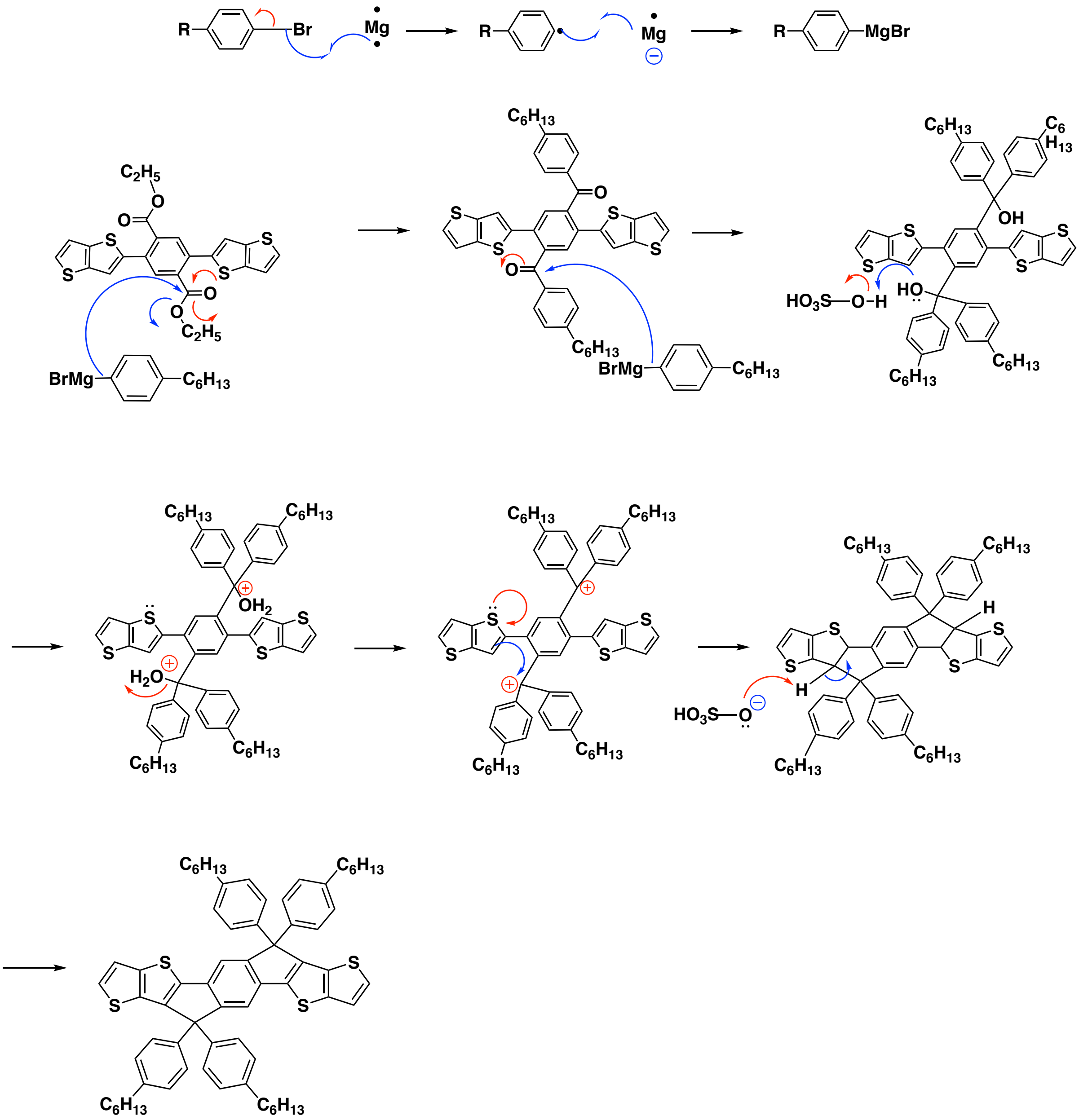

Scheme 2.3: The proposed mechanism of synthesis **IDTT.**

The first step was to prepare the Grignard reagent, starting with the two electrons of the covalent bond between bromine and phenyl group breaking to form two radicals of phenyl and bromine. Then the bromine radical is attacked by an electron from Mg, resulting in the formation of the radical magnesium bromide. The next step of forming a Grignard reagent was to couple the phenyl radical with radical Mg. As the nucleophilicity of the Grignard reagent attacks the ester group, tertiary alcohol generated and is then protonated. In the next step, the tertiary alcohol is treated with acid to promote cyclisation. The double bond of the adjacent thiophene ring performs the ring closure reaction. Eventually, the proton positioned on 3-thiophene position substituted to produce the **IDTT** product.

For final step to **IDTT-Br2 (M1)** compound (**6**) was brominated by N-bromosuccinimde (**NBS**) to afford compound **(M1)** with an excellent yield of 93%. The reaction mechanism describes as an electrophilic aromatic substitution as shown in **Scheme 2.4**.

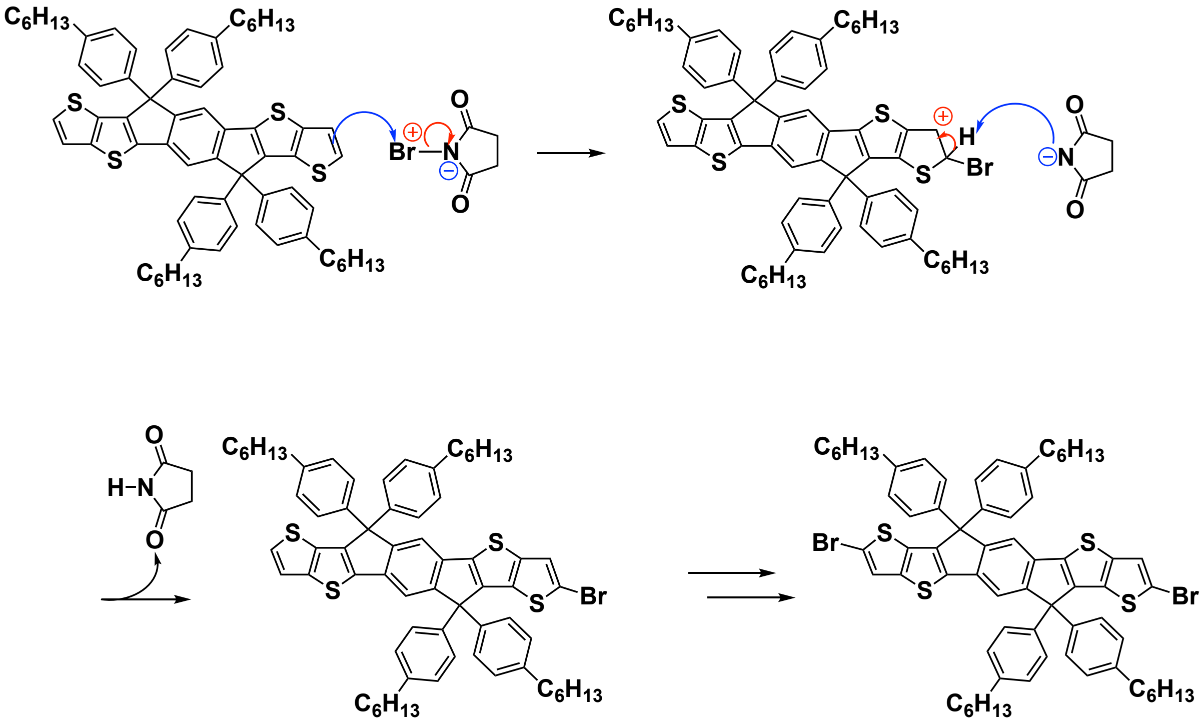

Scheme 2. 4: The proposed mechanism of synthesis **IDTT-Br$_2$ (M1).**

Position 5 of the thiophene ring is more nucleophilic than the other positions due to the influence of the resonance effect. The N-bromosuccinimide (**NBS**) molecule exhibits different electron affinity between the oxygen and nitrogen atoms, which makes the bromine atom partially positive. The mechanism expected to be responsible for this reaction starts with the bromine cation attacking by the thiophene to result in the generation of succinimide anion. The anion is responsible for deprotonation of the thiophene ring, producing the brominated ring. The same steps are repeated to end up with a target product **M1**.

^{1}H and ^{13}C NMR were conducted to identify all materials and prove the reactions had been achieved successfully. The ^{1}H NMR spectrum of **M1** is depicted in **Figure 2.3**. The aromatic region revealed the predicted splitting pattern of two doublets at 7.15 ppm and 7.10 ppm, which are assigned to the sixteen protons of the phenyl ring. The two singlet peaks at 7.50

ppm and 7.29 ppm correspond to the protons on the thiophene and benzene rings. The peaks below 2.55 ppm belong to the hexyl chain.

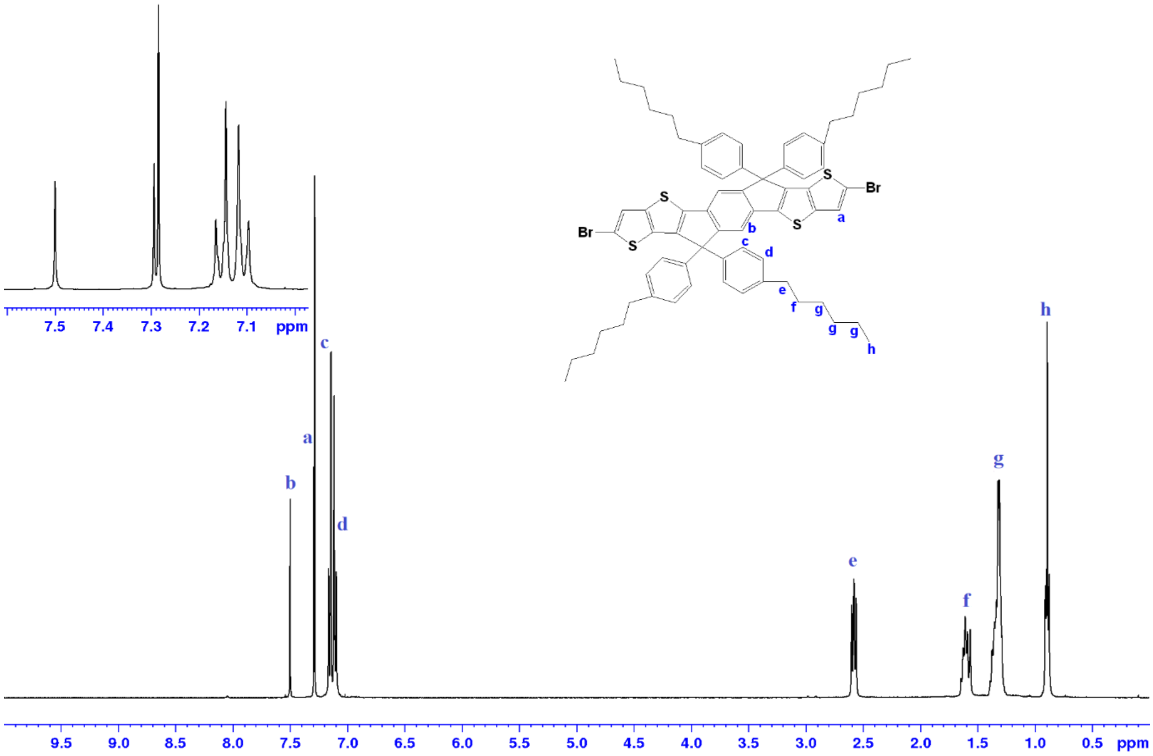

Figure 2. 3: The ^{1}**H** NMR of **IDTT-Br$_2$ (M8)** in $CDCl_3$.

Scheme 2.5 illustrates the synthesis pathway of two different withdrawing groups based on thieno[3,4c]pyrrole-4,6(5H)-dione **(TPD)** including 2-phenyl thiophene-5-(3,7-dimethyloctyl)-4H-thieno[3,4c]pyrrole-4,6(5H)-dione **(TPD-PHT) (M2)** and 5'-(5-(3,7-dimethyloctyl)-4,6-dioxo-5,6-dihydro -4 *H* - thieno [3,4-*c*] pyrrol-1-yl)-[2,2'-bithiophene]-5-carbaldehyde **(TPD-CHO) (M3)**.

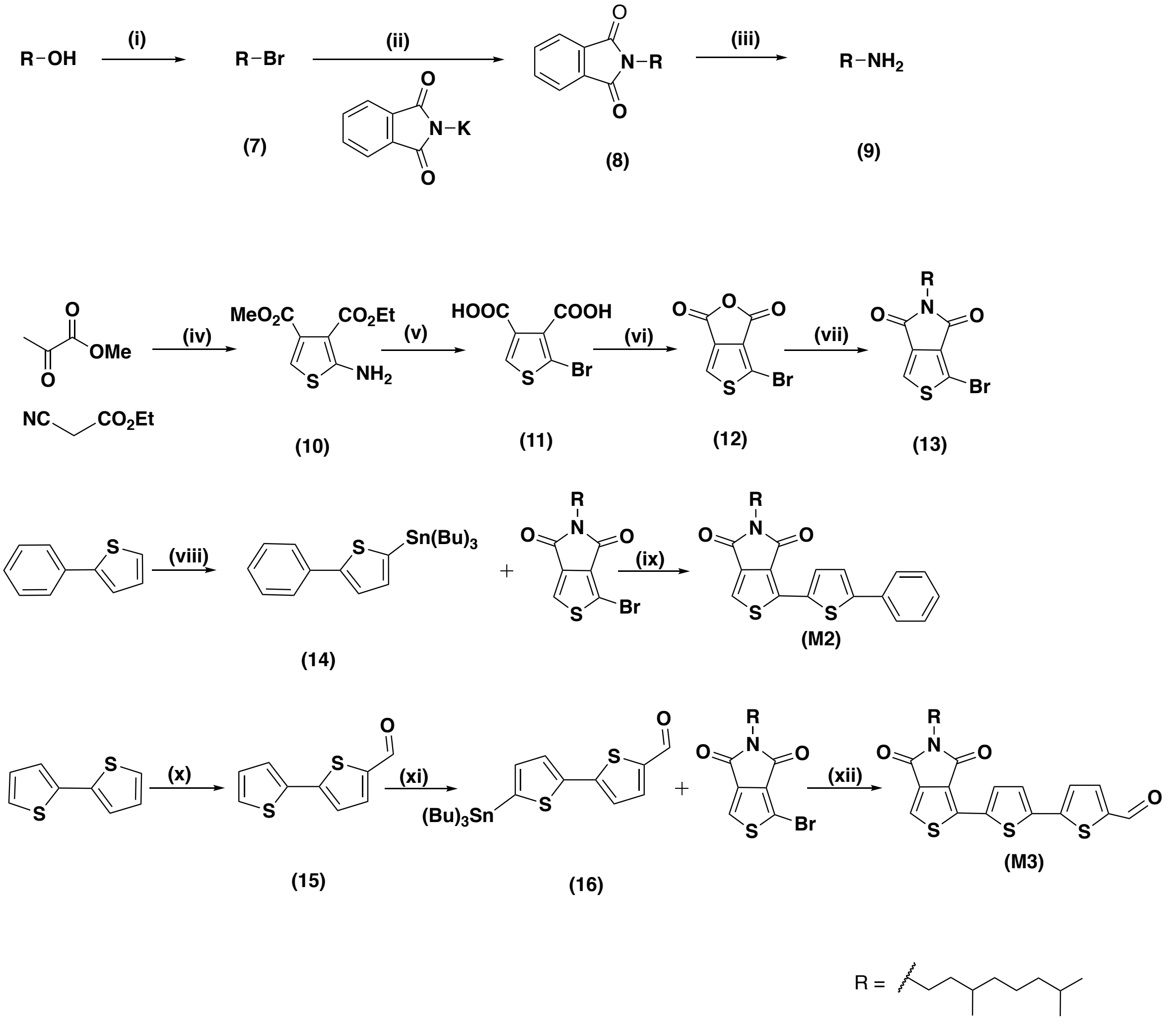

Scheme 2. 5: The synthetic steps of **M2** and **M3.**

Reagents and Reaction condition: (i) PPh_3, NBS, DCM (ii) DMF, 90 ^oC, 16 h (iii) N_2H_4, EtOH, 3 h, HCl (iv) Et_3N, S, DMF, 50^oC, overnight (v) Cu(I)Br, $NaNO_2$, 20%HBr, 2M NaOH (vi) Ac_2O, 110^oC, 2h (vii) $SOCl_2$, THF (viii) n-BuLi, $C_5H_{12}N_2$, $(Bu)_3SnCl$, -78^oC (ix) $Pd(PPh_3)_4$, toluene, 110^oC (x) n-BuLi, DMF, THF, -78^oC; (xi) n-BuLi, $(Bu)_3SnCl$, -78 ^oC (xii) $Pd(PPh_3)_4$, toluene, 110^oC.

The preparation of 3-ethyl-4-methyl-2- aminothiophene-3,4-dicarboxylate **(10)** was obtained according to the Gewald reaction, [176] which is a condensation of methyl-2-oxopropanoate (ketone) with ethyl cyanoacetate (α- cyanoester) in the presence of triethylamine and element sulphur. **Scheme 2.6** demonstrates the mechanism of this reaction.

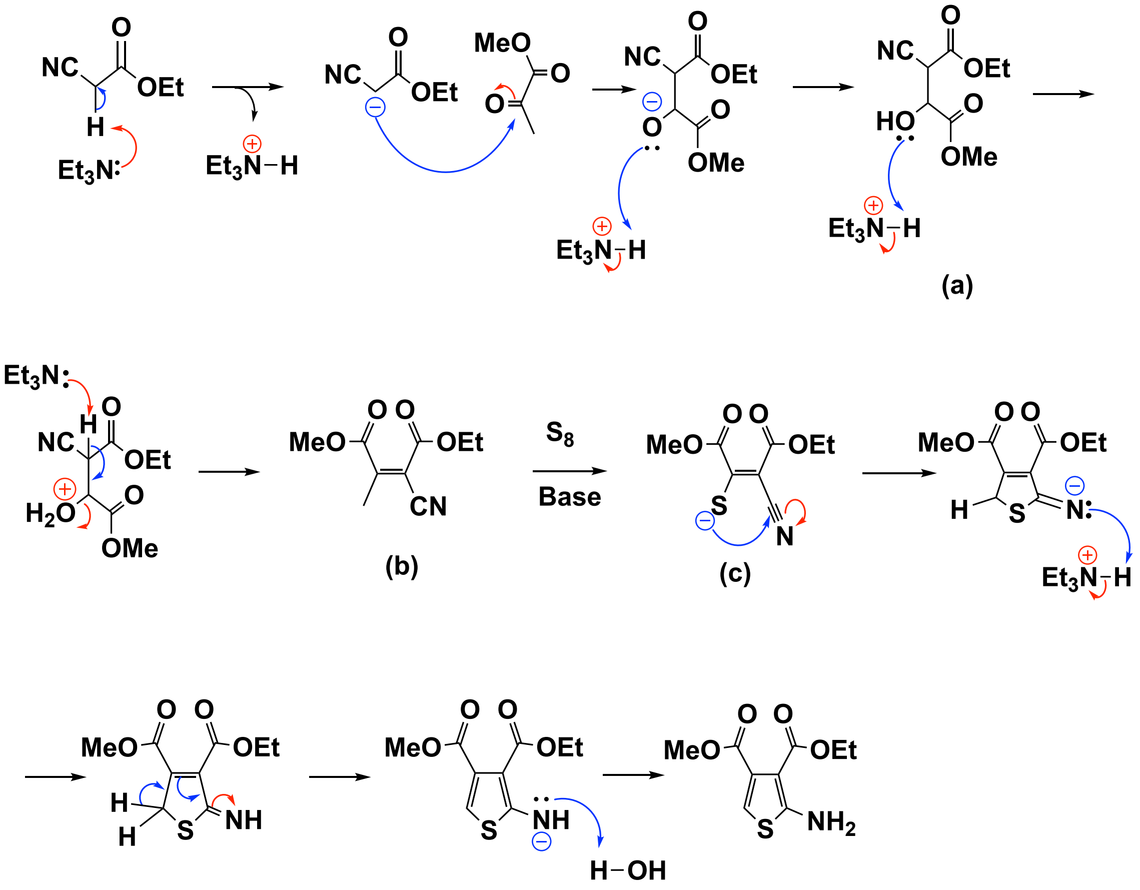

Scheme 2. 6: The suggested mechanism for the synthesis **of 10.**

Synthesis starts with condensation reaction between α-activated methylene nitrile and a ketone in basic condition, leading to the elimination of water, to give the intermediate **(b)**. The pathway of the next step is not clearly understood, but it is anticipated that the elemental sulphur element added in the presence of a base, renders an ylidene-sulphur adduct as the intermediate **(c)**, which is cyclised then undergoes tautomerisation to create the product. [177]

The functionalised aminothiophene was then transformed into bromothiophene *via* Sandmeyer reaction, which was followed by the hydrolysis of the ester group to provide 2-bromothiophene-3,4-dicarboxylic acid **(11)**. **Scheme 2.7** depicts the expected mechanism of the Sandmeyer reaction. This reaction is an effective synthetic approach to convert an amino group on an aryl group into various functional groups; and it is an example of radical nucleophilic aromatic substitution (SAr). The mechanism of this reaction commences with the in situ formation of nitrous acid from sodium nitrite acid, followed by a loss of water to produce nitrosonium salt, which acts as an electrophile, interacting with aminothiophene to generate the diazonium salt. The transformation of diazonium salt into bromothiophene starts from the transfer of a single electron from Cu(I)Br catalyst to form thiophene radical, Cu^{+2} with releasing N_2 gas. Then the thiophene radical reacts with the $Cu(II)Br_2$ to obtain the aryl halide product and the Cu(I)Br catalyst.

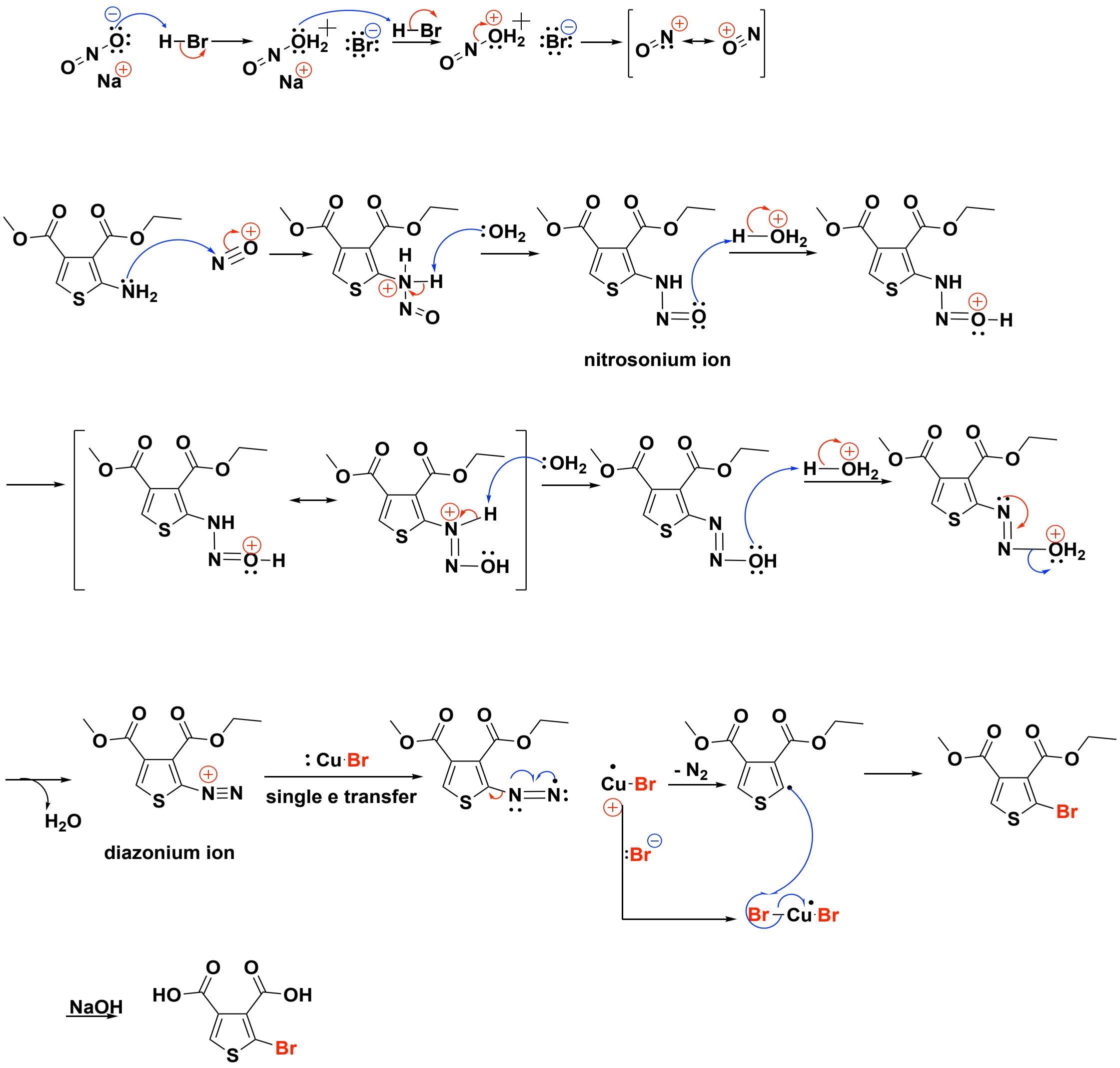

Scheme 2. 7: The proposed mechanism of the Sandmeyer reaction.

To synthesise 4-bromothieno[3,4-c]furan-1,3-dione, compound **(11)** was heated in acetic anhydride, which was utilised as a dehydration reagent to form the cyclic anhydride, **(12).** The next step of preparing the **TPD** monomer involved a reaction between cyclic anhydride and 3,7 dimethyloctylamine, followed by a reaction with thionyl chloride to afford 2-bromo-5-(3,7-dimethyloctyl)-4H-thieno[3,4c]pyrrole-4,6(5H)-dione, **(13).** The reaction mechanism is represented in **Scheme 2.8**.

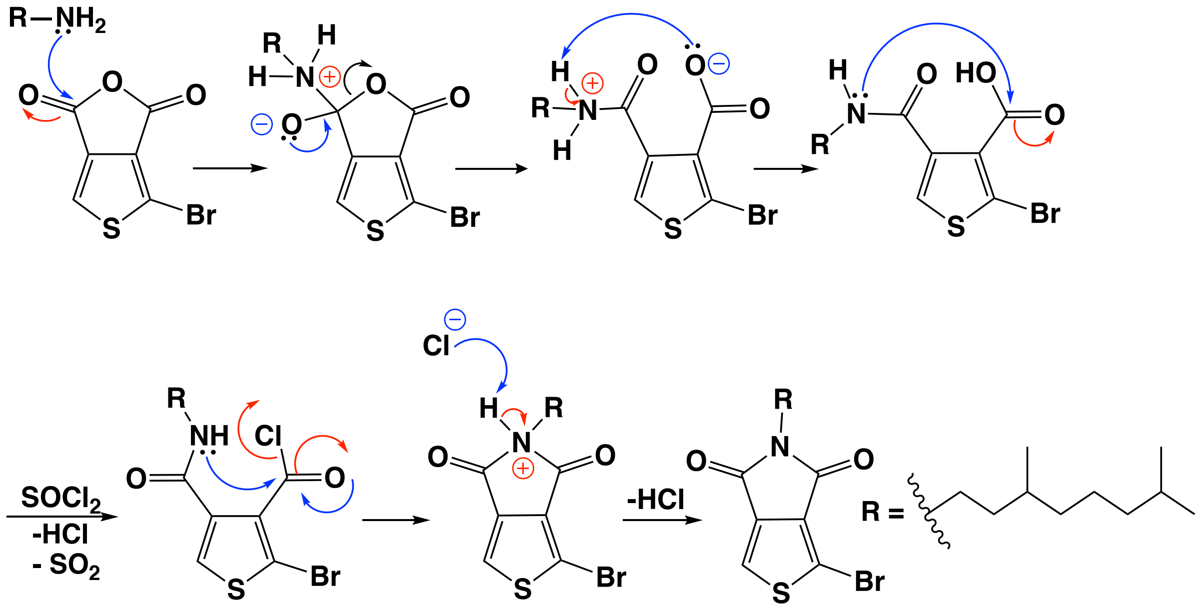

Scheme 2. 8: The mechanism of synthesis **13.**

Incorporating an alkyl chain into the molecule would improve the solubility of the monomer produced. In addition, this action leads to the formation of an electron accepting imide group, which is a prerequisite for the monomer's electron withdrawing properties. Then, 2-phenylthiophene was lithiated and quenched with $(Bu)_3SnCl$ to furnish monostannylated compound **(14)**. Then in the presence toluene as solvent and $Pd(PPh_3)_4$ as the catalyst, **(14)** was reacted with compound **(13)** to obtain the **(M2)** with a yield of 73%.

The synthetic route toward the **M3** monomer is described in S**cheme 2.4**. It starts with the commercially available 2,2-bithiophene, which was lithated using n-BuLi following by the addition of DMF as an acylating agent. A good yield (87%) of the 2,2-bithiophene-5-carboxaldehyde (15) intermediate was obtained. Then compound **(15)** was lithiated and quenched with trimethyltin chloride and the corresponding mono-stannylated **(16)** was produced, at a yield of 83%. Stille coupling reaction of compound **(13)** with **(16)** was accomplished to arrive at the final monomer, **(M3).** The ^{1}H and ^{13}C NMR identified the chemical structures of the **TPD** monomers.

The ^{1}H NMR spectra of **M2** and **M3** are represented in **Figures 2.4** and **2.5**, respectively. The aromatic region of both monomers showed a singlet peak at 7.61 ppm and 7.67 ppm, which are attributed to the protons on the thiophene ring of **M2** and **M3**, respectively. The **M3** spectrum showed a singlet resonance at 9.90 ppm, which corresponds to the aldehyde group. The spectrum peaks positioned from 3.71 ppm to 0.86 ppm possess to the protons located on the alkyl chains.

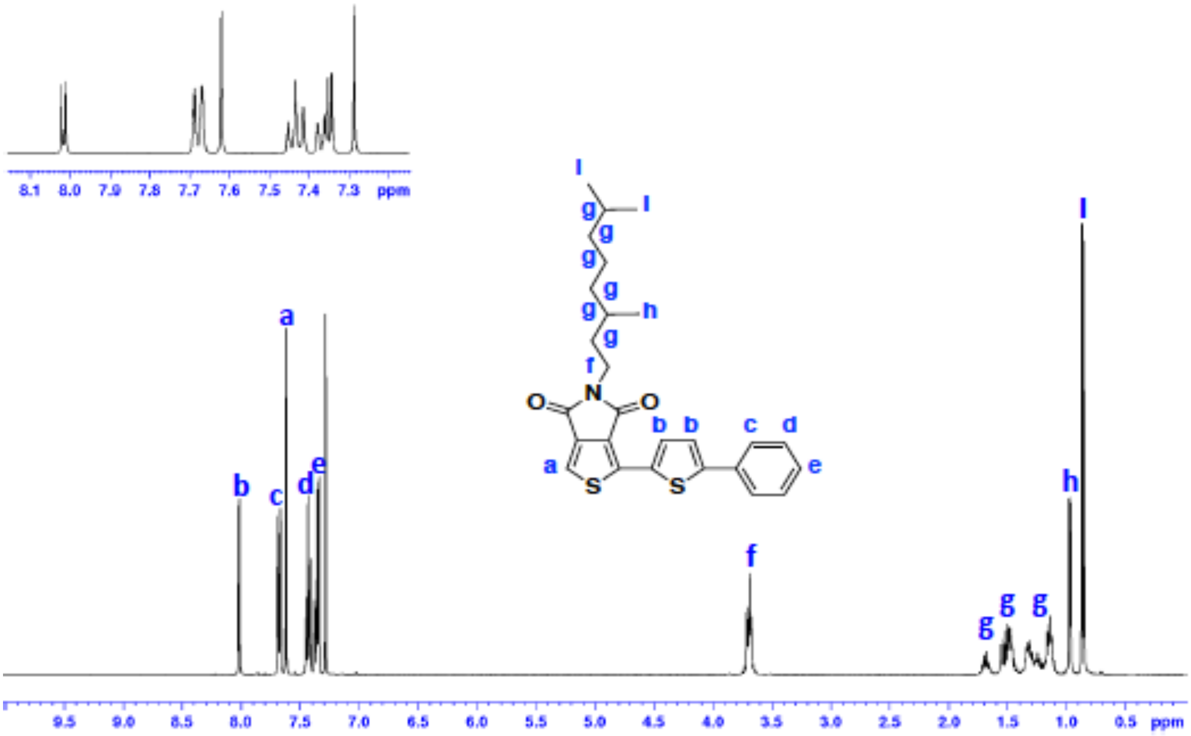

Figure 2. 4: The ^{1}H NMR of **M2 in $CDCl_3$.**

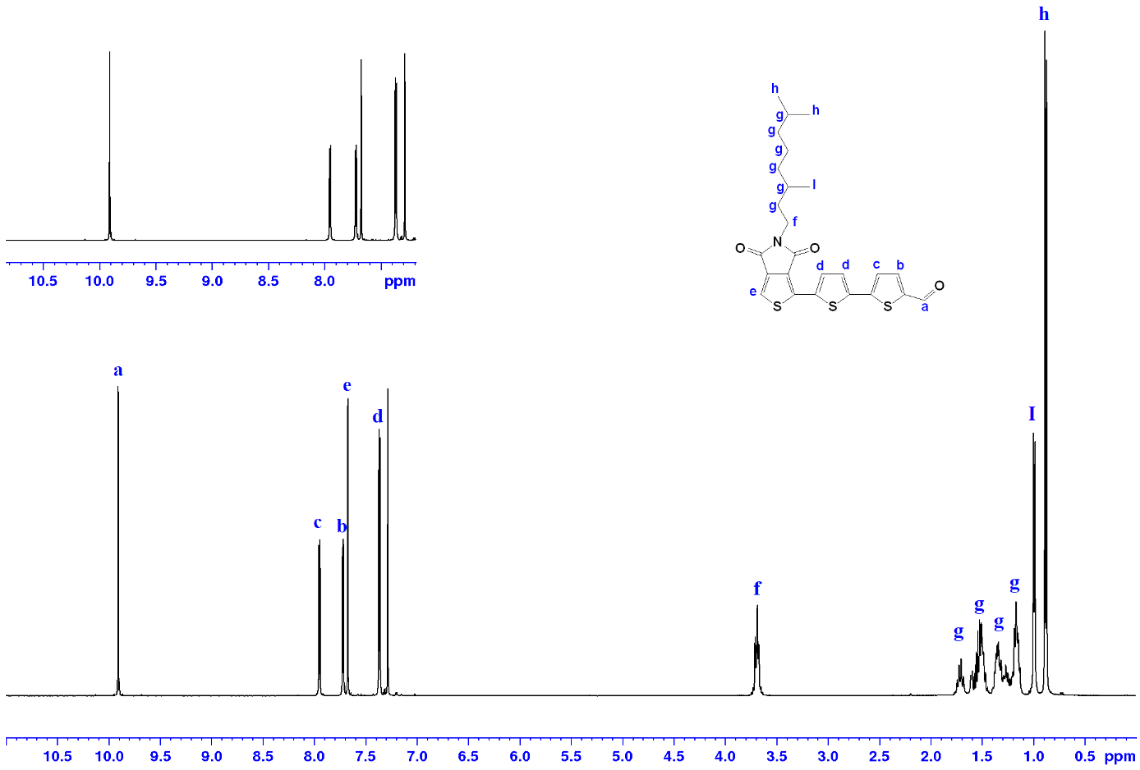

Figure 2. 5: The ^{1}H NMR of **M3 in** $\mathbf{CDCl_3}$**.**

The synthesis approach for the three small molecules is depicted in **Scheme 2.9**. **IDTT-TPD-PHT** was obtained through a conventional direct arylation (**DA**) reaction between **IDTT-Br2** with **TPD-PHT** using Pd$_2$(dba)$_3$ as the catalyst, (o-OMePh)$_3$P as the ligand, pivalic acid (PivOH) and dry THF at 100 ^{o}C and the yield was 52%. In addition, the **DA** reaction was also conducted between **IDTT-Br$_2$** with **TPD-CHO** to obtain the intermediate compound of **IDTT-TPD-CHO.**

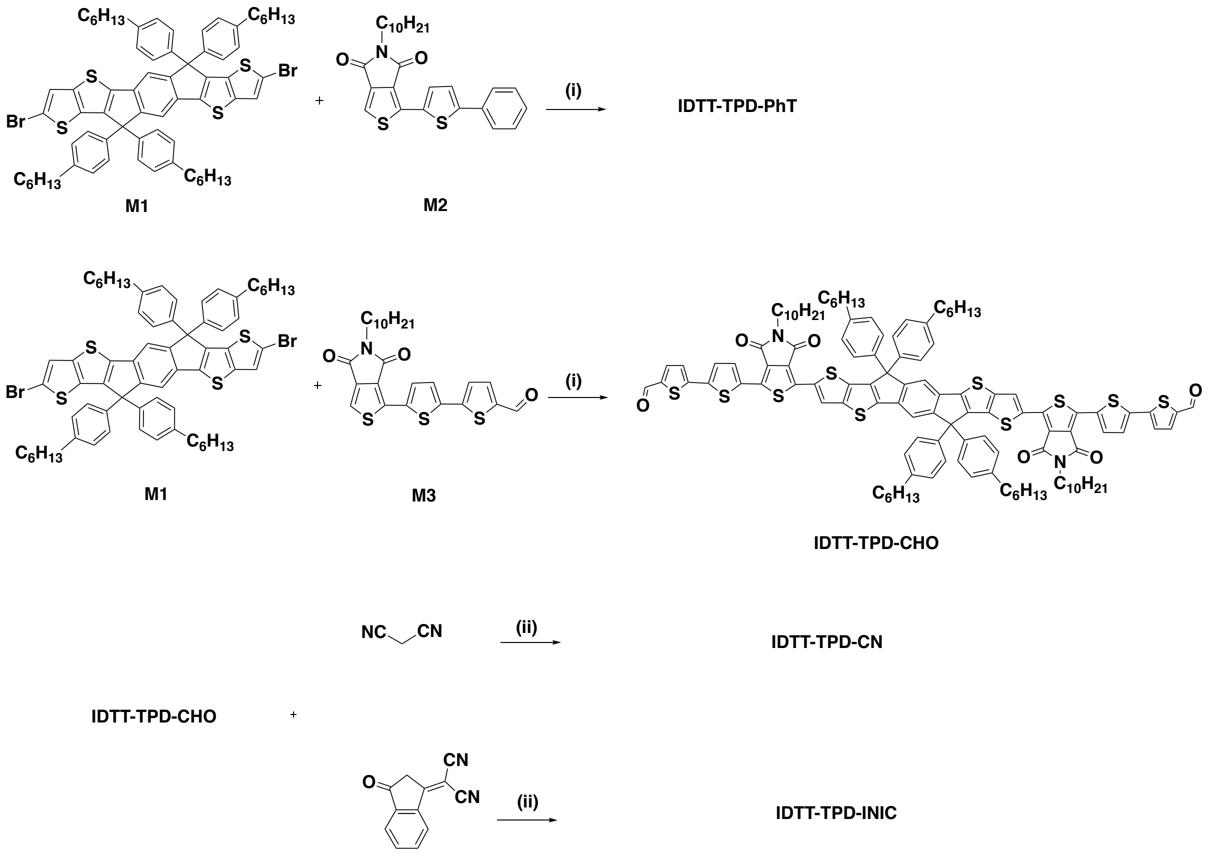

Scheme 2. 9: The synthetic routes of **IDTT-TPD-PHT, IDTT-TPD-CN** and **IDTT-TPD-INIC**

Reagents and condition: (i) Pd$_2$(dba)$_3$, P(o-OMePh)$_3$, CsCO$_3$ PivOH, THF, 100^{o}C (ii) pyridine, CHCl$_3$, refluxed.

IDTT-TPD-CHO was used to synthesise **IDTT-TPD-CN** and **IDTT-TPD-INIC** *via* Knoevenagel condensation reaction with malononitrile and 2-(3-Oxo-2,3-dihydro-1H-inden-1-ylidene) malononitrile. In the presence of pyridine as a base, the respective yields were 47% and 81%. While malononitrile is commercially available, 2-(3-Oxo-2,3-dihydro-1H-inden-1-ylidene) malononitrile (**INIC**) was synthesised as described in the experiment section **Chapter 6**. The proposed mechanism of the Knoevenagel reaction is illustrated in **Scheme 2.10.**

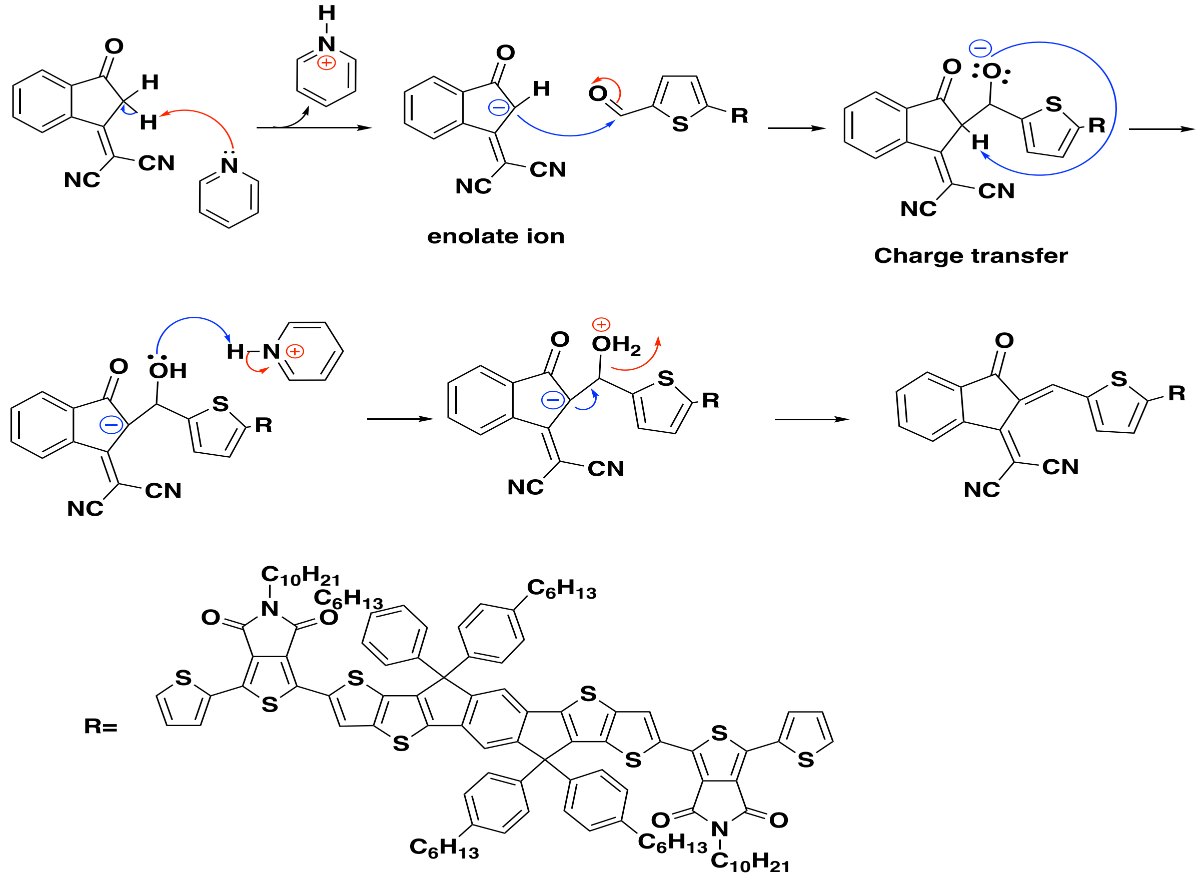

Scheme 2. 10: The mechanism of Knoevenagel reaction.

The reaction mechanism initiates with the deprotonation of activated methylene, using base (pyridine) to produce an enolate ion. Then the aldehyde group is attacked by enolate ion to form an intermediate compound, which is then subjected to proton transfer, terminating with alcohol. In the next step, this intermediate is protonated and rearranged, concluding with olefin material.

The chemical structures of these non-fullerene acceptors **(NFA)** were identified by ^{1}H NMR, ^{13}C NMR, matrix-assisted laser desorption/ionisation (MALDI-TOF MS), and elemental analysis. The **IDTT-TPD-PHT** was readily soluble in common organic solvents such as dichloromethane and chloroform. **IDTT-TPD-INIC** showed a strong lack of solubility in organic solvents. This may be attributed to the alkyl chain substituent, located on the TPD monomer not being adequate to enhance the processability of these two NFA at higher molecular weight due to the increase of the conjugation backbone. On the other hand, **IDTT-TPD-CN** exhibited better solubility in organic solvents compared to **IDTT-TPD-INIC**. It was anticipated that the **IDTT-TPD-CN** and **IDTT-TPD-INIC** would exhibit a noticeably lower solubility than **IDTT-TPD-PHT** in common organic solvents.

The ^{1}H NMR spectra of two **NFAs** were in agreement with their chemical structure. In addition, the ^{13}C NMR spectrum was consistent with the number of carbon environments of the **IDTT-TPD-PHT**. However, due to low solubility of **IDTT-TPD-CN** in $CDCl_3$**,** ^{13}C NMR limits detection, particularly the signals in the aromatic areas. All NMR spectra for the two **NFAs** can be found in supplementary information, **Chapter 6.**

2.2.2 Optical Properties

The optical properties of materials in OSCs play an essential role in the performance of solar cell devices. Ultraviolet-visible (UV-vis) absorption spectroscopy was used to investigate some important parameters, such as the absorption window of the chemical compounds, the optical band gap, the strength of the absorption. The UV-vis absorption spectroscopy was recorded for the three NFA molecules, including **IDTT-TPD-PHT, IDTT-TPD-CN** and **IDTT-TPD-INIC** in a chloroform solution and as thin film. **Figure 2.6 (a** and **b)** demonstrates the absorption spectrum of the three NFAs in the solution and thin film, respectively. The collected data are summarised in **Table 2.1.** In chloroform solution, these three NFA compounds exhibit a strong absorption from approximately ~320 to 800 nm. This may be ascribed to the intramolecular charge transfer (ICT) [178] from the donor unit to acceptors' arms, where the maximum absorption for **IDTT-TPD-PHT** and **IDTT-TPD-CN** molecules is almost similar ~550 nm; however, the maximum absorption of **IDTT-TPD-INIC** is lower by about ~20 nm. Relative to their solution, the absorption band in the solid state of these acceptors displays a red shifted by 17, 21 and 40 nm. This is presumably attributable to the self-organisation, which leads to the formation of π-π stacking interactions in the film. This could be helpful for charge transportation through the backbone of the molecules.

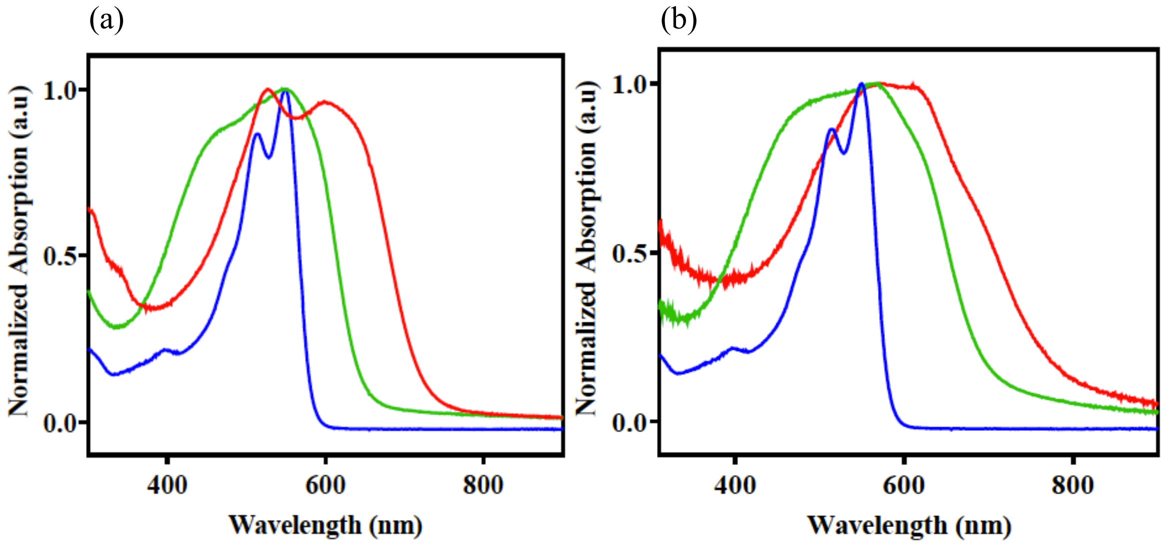

Figure 2. 6: The normalised UV-vis absorption spectra of **IDTT-TPD-PHT**, **IDTT-TPD-CN and IDTT-TPD-INIC** in a) chloroform solution; and b) thin-film**.**

The maximum coefficient absorption for each NFA was calculated and listed in **Table 2.1**. The absorption peaks characteristic of **IDTT-TPD-PHT** reaches 1.3 × 10^5 M^{-1} cm^{-1} at 550 nm, which is the highest value. At 7.6 × 10^4 M^{-1} cm and 9.7 × 10^4 M^{-1} cm, respectively, the absorptivity of **IDTT-TPD-CN** and **IDTT-TPD-INIC** were lower than **IDTT-TPD-PHT.** The approximate calculation of the optical bandgaps for **IDTT-TPD-PHT, IDTT-TPD-CN** and **IDTT-TPD-INIC** were 2.03, 1.75 and 1.55 eV from the absorption edge of the film. The smaller optical band gap of **IDTT-TPD-INIC** by 0.2 eV is suggested to be due to the withdrawing group of **INIC** being stronger compared to malononitrile, which was used as an end capping in **IDTT-TPD-CN.** On the other hand, the larger bandgap of **IDTT-TPD-PHT** resulted from the presence of the electron-rich moiety phenylthiophene, on **the TPD** compound, which was mainly responsible for the increase in the optical bandgap.

Overall, these three NFAs have revealed a broad absorption, which is noticeably stronger than fullerene acceptor, which overlaps with the solar spectrum of the incident light **Figure 1.14.** The maximum coefficient absorption of the three NFAs showed that they have a superior ability to harvest the sunlight compared to the fullerene acceptor ($PC_{60}BM$ 3.9 ×10^3

M^{-1}cm at 400 nm). However, The maximum coefficient absorption for **ITIC** and **IT-4F** are higher than the three NFAs, with 1.90×10^5 M^{-1} cm at 700 nm and 2.10×10^5 M^{-1} cm at 717 nm, respectively. Moreover, the optical bandgap of **IDTT-TPD-INIC** is larger than that of **IT-4F** (1.46 eV) but slightly smaller than that of **ITIC** (1.59 eV). It is suggested that **IT-4F** possesses more acceptor characteristics compared to **IDTT-TPD-INIC**.

Table 2. 1: The optical properties of **IDTT-TPD-PHT, IDTT-TPD-CN and IDTT-TPD-INIC** and their band gap.

Acceptor	λ_{max} Solution (nm)	λ_{max} Film (nm)	Onset (nm)	Eg^{opt} (eV)	Coefficient absorption M^{-1} cm^{-1}
IDTT-TPD-TPH	550	567	610	2.03±0.0067	1.3 × 10^5
IDTT-TPD-CN	547	568	708	1.75±0.0049	7.6 × 10^4
IDTT-TPD-INIC	527	567	800	1.55±0.0038	9.7 × 10^4

2.2.3 Electrochemical properties

Cyclic voltammetry (CV) was used to investigate the electrochemical properties of the synthesised acceptors molecules and to locate the highest occupied molecular orbital (HOMO) and lowest unoccupied molecular orbital (LUMO) energy levels. A thin film of **IDTT-TPD-PHT, IDTT-TPD-CN and IDTT-TPD-INIC** was cast on a platinum electrode and cycled in CH_3CN, containing tetrabutylammonium perchlorate as the supporting electrolyte; the potential scan rate was 100 mV^{-1}.

Figure 2.7 depicts the electrochemical curves for the three NFAs and **Table (2.1)** summarises the collected data of the onset oxidation potential, onset reduction potential, HOMO, LUMO energy levels and electrochemical bandgap values. The oxidation potential is modestly influenced; oxidation wave onsets were recorded as 0.64 V, 0.51 V and 0.57 V for **IDTT-TPD-PHT, IDTT-TPD-CN and IDTT-TPD-INIC;** these values indicate that the HOMO energy levels were at -5.36 eV, -5.30 eV and -5.26 eV, respectively. Compared with **IDTT-TPD-CN IDTT-TPD-INIC,** the higher HOMO level of **IDTT-TPD-PHT** may be ascribed to the presence of electron rich molecule linked to the **TPD** and less conjugation in **IDTT-TPD-PHT**. Furthermore, the replacement of electron rich **PHT** units in **IDTT-TPD-PHT** by electron deficient moieties, such as malononitrile and 2-(3-oxo-2,3-dihydro-1H-inden-1-ylidene) malononitrile (**INIC**) and arm units in **IDTT-TPD-CN** and **IDTT-TPD-INIC** has a significant impact on the reduction potential, resulting in a low laying of LUMO energy level compared to the LUMO of **IDTT-TPD-PHT.** The onset reduction potential of **IDTT-TPD-PHT, IDTT-TPD-CN and IDTT-TPD-INIC** were observed at -1.49 V, -1.08 V, and -0.82 V, which corresponded to the LUMO energy level at -3.22 eV, - 3.64 eV and -3.89 eV, respectively. The deeper LUMO of **IDTT-TPD-INIC,** as compared to the LUMO of **IDTT-TPD-PHT** and **IDTT-TPD-CN** is expected due to the stronger withdrawing property of **INIC**, which leads to the downshift of LUMO below other end capping. However, the LUMO level of **IDTT-TPD-CN** located at shallower energy level (-3.64 eV) relative to LUMO of **IDTT-TPD-INIC** (-3.89 eV), is due to the weaker withdrawing ability of malononitrile compared to **INIC.** The electrochemical band gaps of **IDTT-TPD-PHT, IDTT-TPD-CN and IDTT-TPD-INIC** were estimated to be 2.14 eV, 1.84 eV and 1.37 eV, respectively.

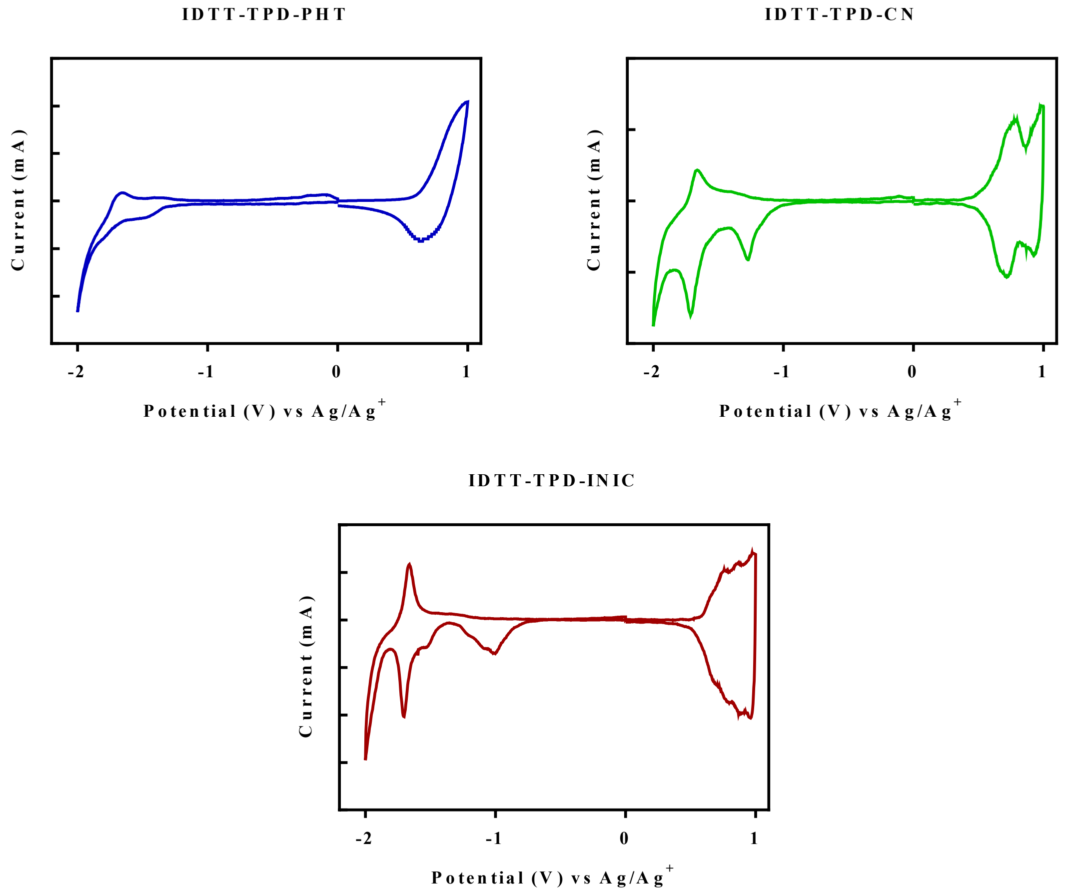

Figure 2. 7: Cyclic voltammograms of **IDTT-TPD-PHT**, **IDTT-TPD-CN** **and** **IDTT-TPD-INIC** on Pt electrode in Bu_4NClO_4/CH_3CN at 100 mV/s.

Table 2. 2: The collected data of the onset oxidation potential, onset reduction potential, HOMO, LUMO energy levels and electrochemical band gap values.

Acceptor	**$E^{(onset-OX)}$ (volts)**	**$E^{(onset-red)}$ (volts)**	**HOMO (eV)**	**LUMO (eV)**	**Eg^{elect} (eV)**
IDTT-TPD-PHT	0.64	-1.49	-5.36±0.007	-3.22±0.009	2.14±0.017
IDTT-TPD-CN	0.59	-1.08	-5.30±0.005	-3.64±0.004	1.84±0.021
IDTT-TPD-INIC	0.54	-0.82	-5.26±0.009	-3.89±0.007	1.37±0.030

All three acceptors demonstrated lower HOMO energy level than the fullerene acceptor, $PC_{60}BM$ that has a low lying energy level of -6.1 eV. This might be attributed to the higher degree of conjugation system of the spherical of fullerene acceptors. Due to more electron withdrawing units incorporated into this NFA, the LUMO energy level of $PC_{60}BM$ was at (-3.7 eV), which is lower compared to **IDTT-TPD-PHT** and **IDTT-TPD-CN,** but higher than **IDTT-TPD-INIC**. In comparison to other published NFAs, the HOMO energy level of the **ITIC** and **IT-4F** were determined to be at -5.50 eV and -5.66 eV, respectively, which is deeper than all three NFAs. The LUMO energy level of **IDTT-TPD-PHT** and **IDTT-TPD-CN** is smaller than **ITIC** (-3.89 eV) and **IT-4F** (-4.14 eV). On the other hand, **IDTT-TPD-INIC** has a similar LUMO energy level to **ITIC**, which is larger than **IT-4F**.

2.2.4 Thermal Properties

To investigate the thermal properties of the three NFAs materials synthesised, thermogravimetric analysis (TGA) measurements were conducted under an inert atmosphere using a heating rate of 10 ^{o}C/min. **Figure 2.8** demonstrates the representative TGA thermo diagrams of these materials, and their data are summarised in **Table 2.2**. These compounds exhibited high thermal stability, with decomposition temperatures (T_d) being between 347°C and 404°C. Also, the melting points of these three NFAs were not observed over 380°C, which indicates the excellent thermal stability of these compounds. Differential scanning calorimetry (DSC) thermal analysis exhibited no evidence of melting or crystalline peaks on the DSC traces. This may be indicated that the melting point temperatures of three NFAs are higher than their decomposition temperatures.

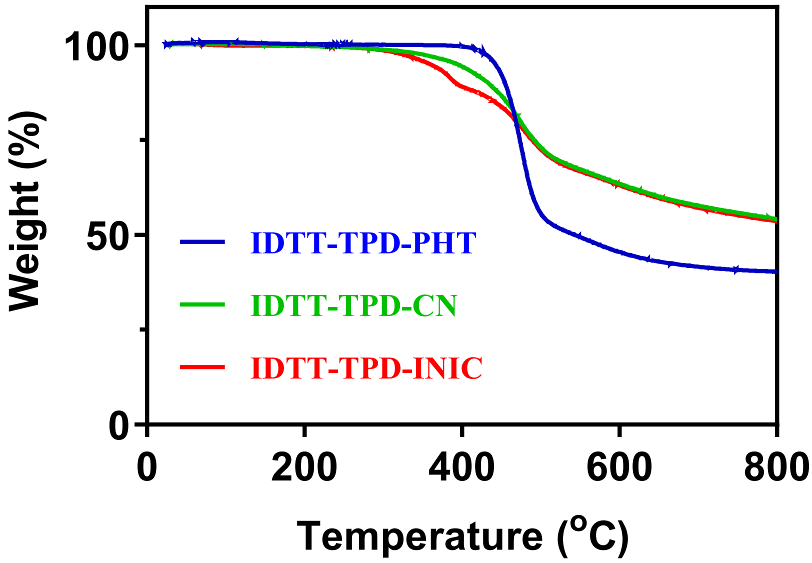

Figure 2. 8: The TGA curves of **IDTT-TPD-PHT**, **IDTT-TPD-CN** and **IDTT-TPD-INIC**.

Table 2. 3: The thermal data of **IDTT-TPD-PHT, IDTT-TPD-CN and IDTT-TPD-INIC**.

Acceptors	Td (°C)
IDTT-TPD-PHT	410
IDTT-TPD-CN	404
IDTT-TPD-INIC	347

T_d: decomposition temperature,

2.2.5 Photovoltaic Properties

The photovoltaic properties of the three NFAs were studied. BHJ devices were fabricated to have a conventional architecture of glass/indium tin oxide (ITO)/ poly(3,4-ethylenedioxythiophene) (PEDOT): polystyrene sulfonate (PSS)/ active layer/BCP/Ag to assess the photovoltaic performance of PBDB-T-NFAs. In addition, for all acceptors attempted and inverted stack (ITO/ZnO/Active Layer/MoO_3/Ag) have been tried to make BHJ devices with a donor of P3HT. Unfortunately, devices using either of these structures have demonstrated very low efficiency. Poor efficiencies may be due to the formation of large grains and non-optimal energy offset. However, PSCs based on **IDTT-TPD-PHT** as a donor with a PNDI(2OD)2T acceptor blends were also prepared using the same conditions and device configuration. The detailed device performance data are summarized in **Tables 2.3** and **Figure 2.9** showed the current density versus voltage (J–V) curves. The highest efficiency achieved was 0.83% PCE with a high short-circuit current density (J_{SC}) of 5.03 mA cm^{-2}, open-circuit voltage (V_{OC}) of 0.32 V and 49.15 fill factor (FF) using **IDTT-TPD-PHT** as a donor with a PNDI(2OD)2T acceptor.

Table 2. 4: Photovoltaic performance of PSCs of **IDTT-TPD-PHT.**

	PCE%	**Jsc(mA/cm2)**	**FF%**	**Voc(V)**
Standard deviation	0.48 ± 0.24	4.19 ± 0.78	40.17 ± 8.24	0.26 ± 0.05
IDTT-TPD-PH	0.80	5.03	49.15	0.32

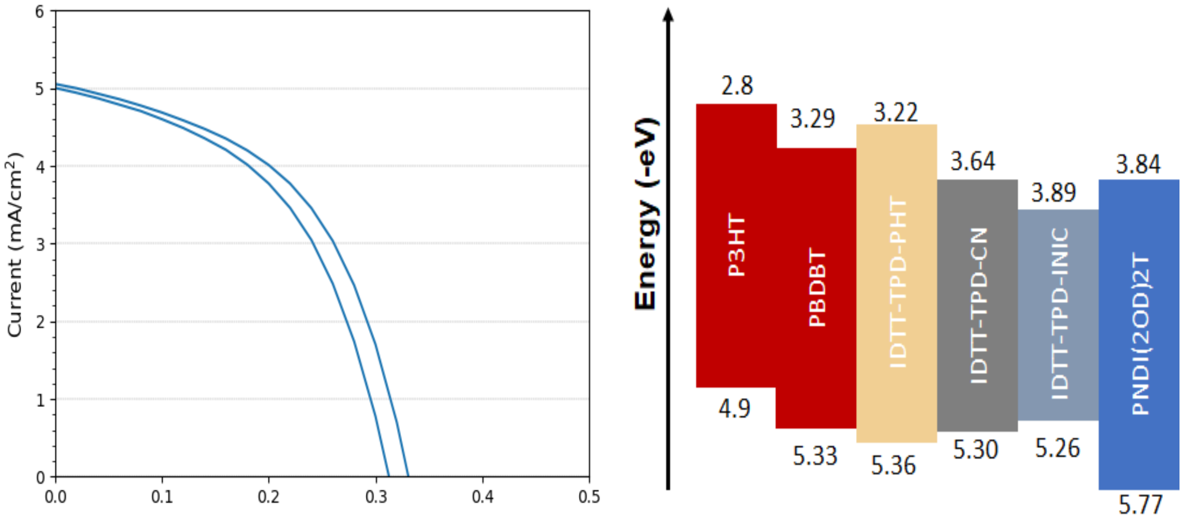

Figure 2. 9: The J-V characteristic curves of **IDTT-TPD-PHT** device**.**

2.3 Conclusion

In summary, we designed and prepared three novel NFAs, **IDTT-TPD-PHT, IDTT-TPD-CN** and **IDTT-TPD-INIC.** In these three NFA acceptors, the **IDTT** fused ring was used as the electron donor to three different of **TPD** moieties with phenylthiophene, malononitrile, and 2-(3-oxo-2,3-dihydro-1H-inden-1-ylidene)malononitrile respectively. Flanking the **IDTT** with various electron withdrawing groups can help to ascertain the influence of these acceptors. Moreover, this would serve to understand the consequences of incorporating these **TPD** deficient electrons units into optical, electrochemical and thermal properties of the resulting NFAs. The **IDTT-TPD-INIC** suffered a lack of solubility, which may be due to having insufficient solubilising substituents on the **TPD** monomer moieties. **IDTT-TPD-PHT, IDTT-TPD-CN** and **IDTT-TPD-INIC** exhibit strong absorption, ranging from around 350 nm to 750 nm with a molar extinction coefficient of $1.3 \times 10^5 M^{-1}$ cm^{-1}, $7.6 \times 10^4 M^{-1}$ cm^{-1} and $9.7 \times 10^4 M^{-1}$ cm^{-1} respectively. Furthermore, the **IDTT-TPD-PHT** showed the highest optical band gap of 2.03 eV. However, **IDTT-TPD-CN** and **IDTT-TPD-INIC** displayed lower optical band gaps of 1.75 eV and 1.55 eV respectively. The electrochemical properties of the three NFAs were investigated; it was demonstrated that the HOMO level of **IDTT-TPD-PH** (-5.36 eV) is higher than acceptors **IDTT-TPD-CN** (-5.30 eV) and **IDTT-TPD-INIC** (-5.26 eV). However, the LUMO level **IDTT-TPD-INIC** is -3.89 eV, which is significantly lower than **IDTT-TPD-CN** and **IDTT-TPD-PH** with **a** LUMO level of -3.64 eV and -3.22 eV, respectively. Employing electron withdrawing units such as malononitrile and **INIC** could possibly downshift the LUMO level, but phenylthiophene is a donating group that mainly affects the HOMO, resulting in the larger HOMO level. The LUMO level of **IDTT-TPD-INIC** is lower than the LUMO level of **IDTT-TPD-CN,** suggesting the withdrawing unit of **INIC** is stronger compared to malononitrile, leading to a downshift of the LUMO level. These NFAs exhibited high thermal stability with onset decomposition temperatures (Td) around 347°C. The solar cell devices of three NFAs have shown a very low PCE. However, the photovoltaic performance device based on **IDTT-TPD-PHT** as donor showed a PCE around 1%. In addition, the investigation is still in progress to improve solar cell performance.

Chapter (III)

Preparation of non-fullerene acceptors based on indacenodithiophene and diketopyrrolopyrrole for solution processed organic solar cells

Abstract

This chapter reports on the preparation of a series of four electron acceptors based on **IDTT** as the electron-rich unit flanked by the electron withdrawing derivatives of diketopyrrolopyrrole (**DPP**) such as (**DPP-PH**), (**DPP-PHT**), (**DPP-CN**) and (**DPP-INIC**). The effect of replacing the **TPD** electron withdrawing units with **DPP** on the optical, electrochemical thermal and photovoltaic properties of these small molecules has been studied. **IDTT-DPP-PH,** **IDTT-DPP-PHT,** **IDTT-DPP-CN** and **IDTT-DPP INIC** were synthesised *via* the Stille coupling reaction and Knoevenagel condensation; they are soluble in common organic solvents. The significantly enhanced solubility was expected due to the increase in the number the solubilising groups on the imide units of **DPP**. The UV-Vis spectroscopy for these small molecules revealed a red-shifted absorption from nearly 500 nm to 900 nm with low optical band gap of 1.43 eV, 1.42 eV, 1.42 eV and 1.28 eV. The molar absorption coefficients were 1.54×10^5 M^{-1} cm^{-1} at 658 nm, 1.59×10^5 M^{-1} cm^{-1} at 665 nm 1.41×10^5 M^{-1} cm^{-1} at 709 nm and 1.31×10^5 M^{-1} cm^{-1} at 723 nm respectively. The incorporation of **DPP** moieties does not only affect the optical properties, but also deepens the energy levels of the HOMO (-5.26, -5.15, -5.26, -5.11eV) and LUMO (-3.32, -3.34, -3.57, -3.93 eV) levels. All compounds exhibited good thermal stability, with a T_d above 380°C.

3.1 Introduction

Organic solar cells with BHJ architectures have gained considerable attention over the past decade due to their lightweight, ease of synthesis, low cost, and excellent processability.[179-186] Recently, the BHJ structure achieved power conversion PCE of 14%.[187] The fullerene materials including phenyl-C_{71}-butyric acid methyl ester ($PC_{71}BM$) and phenyl-C_{61}-butyric acid methyl ester ($PC_{61}BM$) are commonly applied as acceptors in solar cell devices. However, fullerene derivatives have some disadvantages, including, weak absorption, high cost and poor tunability, which leads to restricted OSC performance.[188,189] Therefore, tremendous efforts have been directed to design NFA materials, which have superior properties over fullerene materials.[190-193]

The design of NFAs presents a number of advantages over fullerene derivatives, such as ease of purification and good control of reproducibility.[191,193-195] In recent years, the development of NFAs based on acceptor – donor-acceptor structure is one of the most common designs and has been found to lead to the highest performing acceptor compounds. Recently, compounds with fused-ring ladder structure, such as **IDT** and **IDTT**, have generally used as core donors to manufacture acceptor materials due to their excellent charge transfer, well-matched levels of energy to donor moieties and broad absorption.[196-201] Upon flanking the **IDTT,** with high electron affinity compounds, such as 2-(3- oxo-2,3-dihydroinden-1-ylidene)malononitrile (**INIC**) as end capping moieties, an excellent NFA named **ITIC** was prepared. BHJ devices using **ITIC** as acceptor exhibited similar or superior performances when compared to those of fullerene derivatives.[202-206]

The innovative design and synthetic approaches have evolved to promote the characteristics of **IDTT**-based NFAs, including the horizontal extension of the conjugation of **IDTT**,[207-209] the engineering of the alkyl chain on the **IDTT** unit[210-213] and flanking the **IDTT** unit with various electron deficient molecules.[214-216] Among these approaches, the nature of the end-capping moieties is the most convenient means of controlling the optical properties and energy levels of NFAs, so as to be comparable with donor polymers, resulting in better performance of OSCs.

The electron-deficient molecule, such as **INIC** has been used widely for end capping. For instance, **ITIC** was reported as having the **IDTT** as core and flanked with the **INIC** unit as an acceptor; when blended with **PBDBT** polymer, the PCE of 11.21%. In addition, four fluorine atoms were attached to the **INIC** withdrawing group to yield **IT-4F**. Therefore, the energy levels were downshifted, developeding a broad the absorption range, resulting in the OSC having excellent PCE of 13.2%.[215] The electron-withdrawing group of 2-(benzo[c][1,2,5]-thiadiazol-4-yl-methylene)-malononitrile (**BM**) was connected to the **IDTT** fused-ring to produce **IDTT-2BM**, which exhibited a PCF of 4.7%.[217] **Figure 3.1** represents the chemical structure of ITIC, PBDB, IT-4F and IDTT-2BM.

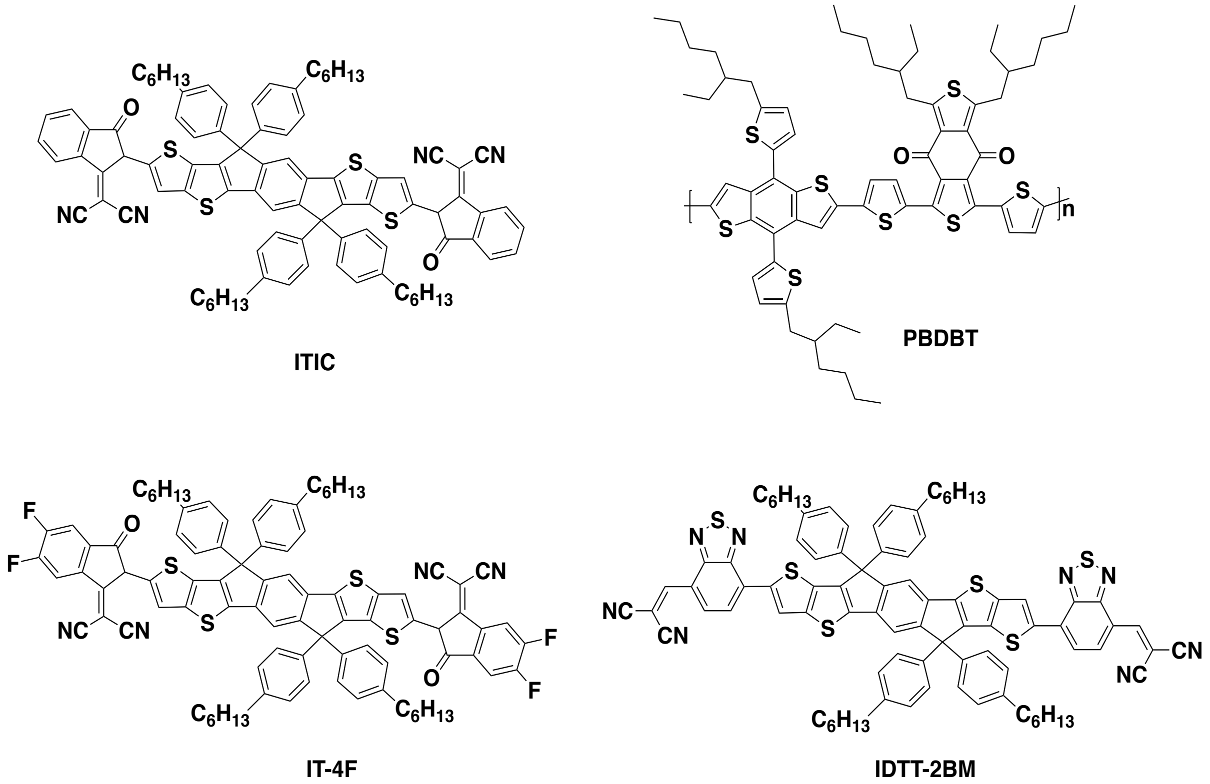

Figure 3. 1: Schematic representations of ITIC, PBDB, IT-4F and IDTT-2BM.

In recent years, **DPP** based small molecules in BHJ have been employed widely for OSCs due to their exceptional optical thermal and mechanical properties. [218-224] In 1974, Farnum et al. reported the first synthesis of pyrrolo [3,4- c] pyrrole-1,4-dione. [225] The planar structure of the **DPP** improves the strong π-π stacking and the presence of the lactam units make **DPP** strong electron withdrawing materials. The incorporation of a solubilising group on the lactam unit of the DPP is achievable to make the **DPP** soluble in most organic solvents and suitable for application in OSC devices.

In this chapter, we designed and prepared four NFAs denoted **IDTT-DPP-PH, IDTT-DPP-PHT**, **IDTT-DPP-CN,** and **IDTT-DPP-INIC** with A-D-A molecular architecture, in which the **IDTT** fused ring is used as electron donating core with four different electron withdrawing groups based on **DPP** moieties as terminal groups **Figure 3.2**. These four molecules extended the planar backbone by incorporating the **DPP** monomers, which deepen the energy levels due to their high electron affinity. Different end capping molecules could not only alter the optical and electrochemical properties of the related NFA materials, but also the solar cell factors such as the short circuit current density (J_{SC}), open-circuit voltage (V_{OC}), fill factor (FF) and thus the PCE.

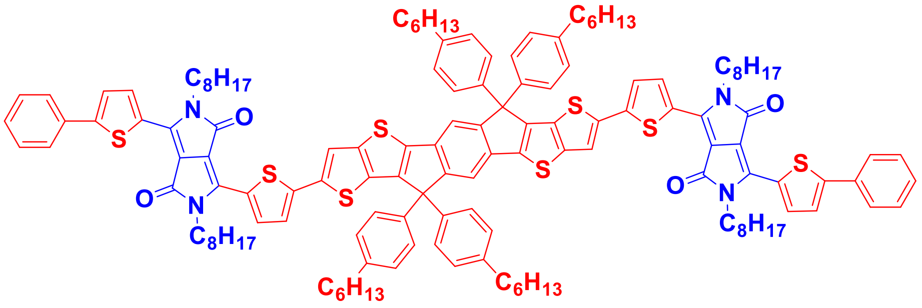

IDTT-DPP-PH

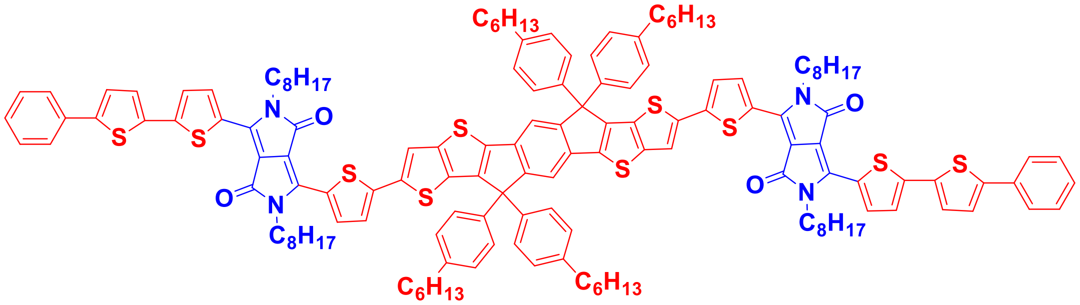

IDTT-DPP-PHT

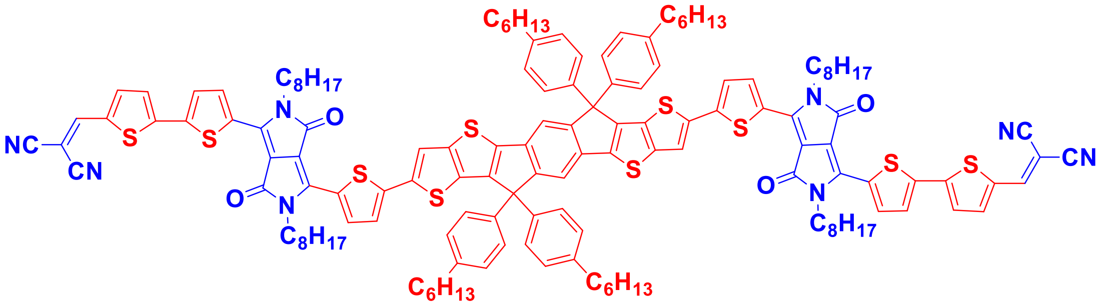

IDTT-DPP-CN

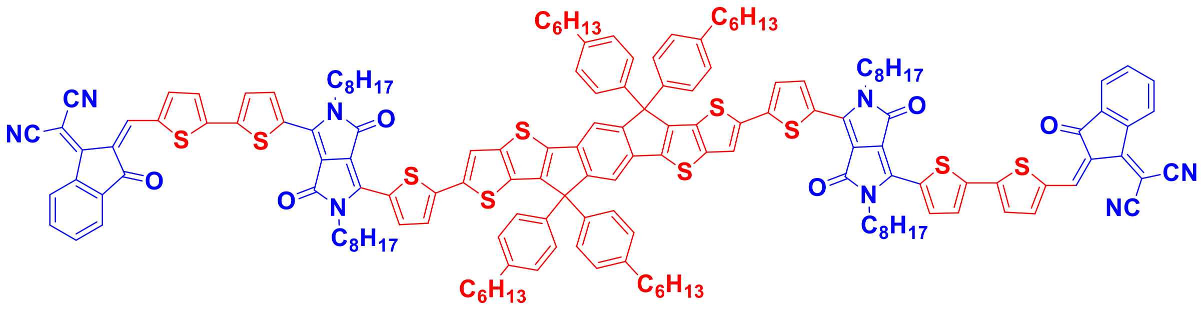

IDTT-DPP-CN

Figure 3. 2: Schematic representations of **IDTT-DPP-PH, IDTT-DPP-PHT, IDTT-DPP-CN** and **IDTT-DPP-INIC** (red: donor unit and blue: acceptor unit)**.**

3.2 Result and discussion

3.3.1 Synthesis of the monomer

The synthetic pathway to **IDTT** was described in the previous **chapter**. The n-BuLi was used to deprotonate the **IDTT,** which was then quenched by trimethyltin chloride (Me_3SnCl) **Scheme 3.1**. The corresponding bis-stannylated monomer **M4** was obtained in a good yield of 91%.

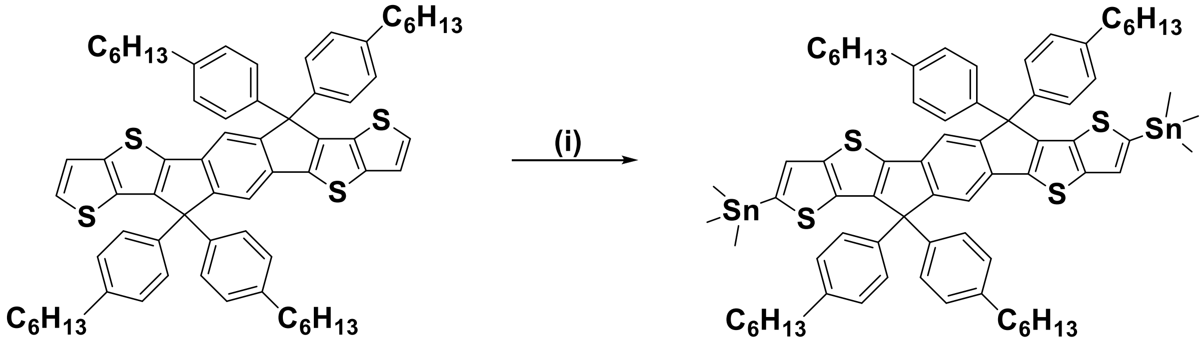

IDTT **(M4)**

Scheme 3. 1: The synthesis of **IDTT-Sn2 (M4)**

Reagents and conditions: n-BuLi, $(CH_3)_3SnCl$, THF, -78°C

^{1}H NMR was conducted to characterise the product and to prove the reaction has been successfully achieved. ^{1}H NMR spectrum of **M4** is shown in **Figure 3.3** and it reveals the expected splitting pattern of two doublet and two singlet peaks in the aromatic area, which indicates the aromatic protons of **M4**. The distinguishing resonance at 0.37 ppm is attributed to the protons on the methyl groups. The two peaks on both sides of this singlet result from ^{119}Sn and ^{117}Sn satellites. The triplet peak at 2.6 ppm is attributed to the α-methylene unit, which is attached directly to the phenyl group.

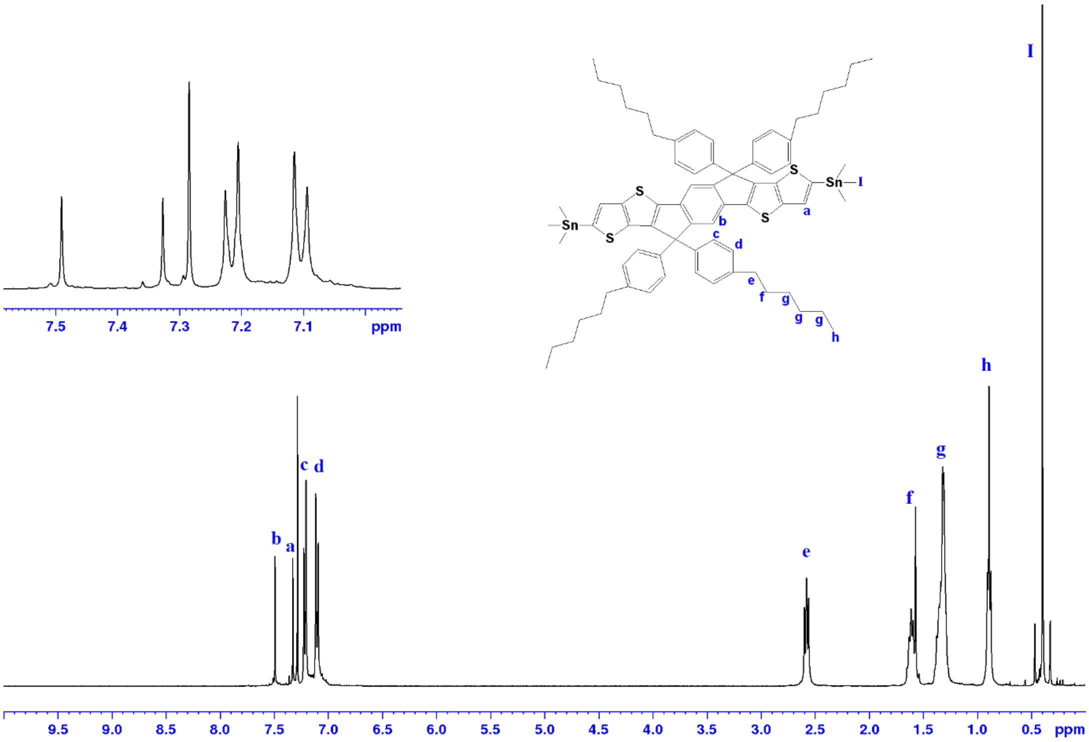

Figure 3. 3: The ^{1}H NMR spectrum of **IDTT-Sn2** (**M4) in CDCl$_3$.**

The synthetic routes to prepare 3-(5-bromothiophen-2-yl)-2,5-bis(2-ethylhexyl)-6-(5-phenylthiophen-2-yl)-2,5-dihydropyrrolo[3,4-*c*]pyrrole-1,4-dione (**M5)**, 3-(5-bromothiophen-2-yl)-2,5-bis(2-ethylhexyl)-6-(5'-phenyl-[2,2'-bithiophen]-5-yl)-2,5 dihydropyrrolo[3,4-*c*]pyrrole-1,4-dione (**M6)** and 5'-(4-(5-bromothiophen-2-yl)-2,5-bis(2-ethylhexyl)-3,6-dioxo-2,3,5,6-tetrahydropyrrolo[3,4-*c*]pyrrol-1-yl)-[2,2'-bithiophene]-5-carbaldehyde (**M7)** are outlined in **Scheme 3.2.**

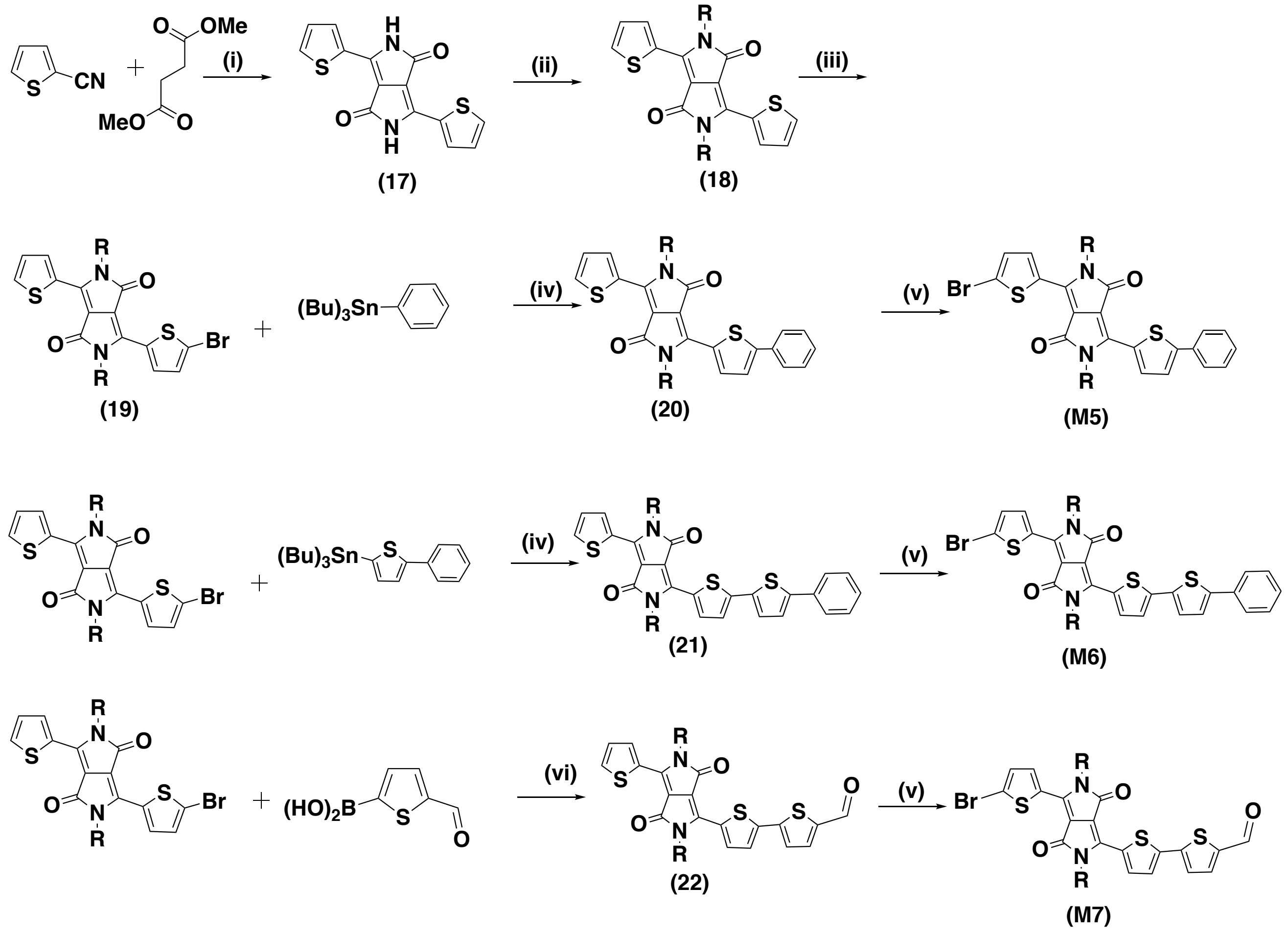

R: 2-ethylhexyl

Scheme 3. 2: The synthetic route of the three **DPP** monomers, **M5, M6 and M7.**

Reagent and condition: (i) KOtBu, amyl alcohol, 110 ^{o}C, N_2, 4h; (ii) R-Br, K_2CO_3, DMF, 130 ^{o}C; (iii) NBS, $CHCl_3$; (iv) $PdCl_2(PPh_3)_2$, toluene, 110 ^{o}C; (v) NBS, $CHCl_3$. (vi) K_2CO_3, $Pd_2(dba)_3$ and P(o-tol)$_3$, H_2O, THF.

3,6-Di(thiophen-2-yl)pyrrolo[3,4-c]pyrrole-1,4(2H,5H)- dione **(17)** is generally synthesised through the succinic ester route, as reported by Iqbal and co-workers. [226] The initial step comprises condensation of two equivalents thiophene-2-carbonitrile and succinic ester in the presence of tert-amyl alcohol and a strong base. The plausible mechanism toward 3,6-di(thiophene-2-yl)pyrrole[3,4-*c*]pyrrole-1,4-(2*H*, 5*H*)-dione(**DPP**) is depicted in **Scheme 3.3.** In the first step, a strong base was used the deprotonate the α-proton on the dimethyl succinate ester to generate a nucleophile, which attacks the thiophene-carbonitrile. This leads to the formation of an enaminoester **(c)**, and subsequently, ring cloure occurs to generate pyrroline ester **(e)**. These steps were continued to prepare **(DPP)** **(17)**.

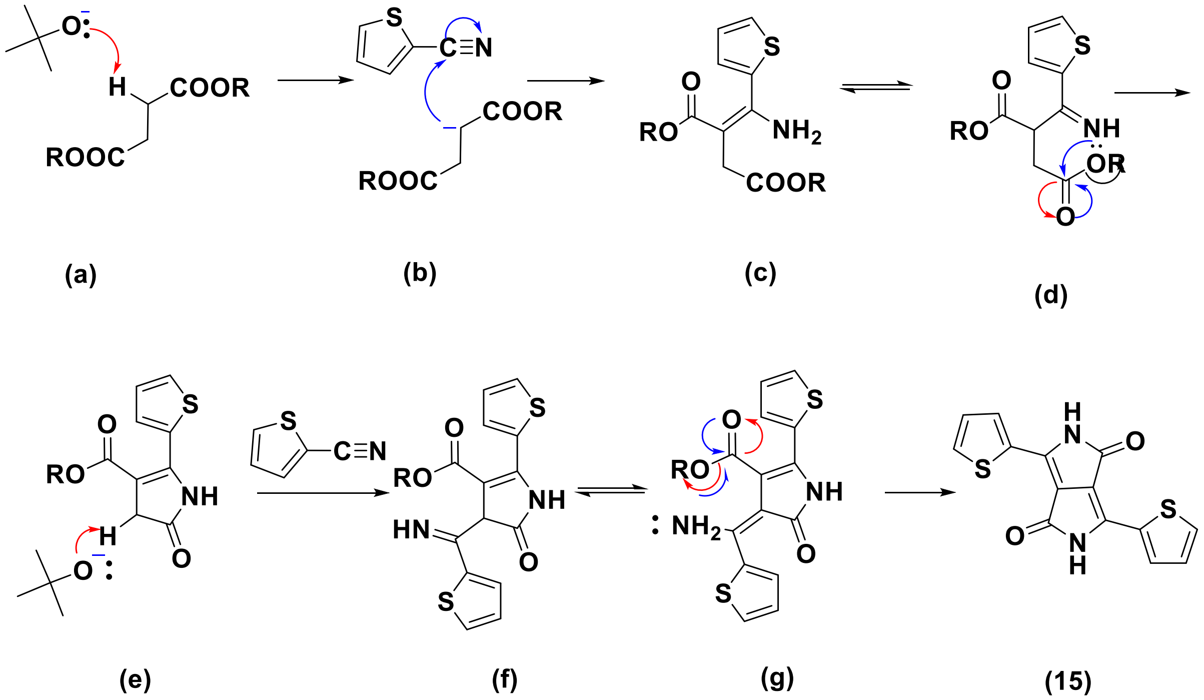

Scheme 3. 3: The mechanism pathway of (**DPP**).

The chemical structure of **DPP** consists of two five-membered ring γ-lactam units, which due to the presence of the cyclic amide, are electron withdrawing-moieties. In addition, the unsubstituted nitrogen atoms in the γ-lactam units result in the formation of intramolecular hydrogen bonding between the nitrogen and the adjacent thiophene aromatics. Therefore, the unfunctionalised; **DPP** is not soluble in most organic solvents; [227] it was used in the next step without further purification.

Compound **15** was alkylated by incorporating 2-ethylhexyl in the presence of K_2CO_3; wnich enhanced its solubility and processability. 2,5-Bis(2-ethylhexyl)-3,6-di(thiophen-2-yl)-2,5-dihydropyrrolo[3,4-*c*]pyrrole-1,4-dione **(18)** was obtained in a low yield of 19%. Then compound **18** was mono brominated using NBS in $CHCl_3$, achieving a yield of 52%. Next, compounds **20** and **21** were generated *via* Stille coupling of tributyl-phenyl-tin and 2-(tributylstannyl) 5-phenylthiophene using $PdCl_2(PPh_3)_2$ as a catalyst. However, compound **22** was synthesised *via* the Suzuki coupling reaction of 5-formyl thiophene-2-yl boronic acid with compound **19** in the presence of K_2CO_3, $Pd_2(dba)_3$ and $P(o\text{-}tol)_3$ in dry THF; the yield was 91%. Lastly, NBS was then used to brominate **20**, **21** and **22** in $CHCl_3$. This led to the formation of the final monomers **M5, M6** and **M7**. Finally, the approach to synthesis the small molecules of **IDTT-DPP-PH, IDTT-DPP-PHT, IDTT-DPP-CN** and **IDTT-DPP-INIC** is demonstrated in **Scheme 3. 4.**

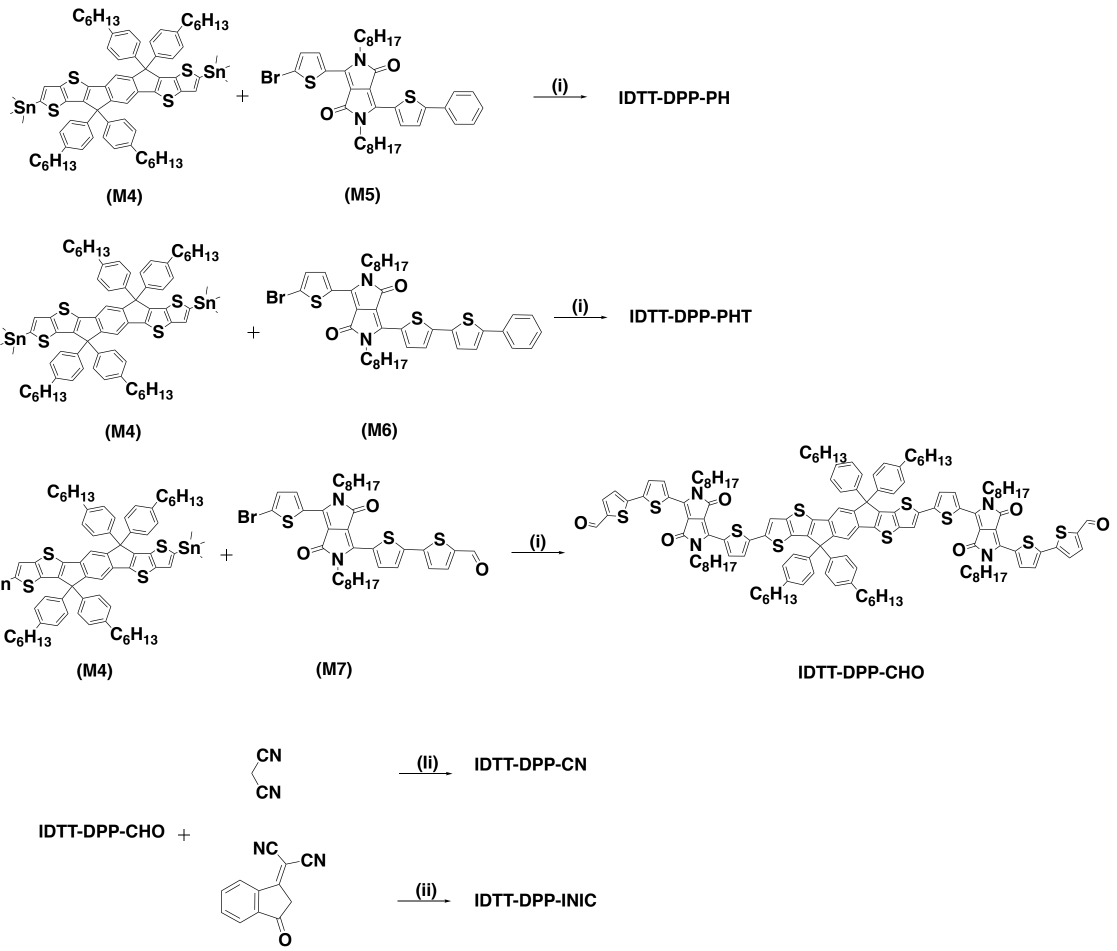

Scheme 3. 4: the synthetic approach toward the small molecules of **IDTT-DPP-PH, IDTT-DPP-PHT, IDTT-DPP-CN** and **IDTT-DPP-INIC.**

Reagent and condition: (i) $Pd_2(dba)_3$ and $P(o\text{-}tol)_3$, toluene 110°C (ii) pyridine, $CHCl_3$, refluxed.

The target molecules of **IDTT-DPP-PH and IDTT-DPP-PHT** were synthesised *via* the Stille coupling reaction between **M4** and the monomers M5 or M6 using $Pd_2(dba)_3$ and P(o-tol)$_3$ with a yield of 66% and 61% respectively. Also, the Stille coupling reaction of **M4** with **M7** was conducted to prepare **IDTT DPP-CHO** followed by the Knoevenagel condensation reaction with malononitrile and 2-(3-oxo-2,3-dihydro-1H-inden-1-ylidene)malononitrile to obtain **IDTT-DPP-CN** and **IDTT-DPP-INIC** in yields of 66% and 61%, respectively. The ^{1}H NMR and ^{13}CNMR analysis were used to characterise these monomers and **NFAs** and verify that the reactions had been conducted successfully. (See supplementary information). However, the ^{13}C NMR for **NFAs** was not detected due to aggregation. The matrix-assisted laser desorption/ionisation (MALDI-TOF MS) (TOF-Ms) and elemental analysis exhibited an agreement with their chemical structures.

3.2.2 Optical Properties

The optical properties of the four **NFAs** including **IDTT-DPP-PH, IDTT-DPP-PHT, IDTT-DPP-CN,** and **IDTT-DPP-INIC,** were investigated using UV-Vis. **Figures 3.4a** and **3.4b** show the normalised UV-Vis absorption spectra of the four NFAs in chloroform and as a thin film, respectively. **Table 3.1** summarises the results of all four **NFAs**. In solution, these acceptors exhibited a strong absorption band from nearly 500 nm to 900 nm region, which illustrates enhanced overlap with the incident solar spectrum compared to $PC_{60}BM$, which has a significantly lower absorption visible wavelength. This absorption can be referred to the ICT between the donor (**IDTT**) and acceptors (**DPP**) moieties. Additionally, the absorption band at a low wavelength from about 330 nm to 490 indicates the π-π* transition. The maximum absorption of these small molecules increases from 658 nm to 723 nm. The tendency can be correlated to the substitution of the electron rich **PH** units in the case of **IDTT-DPP-PH,** and **PHT** in **IDTT-DPP-PHT** with electron withdrawing units of malononitrile in **IDTT-DPP-CN** and **INIC** in **IDTT-DPP-INIC**. The maximum coefficient absorptions of these acceptors were determined to be 1.54×10^5 $M^{-1}cm^{-1}$ at 658 nm, 1.59×10^5 M^{-1} cm^{-1} at 665 nm 1.41×10^5 M^{-1} cm^{-1} at 709 nm and 1.31×10^5 M^{-1} cm^{-1} at 723 nm respectively, which is substantially lower for $PC_{60}BM$ 3.9×10^3 M^{-1} cm^{-1} at 400 nm.

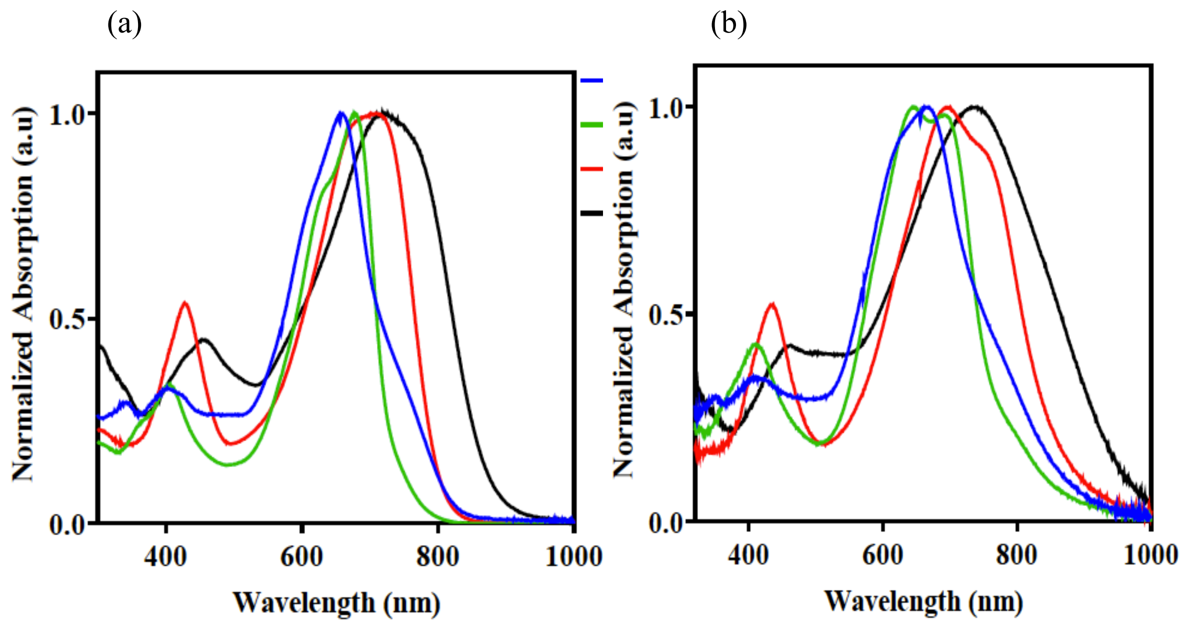

Figure 3. 4: Normalised UV-vis absorption spectra of **IDTT-DPP-PH**, **IDTT-DPP-PHT**, **IDTT-DPP-CN** and **IDTT-DPP-INIC** in a) chloroform solutions; and b) thin-films.

In the solid state, the absorption behaviour of these four compounds exhibits broader absorption compared to their solution in $CHCl_3$. Bathochromic shifts to 667 nm, 697 nm, and 748 were observed for **IDTT-DPP-PH, IDTT-DPP-PHT** and **IDTT-DPP-INIC,** respectively**.** This phenomenon is probably interpreted to the stronger π-π stacking and a higher planar structure. However**, IDTT-DPP-CN** revealed the absorption maxima at 709 nm in diluted chloroform and 698 nm in film. The weakness of a notable red-shifted from solution to film suggests that the **IDTT-DPP-CN** adopts identical energetic arrangements in both solution and film. The optical band gap of four **NFAs** was estimated to be 1.43 eV, 1.42 eV, 1.42 eV, and 1.28 eV, respectively.

In terms of the acceptor molecule in the synthesised NFAs in **Chapter 2** and **3**, it is worth mentioning that the incorporation of **DPP** into the molecules has reduced the optical bandgap more than **TPD**. This can be ascribed to two aspects. First, the molecular weight of **DPP** is greater than the molecular weight of **TPD**. Second, The **DPP** is more electron deficient than TPD, due to the presence of two amide groups, resulting in the **DPP** molecules having more D-A property over **TPD**.

According to the literature, **ITIC** demonstrates the maximum absorption of 664 nm with a maximum coefficient absorption of 1.3 × 10^5 M^{-1} cm^{-1}, which is almost the identical **IDTT-DPP-INIC**, and the optical band gap of **ITIC** was predicted to be 1.59 eV, which is higher than **IDTT-DPP-INIC.** This can be ascribed to the incorporation of **DPP** between the core and **INIC** has led to the broader absorption and narrow the bandgap**.** Moreover, the **ITIC** was fluorinated to synthesise **IT-4F**, which showed somewhat a bathochromic shifted, compared to the **ITIC** with the higher maximum coefficient absorption 2.10× 10^5 M $^{-1}$ cm $^{-1}$ at 723 nm than **ITIC** and **IDTT-DPP-INIC.** The **IDTT** core was flanked with the electron-withdrawing units, 2-(benzo[c][1,2,5]-thiadiazol-4-ylmethylene)-malononitrile **(IDTT-2BM)**. Compared to **IDTT-DPP-CN**, **IDTT 2BM** demonstrated a much lower maximum absorption of 672 nm in $CHCl_3$ solution and 668 nm in the film, with a maximum coefficient absorption of 5.6 × 10^4 M $^{-1}$ cm $^{-1}$. It can be deduced that the **DPP** moieties have greater influence on the optical properties due to their high electron affinity.

Table 3. 1: The optical properties of **IDTT-DPP-PH, IDTT-DPP-PHT, IDTT-DPP-CN** and **IDTT-DPP-INIC** and their band gap.

Acceptor	λ max Solution (nm)	λ max Film (nm)	Onset (nm)	Eg^{opt} (eV)	Coefficient absorption M^{-1} cm^{-1}
IDTT-DPP-PH	658	667	867	1.43±0.003	1.54 × 10^5
IDTT-DPP-PHT	665	695	873	1.42±0.002	1.59 × 10^5
IDTT-DPP-CN	709	698	885	1.40±0.0043	1.41 × 10^5
IDTT-DPP-INIC	723	748	969	1.28±0.003	1.31 × 10^5

3.2.3 Electrochemical properties

The CV was used to investigate the frontier energy levels of four **NFAs** in tetrabutylammonium perchlorate in acetonitrile solutions as an electrolyte. **Figure 3.5** represents the cyclic voltammograms for **IDTT-DPP-PH, IDTT-DPP-PHT, IDTT-DPP-CN,** and **IDTT-DPP-INIC**, and their HOMO and LUMO energy levels; they were measured from the onset oxidation and reduction potential. The HOMO of **IDTT-DPP-PH,**

IDTT-DPP-PHT, IDTT-DPP-CN and **IDTT-DPP-INIC** values are estimated to -5.26 eV, -5.15 eV, -5.23 eV and -5.11 eV while, the LUMO energy levels for acceptors were predicted to be -3.32 eV, -3.34 eV, 3.57 eV, and -3.93 eV, respectively. Clearly, the LUMO level has been affected significantly by flanking the withdrawing groups malononitrile and **INIC** in **IDTT-DPP-CN (-**3.57 eV)**,** and **IDTT-DPP-INIC** (-3.93 eV). This effect is more significant than that of terminal donating groups such as phenyl or 2-phenylthiophen in **IDTT-DPP-PH, IDTT-DPP-PHT** with -3.32 eV and -3.34 eV, respectively. The **IDTT-DPP-PHT** demonstrates a HOMO energy level around 0.11 eV deeper than compared to **IDTT-DPP-PH,** which can probably be attributed to the horizontal extension of the conjugated backbone. Furthermore, the incorporation of the strong withdrawing group, **INIC,** resulted in reducing the HOMO to -5.11 eV in **IDTT-DPP-INIC**. The electrochemical band gaps of **IDTT-DPP-PH, IDTT-DPP-PHT, IDTT-DPP-CN and IDTT-DPP-INIC** were estimated to be 1.94 eV, 1.81 eV, 1.66 eV, and 1.18 eV, respectively. In comparison to the small molecules based on the **TPD** withdrawing units in Chapter **2**, the employment of **DPP** moieties to design these NFAs with the same **IDTT** core, produces noticeable changes on the determination of HOMO and LUMO energy levels due to the high affinity of **DPP**.

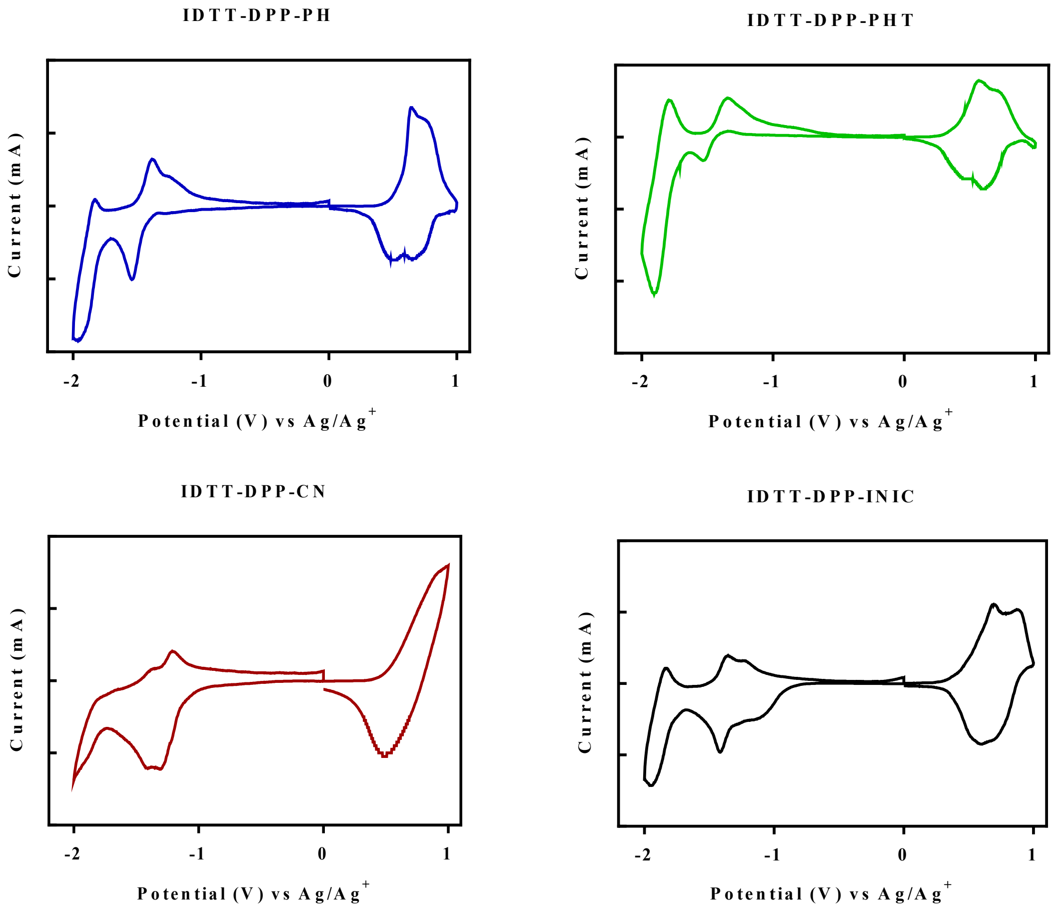

Figure 3. 5: Cyclic voltammograms of **IDTT-DPP-PH**, **IDTT-DPP-PHT**, **IDTT-DPP-CN** and **IDTT-DPP-INIC (black)** on Pt electrode in Bu_4NClO_4/CH_3CN at 100 mV/s.

Table 3. 2: The electrochemical properties of **IDTT-DPP-PH, IDTT-DPP-PHT, IDTT-DPP-CN and IDTT-DPP-INIC.**

Acceptor	$E^{(onset-OX)}$ (volts)	$E^{(onset-red)}$ (volts)	HOMO (eV)	LUMO (eV)	Eg^{elect} (eV)
IDTT-DPP-PH	0.54	-1.39	-5.26±0.008	-3.32±0.007	1.94±0.0088
IDTT-DPP-PHT	0.44	-1.37	-5.15±0.003	-3.34±0.01	1.81±0.009
IDTT-DPP-CN	0.51	-1.14	-5.23±0.01	-3.57±0.004	1.66±0.009
IDTT-DPP-INIC	0.39	-0.79	-5.11±0.008	-3.93±0.01	1.18±0.011

Published literature showes that the LUMO energy level of **IDTT-DPP-INIC** -3.93 eV is higher than **ITIC** (-3.83 eV), but it is lower than **IT-4F** (-4.14 eV). The strength of the acceptor species plays a fundamental role in decreasing the LUMO level energy. As a result, the presence of four high electronegative F atoms could downshift the LUMO energy level more deeply compared to **IDTT-DPP-INIC** and **ITIC**. On the other hand, **IDTT-DPP-INIC** exhibited higher HOMO energy level compared to **ITIC** and **IT-4F** with respective values being -5.11 eV, -5.48 eV and -5.66 eV**.** The inference is that **ITIC** and **IT-4F** have more acceptor characteristics compared **IDTT-DPP-INIC**, even though the presence of the conjugation system is greater in **IDTT-DPP-INIC**. The HOMO level of **IDTT-2BM** and **IDTT-DPP-CN** were estimated to be -5.5 eV and -5.26 eV, respectively. The difference in HOMO energy level can be ascribed to the **IDTT-DPP-CN** possessing more electron donating characteristics. Whereas the LUMO level energy of both NFAs was computed to be -3.8 eV and -3.57 eV. The variation between these values is anticipated to be due to malononitrile having a low withdrawing ability.

3.2.4 Thermal properties

The thermal properties of four NFAs **IDTT-DPP-PH, IDTT-DPP-PHT, IDTT-DPP-CN** and **IDTT-DPP-INIC** were investigated by TGA under an inert atmosphere at a heating rate of 10°C/min **Figure 3.6**. The TGA plots of these compounds and the thermal data are summarised in **Table 3.3**. All compounds revealed good thermal stability, with T_d 380 °C and above, while the melting points of the materials were not detected up to 385 °C. No observation for the glass transition was recorded for all acceptors using DSC.

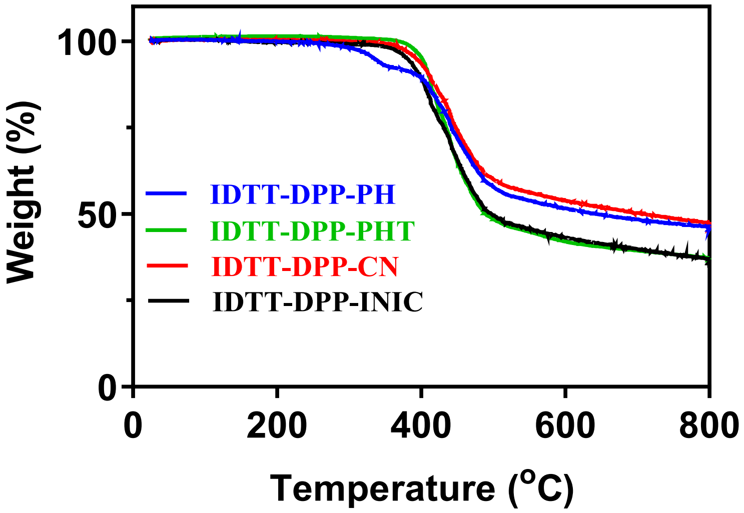

Figure 3. 6: The TGA curves of **IDTT-DPP-PH**, **IDTT-DPP-PHT**, **IDTT-DPP-CN** and **IDTT-DPP-INIC**

Table 3. 3: The thermal data of **IDTT-DPP-PH, IDTT-DPP-PHT, IDTT-DPP-CN and IDTT-DPP-INIC.**

Acceptors	T_d (°C)
IDTT-DPP-PH	380
IDTT-DPP-PHT	391
IDTT-DPP-CN	394
IDTT-DPP-INIC	388

T_d: decomposition temperature,

3.2.5 Photovoltaic properties

The photovoltaic properties of the four NFAs were investigated. OSC devices were fabricated to have a conventional structure of glass/indium tin oxide (ITO)/ poly(3,4-ethylenedioxythiophene) (PEDOT): polystyrene sulfonate (PSS)/ active layer/PFN-Br/Ag to evaluate the photovoltaic performance of PBDB-T-NFAs. Further, all acceptors attempted and inverted stack (ITO/ZnO/Active Layer/MoO_3/Ag) have been tried to make OSC devices with a donor of P_3HT. Unfortunately, devices using any of these four structures have demonstrated very low efficiency. This may be attributed to some significant factors such as non-optimal energy offset, absorption or morphology of the donor acceptors blend. The investigation of the PV performance of four NFAs is still in progress; the aim is to find appropriate polymer donors with an energy level well matched for acceptors and proper morphology that improve the PCE.

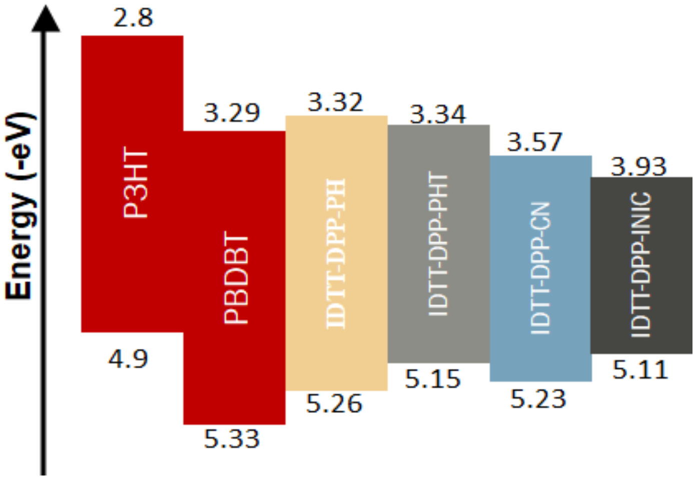

Figure 3. 7: The energy level of the polymer donors and the four NFAs.

3.3 Conclusion

In summary, we designed and prepared four new low bandgaps NFAs materials denoted **IDTT-DPP-PH, IDTT-DPP-PHT, IDTT-DPP-CN,** and **IDTT-DPP-INIC** with an A-D-A molecular architecture, in which the **IDTT** spiro fused ring used as an electron donating molecule and four different withdrawing **DPP** moieties used as terminal groups. The **IDTT-DPP-PH, IDTT-DPP-PHT** small molecules were synthesised *via* Stille coupling, whereas the **IDTT-DPP-CN,** and **IDTT-DPP-INIC** acceptors were prepared *via* Knoevenagel condensation reaction. The UV-Vis of all theses NFAs displayed good absorption in the wavelength range from 350 nm to 900 nm, which is comparable with the maximum solar photon flux (300- 800 nm). Furthermore, these NFAs showed a low optical bandgap ranging from 1.43 eV to 1.28 eV. It is hypothesised that the NFAs adopt a better coplanar structure in the solid-state leading to developing $\pi - \pi$ interchain stacking. In comparison to **IDTT-DPP-PH,** the increase to the conjugation backbone by adding a thiophene ring into **IDTT-DPP-PHT** acceptor does not exert a significant effect in the optical properties. In terms of electrochemical properties, the HOMO energy level of **IDTT-DPP-PH, IDTT-DPP-PHT** and **IDTT-DPP-CN** are similar. Extending the π-conjugation in **IDTT-DPP-PHT** and **IDTT-DPP-CN** has a small influence on the resulting energy levels. However, the replacement of phenyl group of **IDTT-DPP-PHT** by weaker electron deficient malononitrile significantly lowers the LUMO to -3.60 eV. The malononitrile was replaced with the stronger electron accepting **INIC**, which has a noticeable effect not only on the LUMO level but also on HOMO by downshifting the energy level to -5.11/-3.91 eV. The high onset thermal decomposition of these NFAs is above 380°C indicating excellent thermal stability. The solar cell devices have shown a very low PCE, but the investigation is still in progress to improve solar cell performance.

Chapter (IV)

Preparation of non-fullerene acceptors based on IDT and diketopyrrolopyrrole for solution processed organic solar cells

Abstract

Four new small molecules were synthesised based on indacenodithiophene (**IDT**) as the electron donating unit with various electron deficient moieties based on **DPP**, such as **DPP-PH**, **DPP-PHT**, **DPP-CN** and **DPP-INIC** units. The Stille coupling reaction and Knoevenagel condensation reaction were used to prepare these materials and their optical, electrochemical and thermal properties have been studied. The UV-Vis of **IDT-DPP-PH, IDT-DPP-PHT, IDT-DPP-CN** and **IDT-DPP-INIC** non-fullerene acceptors showed strong absorption in the region between 350 nm to 950 nm of the electromagnetic spectrum, which is roughly comparable to the solar spectrum. The optical band gap for **IDT-DPP-PH, IDT-DPP-PHT, IDT-DPP-CN,** and **IDT-DPP-INIC** were estimated to be at 1.42 eV, 1.43 eV, 1.39 eV and 1.29 eV with maximum molar absorption coefficients of 1.37×10^5 M^{-1} cm^{-1} at 663 nm, 1.21×10^5 M^{-1} cm^{-1} at 683 nm 1.47×10^5 M^{-1} cm^{-1} at 726 nm and 1.31×10^5 M^{-1} cm^{-1} at 738 nm respectively. All of the NFAs possess deep energy levels for both the HOMO (-5.25 eV, -5.21 eV and -5.20 eV) and the LUMO (-3.34 eV, -3.38 eV, -3.60 eV and -3.91 eV), respectively. Flanking the **IDT** with electron deficient moieties, such as malononitrile and **INIC,** results in a low lying LUMO energy level depending on the nature of acceptor unit compared to the rich units of phenyl and 2-phenylthiophene in **IDT-DPP-PH, IDT-DPP-PHT,** respectively. TGA revealed that these NFAs have excellent thermal stability with decomposition onsets above 380°C.

4.1 Introduction

Fullerenes and their derivatives based electron acceptors have played a significant role in the development of BHJ for OSCs in the last two decades. [228-233] [6,6]-phenyl-C_{61}-butyric acid methyl ester ($PC_{61}BM$) or [6,6]-phenyl-C_{71}-butyric acid methyl ester ($PC_{71}BM$) were predominately utilised as electron acceptors in polymer solar cell devices, which have demonstrated increase in PCE from 2.5% to above 10%.[234-237] Fullerene derivatives have remarkable features such as high electron affinity, their favourable LUMO energy, excellent electron transporting ability and their ability to produce favourable nanoscale morphology upon mixing with donor polymer. [238-240] Nevertheless, some intrinsic drawbacks of fullerene derivatives include lack of photostability in air, weak absorption in the visible region and near infrared NIR, unstable morphology over the time in film blends, difficult to purify and limited electronic tuning. [241-243] Therefore, researchers' attention has concentrated on overcoming the disadvantages of fullerenes as acceptors in OSCs, while maintaining the good characteristics offered by fullerenes, by designing new non-fullerene electron acceptor molecules, which have well-match energy levels with donor and strong, broad absorption in the visible and NIR regions. [244-248] Apparently, the design of novel NFAs will contribute significantly to the selection of appropriate donor and acceptors for the development PCEs. Up to date, there is a wide range of new NFA small molecules with different electron-withdrawing moieties that have been explored; PCEs of these exceed 13%.[249-255]

In recent years, various types of acceptor–donor–acceptor (A–D–A) small molecules non-fullerene acceptors have been reported, consisting of **IDT** or **IDTT** molecules as electron donor moieties with different electron – deficient capping moieties as electron acceptor moieties. [256-259] In the A-D-A construction, the incorporation of different electron withdrawing groups can be an efficient approach to tune the HOMO and LUMO energy levels. In addition, the conjugation of the **IDT** core enhances the π-π interaction, resulting in a decrease of the band gap and broad absorption. The torsional or conformational modification of **IDT** can be inhibited due to the rigid and coplanar structure leading to excellent electron mobility. [260,261] Moreover, the presence of tetra-hexylphenyl substituents on the electron donating units is found to be beneficial to avoid strong self-aggregation and large phase separation in BHJ and improving solution processability.

Among many electron withdrawing acceptor molecules, semiconductor compounds based on diketopyrrolopyrrole **(DPP)** have found applications in organic photovoltaic devices, organic light emitting diodes and organic-field effect transistors, [262-268] due to their excellent good thermal, chemical and mechanical stability, [269] good charge carrier mobility and outstanding optical properties. [270-272] Moreover, the **DPP** based compounds are planar and their capability to make hydrogen bonds promotes strong π-π stacking, leading to high electron mobiliy. [273,274] The PCE of organic photovoltaic solar cell (OPVs) based on **DPP** polymers was around 6.5%. However, the PCE is 5.8% in terms of small molecules. [272,275,276] Furthermore, **DPP** based on small molecules as acceptors were reported and the PCE of blending **DPP** as acceptor with **P3HT** was reached to 2%.[277,278] Huitao and his colleagues synthesised **IDT-2DPP**, in which the spiro compound **IDT** was used as the donor core and flanked with **DPP** as end capping. Solar devices using **IDT-2DPP** as acceptor and **P3HT** as donor have been manufactured with a PCE of 0.83%.[259] In 2018, two new small molecular acceptors have been reported in which the **IDT** core was flanked with weakly accepting unit of methyl-3-thiophenecarboxylate between the IDT core and INIC end capping to produce **IDT-3MT** and the electron-rich thiophene replace the **3MT** in **IDT-T**. The BHJ solar device based on **PBDB-T:IDT-3MT** blend film exhibited a higher PCE 8.40% compared to that of the **PBDB-T:IDT-T**-based device PCE 6.36%.[279]

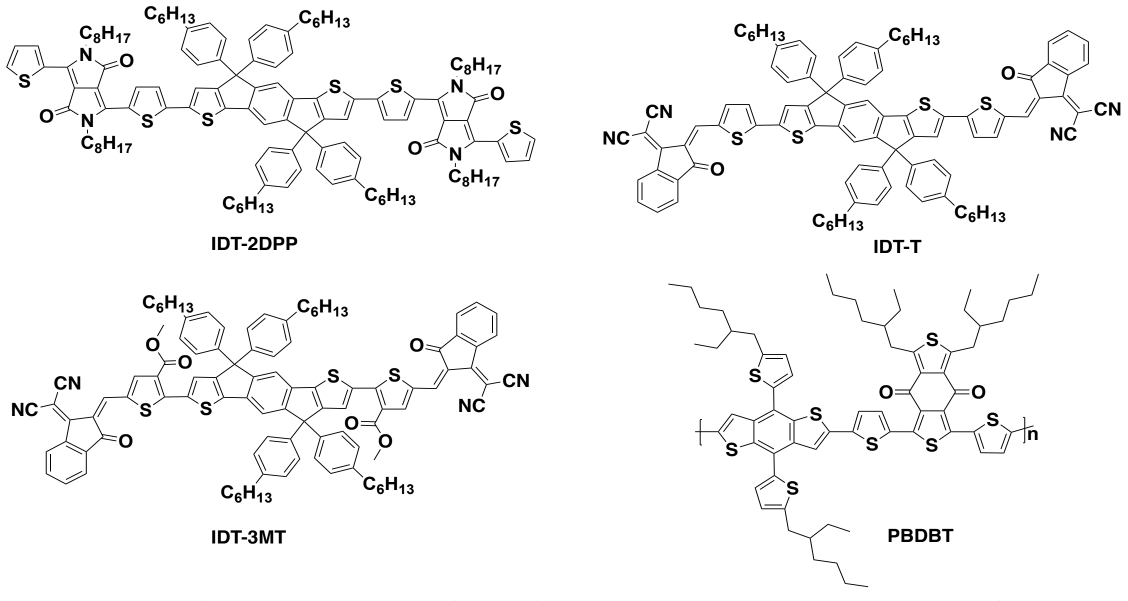

Figure 4. 1: Schematic representations of **IDT-2DPP**, **IDT-T, IDT-3MT** and **PBDBT**.

In this chapter, we report the synthesis of four new A-D-A non-fullerene acceptors **IDT-DPP-PH, IDT-DPP-PHT, IDT-DPP-CN** and **IDT-DPP-INIC** for OSCs application **Figure 4.2.** The **IDT** core is connected with the four different end capping including **DPP-PH**, **DPP-**

PHT, **DPP-CN** and **DPP-INIC**. The effect of changing the end capping on the electrochemical, optical and thermal properties of these NFAs is investigated.

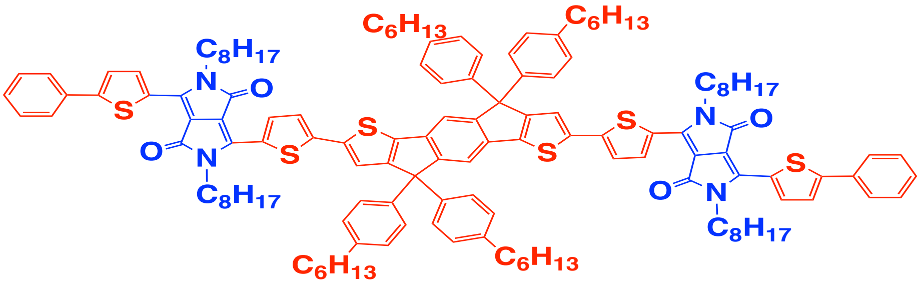

IDT-DPP-PH

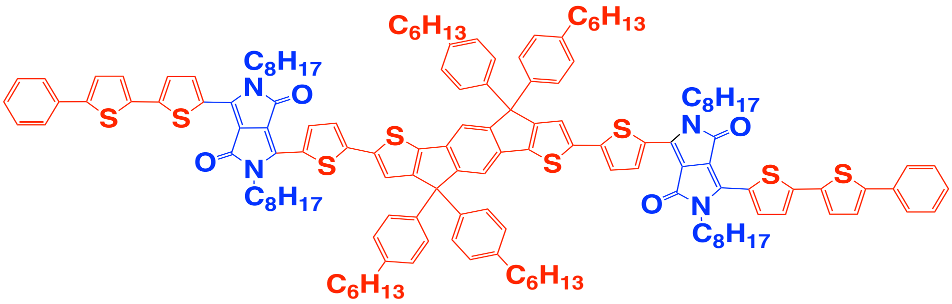

IDT-DPP-PHT

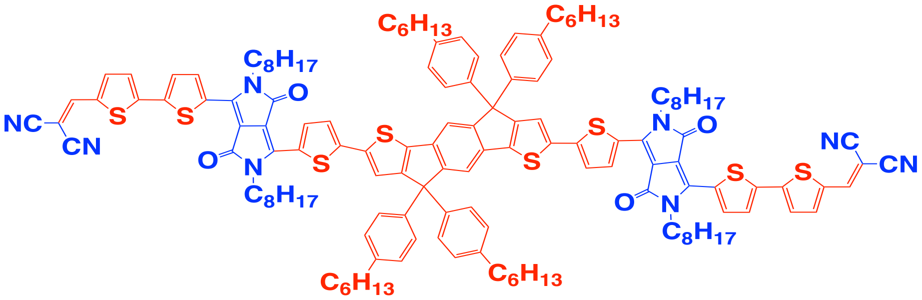

IDT-DPP-CN

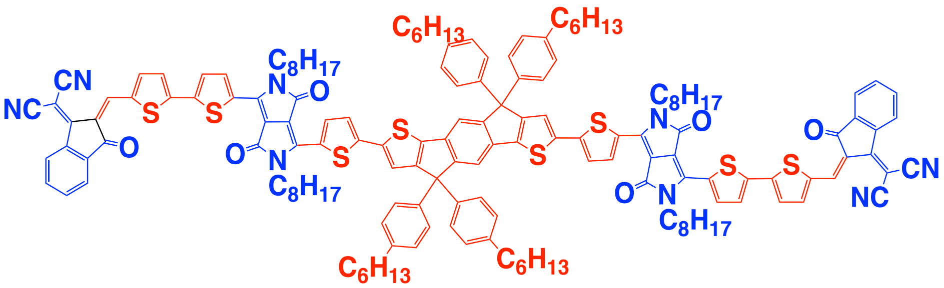

IDT-DPP-INIC

Figure 4. 2: The chemical structures of four NFAs (red: donor unit and blue: acceptor unit).

4.2 Result and discussion

4.2.1 Synthesis of the monomer

The preparation of (4,4,9,9-tetrakis(4-hexylphenyl)-4,9-dihydro-*s*-indaceno[1,2-*b*:5,6-*b′*]dithiophene-2,7-diyl)bis(trimethylstannane) **(IDT-Sn_2) M8** was undertaken as described in the literature. The synthetic route of **(IDT-Sn_2) M8** is outlined in **Scheme 4.1.** The diethyl 2,5-di(thiophen-2-yl)terephthalate compound **23** was prepared *via* Stille coupling reaction of tributyl(thiophen-2-yl)stannane with diethyl 2,5-dibromoterephthalate in the presence of $Pd(PPh_3)_4$ as a catalyst in dry toluene in a good of yield of 84%. Then 1-bromo-4-hexyl benzene was lithated with n-BuLi and quenched with a solution of **23** in THF to perform a double nucleophilic addition reaction on each ester; this was followed by a ring closure reaction under an acidic condition to obtain 4,4,9,9-tetrakis(4-hexylphenyl)-4,9-dihydro-*s*-indaceno[1,2-*b*:5,6*b′*] dithiophene **(IDT) 24**. The crude product was purified *via* column chromatography using a mixture of petroleum ether and DCM 10:2. The target product was obtained in a good yield of **87%.** After lithiation of **24** using n-BuLi, trimethyltin chloride was added to prepare the corresponding bis-stannylated **M8,** with an excellent yield of 92%.

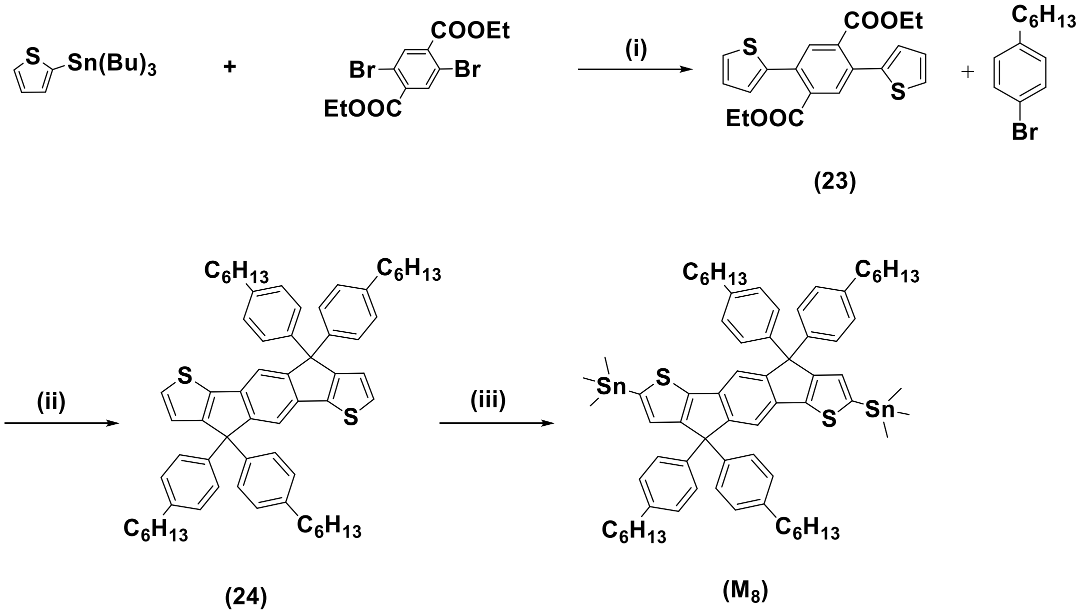

Scheme 4. 1: The synthesis of **IDT-Sn_2 M8**.

Reagent and condition: (i) $Pd(PPh_3)_4$, toluene (ii) n-BuLi, -78°C, H_2SO_4, AcOH, (iii) n-BuLi, $(CH_3)_3SnCl$, THF, -78°C.

The chemical structure and the purity of **M8** were characterised by NMR spectroscopy to confirm the reaction was accomplished successfully. **Figure 4.3** shows the ^{1}H NMR spectrum of M**8**, which illustrates a split pattern of two doublet and two singlet peaks in the aromatic region as expected. The appearance of a new singlet peak at 0.38 ppm refers to the protons on the methyl groups.

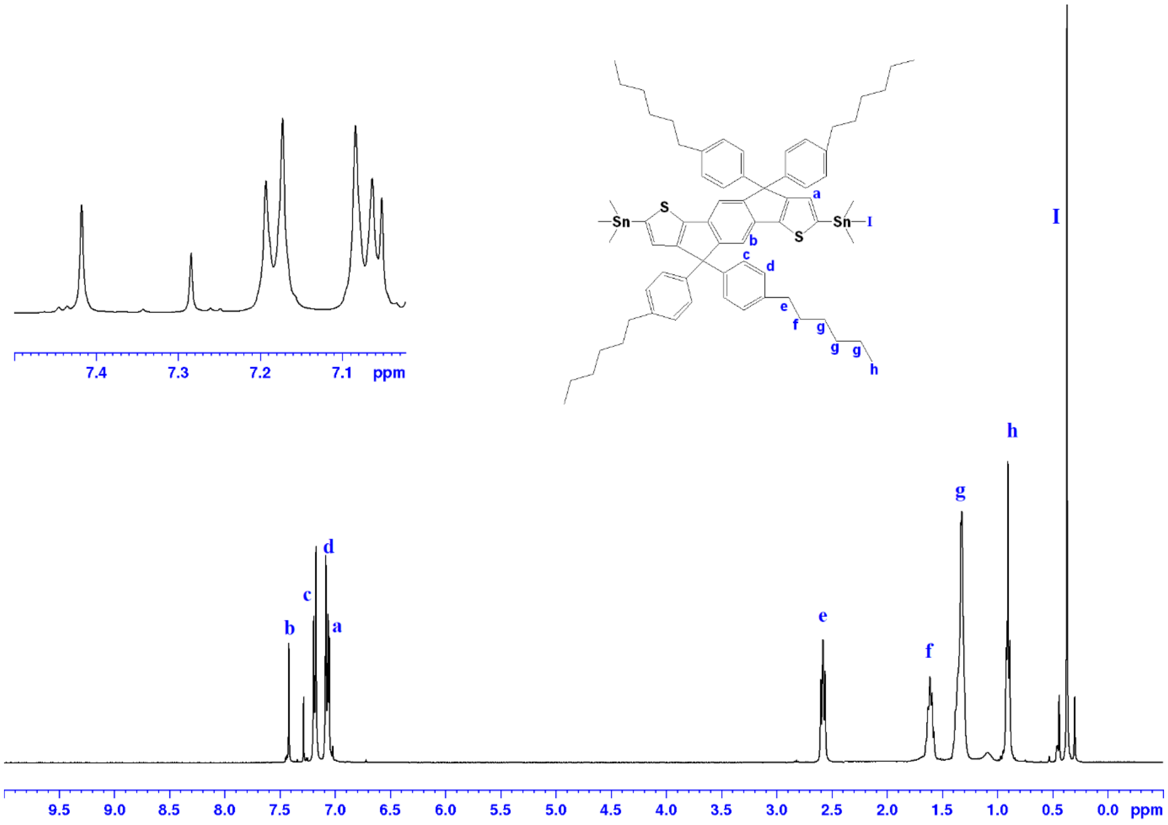

Figure 4. 3: ^{1}H NMR spectrum of **M8** in **$CDCl_3$**.

The same methodology of preparing the NFAs as described in **Chapter 3** was used to synthesise four different NFAs, **IDT-DPP-PH, IDT-DPP-PHT, IDT-DPP-CN** and **IDT-DPP-INIC.** These NFAs were synthesised using a palladium catalyst in toluene through Stille coupling reaction between **M8** and the synthesized monomers **M5, M6**, and **M7**. The synthetic route to monomers **M5, M6**, and **M7** were described in detail in the experimental section in **Chapter 6. Scheme 4.2** shows the chemical structures of these **NFAs,** which were identified by ^{1}H NMR, (MALDI-TOF MS) and elemental analysis. Due to the aggregation of these acceptors **IDT-DPP-PH, IDT-DPP-PHT, IDT-DPP-CN** and **IDT-DPP-INIC** in $CHCl_3$, ^{13}C NMR spectra were not collected.

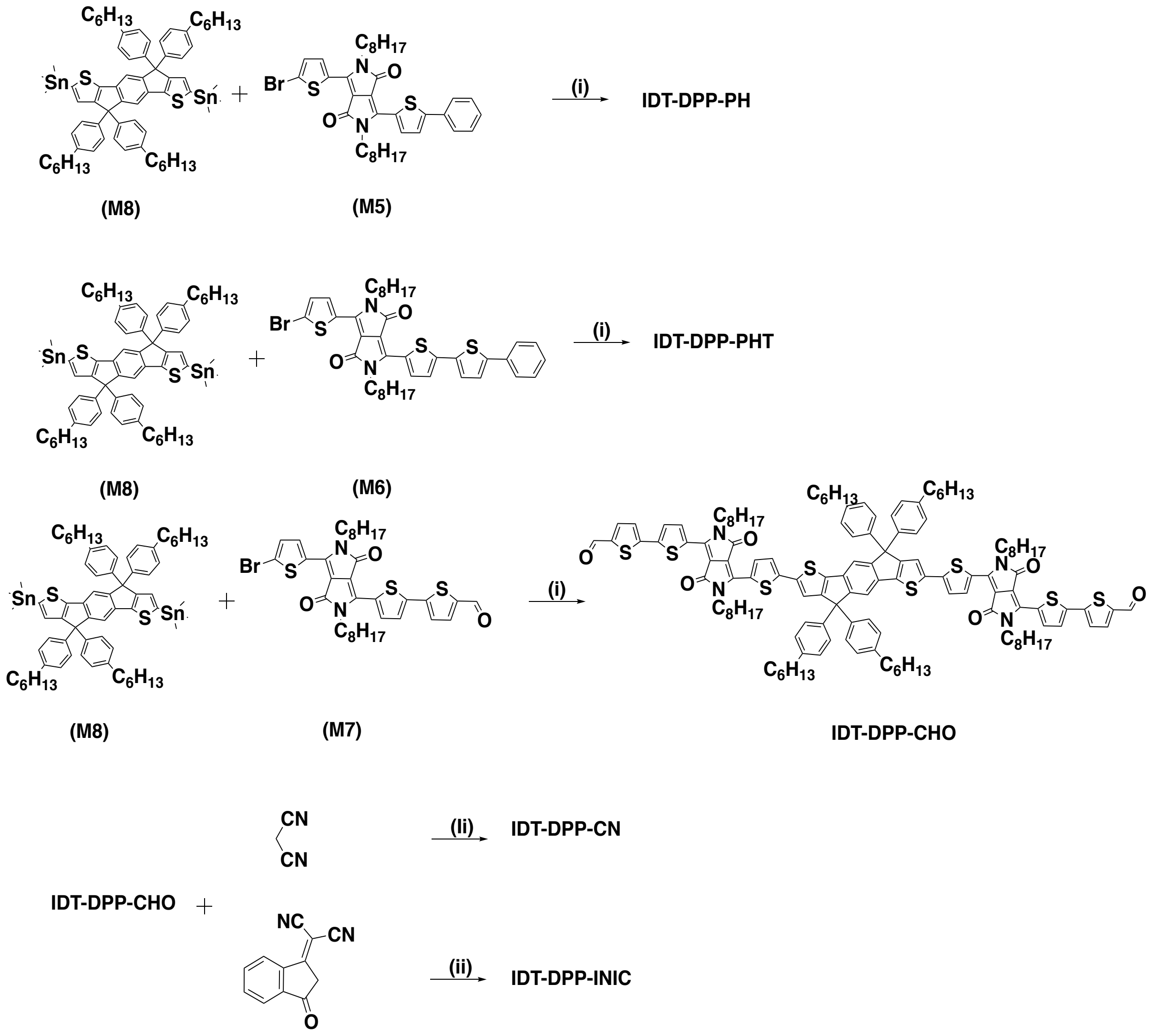

Scheme 4. 2: The synthetic approach toward the small molecules of **IDT-DPP-PH, IDT-DPP-PHT, IDT-DPP-CN** and **IDT-DPP-INIC.**

Reagent and condition: (i) $Pd_2(dba)_3$ and $P(o\text{-}tol)_3$, toluene 110°C (ii) pyridine, $CHCl_3$, refluxed.

4.2.2 Optical properties

The optical properties of small molecular acceptors **IDT-DPP-PH, IDT-DPP-PHT, IDT-DPP-CN** and **IDT-DPP-INIC** were recorded using UV-vis. The absorption spectra of these NFAs in diluted chloroform and film are presented in **Figures 4.4a, 4.4b**, and **Table 4.3** outlines the spectroscopic data.

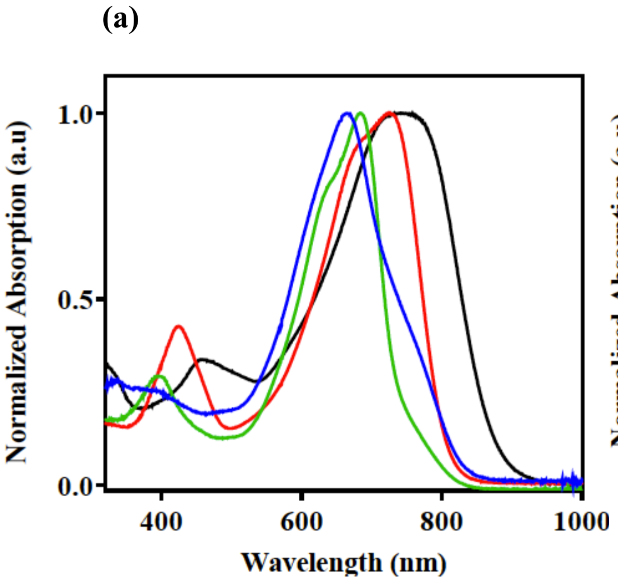

Figure 4. 4: Normalised UV-vis absorption spectra of **IDT-DPP-PH**, **IDT-DPP-PHT**, **IDT-DPP-CN** and **IDT-DPP-INIC** in a) chloroform solutions; and b) thin-films.

In chloroform solution, the absorption spectra of the four **IDT**-based NFAs exhibited analogous behavior to that using the **IDTT** core in **Chapter 3**. The main absorption regions of **IDT** NFAs extend from 480 nm to 930 nm, corresponding to ICT between the rich electron **IDT** and the electron deficient **DPP** moieties, with maximum absorptions of 655 nm, 673 nm, 715 nm and 739 nm**,** and maximum coefficient absorptions of 1.37 × 10^5 M^{-1} cm^{-1} at 663 nm, 1.21 × 10^5 M^{-1} cm^{-1} at 683 nm 1.47 × 10^5M^{-1} cm^{-1} at 726 nm and 1.31 × 10^5M^{-1} cm^{-1} at 738 nm respectively. The increase of maximum absorptions may infer a horizontal extension of the conjugation system. However, the **IDT-DPP-PHT** and **IDT-DPP-CN** showed an absorption band from around 330 nm to 480 nm, resulting from the π-π* transition. Compared to the four NFAs using **IDTT** core, the maximum absorption values observed for all NFAs based on **IDT** demonstrated a bathromic shift, which can be ascribed to the aggregation of the NFAs using **IDTT**.

In the solid state, the absorption spectram of **IDT-DPP-PH, IDT-DPP-PHT** and **IDT-DPP-INIC** displayed broader signals and a slightly higher red-shifted relative to their solution, indicating stronger π-π stacking and higher coplanar structures. The optical band gap for these small molecules were estimated from the onset edge absorption to be 1.42 eV, 1.43 eV, 1.39 eV and 1.29 eV respectively for **IDT-DPP-PH, IDT-DPP-PHT, IDT-DPP-CN** and **IDT-DPP-INIC**; these values are quite similar to those of the NFAs using **IDTT** described in **Chapter 3.** **IDT-DPP-INIC** demonstrates the highest maximum absorption at 738 nm and the lowest optical band gap of 1.29 eV, which are consequences of containing more acceptors groups.

Table 4. 1: The optical properties of **IDT-DPP-PH, IDT-DPP-PHT, IDT-DPP-CN** and **IDT-DPP-INIC** and their band gap.

Acceptor	λ_{max} Solution (nm)	λ_{max} Film (nm)	Onset (nm)	Eg^{opt} (eV)	Coefficient absorption M^{-1} cm^{-1}
IDT-DPP-PH	663	676	867	1.42±0.0040	1.37×10^5
IDT-DPP-PHT	683	637-697	873	1.43±0.0058	1.21×10^5
IDT-DPP-CN	726	698	892	1.39±0.0027	1.47×10^5
IDT-DPP-INIC	738	748	961	1.29±0.0027	1.31×10^5

Previous literature has reported that **IDT** flanked only with **DPP** as the end capping shows smaller maximum absorption of 640 nm and optical bandgap 1.74 eV compared to those four NFAs. In addition, it is published that when a thiophene ring and weak acceptors methyl-3-thiophene carboxylate replaced the **DPP** moiety of **IDT-DPP-INIC** in **IDT-T** and in **IDT-3MT,** respectively they showed maximum absorptions of 698 nm and 683nm. The estimated optical band gap for **IDT-T** and **IDT-3MT** was 1.56 eV and 1.52 eV, respectively, which is higher than four NFAs. Relative to that of **IDT-2BM, IDT-DPP-CN** exhibited a higher maximum absorption peak by ~66 nm and a lower optical bandgap by 0.21 eV.

4.2.3 Electrochemical properties

CV was used to study the electrochemical properties of **IDT-DPP-PH, IDT-DPP-PHT, IDT-DPP-CN** and **IDT-DPP-INIC** under an inert atmosphere. The CV curves of these molecules are displayed in **Figure 4.5**, and the collected data are summarised in **Table 4.2**. The HOMO/LUMO energy levels of four NFAs were estimated from the onset oxidation potential and the onset of reduction potential. The HOMO of **IDT-DPP-PH, IDT-DPP-PHT,**

IDT-DPP-CN and **IDT-DPP-INIC** values are estimated to be -5.26 eV, -5.21 eV, -5.20 eV and -5.12 eV, while, the LUMO energy levels for acceptors were predicted to be -3.34 eV, -3.38 eV, -3.60 eV and -3.91 eV, respectively.

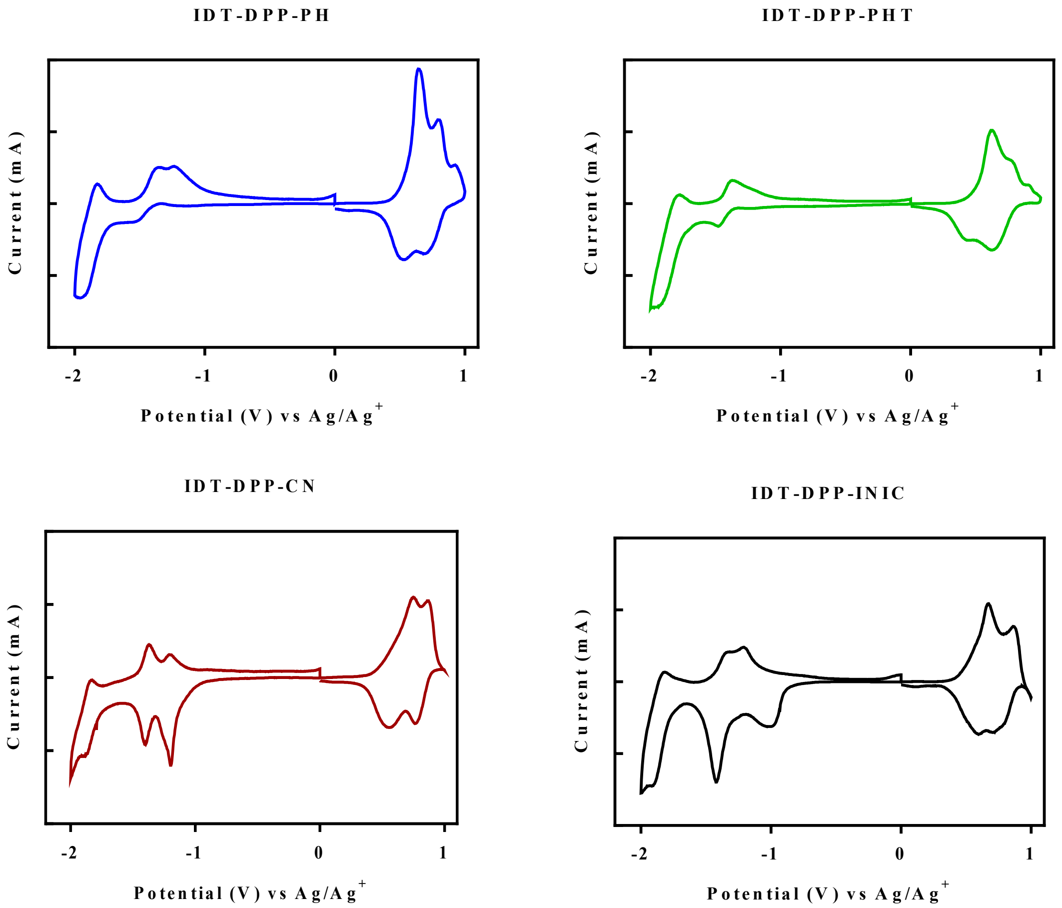

Figure 4. 5: Cyclic voltammograms **of IDT-DPP-PH**, **IDT-DPP-PHT**, **IDT-DPP-CN** and **IDT-DPP-INIC on Pt** electrode **in Bu_4NClO_4/CH_3CN at 100 mV/s.**

Of all the acceptors synthesised, **IDT-DPP-INIC** has deepest LUMO energy level with a value of -3.91 eV, and the HOMO level was estimated to be -5.11 eV. The LUMO/HOMO level of **IDT-DPP-CN** were estimated to be -3.60/-5.26 eV. It was anticipated that the deeper LUMO level of **IDT-DPP-INIC** relative to **IDT-DPP-CN** is the consequence of the higher electron affinity of **IDT-DPP-INIC.** The HOMO/LUMO energy levels of **IDT-DPP-PH** and **IDT-DPP-PHT** were estimated to be -5.26/-3.34 eV and -5.21/-3.39 eV, respectively. The insertion of the thiophene ring has a slight influence on the resulting energy levels.

In the literature, compared to the energy levels of **IDT-DPP-CN**, **IDT-2BM** showed higher HOMO with a value of -5.6 eV, but lower LUMO -3.8 eV level relative to that of LUMO of **IDT-DPP-CN**. This can be explained by the presence of a higher degree of conjugation system. However, **IDT-2BM** has more D-A characteristics due to the reduced presence of donating groups. The presence of weaker acceptor of methyl-3-thiophenecarboxylate groups in **IDT-3MT** has mainly affected to LUMO energy level, which exhibited deeper LUMO of -4.16 eV relative to that of **IDT-T** and **IDT-DPP-CN** with LUMO value of - 4.01eV and 3.91 eV respectively. In terms of HOMO energy level, the **IDT-DPP-CN** displayed a higher HOMO level by -0.56 eV and -0.45 eV for **IDT-3MT** and **IDT-T** respectively. Overall, these NFAs exhibited relatively comparable behaviour to that of NFAs using **IDTT** core in **Chapter 3**. Also, it is apparent that changing the donor units from **IDTT** to **IDT** does not modify significantly on the electronic properties of the resulting acceptors.

Table 4. 2: The electrochemical properties of **IDT-DPP-PH, IDT-DPP-PHT, IDT-DPP-CN and IDT-DPP-INIC**

Acceptor	$E^{(onset-ox)}$ (volts)	$E^{(onset-red)}$ (volts)	HOMO (eV)	LUMO (eV)	Eg^{elect} (eV)
IDT-DPP-PH	0.54	-1.37	-5.26±0.009	-3.34±0.005	1.91±0.011
IDT-DPP-PHT	0.50	-1.35	-5.21±0.006	-3.38±0.01	1.83±0.023
IDT-DPP-CN	0.48	-1.12	-5.20±0.01	-3.60±0.003	1.60±0.003
IDT-DPP-INIC	0.41	-0.80	-5.12±0.008	-3.91±0.009	1.21±0.001

4.2.4 Thermal properties

The thermal characteristics of **IDT-DPP-PH**, **IDT-DPP-PHT**, **IDT-DPP-CN** and **IDT-DPP-INIC** were investigated *via* TGA under inert condition using a heating rate of 10°C/min. **Figure 4.6** demonstrates the TGA thermo diagrams of these NFAs and the thermal data is summarised in **Table 4.3**. All compounds exhibited great thermal stability with onset decomposition temperature T_d higher than 380°C. The melting points of these NFAs were not recorded until above 380°C. DSC does not show any glass transition for all four acceptors.

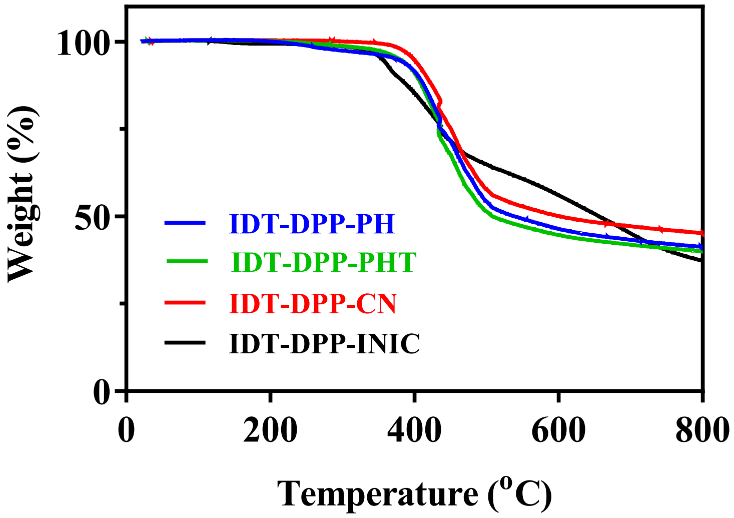

Figure 4. 6: **The TGA curves of IDT-DPP-PH**, **IDT-DPP-PHT**, **IDT-DPP-CN** and **IDT-DPP-INIC**.

Table 4. 3: The thermal data of **IDT-DPP-PH, IDT-DPP-PHT, IDT-DPP-CN** and **IDT-DPP-INIC**

Acceptors	T_d (°C)
IDT-DPP-PH	383
IDT-DPP-PHT	382
IDT-DPP-CN	385
IDT-DPP-INIC	388

T_d: decomposition temperature.

4.2.5 Photovoltaic properties

The OSC devices of the four NFAs were fabricated following the similar structures in described **Chapter 3**. (ITO/PEDOT) (PSS)/ active layer/PFN-Br/Ag to investigate photovoltaic performance of PBDB-T-NFAs. The fullerene free acceptors have been investigated and an inverted stack of (ITO/ZnO/Active Layer/MoO_3/Ag) has been used in attempts to fabricate OSC devices with a donor of P3HT. **Figure 4.7** shows the energy level of the donors and four NFAs. The PEC of PV devices was very poor as in the NFAs **Chapter 3**. The low PCE for all acceptors is suggested due to the aforementioned reasons such as non-optimal energy offset, absorption or morphology of donor acceptors blend. The study of PV performance of four NFAs is still in ongoing to improve the PCE.

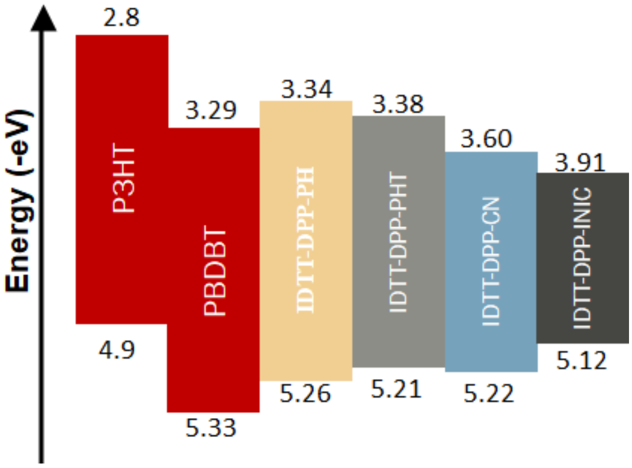

Figure 4.7: The energy level of the donors and four NFAs.

4.3 Conclusion

Four fullerene – free acceptor molecules were designed and synthesised *via* Stille coupling for **IDT-DPP-PH, IDT-DPP-PHT** and *via* Knoevenagel condensation reaction for **IDT-DPP-CN**, **IDT-DPP-INIC**, where **IDT** was used as the donor unit and four different **DPP** monomers as acceptors moieties. These fullerene-free acceptors showed absorption regions between 350 nm to 950 nm with a low optical band gap value of 1.42 eV, 1.43 eV, 1.39 eV and 1.29 eV, respectively. It is assumed that the acceptors form a more coplanar structure in the solid-state, resulting in the promotion of π-π stacking. These acceptors are soluble in common organic solvents at an elevated temperature. The electrochemical properties of these NFAs were investigated, and the location of the HOMO level for **IDT-DPP-PH, IDT-DPP-PHT** and **IDT-DPP-CN** do not show a noticeable change, with values of -5.25 eV, -5.21 eV and -5.20 eV, respectively. It may be attributed to the similarity of the conjugation backbone of these acceptors. However, the LUMO level does not show a significant change in **IDT-DPP-PH, IDT-DPP-PHT**, while is smaller in **IDT-DPP-CN** with -5.60 eV arising from the weaker acceptor of malononitrile, which downshifts the LUMO level. **IDT-DPP-INIC** demonstrates the deepest HOMO/LUMO energy levels of all the acceptors with -5.12 / -3.91 eV, resulting from the strong electron deficient of **INIC**, which is responsible for low lying of energy levels. TGA revealed that these NFAs have thermal stability with onset decomposition above 380°C. All acceptors exhibited poor PCE in OSC devices. However, the investigation is still in progress to develop the PCE.

Chapter (V): Conclusions

5.1 Conclusion

The motivation of this thesis was devoted to prepare and characterize new small molecules based on non-fullerene acceptors with low band gap in A-D-A structure for organic photovoltaic devices. The objectives behind the synthesis of non-fullerene acceptors stemmed from the advantage of addressing the shortcoming of fullerenes disadvantages. The work presented in **Chapter 2, Chapter 3** and **Chapter 4** explores the objective of designing the 3D small molecule acceptors using the spiro structures of **IDTT** and **IDT** as a electron donor moities linked with electron-deficient molecules such as **TPD** and **DPP** to regulate the HOMO and LUMO energy levels. The idea of employing these spiro compounds is to produce small molecules with highly rigid conjugated backbone to facilitate the charge mobility and prevent the self-aggregation and resulted in enhancing the solubility characteristics of these non-fullerene acceptors. The main findings of the thesis are as following:

In Chapter II, we designed and prepared three novel NFAs, **IDTT-TPD-PHT, IDTT-TPD-CN** and **IDTT-TPD-INIC.** In these three acceptors, the **IDTT** fused ring as a donor, and three different derivatives of **TPD** moieties with phenylthiophene, malononitrile, and 2-(3-Oxo-2,3-dihydro-1H-inden-1-ylidene)malononitrile. Flanking the **IDTT** with various electron withdrawing groups can help to ascertain the influence of these acceptors. Moreover, this would serve to understand the consequences of incorporating these TPD deficient electrons units into optical, electrochemical and thermal properties of the resulting NFAs. The **IDTT-TPD-INIC** possessed a lack of solubility, which may be due to having insufficient solubilising substituents on the **TPD** monomer moiety. **IDTT-TPD-PHT, IDTT-TPD-CN** and **IDTT-TPD-INIC** exhibit strong absorption, ranging from around 350 nm to 750 nm with a molar extinction coefficient of $1.3 \times 10^5 M^{-1} cm^{-1}$, $7.6 \times 10^4 M^{-1} cm^{-1}$ and $9.7 \times 10^4 M^{-1} cm^{-1}$ respectively. Furthermore, the **IDTT-TPD-PHT** showed the highest optical band gap of 2.03 eV. However, **IDTT-TPD-CN** and **IDTT-TPD-INIC** displayed lower optical band gaps of 1.75 eV and 1.55 eV. The electrochemical properties of the three NFAs were investigated; it was demonstrated that the HOMO level of **IDTT-TPD-PH** (-5.36 eV) is higher than acceptors **IDTT-TPD-CN** (-5.30 eV) and **IDTT-TPD-INIC** (-5.26 eV). However, the LUMO level **IDTT-TPD-INIC** is -3.89 eV, which is significantly lower than **IDTT-TPD-CN** and **IDTT-TPD-PH** with **a** LUMO level of -3.64 eV and -3.22 eV, respectively. Employing electron withdrawing units such as malononitrile and **INIC** could possibly downshift the LUMO level, but phenylthiophene is a donating group that mainly affects the HOMO, resulting in the larger HOMO level. The LUMO level of **IDTT-TPD-INIC** is lower than the LUMO level of **IDTT-TPD-CN,** suggesting the withdrawing unit of **INIC** is stronger compared to malononitrile, leading to a downshift of the LUMO level. These NFAs exhibited high thermal stability with onset decomposition temperatures (Td) around 347°C. The solar cell devices of three NFAs have shown a very low PCE. However, the photovoltaic performance device based on **IDTT-TPD-PHT** as donor showed a PCE around 1%. In addition, the investigation is still in progress to improve solar cell performance.

In Chapter III, we designed and prepared four new low bandgaps NFAs materials denoted **IDTT-DPP-PH, IDTT-DPP-PHT, IDTT-DPP-CN,** and **IDTT-DPP-INIC** with an A-D-A molecular architecture, in which the **IDTT** spiro fused ring used as an electron donating molecule and four different withdrawing **DPP** moieties used as terminal groups. The **IDTT-DPP-PH, IDTT-DPP-PHT** small molecules were synthesised *via* Stille coupling, whereas the **IDTT-DPP-CN,** and **IDTT-DPP-INIC** acceptors were prepared *via* Knoevenagel condensation reaction. The UV-Vis of all theses NFAs displayed good absorption in the wavelength range from 350 nm to 900 nm, which is comparable with the maximum solar photon flux (300- 800 nm). Furthermore, these NFAs showed a low optical bandgap ranging from 1.43 eV to 1.28 eV. It is hypothesised that the NFAs adopt a better coplanar structure in the solid-state leading to developing $\pi - \pi$ interchain stacking. In comparison to **IDTT-DPP-PH,** the increase to the conjugation backbone by adding a thiophene ring into **IDTT-DPP-PHT** acceptor does not exert a significant effect in the optical properties. In terms of electrochemical properties, the HOMO energy level of **IDTT-DPP-PH, IDTT-DPP-PHT** and **IDTT-DPP-CN** are similar. Extending the π-conjugation in **IDTT-DPP-PHT** and **IDTT-DPP-CN** has a small influence on the resulting energy levels. However, the replacement of phenyl group of **IDTT-DPP-PHT** by weaker electron deficient malononitrile significantly lowers the LUMO to -3.60 eV. The malononitrile was replaced with the stronger electron accepting **INIC**, which has a noticeable effect not only on the LUMO level but also on HOMO by downshifting the energy level to -5.11/-3.91 eV. The high onset thermal decomposition of these NFAs is above 380°C indicating excellent thermal stability. The solar cell devices have shown a very low PCE, but the investigation is still in progress to improve solar cell performance.

In Chapter IV, four fullerene – free acceptors molecules were designed and synthesised *via* Stille coupling for **IDT-DPP-PH, IDT-DPP-PHT** and *via* Knoevenagel condensation reaction for **IDT-DPP-CN**, **IDT-DPP-INIC**, where **IDT** was used as the donor unit and four different **DPP** monomers as acceptors moieties. These fullerene-free acceptors showed absorption regions between 350 nm to 950 nm with a low optical band gap value of 1.42 eV, 1.43 eV, 1.39 eV and 1.29 eV, respectively. It is assumed that the acceptors form a more coplanar structure in the solid-state, resulting in the promotion of π-π stacking. These acceptors are soluble in common organic solvents at an elevated temperature. The electrochemical properties of these NFAs were investigated, and the location of the HOMO level for **IDT-DPP-PH, IDT-DPP-PHT** and **IDT-DPP-CN** do not show a noticeable change, with values of -5.25 eV, -5.21 eV and -5.20 eV, respectively. It may be attributed to the similarity of the conjugation backbone of these acceptors. However, the LUMO level does not show a significant change in **IDT-DPP-PH, IDT-DPP-PHT**, while is smaller in **IDT-DPP-CN** with -5.60 eV arising from the weaker acceptor of malononitrile, which downshifts the LUMO level. **IDT-DPP-INIC** demonstrates the deepest HOMO/LUMO energy levels of all the acceptors with -5.12 / -3.91 eV, resulting from the strong electron deficient of **INIC**, which is responsible for low lying of energy levels. TGA revealed that these NFAs have thermal stability with onset decomposition above 380°C. All acceptors exhibited poor PCE in OSC devices. However, the investigation is still in progress to develop the PCE.

5.2: Future work

In this thesis, a series of non-fullerene small molecules have been designed and prepared as electron acceptor components for organic solar cells application. Different electron acceptors have been successfully synthesised based on the spiro compounds of **IDTT** and **IDT** as donor units and various derivatives of **TPD** and **DPP** as electron deficient units. On the other hand, there is an opportunity for further study of the effect of linking various withdrawing groups to the donor units. Moreover, there is an opportunity to design and synthesise novel non-fullerene acceptors based on a wide range of electron withdrawing pigments, for instance, furan flanked diketopyrrolopyrrole, perylene diimide, benzonthiadiazole.

Furthermore, it is beneficial to formulate novel polymers as donors as it is imperative to maintain similar functions to the originals in BHJ as it will lead to the enhancement of organic solar cell devices. The morphology of the blend plays an important role in PV devices. In terms of future study, it would be worth investigating the influence of the chemical structure on the morphology for better development of OPV devices.

There is also a room of incorporating different alkyl groups, which can ensure the new materials to be soluble in common organic solvents. Generally, the insertion of large side chains on the backbone of conjugated small molecules can enhance the solubility but decreases the π−π interchain interaction, resulting in lower performance of the solar cell device. As a result, the natural properties of side chains are an essential component in OSCs properties, and it has to be considered in the design of new small molecules materials. It is proposed that upon engineering new small molecules, the aromatic side-chain including benzene/thiophene derivatives can be attached to enhance the π−π interchain interaction and charge transportation.

Furthermore, the introduction of a fluorine atom into the backbone of NFAs and polymers is suggested to improve several parameters of OSCs such as morphology, tune carrier charge transport and deepen the HOMO/LUMO level and molecular organisation, which can ultimately enhance the PCE of the solar cell devices. As future work, it is proposed to incorporate different degrees of fluorine atoms into **IDTT-DPP-INIC, IDT-DPP-INIC** and other acceptors.

Moreover, there is an opportunity to flank the donor units with various high electron affinities groups such as 3-ethylrhodanine, 3-diethyl-2-thiobarbituric acid, 2-(1,1- dicyanomethylene) rhodamine, 1,3-diethyl-2-thiobarbituric acid and others, Ultimately, these substances are beneficial in that they can efficiently modify the energy consumption, absorb small molecules and essentially enhance the yield from the solar cell devices.

Chapter (VI): Experimental Section

6.1. General procedures

6.1.1 Reagents and Solvents

All chemicals purchased from the chemical suppliers were used as received unless otherwise stated. Dry solvents were utilised for reactions unless otherwise stated. The majority, including diethyl ether, dimethylformamide, chloroform, toluene, hexane, and tetrahydrofuran, were obtained using the Grubbs solvent purification system.

6.1.2 Nuclear Magnetic Resonance Spectra

^{1}H NMR and ^{13}C NMR spectra were recorded on a Bruker 250MHz, AMX400 400 MHz, or DRX 500 MHz NMR spectrometer 22 °C in chloroform-d_1, DMSO-d_6, acetone-d_6 solution. Chemical shifts were recorded in ppm relative to the internal standard (or δ). Observations given are as follows: s (singlet), d (doublet), dd (doublet of doublet), m (multiplet). Coupling constants were measured in Hz.

6.1.3 Thin Layer Chromatography (TLC)

TLCs (silica-coated aluminium plates) were used to detect the chromophore materials under an ultraviolet (UV) lamp. A solution of *p*-anisaldehyde was also sprayed onto the TLCs, followed by heating using a heat gun, to detect inactive UV materials.

6.1.3 Mass Spectral Data

Mass spectral data were obtained from the PerkinElmer Turbomass Mass Spectrometer Equipped with PerkinElmer PE-5MS Capillary Column for GCMS. Ms were obtained *via* chemical ionization (Cl) or electron impact (El).

6.1.4 Elemental Analysis

Elemental analyses were conducted using the PerkinElmer 2400 CHN Elemental Analyser for CHN analysis, and the Schöniger oxygen flask combustion method for sulphur and halides (anions). The weights submitted were 10 mg for CHN analysis and 10 mg for anion analysis.

6.1.5 Melting point

Melting points were collected using a Gallenkamp melting point apparatus. Samples were injected into open-ended capillary tubes and placed in the dedicated position on the apparatus.

6.1.6 Cyclic voltammetry

Cyclic voltammograms were collected from a Princeton Applied Research Model 263A Potentiostat/Galvanostat. All measurements were conducted in in CH_3CN containing 0.1 M tetrabutylammonium perchlorate ($n\text{-}Bu_4NClO_4$) as the supporting electrolyte at a potential scan rate of 100 mV^{-1}. The CV experiments were conducted in a three-electrode cell including reference electrode: Ag/Ag^+, a platinum wire as a counter electrode, and a platinum disc as a working electrode. Thin films of all acceptors from a solution of $CHCl_3$ were cast on a platinum electrode and the three electrodes were submerged in the prepared electrolyte during the measurements, followed by cycling in the electrolyte under an inert atmosphere. Ferrocene was employed as the reference redox system based on IUPAC's recommendations.

6.1.7 UV-Visible absorption spectroscopy analysis

A Hitachi U-2010 Double Beam UV/Visible Spectrophotometer was used to obtain UV–visible absorption spectra in diluted chloroform solutions. A quartz cuvette with a path length of 1 cm was used for the measurements. In the solid state, thin films of all acceptors were cast on quartz substrates using approximately 1 mg chloroform.

6.1.8 Thermogravimetric analysis

A TGA (PerkinElmer TGA-1 Thermogravimetric Analyser) was used to obtain thermogram curves of all acceptors. The samples were placed in a platinum pan conducted in an inert atmosphere at a heating rate of 10 °C/min.

6.2 Preparation of the Monomers

6.2.1 Synthesis of 1,2-bis (2,2-diethoxyethyl) disulfide (1) [280]

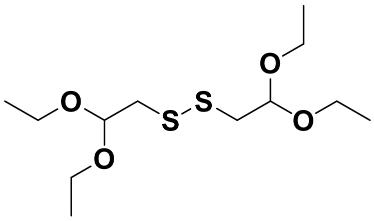

The procedures of Henssler and Matzger were followed to synthesize 1,2-bis (2,2-diethoxyethyl)disulphide. Sodium sulphide (118.75 g, 0.495 mol), sulphur (19.80 g, 0.617 mol), potassium iodide (4.97 g, 0.029 mol), and 2-bromo-1,1-diethoxyethane (95 mL, 0.617 mol) were mixed by stirring in ethanol (250 mL) and refluxed overnight. The ethanol was removed by distillation, and the residue was filtered to remove the salts, followed by washing with ethyl acetate. The filtrate was then washed three times with water. Subsequently, the aqueous phases were extracted with ethyl acetate, after which the organic phases were collected, washed with brine solution, and dried over anhydrous $MgSO_4$. After removing the solvent *in vacuo*, a yellow oily product was produced (65 g, 88%). ^1H NMR (400 MHz, $CDCl_3$) δ (ppm): 4.71 (t, *J* =5.5 Hz, 2H), 3.68 (m, 4H), 3.56 (m, 4H), 2.96 (d, *J* = 5.5 Hz, 4H), 1.22 (t, *J* =7.0 Hz, 12H). ^{13}C NMR (400 MHz, $CDCl_3$) δ (ppm): 101.4, 62.0, 42.9, 15.2. Mass calculated: $C_{12}H_{26}O_4S_2$: 298.46. Found (El); (m/z): 298.44.

6.2.2 Synthesis of 3-(2,2-diethoxy-ethylsulfanyl) thiophene (2) [281]

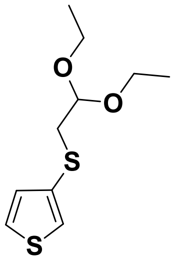

In a 500 ml dry round-bottom flask, 1.7 M *tert*-butyllithium in pentane (9.74 mL, 16.5 mmol) was added slowly to 3-bromothiophene (1.35 g, 8.28 mmol) in dry ether (200 ml) at -78 °C under an inert atmosphere. The reaction mixture was left to stir for 30 min at this temperature, followed by the slow addition of 1,2-bis (2,2-diethoxyethyl) disulphide

compound (1) (2.71 g, 9.10 mmol). The reaction was left to stir for a further 10 h at room temperature. The reaction was quenched with distilled water, and the organic phase was washed three times with aqueous NaOH (1 M) followed by a brine solution. The organic phase was dried over anhydrous $MgSO_4$, and the solvent was removed *in vacuo* to yield **compound (2)** (1.35 g, 70%). ^{1}H NMR (400 MHz, $CDCl_3$) δ (ppm): 7.31 (dd, *J* = 5.0, 3.0 Hz, 1H), 7.20 (dd, *J* = 3.0, 1.5 Hz, 1H), 7.06 (dd, *J* = 5.0, 1.5 Hz, 1H), 4.63 (t, *J* = 5.5 Hz, 1H), 3.66 (m, 2H), 3.54 (m, 2H), 3.05 (d, *J* = 5.5 Hz, 2H), 1.20 (t, *J* = 7.0 Hz, 6H). ^{13}C NMR (400 MHz, $CDCl_3$) δ (ppm): 131.6, 129.7, 126.1, 123.5, 101.6, 61.9, 38.6, 15.2. Mass calculated: $C_{10}H_{16}O_2S_2$: 232.36. Found (El); (m/z): 232.1.

6.2.3 Synthesis of thieno[3,2-b]thiophene (3) [281]

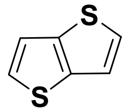

In a dry 500 ml round-bottom flask, (350 mL) dry ether was added to 3-(2,2-diethoxy-ethylsulfanyl) thiophene **compound (2)** (16.2 g, 70 mmol) under an inert atmosphere, followed by a quick addition of anhydrous Amberlyst 15 ion exchange resin (16.4 g, 77 mmol acid sites). The reaction was stirred and refluxed for 10 h. The reaction was then decanted and poured through a Buchner funnel fitted with filter paper. Next, the Amberlyst beads were collected, and fresh dry ether was added and refluxed to extract the residual product. The solution was collected with the reaction mixture upon decanting through the Buchner funnel. The solvent was evaporated *in vacuo*, and the crude product was purified by column chromatography on silica gel using petroleum ether as an eluent to yield thieno[3,2-b]thiophene **compound (3)** (6.95 g, 71%). M.P: 55°C. ^{1}H NMR (400 MHz, $CDCl_3$) δ (ppm): 7.25 (d, *J* = 5.0 Hz, 2H), 7.37 (d, *J* = 5.0 Hz, 2H). ^{13}C NMR (400 MHz, $CDCl_3$) δ (ppm): 139.4, 127.3, 119.3. Mass calculated: $C_6H_4S_2$: 140.22. Found (El); (m/z): 140.1; Elemental analysis (%): calculated for $C_6H_4S_2$: C, 51.40; H, 2.88; S, 45.73. Found: C, 51.22; H, 6.72; S, 27.22.

6.2.4 Synthesis of 2-(tributylstannyl) thieno[3,2-b]thiophene (4) [282]

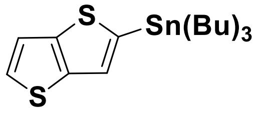

Synthesis of 2-(tributylstannyl)thieno[3,2-b]thiophene **(4)** was prepared using a procedure modified from Prim and Kirsch. In a 200 ml dry flask, 2.5 M *n*-butyllithium in hexane (2.86 mL, 7.2 mmol) was added gradually to a solution of thieno[3,2-b]thiophene **compound (3)** (1.01 g, 7.2 mmol) in dry THF (100 mL) at -78 °C under an argon atmosphere. After 2h of stirring at this temperature, tributylstannyl chloride (2.33g, 7.2 mmol) was added quickly, and the mixture was stirred for 1h at -78 °C. The reaction was then allowed to warm to room temperature and stirred overnight. Subsequently, the solvent was evaporated *in vacuo*. The crude product (2.94 g) was used in the subsequent step without any additional purification.

6.2.5 Synthesis of 1,4-benzendicarboxylic acid, 2,5 dithiono[3,2-b]thien-2-yl,1,4 diethyl ester (5) [283]

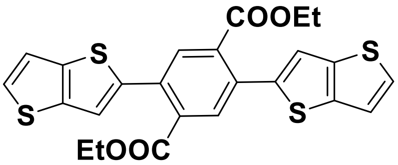

A mixture of diethyl 2,4-dibromoterephthalate (1.14 g, 3 mmol), 2-(tributylstannyl)thieno[3,2-b]thiophene (2.96 g, 6.90 mmol), Pd(PPh_3)$_4$ (0.74 g, mmol), and dry toluene (50 mL) was refluxed at 110 °C under an argon atmosphere overnight. The reaction mixture was poured into water and extracted with DCM. The organic layers were combined and dried over $MgSO_4$, and the solvent was evaporated *in vacuo*. The residue was purified by column chromatography on silica gel using a mixture of (petroleum ether/ethyl acetate, 20/1), producing a light yellow solid (2.2 g, 74%). ^{1}H NMR (400 MHz, $CDCl_3$) δ (ppm): 7.89 (s, 2H), 7.40 (d, *J* = 5.5 Hz, 2H), 7.29 (s, 2H), 7.28 (d, *J* = 5.5 Hz, 2H), 4.25 (q, *J* = 7.0 Hz, 4H), 1.13 (t, *J* = 7.0 Hz, 6H). ^{13}C NMR (400 MHz, $CDCl_3$) δ (ppm): δ: 167.4, 142.0, 139.9, 139.3, 134.1, 133.8, 132.1, 127.4, 119.4, 119.3, 61.8, 13.8. Mass calculated:

$C_{24}H_{18}O_4S_4$: 498.64. Found (El); (m/z): 498.51; Elemental analysis (%): calculated for $C_{24}H_{18}O_4S_4$: C, 57.81; H, 3.64; S, 25.72. Found: C, 57.12; H, 4.29; S, 25.10.

6.2.6 Synthesis of indacenodithieno[3,2-b]thiophene (IDTT) (6) [284]

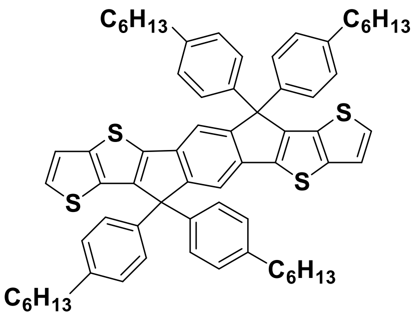

A freshly prepared Grignard reagent was synthesized by the addition of 4-hexyl-1-bromobenzene (3 g, 12.55 mmol) to a suspension of magnesium (361 mg, 15.06 mmol) in dry THF (20 mL) under an inert atmosphere, and the mixture was refluxed for 2h. Next, 4-hexyl-1- magnesium bromobenzene was added dropwise to a solution of 1,4-benzenedicarboxylic acid and 2,5-dithiono[3,2-b]thien-2-yl,1,4 diethyl ester **compound (5)** (250 mg, 0.502 mmol) in dry THF (10 mL) at room temperature. The reaction was refluxed overnight, before being cooled to room temperature and poured into water (150 mL). The mixture was extracted with DCM (3 × 100 mL). The organic layers were collected and dried over $MgSO_4$, and the solvent was evaporated. The yellow crude product was redissolved in (30 mL) acetic and (0.4 mL) sulphuric acid, and the mixture was refluxed for 3 h. After cooling to room temperature, the reaction mixture was poured into water (100 mL). The mixture was extracted with DCM (3 × 100 mL) and dried over $MgSO_4$. After evaporating the solvent, the residue was subjected to column chromatography on silica gel using a mixture of petroleum ether and DCM as an eluent (10/2) to produce a light yellow solid (173.7 mg, 34%); M.P > 350 °C.^{1}H NMR (400 MHz, $CDCl_3$) δ (ppm): 7.50 (s, 2H), 7.28 (d, J = 5.0 Hz, 2H), 7.25 (d, J = 5.0 Hz, 2H), 7.18 (d, J = 8.5 Hz, 8H), 7.07 (d, J = 8.5 Hz, 8H), 2.55 (t, J = 8.0 Hz, 8H), 1.60-1.53 (m, 8H), 1.35-1.29 (m, 24H), 0.86 (t, J = 6.5 Hz, 12H). ^{13}C NMR (400 MHz, $CDCl_3$) δ (ppm): 153.2, 145.9, 143.2, 141.7, 141.6, 140.3, 136.1, 133.8, 128.4, 128.1, 126.3, 120.3, 116.9, 62.9, 35.6, 31.7, 31.2, 29.2, 22.6, 14.1. (MALDI) m/z :M$^+$, calculated for $C_{68}H_{74}S_4$, 1019.58; found, 1019.38 Elemental analysis (%): calculated for $C_{68}H_{74}S_4$: C, 80.11; H, 7.32; S, 12.58. Found: C, 79.91; H, 7.35; S, 12.42.

6.2.7 Synthesis of dibromo indacenodithieno[3,2-b]thiophene (IDTT-Br$_2$) (7) (M1) [285]

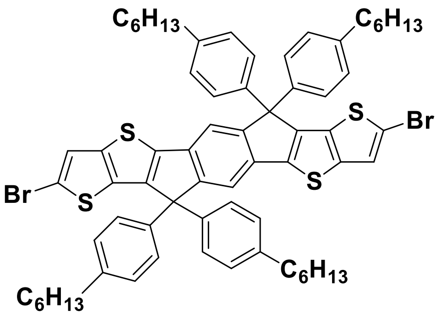

Under protection from the light, N-bromosuccinimide (**NBS**) (192.2 mg, 1.080 mmol) was added portion-wise to a solution of indacenodithieno[3,2-b]thiophene (**IDTT**) **compound (6)** (500 mg, 0.491 mmol) in chloroform (35 mL) at room temperature. The reaction was stirred overnight. Subsequently, the reaction mixture was poured into water (100 mL) and extracted with DCM. The organic layers were collected and dried over $MgSO_4$. The crude solid was purified *via* column chromatography on silica gel using a mixture of petroleum ether and DCM as an eluent (10/2) to produce a yellow solid (537 mg, 93%). M.P > 350 °C. ^{1}H NMR (400 MHz, $CDCl_3$) δ (ppm): 7.50 (s, 2H), 7.29 (s, 2H), 7.15 (d, *J* = 8.5 Hz, 8H), 7.1 (d, *J* = 8.5 Hz, 8H), 2.57 (t, *J* = 8.0 Hz, 8H), 1.65-1.57 (m, 8H), 1.40-1.25 (m, 24H), 0.86 (t, *J* = 7.0 Hz, 12H). ^{13}C NMR (400 MHz, $CDCl_3$) δ (ppm): 153.2, 146.3, 142.3, 142.0, 140,0 139.9, 135.9, 134.1, 128.6, 127.9, 123.0, 117.0, 112.5, 65.1, 35.6, 31.7, 31.3, 29.2, 22.6, 14.1. (MALDI) m/z :M$^+$, calculated for $C_{68}H_{72}Br_2S_4$, 1177.37; found, 1176.4; Elemental analysis (%): calculated for $C_{68}H_{72}Br_2S_4$: C, 69.37; H, 6.16; Br, 13.57; S, 12.58. Found: C,68.60; H,5.69; Br,12.81; S, 9.17. + 0.3 DCM.

6.2.8 Synthesis of 1-bromo-3,7-dimethyloctane (8) [286]

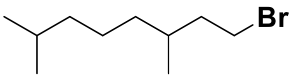

Triphenylphosphine (21.1 g, 80.5 mmol), 3,7-dimethyl-1-octanol (12.6 g, 67.7 mmol), and DCM (250 mL) were stirred until fully dissolved. **NBS** (14.2 g, 80.1 mmol) was then added portion-wise, and the reaction was left to stir at room temperature for 1 h. Subsequently, the reaction mixture was washed with saturated sodium hydrogen carbonate $NaHCO_3$ (3 × 180 mL), dried over $MgSO_4$, filtered, and the solvent removed *in vacuo*. The resulting product was charged in a round-bottom flask and stirred in petroleum ether for 30 min at room temperature. The mixture was then filtered off, and the solvent was evaporated *in vacuo*. The crude product was purified *via* column chromatography on silica gel using a mixture of petroleum ether as an eluent to yield 1-bromo-3,7-dimethyloctane as a colourless oil (12.42 g, 70 %). ^1H NMR (400 MHz, $CDCl_3$) δ (ppm): 3.44 (m, 2H), 1.89 (m, 2H), 1.69 (m, 1H), 1.55 (m, 1H), 1.31 (m, 3H), 1.17 (m, 3H), 0.90 (t, $J = 8.5$ Hz, 9H). ^{13}C NMR (400 MHz, $CDCl_3$) δ (ppm): 40.1, 39.2, 36.7, 32.4, 31.6, 27.9, 24.5, 22.7, 22.6, 18.9. EI-MS (m/z): [M]+ calculated for $C_{10}H_{21}Br$, 220.08; found, 220.08.

6.2.9 Synthesis of N-(3,7-dimethyloctyl) phthalimide (9) [287]

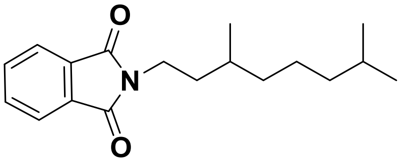

Potassium phthalimide (15 g, 80 mmol) was added to a solution of 1-bromo-3,7-dimethyloctane **compound (8)** (16.28 g, 74 mmol) in DMF (90 mL). The reaction was left to stir at 90 °C for 16 h. The reaction was then cooled to room temperature and poured into H_2O (60 mL). The product was extracted with DCM (3 × 200 mL). The organic phases were combined and washed with H_2O many times. The organic layer was dried over $MgSO_4$, and the solvent evaporated *in vacuo*. The product was purified *via* column chromatography using DCM as an eluent to obtain **compound (9)** as a colourless oil (18.96 g, 89 %). ^{1}H NMR (400 MHz, $CDCl_3$) δ (ppm): 7.82 (m, 2H), 7.72 (m, 2H), 3.81-3.66 (m,2H), 1.76-1.67 (m, 1H), 1.52-1.42 (m, 3H), 1.40-1.24 (m, 3H), 1.19-1.10 (m, 3H) 0.95 (d, *J* = 6.5 Hz, 3H), 0.83 (d, *J* = 6.5 Hz, 6H). ^{13}C NMR (400 MHz, $CDCl_3$) δ (ppm): 168.3, 133.7, 132.2, 123.1, 39.2, 36.9, 36.3, 35.3, 30.7, 27.9, 24.5, 22.6, 22.56, 19.8. EI-MS (m/z): [M]+ calculated for $C_{18}H_{25}NO_2$, 287.18; found, 287.1. Elemental analysis (%): C, 75.22; H, 8.77; N, 4.87; Found: C, 74.94; H, 8.13; N, 4.74.

6.2.10 Synthesis 3,7-dimethyloctan-1-amine (10) [288]

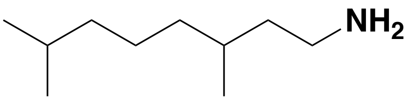

N-(3,7-dimethyloctyl)phthalimide **compound (9)** (3.01 g, 10.5 mmol) and hydrazine hydrate (51%, 2 mL, 32.5 mmol) were dissolved in ethanol (60 mL) and refluxed for 3 h. HCl conc. (1 mL) was then added, and the reaction mixture was refluxed for an additional hour and cooled to room temperature. The precipitate was filtered off and washed with H_2O. The ethanol was evaporated, and the crude product was dissolved in DCM (70 mL). The organic layer was washed with 10% NaOH (3 × 50 mL). The combined aqueous layer was extracted with DCM (3 × 100 mL). The organic layer was combined and washed with brine (2 × 100 mL), dried over $MgSO_4$, and the solvent removed *in vacuo* to obtain the product as a light brown oil, which was used in the next step without further purification (1.51 g, 87 %).

6.2.11 3-Ethyl-4-methyl-2-Aminothiophene-3,4-Dicarboxylate (11) [176]

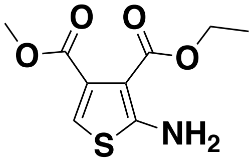

A mixture of methyl pyruvate (12.15 g, 0.119 mmol), (12.15 g, 0.119 mol), ethyl cyanoacetate (12.2 g, 0.119 mol), and sulphur (4.2 g, 0.131 mol) was placed in a three-necked round-bottom flask (500 mL) under an argon atmosphere and degassed for 5 min, followed by the addition of dry (60 mL) DMF. A solution mixture of triethylamine (28 mL) in dry DMF (60 mL) was then added dropwise, after which the reaction was allowed to stir at 50 °C overnight. After cooling to room temperature, the solution mixture was poured into water (300 mL) and left to crystallise for 3 days. The crystals were filtered and 3-ethyl-4-methyl-2-aminothiophene-3,4-dicarboxylate was produced as ivory-coloured crystals, and used in the next step without further purification (12.44 g, 46 %). M.P: 112 °C. ^{1}H NMR (400 MHz, $CDCl_3$) δ (ppm): 6.63 (s, 1H), 6.01 (s, br, 2H), 4.28 (q, *J* = 7.0 Hz, 2H), 3.86 (s, 3H), 1.33 (t, *J* = 7.0 Hz, 3H). ^{13}C NMR (250 MHz, $CDCl_3$) δ (ppm): 165.6, 164.6, 162.8, 132.4, 111.3, 104.9, 60.2, 52.3, 14.2. EI-MS (m/z): [M]+ calculated for $C_9H_{11}NO_4S$, 230.04; found, 230.10.

6.2.12 Synthesis of 2-bromothiophene-3,4-dicarboxylic acid (12) [176]

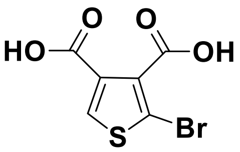

A diluted solution (10% aqueous, 100 mL) of HBr was added to (2.5 g, 10.91 mmol) of 3-ethyl 4-methyl 2-aminothiophene-3,4-dicarboxylate **compound (11)** in a 250 mL round-bottom flask. The solution mixture was allowed to stir for 30 min at room temperature and then cooled to 0 °C (ice bath), followed by the addition of (1.45 g, 21.94 mmol) of $NaNO_2$, and the reaction was stirred at 0 °C for 1 h. Subsequently, (4.95 g, 32.74 mmol) of Cu(I)Br was added portion-wise. Once this was complete, the reaction was heated to 80 °C for 3 h. After cooling to room temperature, the reaction mixture was washed with diethyl ether (10 × 70 mL) and the organic layer was washed with a saturated solution of sodium bicarbonate solution (5 × 70 mL) and water (5 × 100 mL). The organic layer was dried over $MgSO_4$ and concentrated *in vacuo*. The crude material was purified *via* column chromatography on silica gel using an eluent of (3:7) of ethyl acetate and petroleum ether to obtain a brown oily product (1.1 g, 17.46 %), which was then placed in a 100 mL round-bottom flask and diluted in 50 mL of NaOH (2 M). The reaction mixture was stirred at 95 °C overnight. After cooling to room temperature, the solution mixture was acidified to a pH of 1–2 by addition of HCl and then extracted with diethyl ether (10 × 90 mL). The organic layer was combined and dried over $MgSO_4$, and then evaporated to obtain a dark brown solid (0.95 g, 33%). M.P: 155 °C. ^1H NMR (400 MHz, acetone-d_6) δ (ppm): 8.30 (s, 1H); ^{13}C NMR (400 MHz, acetone-d6) δ (ppm): 164.0, 161.4, 136.0, 134.7, 132.5, 113.4; Mass calculated for $C_6H_3BrO_4S$: 251.05. Found (ES); (m/z): 250.9,; Elemental analysis (%): calculated for $C_6H_3BrO_4S$: C, 28.71; H, 1.20; Br, 31.83; S, 12.77. Found: C, 28.89; H, 1.96; Br, 28.34; S, 11.92.

6.2.13 Synthesis of 4-bromothieno[3,4-c]furan-1,3-Dione (13) [176]

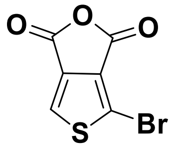

In a round-bottom flask (100 ml), (2.5 g, 7.6 mmol) of 2-bromothiophene-3,4-dicarboxylic acid **compound (12)** was added to acetic anhydride (40 ml). The reaction mixture was heated to 110 °C for 1 h while stirring. After cooling to room temperature, the acetic anhydride was evaporated to obtain a solid product, which was then washed with hexane and filtered to yield the target compound as a brown crystalline material (1.88 g, 6.01mmol, 80 %). M.P: 168 °C. ^1H NMR (400 MHz, $CDCl_3$) δ (ppm): 8.03 (s, 1H); ^{13}C NMR (400 MHz, $CDCl_3$) δ (ppm): 155.3, 154.9, 135.13, 133.5, 130.2, 117.7; EI-MS (m/z): [M]+ calculated for C_6HBrO_3S, 311.72; found, 311.79. Elemental analysis (%): calculated for $C_6H_1BrO_3S$: C, 30.92; H, 0.43; Br, 34.29; S, 13.76 found C, 29.12; H, 0.28; Br, 35.22; S, 13,13. +0.2 ether, 0.1 water.

6.2.14 Synthesis of 2-bromo-5-(3,7-dimethyloctyl)-4H-thieno[3,4c]pyrrole-4,6(5H)-dione (14)[289]

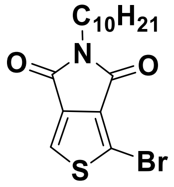

In a two-necked round-bottom flask (100 mL) under an argon atmosphere, 2-bromothieno[3,4-c]furan-1,3-dione (0.7 g, 3.0 mmol) **compound (13)** and 3,7-dimethyloctamine (0.519 mg, 3.33 mmol) **compound (10)** were dissolved in (10 mL) of dry THF. The resulting mixture was heated to 55 °C for 3 h. The reaction mixture was then cooled to room temperature and (3 mL) of thionyl chloride was added dropwise. The resulting mixture was heated to 60 °C for 4 h. After cooling to room temperature, the reaction solution was precipitated in methanol and filtered off. The crude product was then subjected to flash chromatography using DCM as an eluent (0.78 g, 1.73 mmol, 54 %). M.P: 84°C ^{1}H NMR (400 MHz, $CDCl_3$) δ (ppm): 7.71 (s, 1H); 3.71-3.65 (m, 2H), 1.75-1.43 (m, 4H), 1.40-1.11 (m, 6H), 0.99 (d, *J* =6.0 Hz, 3H), 0.87 (d, *J* =6.0 Hz, 6H). ^{13}C NMR (400 MHz, $CDCl_3$) δ (ppm): 161.6, 161.2, 136.8, 134.3, 126.5, 113.3, 39.2, 36.9, 35.2, 30.7, 27.9, 24.5, 22.7, 22.2, 19.3; EI-MS (m/z): [M]+ calculated for C_6HBrO_3S, 372.32; found, 372.32. Elemental analysis (%): calculated for $C_{16}H_{22}BrNO_2S$: C, 51.62; H, 5.96; Br, 21.46; N, 3.76; S, 8.61, found C, 51.99; H, 5.64; Br, 20.68; N, 3.44; S, 7.90.

6.2.15 Synthesis of 2-(tributylstannyl) 2-phenylthiophene (15)[290]

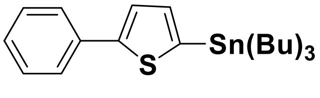

2-Phenylthiophene (1g, 6 mmol) was dissolved in dry THF (30 mL) in a 100 mL two-necked round-bottom flask under an argon atmosphere. The solution mixture was cooled to -78 °C and n-butyllithium (2.4 mL, 2.5 M in hexane) was added dropwise. The reaction was kept at -

78 °C for 2 h. Subsequently, the lithiated 2-phenylthiophene was quenched by a quick addition of tributyltin chloride (2.54 g, 7.8 mmol) and the reaction was stirred at this temperature for another hour. The reaction was then warmed to room temperature overnight. After evaporating the solvent, the crude product was used in the next step without further purification.

6.2.16 Synthesis of 2-phenyl thiophene-5-(3,7-dimethyloctyl)-4H-thieno[3,4-c]pyrrole-4,6(5H)-dione (TPD-PHT) (16) (M2)

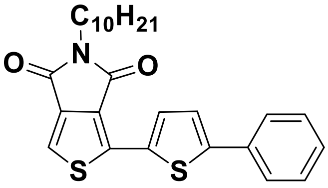

In a 100 ml two-necked round-bottom flask under an argon atmosphere, 2-bromo-5-(3,7-dimethyloctyl)-4H-thieno[3,4-c]pyrrole-4,6(5H)-dione (1g, 2.68 mmol) **compound (14)**, 2 (tributylstannyl) 2-phenylthiophene **compound (15)** (1.44 g, 3.22 mmol), and tetrakis(triphenylphosphine)palladium(0) Pd(PPh_3)$_4$ (0.155g, 0.134 mmol) were mixed and degassed for 5 min, before dry toluene (60 mL) was added to the mixture. The reaction was heated to 110 °C overnight. After cooling, water (200 mL) was added, extracted with dichloromethane (DCM) (3 × 100 mL), and dried over $MgSO_4$. The solvent was evaporated under reduced pressure, and the brown crude product was purified *via* column chromatography using a mixture of 10:1 of petroleum ether and dichloromethane to obtain a yellow solid product (0.88 g, 73%). M.P: 83 °C ^{1}H NMR (400 MHz, $CDCl_3$) δ (ppm): 8.01 (s, 1H), 7.67 (d, *J* = 7.5 Hz, 2H), 7.61 (s, 2H), 7.43 (t, *J* = 7.5 Hz, 1H), 7.38-7.35 (m, 2H), 3.70-3.66 (m, 2H), 1.73-1.42 (m, 4H), 1.38-1.13 (m, 6H), 0.98 (d, *J* =6.5 Hz, 3H), 0.88 (d, *J* =6.5 Hz, 6H); ^{13}C NMR (400 MHz, $CDCl_3$) δ (ppm): 162.9, 162.4, 147.6, 140.0, 137.5, 133.4, 131.8, 129.1, 128.5, 127.7, 126.1, 124.3, 122.1, 39.23, 37.04, 36.87, 35.46, 30.84, 27.94, 24.59, 22.62, 19.42; EI-MS (m/z): [M]+ exact mass calculated for $C_{26}H_{29}NO_2S_2$, 451.1634; Found, 451.1654; Elemental analysis (%):calculated for C_{26} $H_{29}NO_2S_2$: C, 69.14; H, 6.47; N, 3.10; S, 14.20 Found: C, 68.05; H; 6.61; N, 2.67; S, 12.53.

6.2.17 Synthesis of 2,2-bithiophene-5-carboxaldehyde (17) [291]

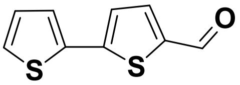

The synthesis procedure of 2,2-bithiophene-5-carboxaldehyde was followed as described. In a 100 mL round-bottom flask, 2,2-bithiophene (2.5 g, 15 mmol) was dissolved in dry THF (50 mL) under an argon atmosphere. The solution mixture was cooled to -78 °C and 1.6 M n-BuLi in hexane (9 mL) was added dropwise. The reaction was left to stir for 1 h. Subsequently, (3 mL, 39 mmol) of dimethylformamide was added slowly. The reaction was allowed to warm to room temperature and stir overnight. Water (10 mL) was added to quench the reaction, and then was acidified by adding (1 M) of HCl. The reaction mixture was then extracted with DCM (3 × 50 mL) and dried over $MgSO_4$. The solvent was evaporated, and the crude product was subjected to column chromatography using silica gel to obtain a red solid product (2.40 g, 87%). M.P: 83-85 °C ^{1}H NMR (400 MHz, $CDCl_3$) δ (ppm); 9.89 (1H, s); 7.70 (1H, d, *J* = 4.0 Hz) 7.40 (2H, d, *J* = 4.0 Hz), 7.28 (1H, d, *J* = 4.0 Hz), 7.12 (1H, dd, *J* = 4.5 Hz, 4.0 Hz); ^{13}C NMR (400 MHz, $CDCl_3$) δ (ppm): 182.6, 147.2, 137.4, 136.1, 128.4, 127.1, 126.2,124.3. Mass calculated: $C_9H_6OS_2$: 194.27, Found (El); (m/z): 194.0; Elemental analysis (%): calculated for $C_9H_6NOS_2$: C, 55.64; H, 3.11, S, 33.01, Found: C, 54.84; H, 2.98, S, 33.31.

6.2.18 Synthesis of 5-(tributylstannyl)- 2,2-bithiophene-5-carboxaldehyde (18) [290]

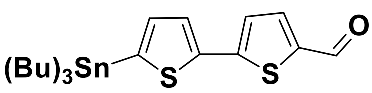

Compound (18) was synthesised following the modification procedure as described in the literature. In a 250 mL round-bottom flask, 2,2-bithiophene-5-carboxaldehyde **compound (17)** (1g, 5.14mmol) was dissolved in dry THF (60 mL) under an argon atmosphere. The reaction mixture was cooled to -78 °C, and N-methyl piperazine (0.626 mL, 5.66 mmol) was added, before n-butyllithium (2.23 mL, 2.5 M in hexane) was added dropwise. The reaction mixture was stirred at -78 °C for 20 min, and then was warmed to -20 °C for 20 min, followed by another addition of n-butyllithium (2.23 mL, 2.5 M in hexane) dropwise. The reaction was stirred at this temperature for 30 min, before tributyltin chloride (1.66 mL, 6.16 mmol) was added. Subsequently, the cooling bath was removed, and the reaction was left to stir overnight at room temperature. 1 M of HCl (40 mL) was added to quench the reaction, and the solvent was evaporated. The crude product was diluted with water and extracted with DCM. The collected organic layers were dried over $MgSO_4$. The solvent was rotationally evaporated *in vacuo* to obtain a dark red liquid (1.95 g, 83%). ^1H NMR (400 MHz, $CDCl_3$) δ (ppm): 9.88 (s, 1H), 7.69 (d, J = 4.0 Hz, 1H), 7.50 (d, J = 3.5 Hz, 1H), 7.27 (d, J = 3.95 Hz, 1H), 7.18 (d, J = 3.6 Hz, 1H), 1.64-1.55 (m, 6H), 1.37 (m, 6H), 1.14-1.11 (m, 6H), 0.96 (t, J = 7.0 Hz, 9H). ^{13}C NMR (400 MHz, $CDCl_3$) δ (ppm): 182.6, 147.6, 141.3, 140.9, 137.5, 136.5, 127.3, 124.0, 29.0, 27.5, 14.1, 11.0. Mass calculated: $C_{21}H_{32}OS_2Sn$: 484.09, Found (El); (m/z): 485.10.

6.2.19 Synthesis of 5'-(5-(3,7-dimethyloctyl)-4,6-dioxo-5,6-dihydro-4*H*-thieno[3,4-*c*]pyrrol-1-yl)-[2,2'-bithiophene]-5-carbaldehyde (TPD-CHO) (19) (M3)

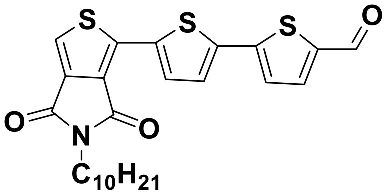

In a 100 ml round-bottom flask under an argon atmosphere, 2-bromo-5-(3,7-dimethyloctyl)-4H-thieno[3,4-c]pyrrole-4,6(5H)-dione (0.5g, 1.34 mmol) **compound (14)**, (0.77 g, 1.16 mmol) of 5-(tributylstannyl)-2,2-bithiophene-5-carboxaldehyde **compound (18)** and (7.75 mg, 67 mmol) of tetrakis(triphenylphosphine)palladium(0) $Pd(PPh_3)_4$ were mixed and degassed for 5 min, before dry toluene (40 mL) was added to the mixture. The reaction was heated to 110 °C overnight. After cooling, it was then added to water (200 ml), extracted with DCM (3 × 100 mL), and dried over $MgSO_4$. The solvent was evaporated, and the brown crude product was washed with methanol to obtain a dark red solid product (0.45 g, 70%). M.P: 119 °C ^1H NMR (400 MHz, $CDCl_3$) δ (ppm): 9.90 (s, 1H), 7.94 (d, J = 4.0 Hz, 1H), 7.71 (d, J = 4.0 Hz, 1H), 7.67 (s, 1H), 7.36 (d, J = 4.0 Hz, 2H), 3.71-3.65 (m, 2H), 1.75-1.43 (m, 4H), 1.40-1.11 (m, 6H), 0.99 (d, J =6.5 Hz, 3H), 0.87 (d, J =6.5 Hz, 6H). ^{13}C NMR (400

MHz, $CDCl_3$) δ (ppm): 182.5, 162.8, 162.6, 145.6, 138.6, 137.6, 137.6, 133.8, 128.7, 127.0, 125.2, 122.9 39.2, 37.0, 36.9, 35.4, 30.8, 27.9, 24.6, 22.7, 22.6, 19.4. Exact mass calculated: $C_{25}H_{27}NO_3S_3$: 485.1148 Found (El); (m/z): 485.1162; Elemental analysis (%): calculated for $C_{25}H_{27}NO_3S_3$: C, 61.83; H, 5.60; N, 2.88, S,19.80, Found: C, 60.88; H, 5.14; N, 2.14; S, 21.02.

6.2.20 Synthesis of 2-(3-oxo-2,3-dihydro-1H-inden-1-ylidene)malononitrile (20) [292]

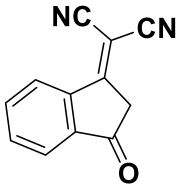

In a 250 ml round-bottom flask, indane-1,3-dione (4 g, 27.36 mmol) and malononitrile (3.6 g, 132.12 mmol) were dissolved in absolute ethanol (60 mL). The solution mixture was stirred at room temperature followed by the addition of (2.68 g, 32.8 mmol) of sodium acetate while stirring. The reaction was left to stir for 40 min. Subsequently, (260 mL) of H_2O was added to the mixture, and the reaction was then acidified to pH 1–2 by adding concentrated hydrochloric acid dropwise. The precipitate was then filtered through a Buchner funnel and washed with a copious amount of H_2O. The solid residue was recrystallized with acetic acid and once with ethanol to produce the target product as a red solid (4.5 g 85%). M.P: 231 °C. ^{1}H NMR (400 MHz, $CDCl_3$) δ (ppm): 8.65 (d, J = 7.5 Hz, 1 H), 8.11 (d, J = 7.5 Hz, 1 H), 7.93-7.84 (m, 2H), 3.77 (s, 2 H), ^{13}C NMR (400 MHz, $CDCl_3$) δ (ppm): 195.2, 166.3, 142.58, 140.6, 136.4, 136.0, 126.2, 125.1, 112.3, 79.6, 43.4, Mass calculated for $C_{12}H_6N_2O$: 194.04 Found (El); (m/z): 195.10; Elemental analysis (%): calculated for $C_{12}H_6N_2O$: C, 74.22; H, 3.11; N, 14.43. Found: C, 73.91; H, 3.20; N, 14.36.

6.2.21 Synthesis of indacenodithieno[3,2-b]thiophene -Phenyl thiophene-5-(3,7-dimethyl octyl)-4H-thieno[3,4c]pyrrole-4,6(5H)-dione. (IDTT-TPD-PHT) (21)

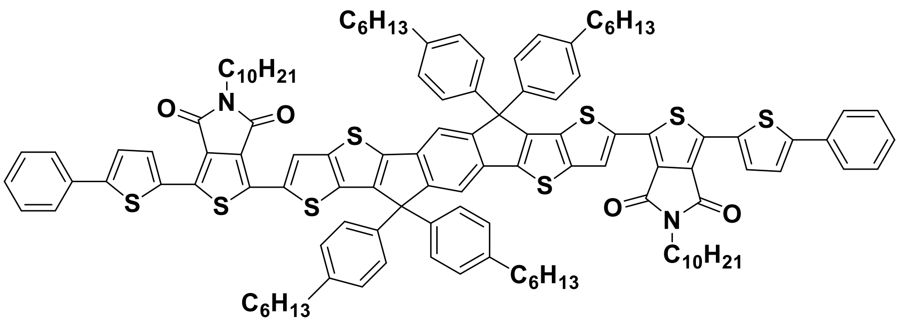

The **IDTT-Br$_2$ compound (7)** (0.2 g, 0.169 mmol), **TPD-PHT compound (16)** (0.3 g, 0.679 mmol), $CsCO_3$ (0.33 g, 1.01 mmol), $Pd_2(dba)_3$ (7 mol %, 10.8 mg, 0.0118 mmol), P(o-OMePh)$_3$ (7 mol %, 4.19 mg, 0.0118 mmol,), and pivalic acid (17.3 mg, 0.169 mmol) were weighed and placed in a top-sealed tube with a magnetic stir bar. The tube was degassed and purged with argon for 5 min, after which 2 mL of dry THF was added. The reaction mixture was degassed again and then left to stir at 100 °C overnight. The reaction was then cooled to room temperature, poured into water, and extracted with DCM (3 × 100 mL). The organics were collected and dried over $MgSO_4$. The solvent was evaporated under reduced pressure. The crude solid was purified *via* column chromatography using silica gel and a mixture of (1:10) of ethyl acetate and petroleum ether, to obtain the desired product as a red solid (52%, 170 mg). M.P > 350 °C. ^{1}H NMR (400 MHz, $CDCl_3$) δ (ppm): 8.57 (s, 2H), 7.98 (d, *J* = 4.0 Hz, 2H), 7.65-7.60 (m, 5H), 7.58 (s, 2H), 7.41-7.30 (m, 7H), 7.29 (d, *J* = 4.0), 7.24 (d, *J* = 8.5, 8H), 7.17 (d, *J* = 8.43, 8H), 3.71 (m, 4H), 2.61 (t, *J* = 8.0 and 8.0, 8H), 1.80-1.47 (m, 18H), 1.42-1.26 (m, 34H), 1.01 (d, *J* = 6.0, 6H), 0.91-0.86 (m, 24H); ^{13}C NMR (400 MHz, $CDCl_3$) δ (ppm): 162.7, 162.5, 154.0, 147.7, 146.4, 146.3, 143.1, 142.1, 139.7, 136.8, 136.3, 136.0, 135.3, 133.3, 133.1, 132.0, 131.6, 131.0, 129.0, 128.7, 128.5, 128.3, 128.4, 128.0, 126.0, 124.3, 123.7, 117.4, 63.0, 39.6, 37.1, 35.6, 31.7, 31.3, 30.9, 29.2, 27.9, 35.6, 31.7, 24.6, 22.7, 22.6, 19.4, 14.1. (MALDI) m/z: M$^+$, calculated for $C_{120}H_{128}N_2O_4S_8$, 1918.83; found, 1917.83 Elemental analysis (%): calculated for $C_{120}H_{128}N_2O_4S_8$: C, 75.11; H, 6.72; N: 1.46, S,13.37. Found: C, 74.85; H, 6.84; N: 1.49; S, 11.97.

6.2.22 Synthesis of indacenodithieno[3,2-b]thiophene 5'-(5-(3,7-dimethyloctyl)-4,6 dioxo -5,6-dihydro-4*H*-thieno[3,4-*c*]pyrrol-1-yl)-[2,2'-bithiophene]-5-carbaldehyde (22)

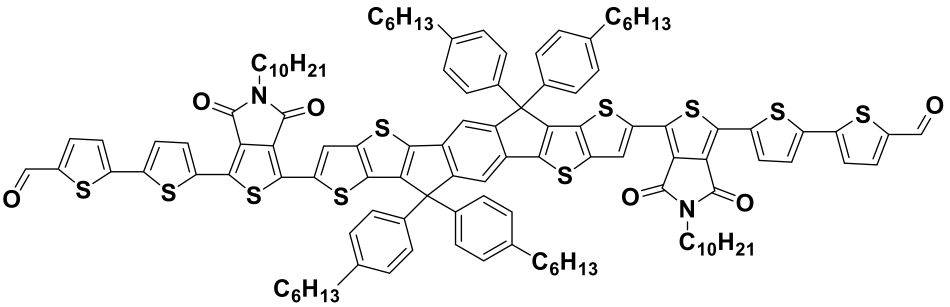

The same procedures used to prepare the **IDTT-TPD-PHT compound (21)** were followed to synthesise the compound **IDTT-TPD-CHO**. The **IDTT-Br$_2$ compound (7)** (0.1 g, 0.084 mmol), **TPD-CHO compound (19)** (0.165 g, 0.339 mmol), CsCO$_3$ (0.166 g, 0.509 mmol), Pd$_2$(dba)$_3$ (7 mol %, 5.4 mg, 0.005 mmol), P(o-OMePh)$_3$ (7 mol %, 2.10 mg, 0.005 mmol), and pivalic acid (7.8 mg, 0.084 mmol) were weighed and placed in a top-sealed tube with a magnetic stir bar. The tube was degassed and purged with argon for 5 min, before 2 mL of dry THF was added. The reaction mixture was then left to stir at 100 °C overnight. The reaction was then cooled to room temperature, poured into water, and extracted with CHCl$_3$ (3 × 100 mL). The organics were collected and dried over MgSO$_4$. The solvent was evaporated under reduced pressure. The crude solid was purified *via* column chromatography using silica gel and a (3:10) mixture of ethyl acetate and petroleum ether, to obtain the desired product as a red solid (62%, 104 mg). M.P > 350 °C. ^{1}H NMR (400 MHz, CDCl$_3$) δ (ppm): 9.91(s, 2H), 8.62 (s, 2H), 7.93 (d, *J* = 4.0, 2H), 7.71 (d, *J* = 3.97 Hz, 2H), 7.57 (s, 2H), 7.36 (t, *J* = 4.0 Hz and 4.0 Hz), 7.21 (d, *J* = 8.5 Hz, 8H), 7.15 (d, *J* = 8.5 Hz, 8H), 3.77-3.67 (m, 4H), 2.59 (t, *J* = 4.0 Hz and 8.0 Hz, 8H), 1.78-1.46 (m, 18H), 1.40-1.16 (m, 34H), 1.01 (d, *J* = 6.0 Hz, 2H), 0.92-0.84 (m, 24H); (MALDI) m/z: M$^+$, calculated for $C_{118}H_{124}N_2O_6S_{10}$, 1986.90; found, 1986.90 Elemental analysis (%): calculated for $C_{118}H_{124}N_2O_6S_{10}$: C, 71.33; H, 6.29; N,1.41; S, 16.14. Found: C, 69.41; H, 6.37; N,1.23; S, 15.97

6.2.23 Synthesis of indacenodithieno[3,2-b]thiophene 5'-(5-(3,7-dimethyloctyl)-4,6-dioxo-5,6-dihydro-4*H*-thieno[3,4-*c*]pyrrol-1-yl)-[2,2'-bithiophene]-5-carbaldehyde malononitrile (23)

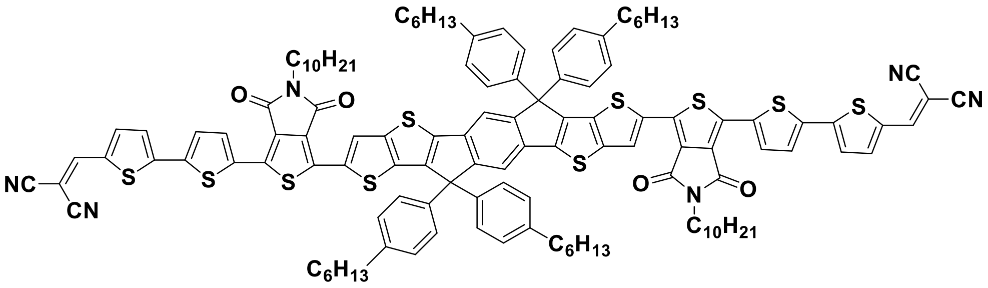

In a dry 100 ml round-bottom flask, the **IDTT-TPD-CHO (22)** compound (150 mg, 0.075 mmol) and malononitrile (99.7 mg, 1.51 mmol) were placed and degassed for 5 min following the addition of chloroform (50 mL) and pyridine (1 mL) at room temperature. The reaction mixture was then refluxed overnight. The reaction was cooled to room temperature and extracted with chloroform. The combined layers were then dried over magnesium sulphate ($MgSO_4$) and the solvent was evaporated under reduced pressure. The crude product was washed with methanol and filtered through a Buchner funnel. Subsequently, the product of compound IDTT-TPD-CN was obtained as a black-purple solid (75 mg, 47%). M.P > 350 °C. ^{1}H NMR (400 MHz, $CDCl_3$) δ (ppm): 8.61 (s, 2H), 7.93 (d, *J* = 4.0 Hz, 2H), 7.75 (s, 2H), 7.65 (d, *J* = 4.0 Hz, 2H), 7.58 (s, 2H), 7.42 (d, *J* = 4.0 Hz, 2H), 7.36 (d, *J* = 4.0 Hz, 2H), 7.21 (d, *J* = 8.5 Hz, 8H), 7.15 (d, *J* = 8.5 Hz, 8H) 3.77-3.67 (m, 4H), 2.59 (t, *J* = 4.0 Hz and 8.0 Hz, 8H), 1.78-1.46 (m, 18H), 1.40-1.16 (m, 34H), 1.01 (d, *J* = 6.0, 6H), 0.92-0.84 (m, 24H); (MALDI) m/z :M^+ , calculated for $C_{124}H_{124}N_6O_4S_{10}$, 2082.99; found, 2084.1 Elemental analysis (%): calculated for $C_{124}H_{124}N_6O_4S_{10}$: C, 71.50; H, 6.00; N; 4.03; S, 15.39. Found: C, 66.80; H, 5.37; N; 4.53; S, 17.22.

6.2.24 Synthesis of indacenodithieno[3,2-b]thiophene 5'-(5-(3,7-dimethyloctyl)-4,6-dioxo-5,6-dihydro-4*H*-thieno[3,4-*c*]pyrrol-1-yl)-[2,2'-bithiophene]-5-carbaldehyde 2-(3-oxo-2,3dihydroinden-1-ylidene)malononitrile (24)

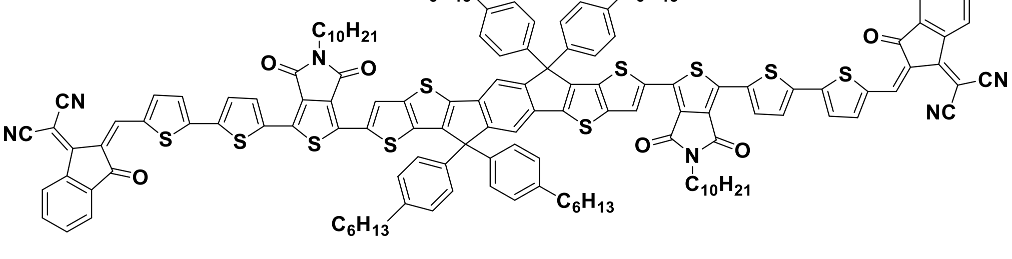

The same procedures used to prepare the **IDTT-TPD-CN compound (23)** were followed to synthesize the **IDTT-TPD-INIC compound (24)**. In a dry 100 mL round-bottom flask, the **IDTT-TPD-CHO compound (22)** (100 mg, 0.206 mmol) and 2-(3-oxo-2,3dihydroinden-1-ylidene)malononitrile **compound (20)** (44 mg, 0.226 mmol) were placed and degassed for 5 min following the addition of chloroform (50 mL) and pyridine (1 mL) at room temperature. The reaction mixture was then refluxed overnight. The reaction was cooled to room temperature and extracted with chloroform. The combined layers were then dried over $MgSO_4$, and the solvent was evaporated under reduced pressure. The crude product was washed with methanol and filtered through a Buchner funnel. Subsequently, the product of compound **IDTT-TPD-INIC** was obtained as a black-purple solid (0.11 mg, 81%). M.P > 350 °C. MALDI m/z: M^+, calculated for $C_{142}H_{132}N_6O_6S_{10}$, 2339.25; found, 2339.30 Elemental analysis (%): calculated for $C_{142}H_{132}N_6O_6S_{10}$: C, 72.91; H, 5.69; N; 3.59; S, 13.71. Found: C, 70.14; H, 5.49; N; 3.84; S, 13.45.

6.2.25 Synthesis of indacenodithieno[3,2-b]thiophene ditin (IDTT) (25) (M4) [293]

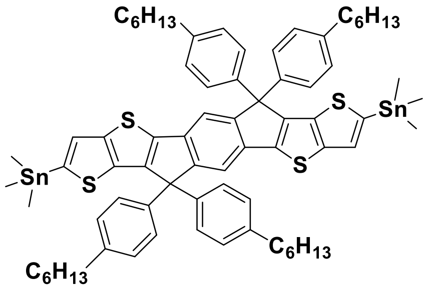

In a dry 100 ml two-necked round-bottom flask, **IDTT compound (6)** (200 mg, 0.098 mmol) was dissolved in anhydrous THF (20 mL) under an argon atmosphere. The solution was cooled to -78 °C, and (0.2 mL, 0.49 mmol) of n-BuLi 2.5 M in hexane was added dropwise. The reaction mixture was maintained at -78 °C for 1 h and then warmed to room temperature for 30 min. Subsequently, the mixture was cooled again to -78 °C, and (0.49 mL, 0.49 mmol) of trimethyltin chloride in hexane was added. The cooling bath was then removed, and the reaction was stirred overnight at room temperature. The resulting mixture was poured into water and extracted with diethyl ether (3 × 100 mL). The organic layers were collected and dried over $MgSO_4$, and the solvent was evaporated under reduced pressure. Subsequently, the precipitate was washed with ethanol to produce the desired compound as a yellow solid (240 mg, 91%). M.P > 350 °C. ^{1}H NMR (400 MHz, $CDCl_3$) δ (ppm): 7.46 (s, 2H), 7.30 (s, 2H), 7.19 (d, *J* = 8.5 Hz, 8H), 7.07 (d, *J* = 8.5 Hz, 8H), 2.55 (t, *J* = 8.0 Hz, 8H), 1.61-1.55 (m, 8H), 1.35-1.27 (m, 24H), 0.86 (t, *J* = 6.5 Hz, 12H), 0.37 (s, 18H). ^{13}C NMR (400 MHz, $CDCl_3$) δ (ppm): 153.0, 145.4, 143.7, 143.2, 141.5, 140.5, 140.3, 139.3, 136.2, 128.4, 128.1, 127.4, 116.8, 62.9, 35.6, 31.7, 31.2, 29.2, 22.6, 14.1, -8.1. (MALDI) m/z : M^+, calculated for $C_{68}H_{90}S_4Sn_2$: 1346,40; found, 1345.4 Elemental analysis (%): calculated for $C_{68}H_{72}S_4Sn_2$: C, 66.07; H, 6.74; S, 9.53. Found: C, 66.91; H, 6.94, S, 8.55.

6.2.26 Synthesis of diethyl 2,5-di(thiophene-2-yl)terephthalate (26) [294]

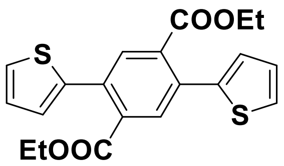

A mixture of diethyl 2,4-dibromoterephthalate (1 g, 2.56 mmol), 2-(tributylstannyl)thiophene (2.10 g, 5.64 mmol), and $Pd(PPh_3)_4$ (147 mg, 0.128 mmol) were placed in a dry 100 mL round-bottom flask under an argon atmosphere. Dry toluene (50 mL) was subsequently added and the reaction was left to reflux overnight at 110 °C. The reaction mixture was then cooled to room temperature, poured into water, and extracted with DCM (3 × 150 mL). The organic layers were combined and dried over $MgSO_4$, and the solvent was evaporated under reduced pressure. The crude solid was purified by column chromatography on silica gel using a mixture of petroleum ether and dichloromethane as an eluent (10:2) to obtain the product as a pale yellow solid (842 mg, 85%). M.P: 119-121°C ^{1}H NMR (400 MHz, $CDCl_3$) δ (ppm): 7.82 (s, 2H), 7.36 (dd, *J* = 5.0 Hz and 1.5 Hz, 2H), 7.09 (m, 2H), 7.06 (m, 2H), 4.21 (q, *J* = 7.0 Hz 4H), 1.14 (t, *J* = 7.0 Hz, 6H). ^{13}C NMR (400 MHz, $CDCl_3$) δ (ppm): 167.7, 140.5, 134.1, 133.5, 131.9, 127.4, 127.0, 126.5, 61.6, 13.8. Mass calculated: $C_{20}H_{18}O_4S_2$: 386.48. Found (El); (m/z): 386.45; Elemental analysis (%): calculated for $C_{24}H_{18}O_4S_4$: C, 62.16; H, 4.69; S, 16.59. Found: C, 62.12; H, 4.53; S, 16.66.

6.2.27 Synthesis of indacenodithiophene (IDT) (27) [295]

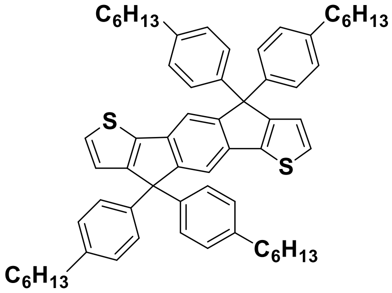

In a 100 mL dry two-necked round-bottom flask, 4-hexyl-1-bromobenezene (748 mg, 3.10 mmol) was dissolved in dry THF (10 mL), and the solution was degassed with argon. The solution was then cooled to -78 °C followed by the addition of *n*-butyllithium (2.5 M in hexane, 1.24 mL, 3.10 mmol) dropwise. The resulting mixture was stirred at this temperature for 1 h. Next, a solution of diethyl 2,5-di(thiophene-2-yl)terephthalate **compound (26)** (0.25 mL, 0.647 mmol) in dry THF was added dropwise to the reaction. After 1 h of stirring at -78 °C, the cooling bath was removed, and the reaction was left to stir at room temperature overnight. The reaction mixture was then poured into water and extracted with DCM (3 × 150 mL). The organic layers were combined and dried over $MgSO_4$, and the solvent was evaporated under reduced pressure. The residue was charged into a 100 ml round-bottom flask containing (15 mL) of acetic acid and (0.4 mL) of concentrated sulphuric acid to reflux for 3 h. This was then added to (50 ml) of water to quench the reaction, and extracted with DCM (3 × 75 mL). The organic layers were collected and dried over $MgSO_4$, and the solvent was evaporated under reduced pressure. The crude solid was purified by column chromatography on silica gel using a mixture of petroleum ether and DCM as an eluent (10:2) to obtain the target product as a yellow solid (416 mg, 71%). M.P > 350 °C. ^{1}H NMR (400 MHz, $CDCl_3$) δ (ppm): 7.44 (s, 2H), 7.26 (d, *J* = 5.0 Hz, 2H), 7.15 (d, *J* = 8.5 Hz, 8H), 7.08 (d, *J* = 8.5 Hz, 8H), 7.02 (d, *J* = 5.0 Hz, 2H), 2.57 (t, *J* =8.0 Hz, 8H), 1.58 (m, 4H), 1.31 (m, 28H), 0.88 (t, *J* = 6.5 Hz, 12H). ^{13}C NMR (400 MHz, $CDCl_3$) δ (ppm): 156.1, 153.6, 142.3, 141.6, 141.5, 135.3, 128.5, 128.1, 127.59, 123.3, 117.7, 62.9, 35.8, 31.9, 31.6, 29.4, 22.8,14.3. Mass calculated: $C_{64}H_{74}O_4S_2$: 907.42 Found (El); (m/z): 907.39; Elemental analysis (%): calculated for $C_{64}H_{74}O_4S_2$: C, 84.71; H, 8.22; S, 7.07. Found: C, 84.60; H, 8.16; S, 6.94.

6.2.28 Synthesis of (4,4,9,9-tetrakis(4-hexylphenyl)-4,9-dihydro-s-indaceno[1,2-b:5,6-b']dithiophene-2,7-diyl)bis(trimethylstannane ($IDT-Sn_2$) (28) (M8) [295]

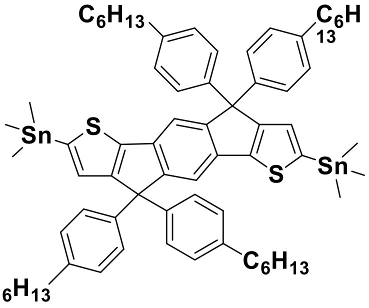

In a dry 100 ml two-necked round-bottom flask, **IDT compound (27)** (200 mg, 0.220 mmol) was dissolved in anhydrous THF (30 mL) under an argon atmosphere. The solution was cooled to -78 °C and (0.194 mL, 0.194 mmol) of *n*-BuLi 2.5 M in hexane was added dropwise. The reaction mixture was kept at -78 °C for 1 h and then warmed to room temperature for 30 min. Subsequently, the mixture was cooled again to -78 °C, and (0.55 mL, 0.551 mmol) of trimethyltin chloride in hexane was added. The cooling bath was then removed, and the reaction was stirred overnight at room temperature. The resulting mixture was then poured into water and extracted with diethyl ether (3 × 100 mL). The organic layers were collected and dried over $MgSO_4$, and the solvent was evaporated under reduced pressure. Subsequently, the precipitate was washed with ethanol to yield the target compound as a yellow solid (231 mg, 85 %). M.P > 350 °C. ^1H NMR (400 MHz, $CDCl_3$) δ (ppm): 7.40 (s, 2H), 7.15 (d, *J* = 8.0 Hz, 8H), 7.07 (d, *J* = 8.0 Hz, 8H), 7.03 (s, 2H), 2.56 (t, *J* = 8.0 Hz 8H), 1.58 (m, 4H), 1.31 (m, 28H), 0.89 (t, *J* = 6.5 Hz, 12H), 0.35 (s, 18H). ^{13}C NMR (400 MHz, $CDCl_3$) δ (ppm): 157.7, 153.8, 147.6, 142.7, 141.4, 141.2, 134.9, 130.8, 128.4, 128.2, 118.0, 62.3, 35.8, 31.9, 31.6, 29.4, 22.8, 14.3, -7.8. (MALDI) m/z: M^+, calculated for $C_{70}H_{90}S_2Sn_2$, 1234.45; found, 1234.40; Elemental analysis (%): calculated for $C_{70}H_{90}S_2Sn_2$: C, 80.11; H, 7.32; S, 12.58. Found: C, 79.91; H, 7.35; S, 12.42.

6.2.29 Synthesis of 3,6-dithiophen-2-yl-2,5-dihydropyrrolo[3,4-c]pyrrole-1,4-dione (29) [296]

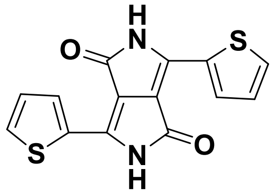

Potassium tert-butoxide (4 g, 35.7 mmol) and t-amyl alcohol (25 mL) were added to a dry 250 mL two-necked round-bottom flask under an argon atmosphere, and the temperature was increased to 110 °C for 1 h. 2-Thiophenecarbonitrile (3.27 g, 30 mmol) was added dropwise while stirring at 110 °C for 30 min. Subsequently, a solution mixture of dimethyl succinate (1.46 g, 10 mmol) in t-amyl alcohol (8 mL) was added slowly over a period of 2 h. Once this was complete, the reaction was left to stir vigorously for a further 2 h at 110 °C. After cooling the reaction to room temperature, the reaction solution was poured into a mixture of of ice (31 g), HCl (8 mL), and methanol (40 mL). The mixture was then stirred for 1 h, and the precipitate was filtered and washed with methanol (15 mL). The solid was dried *in vacuo* to produce a purple solid, and was used in the next step without further purification (3.6 g, 85%). ^{1}H NMR (400 MHz, DMSO-d$_6$): δ (ppm) 11.27 (s, 2H), 8.22 (dd, *J* = 1.0 Hz, 3.81 Hz), 8.97 (dd, *J* = 1.0 Hz, 4.64 Hz), 7.32 (br, 2H). ^{13}C NMR (250 MHz, DMSO-d$_6$): δ (ppm) 162.1, 136.6, 133.2, 131.8, 131.3, 129.2. 109.0 EI-MS (*m/z*): [M]$^+$ calculated for $C_{14}H_9N_2O_2S_2$, 301.01; Found, 301.10.

6.2.30 Synthesis of 2,5-bis(2-ethylhexyl)-3,6-di(thiophen-2-yl)pyrrolo[3,4-c] pyrrole- 1,4 (2H,5H)-dione (30) [297]

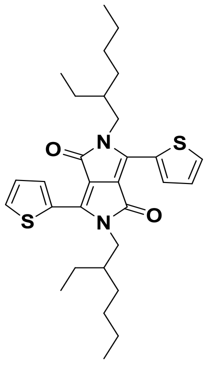

Potassium carbonate (13.82 g, 100 mmol) and 3,6-dithiophen-2-yl-2,5-dihydropyrrolo[3,4-c]pyrrole-1,4-dione **compound (29)** (7.5 g, 250 mmol) were added to a dry 500 mL two-necked round-bottom flask and degassed with argon for 5 min, before dry DMF (250 mL) was added. Subsequently, the reaction solution was stirred rapidly and heated to 140 °C for 2 h. Next, 2-ethylhexyl bromide (19.31 g, 100 mmol) was added dropwise to the reaction mixture. Once this was complete, the reaction was stirred overnight. After cooling to room temperature, the reaction was poured into water, extracted with DCM (6 × 500 mL), and washed several times with water. The organic layers were collected and dried over $MgSO_4$, and the solvent was evaporated under reduced pressure. The crude material was purified by column chromatography on silica gel using a mixture of petroleum ether and DCM as an eluent (1:1), to obtain the target product as a dark red solid (416 mg, 21%). M.P: 130 °C. ^1H NMR (400 MHz, $CDCl_3$) δ (ppm): 8.90 (d, *J* = 3.5 Hz, 1H), 7.64 (d, *J* = 4.0 Hz, 1H), 7.27 (dd, *J* = 5.0 Hz, 4.0 Hz, 1H), 4.06- 3.93 (m, 4H), 1.92-1.80 (m, 2H), 1.42-1.27 (m, 16H), 0.89-0.83 (m, 12H). ^{13}C NMR (400 MHz, $CDCl_3$) δ (ppm): 161.8, 140.5, 135.3, 130.5, 129.8, 128.4, 107.9, 45.9, 39.1, 30.2, 28.4, 23.5, 23.1, 14.0, 10.5; Mass calculated: $C_{30}H_{40}N_2O_2S_2$: 524.2. Found (El); (m/z): 524.7; Elemental analysis (%): calculated for $C_{30}H_{40}N_2O_2S_2$: C, 68.66; H, 7.68; N, 5.34, S, 12.22. Found: C, 68.53; H, 7.42; N, 5.46; S, 12.67.

6.2.31 Synthesis of 3-(5-bromothiophen-2-yl)-2,5-bis(2-ethylhexyl)-6-(thiophen-2-yl)pyrrolo[3,4-c]pyrrole-1,4(2H,5H)-dione (31) [298]

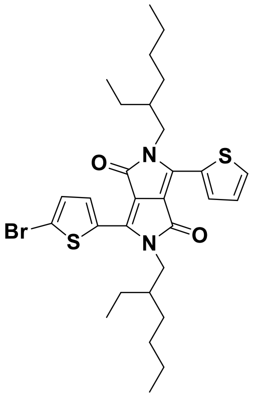

Under protection from the light, **NBS** (338 mg, 1.9 mmol) was added portion-wise to a solution of **compound (30)** (1 g, 1.9 mmol) in chloroform (50 ml) at 0 °C for 1 h. The ice bath was then removed, and the reaction was stirred at room temperature overnight. Subsequently, the solvent was evaporated under reduced pressure. The crude solid was purified *via* column chromatography on silica gel using a mixture of petroleum ether and chloroform as an eluent (1/1) to yield the product as a dark red solid (74 mg, 51%). M.P: 174 °C ^1H NMR (400 MHz, $CDCl_3$) δ (ppm): ^1H NMR (400 MHz, $CDCl_3$) δ (ppm): 8.93 (d, *J* =

4.0 Hz, 1H), 8.64 (d, *J* = 4.0 Hz, 1H), 7.64 (d, *J* = 5.0 Hz, 1H), 7.27 (dd, *J* = 5.0 Hz, 3.95 Hz, 1H) 7.22 (d, *J* = 4.0 Hz, 1H), 4.06- 3.93 (m, 4H), 1.92-1.80 (m, 2H), 1.42-1.27 (m, 16H), 0.89-0.83 (m, 12H). ^{13}C NMR (400 MHz, $CDCl_3$) δ (ppm): 161.7, 161.5, 141.0, 139.0, 135.6, 135.1, 131.4, 131.3, 130.9, 129.8, 128.5, 118.6, 108.2, 107.8, 46.0, 45.9, 39.1, 39.1, 30.2, 28.3, 23.8, 23.6, 23.5, 23.1, 23.0, 14.0, 10.5. Mass calculated for $C_{30}H_{40}BrN_2O_2S_2$: 603.17 Found (ESI-TOF-MS); (m/z): 603.3; Elemental analysis (%) calculated for $C_{30}H_{40}BrN_2O_2S_2$: C, 59.69; H, 6.51; N, 4.64; Br, 13.24; S, 10.62. Found: C, 59.72; H, 6.45; N, 4,71; S, 11.03.

6.2.32 Synthesis of 2,5-bis(2-ethylhexyl)-3-(5-phenylthiophen-2-yl)-6-(thiophen-2-yl)-2,5-dihydropyrrolo[3,4-*c*]pyrrole-1,4-dione (DPP-PH) (32)

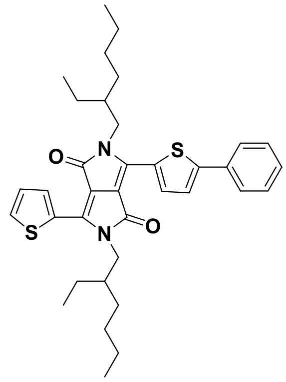

In a 100 mL round-bottom flask under an argon atmosphere, 3-(5-bromothiophen-2-yl)-2,5-bis(2-ethylhexyl)-6-(thiophen-2-yl)pyrrolo[3,4-c]pyrrole-1,4(2H,5H) dione **compound (31)** (100 mg, 0.165 mmol), 2-tributylstannylphenyltin (70 mg, 0.215 mmol), and bis(triphenylphosphine) palladium(II) dichloride $PdCl_2(PPh_3)_2$ (8.13 mg, 0.0116 mmol) were mixed and degassed for 5 min, before dry toluene (40 mL) was added to the mixture. The reaction was heated to 110 °C for overnight. After cooling, the reaction was added to water (200 mL), extracted with DCM (3 × 100 mL), and dried over $MgSO_4$. The solvent was evaporated, and the crude product was purified *via* column chromatography using a (3:1) mixture of petroleum ether and DCM to obtain the product as a dark purple solid (74 mg, 74%). M.P: 177 °C. ^{1}H NMR (400 MHz, $CDCl_3$) δ (ppm): 8.98 (d, *J* = 4.0 Hz, 1H), 8.90 (dd, *J* = 4.0 Hz and 1.0 Hz, 1H), 7.70 (m, 2H), 7.64 (dd, *J* = 5.0 Hz and 1.0 Hz, 1H), 7.50-7.42 (m, 3H), 7.41 – 7.36 (m, 1H), 7.29 (m, 1H), 4.14 – 4.00 (m, 4H), 2.01 - 1.84 (m, 2H), 1.47 – 1.21 (m, 16H), 0.97-0.84 (m, 12H). ^{13}C NMR (400 MHz, $CDCl_3$) δ (ppm): 161.9, 161.7, 149.8, 140.4, 140.0, 136.9, 135.2, 133.2, 130.8, 130.4, 129.9, 129.2, 128.9, 128.8, 128.7, 128.4, 126.2, 124.5, 108.1, 108.0, 45.9, 45.9, 39.2, 39.1, 30.4, 30.2, 28.6, 28.4, 23.7, 23.6, 23.1, 23.1, 14.1, 14.1, 10.6, 10.5; Exact mass calculated for $C_{36}H_{44}N_2O_2S_2$: 600.88. Found (El); (m/z): 601.5; Elemental analysis (%): calculated for $C_{36}H_{44}N_2O_2S_2$: C, 71.96; H, 7.38; N, 4.66; S,10.67. Found: C, 69.98; H, 7.24; N, 4.39; S, 10.48

6.2.33 Synthesis of 2,5-bis(2-ethylhexyl)-3-(5'-phenyl-[2,2'-bithiophen]-5-yl)-6-(thiophen-2-yl)-2,5-dihydropyrrolo[3,4-*c*]pyrrole-1,4-dione (DPP-TPH) (33)

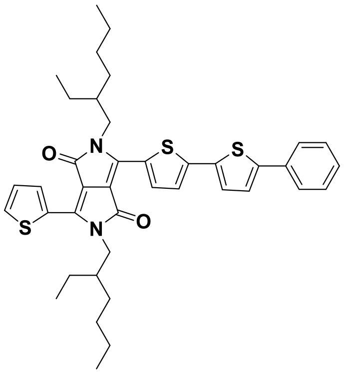

In a 100 mL round-bottom flask under argon atmosphere, (100 mg, 0.165 mmol) of 3-(5-bromothiophen-2-yl)-2,5-bis(2-ethylhexyl)-6-(thiophen-2-yl)pyrrolo[3,4-c]pyrrole 1,4 (2H,5H)-dione **compound (31)**, 2-(tributylstannyl) 2-phenylthiophene **compound (15)** (89.3mg, 0.198 mmol), and bis(triphenylphosphine)palladium(II) dichloride $PdCl_2(PPh_3)_2$ (8.13 mg, 0.0116 mmol) were mixed and degassed for 5 min, before dry toluene (40 mL) was added to the mixture. The reaction was heated to 110 °C overnight. After cooling, the reaction was added to water (200 mL), extracted with DCM (3 × 100 mL), and dried over $MgSO_4$. The solvent was evaporated, and the crude product was purified *via* column chromatography using a (3:1) mixture of petroleum ether and DCM to obtain the product as a dark purple solid (100 mg, 88%). M.P: 175-177 °C. ^{1}H NMR (400 MHz, $CDCl_3$) δ (ppm): 8.98 (d, *J* = 4.0 Hz, 1H), 8.91 (d, *J* = 4.0 Hz, 1H), 7.66-7.61 (m, 3H), 7.45-7.39 (m, 2H) 7.36-7.27 (m, 5H), 7.30 – 7.27 (m, 1H), 4.13 – 4.03 (m, 4H), 2.00 - 1.84 (m, 2H), 1.47 – 1.22 (m, 16H), 0.98-0.85 (m, 12H). ^{13}C NMR (400 MHz, $CDCl_3$) δ (ppm): 161.8, 161.6, 145.3, 142.8, 140.0, 139.8 136.9, 135.3, 135.2, 133.6, 130.4, 129.9, 129.1, 128.4, 128.1, 128.0, 126.1, 125.8, 124.6, 124.2, 108.2, 108.1, 45.9, 46.0, 39.3, 39.1, 30.4, 30.2, 28.6, 28.4, 23.7, 23.6, 23.1, 23.1, 14.1, 14.0, 10.6, 10.5; Exact mass calculated for $C_{40}H_{46}N_2O_2S_3$: 683.2800.

Found (El); (m/z): 683.2790; Elemental analysis (%): calculated for $C_{40}H_{46}N_2O_2S_3$: C, 70.34; H, 6.79; N, 4.10; S, 14.08. Found: C, 69.53; H, 6.35; N, 3.42; S, 14.69.

6.2.34 Synthesis of 5'-(2,5-bis(2-ethylhexyl)-3,6-dioxo-4-(thiophen-2-yl)-2,3,5,6-tetrahydro pyrrolo[3,4-*c*]pyrrol-1-yl)-[2,2'-bithiophene]-5-carbaldehyde (DPP-CHO) (34)

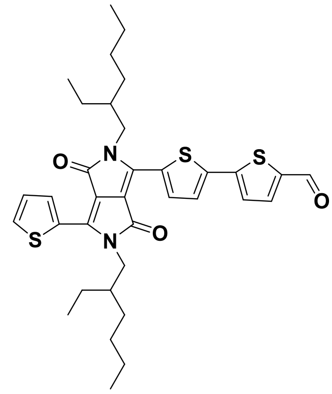

In a 100 mL two-necked round-bottom flask under an argon atmosphere, (500 mg, 0.825 mmol) of 3-(5-bromothiophen-2-yl)-2,5-bis(2-ethylhexyl)-6-(thiophen-2-yl)pyrrolo[3,4-c]pyrrole-1,4(2H,5H)-dione **compound (31)**, (193.5 mg, 1.24 mmol) of 5-formyl thiophene-2-yl boronic acid, and (171.5 mg, 1.24 mmol) of potassium carbonate (K_2CO_3) were dissolved in (30 mL) of dry THF. Next, (15.6 mg, 0.016 mmol) of $Pd_2(dba)_3$, (20.2 mg, 0.066 mmol) of $P(o\text{-}tol)_3$, and (3 mL) of water were added, and the reaction was left to reflux overnight. After cooling to room temperature, the solution mixture was poured into water and extracted with DCM (6 × 100 mL). The organic layers were then collected and dried over $MgSO_4$, and the solvent was evaporated under reduced pressure. The crude material was purified by column chromatography on silica gel using a mixture of petroleum ether and DCM (3:1) as an eluent, yielding the desired product as a dark purple solid (487 mg, 91%). M.P: 181-183 °C. ^{1}H NMR (400 MHz, $CDCl_3$) δ (ppm): 9.91(s, 1H), 8.95 (dd, *J* = 4.0 Hz and 1.0 Hz, 1H), 8.88 (d, *J* = 4.0 Hz, 1H), 7.73 (d, *J* = 4.0 Hz, 1H), 7.67 (d, *J* = 5.0 Hz and 1.0 Hz, 1H), 7.50 (d, *J* = 3.5 Hz, 1H), 7.48 (d, *J* = 3.5 Hz, 1H), 7.30 (dd, *J* = 4.0 Hz and 1.0 Hz, 1H), 4.10-3.98 (m, 4H), 1.95-1.83 (m, 2H), 1.44-1.21 (m, 16H), 0.97-0.84 (m, 12); ^{13}C NMR (400 MHz, $CDCl_3$) δ (ppm): 182.5, 161.7, 161.6, 145.3, 141.1, 140.3, 138.8, 137.2, 136.2, 135.9, 135.7, 131.2, 130.6, 129.7, 128.6, 127.0, 126.1, 125.4, 109.1, 108.0; 46.0, 39.3, 39.1, 30.3, 30.2, 28.5, 28.3, 23.7, 23.5, 23.1, 14.1, 14.0, 10.6, 10.5; Exact mass calculated for $C_{35}H_{42}N_2O_3S_3$: 634.24. Found (El); (m/z): 634.5; Elemental analysis (%): calculated for $C_{35}H_{42}N_2O_3S_3$: C, 66.21; H, 6.67; N, 4.41, S, 15.15. Found: C, 65.83; H, 6.42; N, 3.94, S, 15.49.

6.2.35 Synthesis of 3-(5-bromothiophen-2-yl)-2,5-bis(2-ethylhexyl)-6-(5-phenylthiophen -2 -yl)-2,5-dihydropyrrolo[3,4-*c*]pyrrole-1,4-dione (DPP-PH-Br) (35) (M5)

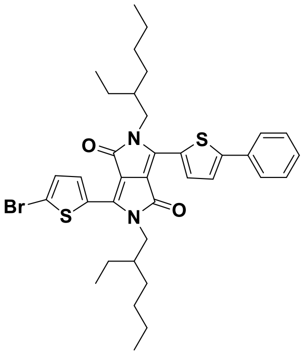

In a 50 mL round-bottom flask protected from the light under an argon atmosphere, **NBS** (82.8 mg, 0.465 mmol) was added in portions to a solution of **DPP-PH compound (32)** (200 mg, 0.333 mmol) in chloroform (25 mL) at room temperature. Once this was complete, the reaction was heated to 60 °C and stirred for 12 h. Subsequently, the solvent was evaporated under reduced pressure. The crude solid was purified *via* column chromatography on silica gel using a mixture of petroleum ether and $CHCl_3$ as an eluent (2:1) to yield the product as a dark purple solid (147 mg, 65%). M.P:180 °C. ^{1}H NMR (400 MHz, $CDCl_3$) δ (ppm): 8.99 (d, *J* = 4.0 Hz, 1H), 8.92 (d, *J* = 4.0 Hz, 1H), 7.70 (d, *J* = 7.5 Hz, 2H), 7.65 (d, *J* = 5.0 Hz, 1H), 7.42 (m, 4H), 7.30 – 7.27 (m, 1H), 4.17 – 4.03 (m, 4H), 2.02 - 1.95 (m, 2H), 1.48 – 1.26 (m, 16H), 0.99-0.87 (m, 12H). ^{13}C NMR (400 MHz, $CDCl_3$) δ (ppm): 161.8, 161.4, 150.2, 140.8, 138.5, 137.2, 135.0, 133.1, 131.4, 131.4, 129.2, 129.0, 128.7, 126.2, 124.6, 118.5, 108.4, 107.9, 46.0, 39.2, 39.1, 30.6, 30.2, 28.6, 28.4, 23.7, 23.6, 23.1, 23.1, 14.1, 14.0, 10.6, 10.5; Exact mass for $C_{36}H_{44}BrN_2O_2S_2$: 678.1996. Found (El); (m/z): 678.2028.

6.2.36 Synthesis of 3-(5-bromothiophen-2-yl)-2,5-bis(2-ethylhexyl)-6-(5'-phenyl-[2,2'-bithiophen]-5-yl)-2,5-dihydropyrrolo[3,4-*c*]pyrrole-1,4-dione (DPP-PHT-Br) (36) (M6)

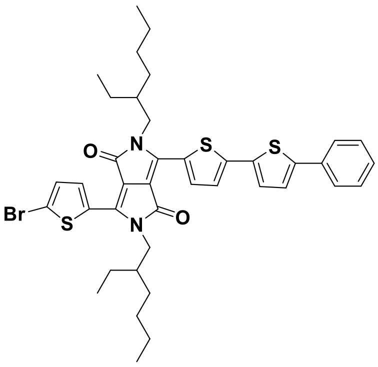

The same method used to prepare **DPP-PH-Br** was followed to synthesize **DPP-PHT-Br**. In a 50 mL round-bottom flask protected from the light under an argon atmosphere, **NBS** (62.5 mg, 0.351 mmol) was added in portions to a solution of **DPP-PHT compound (33)** (200 mg, 0.292 mmol) in chloroform (25 mL) at room temperature. Once this was complete, the reaction was heated to 60 °C and stirred for 12 h. Subsequently, the solvent was evaporated under reduced pressure. The crude solid was purified *via* column chromatography on silica gel using a mixture of petroleum ether and chloroform as an eluent (2:1) to yield the product as a dark purple-black solid (118 mg, 53%). M.P: 180 °C. ^{1}H NMR (400 MHz, $CDCl_3$) δ (ppm): 8.99 (d, *J* = 4.0 Hz, 1H), 8.64 (d, *J* = 4.0 Hz, 1H), 7.67-7.62 (m, 2H), 7.46-7.38 (m, 2H) 7.37-7.29 (m, 4H), 7.24 (d, *J* = 4.0 Hz, 1H), 4.12 – 3.91 (m, 4H), 1.99 - 1.82 (m, 2H), 1.47 – 1.29 (m, 16H), 0.98-0.85 (m, 12H). ^{13}C NMR (400 MHz, $CDCl_3$) δ (ppm): 161.7, 161.3, 145.4, 143.2, 140.4, 138.3, 137.2, 135.2, 135.0, 133.6, 131.4, 129.1, 129.0, 128.1, 127.9, 127.8, 127.6, 126.2, 125.8, 125.6, 124.7, 124.5, 124.2, 123.8, 118.5, 108.4, 108.0, 46.0, 39.3, 39.1, 30.4, 30.2, 28.6, 28.3, 23.7, 23.6, 23.1, 23.1, 14.1, 14.1, 10.6, 10.5; Exact mass calculated for $C_{40}H_{46}BrN_2O_2S_3$: 761.1923. Found (El); (m/z): 761.1905.

6.2.37 Synthesis of 5'-(4-(5-bromothiophen-2-yl)-2,5-bis(2-ethylhexyl)-3,6-dioxo-2,3,5,6-tetrahydropyrrolo[3,4-*c*]pyrrol-1-yl)-[2,2'-bithiophene]-5-carbaldehyde (DPP-CHO-Br) (37) (M7)

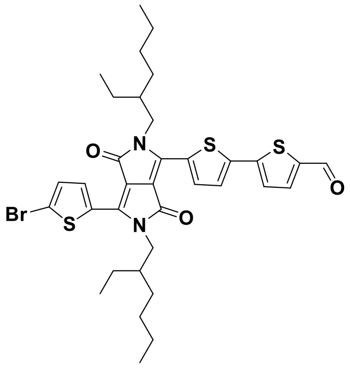

The same method used to prepare **DPP-PH-Br** was followed to synthesize **DPP-CHO-Br**. In a 50 mL round-bottom flask protected from the light under an argon atmosphere, **NBS** (36.4 mg, 0.205 mmol) was added in portions to a solution of **DPP-CHO compound (34)** (100 mg, 0.157 mmol) in chloroform (20 mL) at room temperature. Once this was complete, the reaction was heated to 60 °C and stirred for 12 h. Subsequently, the solvent was evaporated under reduced pressure. The crude solid was purified *via* column chromatography on silica gel using a mixture of petroleum ether and chloroform as an eluent (2:1) to yield the product as a dark purple-black solid (80 mg, 72%). M.P: 181 °C ^{1}H NMR (400 MHz, $CDCl_3$) δ (ppm): 9.92(s, 1H), 8.91 (d, *J* = 4.0 Hz, 1H), 8.70 (d, *J* = 4.0 Hz, 1H), 7.74 (d, *J* = 4.0 Hz, 1H), 7.49 (d, *J* = 4.0 Hz, 1H), 7.40 (d, *J* = 4.0 Hz, 1H), 7.25 (d, *J* = 4.0 Hz, 1H), 4.10-3.91 (m, 4H), 1.94-1.82 (m, 2H), 1.44-1.22 (m, 16H), 0.96-0.85 (m, 12H); ^{13}C NMR (400 MHz, $CDCl_3$) δ (ppm): 182.4, 161.5, 161.4, 145.2, 141.4, 140.7, 139.6, 139.3, 138.1, 137.8, 137.1, 136.4, 136.2 135.7, 131.5, 131.1, 130.9, 127.0, 125.5, 45.1, 39.3, 39.1, 30.3, 30.2, 28.5, 28.3, 23.7, 23.6, 23.1, 23.0, 14.1, 14.0, 10.6, 10.5. Exact mass calculated for $C_{35}H_{42}BrN_2O_3S_3$: 713.1556. Found (El); (m/z): 713.1541.

6.2.38 Synthesis of IDTT-DPP-PH (38)

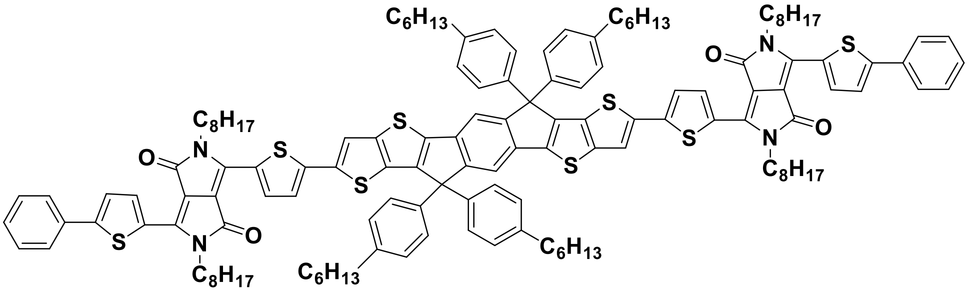

In a 100 mL round-bottom flask under an argon atmosphere, (100 mg, 0.074 mmol) of **IDTT-Sn_2 compound (25)**, (200.2 mg, 0.297 mmol) of **DPP-PH-Br compound (35)**, (4 mg, 0.022 mmol) of $Pd_2(dba)_3$, and (54.2 mg, 0.178 mmol) of $P(o\text{-}tol)_3$ were mixed and degassed for 5 min, before dry toluene (50 mL) was added to the mixture. The reaction was heated to 110 °C overnight. After cooling, the reaction was added to water (300 ml), extracted with $CHCl_3$ (5 × 150 mL), and dried over $MgSO_4$. The solvent was evaporated, and the crude product was purified *via* column chromatography using a (1:3) mixture of petroleum ether and $CHCl_3$ to obtain the target product as a black-blue solid (200 mg, 60%). M.P > 350 °C. ^1H NMR (400 MHz, $CDCl_3$) δ (ppm): 9.00-8.95 (m, 4H), 7.70 (d, *J* = 7.5 Hz, 4H), 7.54 (s, 2H), 7.50-7.35 (m, 10H), 7.30 (d, *J* = 4.0 Hz, 2H), 7.22 (d, *J* = 8.0 Hz, 8H), 7.14 (d, *J* = 8.0 Hz, 8H), 4.17 - 4.00 (m, 8H), 2.60 (t, *J* = 8.0 Hz, 8H), 2.00 - 1.89 (br, 4H), 1.67 - 1.55 (m, 10H), 1.48 - 1.24 (m, 54H), 0.99 - 0.83 (m, 36H). (MALDI) m/z: M^+, calculated for $C_{140}H_{158}N_4O_4S_8$,: 2217.32; found, 2216.6; Elemental analysis (%): $C_{140}H_{158}N_4O_4S_8$: C, 75.84; H, 7.18; N, 2.53 S, 11.57. Found: C, 74.69; H, 6.96; N, 2.37, S, 11.08.

6.2.39 Synthesis of IDTT-DPP-PHT (39)

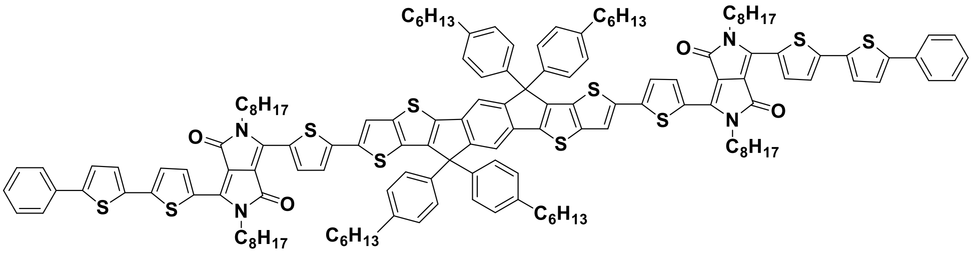

The **IDTT-DPP-PHT** compound was obtained following similar procedures to those for preparing **IDTT-DPP-PH**. (100 mg, 0.074 mmol) of **IDTT-Sn$_2$ compound (25)**, (226.5 mg, 0.297 mmol) of **DPP-PHT-Br compound (36)**, (4 mg, 0.022 mmol) of $Pd_2(dba)_3$, and (54.2 mg, 0.178 mmol) of $P(o\text{-}tol)_3$ were used to synthesize the desired product as a black-blue solid (120 mg, 67%). M.P > 350 °C. ^{1}H NMR (400 MHz, $CDCl_3$) δ (ppm): 8.98-8.95 (m, 4H), 7.36 (d, *J* = 7.5 Hz, 2H), 7.54 (d, *J* = 3.5 Hz, 2H), 7.42 (t, *J* = 7.5 Hz and 7.5 Hz, 6H), 7.37-7.28 (m, 10H), 7.24 (s, 2H), 7.22 (d, *J* = 8.0 Hz, 8H), 7.14 (d, *J* = 8.0 Hz, 8H), 4.15 - 3.97 (m, 8H), 2.60 (t, *J* = 8.0 Hz, 8H), 2.01 - 1.88 (br, 4H), 1.67 - 1.51 (m, 10H), 1.48 - 1.22 (m, 54H), 1.00 - 0.80 (m, 36H). (MALDI) m/z: M$^+$, calculated for $C_{148}H_{162}N_4O_4S_{10}$; 2381.55 found 2380.0; Elemental analysis (%): $C_{148}H_{162}N_4O_4S_{10}$: C, 74.64; H, 6.86; N, 2.35 S, 13.46. Found: C, 73.60; H, 6.83; N, 2.09, S, 12.59.

6.2.40 Synthesis of IDTT-DPP-CHO (40)

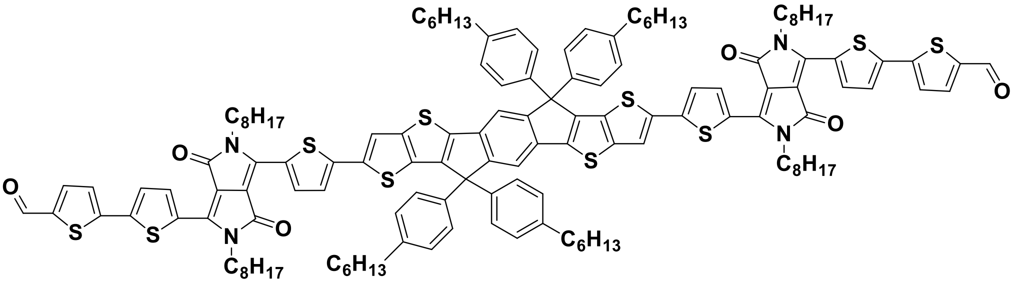

This compound was obtained following similar procedures to those for preparing **IDTT-DPP-PH**. (100 mg, 0.074 mmol) of **IDTT-Sn$_2$ compound (25)**, (212.2 mg, 0.297 mmol) of **DPP-CHO-Br compound (37)**, (4 mg, 0.022 mmol) of $Pd_2(dba)_3$, and (54.2 mg, 0.178 mmol) of $P(o\text{-}tol)_3$ were used to synthesize the desired product as a black-blue solid (113 mg, 67%). M.P > 350 °C. ^{1}H NMR (400 MHz, $CDCl_3$) δ (ppm): 9.90 (s, 2H), 9.02 (d, *J* = 4.0 Hz, 2H), 8.89 (d, *J* = 4.0 Hz, 2H), 7.71 (d, *J* = 4.0 Hz, 2H), 7.55 (d, *J* = 1.5 Hz, 4H), 7.48 (d, *J* = 4.0 Hz, 2H), 7.37 (d, *J* = 4.0 Hz, 2H), 7.31 (d, *J* = 4.0 Hz, 2H), 7.22 (d, *J* = 8.0 Hz, 8H), 7.14 (d, *J* = 8.0 Hz, 8H), 4.06 (br, 8H), 2.59 (t, *J* = 8.0 Hz, 8H), 1.99 - 1.83 (br, 4H), 1.67 - 1.53 (m, 10H), 1.48 - 1.24 (m, 54H), 0.99 - 0.83 (m, 36H); (MALDI) m/z :M$^+$, calculated for $C_{138}H_{154}N_4O_6S_{10}$; 2285.37 found 2284.7; Elemental analysis (%): $C_{138}H_{154}N_4O_6S_{10}$: C, 72.53; H, 6.79; N, 2.45 S, 14.03. Found: C, 71.92; H, 6.82; N, 2.27, S, 13.23.

6.2.41 Synthesis of IDTT-DPP-INIC (41)

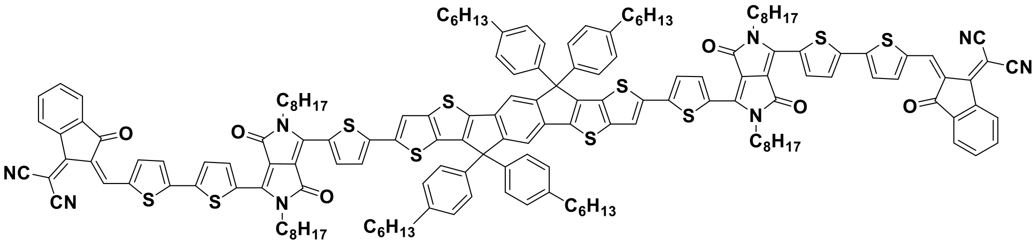

In a dry 100 mL two-necked round-bottom flask under an argon atmosphere, a mixture of (130 mg, 0.0567 mmol) of **IDTT-DPP-CHO compound (40)** compound and (165.6 mg, 0.853 mmol) of 2-(3-oxo-2,3dihydroinden-1-ylidene)malononitrile **compound (20)** were placed and degassed for 5 min following the addition of (50 mL) chloroform and (1 mL) pyridine at room temperature. The reaction mixture was then refluxed overnight. The reaction was cooled to room temperature and extracted with $CHCl_3$ (5× 150 mL). The combined layers were then dried over $MgSO_4$, and the solvent was evaporated under reduced pressure. The crude product was washed with methanol and filtered through a Buchner funnel. Subsequently, the target compound **IDTT-DPP-INIC** was obtained as a black solid (160 mg, 92%). M.P > 350 °C. ^{1}H NMR (400 MHz, $CDCl_3$) δ (ppm): 9.04 (d, *J* = 4.0 Hz, 2H), 8.96 (d, *J* = 4.0 Hz, 2H), 8.81 (s, 2H) 8.64 (d, *J* = 6.5 Hz, 2H), 7.95 (d, *J* = 6.5 Hz, 2H), 7.78 (d, *J* = 4.0 Hz, 2H), 7.67-7.69 (m, 6H), 7.60-7.49 (m, 6H), 7.42 (d, *J* = 4.0 Hz, 2H), 7.23 (d, *J* = 7.0 Hz, 8H), 7.15 (d, *J* = 7.5 Hz, 8H), 4.07 (br, 8H), 2.60 (t, *J* = 7.5 Hz, 8H), 1.99 - 1.87 (br, 4H), 1.67 - 1.53 (m, 10H), 1.48 - 1.22 (m, 54H), 0.99 - 0.81 (m, 36H); (MALDI) m/z :M^+ , calculated for $C_{162}H_{162}N_8O_6S_{10}$; 2637.7 found 2636.4 Elemental analysis (%): $C_{162}H_{162}N_8O_6S_{10}$: C, 73.77; H, 6.19; N, 4.25 S, 12.15. Found: C, 73.50; H, 6.36; N, 3.84, S, 11.64.

6.2.42 Synthesis of IDTT-DPP-CN (42)

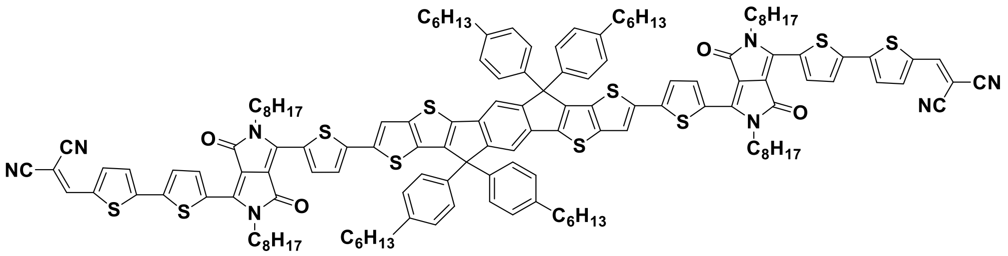

This compound was obtained following similar procedures to those for preparing **IDTT-DPP-INIC**. **IDTT-DPP-CHO compound (40)** (100 mg, 0.044 mmol), malononitrile (43.3 mg, 0.656 mmol), and (1 mL) of pyridine were used to synthesize the desired product as a black-blue solid (113 mg, 67%). M.P > 350 °C. ^{1}H NMR (400 MHz, $CDCl_3$) δ (ppm): 9.06 (d, *J* = 4.0 Hz, 2H), 8.88 (d, *J* = 4.0 Hz, 2H), 7.60 (br, 4H), 7.56-7.53 (m, 4H), 7.52 (d, *J* = 4.0 Hz, 2H), 7.36 (d, *J* = 4.0 Hz, 2H), 7.30 (s, 2H), 7.23 (d, *J* = 8.5 Hz, 8H), 7.15 (d, *J* = 8.5 Hz, 8H) 4.07 (br, 8H), 2.60 (t, *J* = 8.0 Hz, 8H), 1.99 - 1.85 (br, 4H), 1.67 - 1.50 (m, 10H), 1.47 - 1.20 (m, 54H), 0.99 - 0.82 (m, 36H); (MALDI) m/z :M^+, calculated for $C_{162}H_{162}N_8O_6S_{10}$; 2381.47 found 2379.8 Elemental analysis (%): $C_{162}H_{162}N_8O_6S_{10}$: C, 72.63; H, 6.52; N, 4.71 S, 13.46. Found: C, 71.55; H, 6.63; N, 4.04, S, 12.42.

6.2.43 Synthesis of IDT-DPP-PH (43)

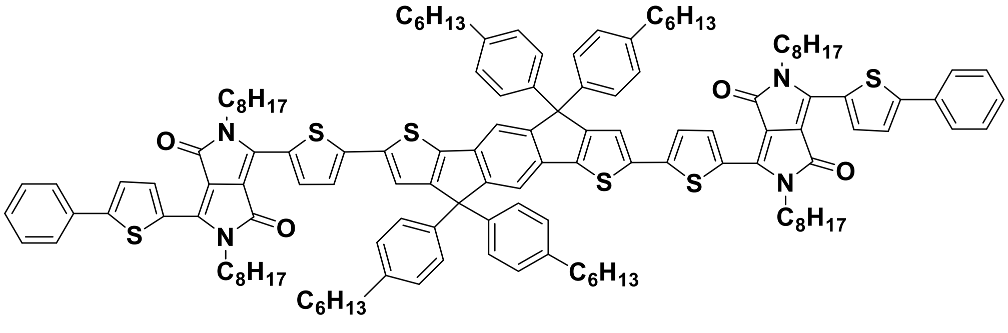

In a 100 mL round-bottom flask under an argon atmosphere, (100 mg, 0.081 mmol) of **IDT-Sn_2 compound (28)**, **DPP-PH-Br compound (35)** (100 mg, 0.324 mmol), $Pd_2(dba)_3$ (4.45

mg, 0.005 mmol) and P(o-tol)$_3$ (5.92 mg, 0.0194 mmol) were mixed and degassed for 5 min, before dry toluene (50 mL) was added to the mixture. The reaction was heated to 110 °C overnight. After cooling, the reaction mixture was added to water (300 ml), extracted with CHCl$_3$ (5× 150 mL) and dried over MgSO$_4$. The solvent was evaporated and the crude product was purified *via* column chromatography using 1:3 mixture of petroleum ether and CHCl$_3$ to obtain a target product as a black-blue solid. (102 mg, 61%). M.P > 350 °C. ^{1}H NMR (400 MHz, CDCl$_3$) δ (ppm): 8.97 (d, *J* = 4.0 Hz, 2H), 8.92 (d, *J* = 4.0 Hz, 2H), 7.70 (d, *J* = 7.5 Hz, 2H), 7.51-7.42 (m, 10H), 7.41 - 7.35 (m, 2H), 7.31 (d, *J* = 4.0 Hz, 2H), 7.24 (s, 2H), 7.21 (d, *J* = 8.0 Hz, 8H), 7.12 (d, *J* = 8.0 Hz, 8H), 4.16 - 3.99 (m, 8H), 2.60 (t, *J* = 7.5 Hz, 8H), 2.02 - 1.90 (br, 4H), 1.67 - 1.53 (m, 10H), 1.48 - 1.24 (m, 54H), 0.99 - 0.82 (m, 36H); (MALDI) m/z :M$^+$, calculated for $C_{136}H_{158}N_4O_4S_6$; 2105.14 found 2013.8; Elemental analysis (%): calculated for $C_{136}H_{158}N_4O_4S_6$: C, 77.60; H, 7.57; N, 2.66, S, 9.14. Found: C, 76.17; H, 7.26; N, 2.64, S, 9.32.

6.2.44 Synthesis of IDT-DPP-PHT (44)

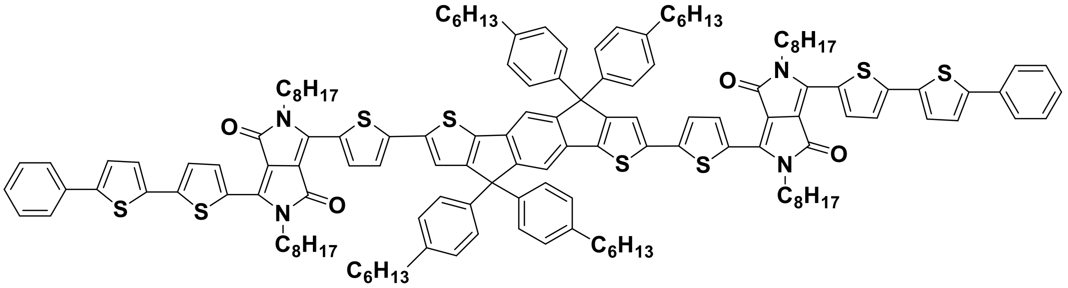

The **IDT-DPP-PHT** compound was synthesized following similar procedures to those for preparing **IDT-DPP-PH. IDT-Sn$_2$ compound (28)** (100 mg, 0.081 mmol), **DPP-PHT-Br compound (36)** (185 mg, 0.243 mmol), Pd$_2$(dba)$_3$ (4 mg, 0.022 mmol) and P(o-tol)$_3$ (54.2 mg, 0.178 mmol) were used to synthesize the desired product as a black-blue solid (125 mg, 68%). M.P > 350 °C. ^{1}H NMR (400 MHz, CDCl$_3$) δ (ppm): 8.96 (d, *J* = 4.0 Hz, 2H), 8.92 (d, *J* = 4.0 Hz, 2H), 7.61-7.58 (m, 4H), 7.43 (m, 6H), 7.37-7.29 (m, 10H), 7.24 (s, 2H), 7.21 (d, *J* = 8.0 Hz, 8H), 7.12 (d, *J* = 8.0 Hz, 8H), 4.15 - 3.97 (m, 8H), 2.60 (t, *J* = 8.0 Hz, 8H), 2.01 - 1.88 (br, 4H), 1.67 - 1.51 (m, 10H), 1.48 - 1.22 (m, 54H), 1.00 - 0.80 (m, 36H). (MALDI) m/z :M$^+$, calculated for $C_{144}H_{162}N_4O_4S_8$; 2269.38 found 2268.8; Elemental analysis (%): calc. for $C_{144}H_{162}N_4O_4S_8$: C, 76.21; H, 7.20; N, 2.47, S, 11.30. Found: C, 74.56; H, 7.05; N, 2.33, S, 10.72.

6.2.45 Synthesis of IDT-DPP-CHO (45)

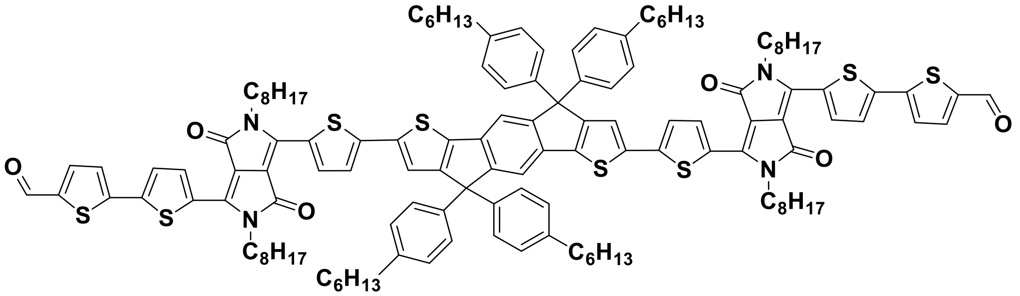

This compound was obtained following the similar procedures of to those for preparing **IDT-DPP-PH**. **IDT-Sn$_2$ compound (28)** (140 mg, 0.0113 mmol), **DPP-CHO-Br compound (37)** (211 mg, 0.295 mmol), $Pd_2(dba)_3$ (44.5 mg, 0.0049 mmol) and P(o-tol)$_3$ (5.92 mg, 0.0194 mmol) were used to synthesize the desired product as a black-blue solid. (192 mg, 78%). M.P > 350 °C. ^{1}H NMR (400 MHz, $CDCl_3$) δ (ppm): 9.91 (s, 2H), 8.98 (d, *J* = 4.0 Hz, 2H), 8.88 (d, *J* = 4.0 Hz, 2H), 7.73 (d, *J* = 4.0 Hz, 2H), 7.49 (d, *J* = 4.0 Hz, 2H), 7.44(s, 2H), 7.39 (d, *J* = 4.0 Hz, 2H), 7.32 (d, *J* = 4.0 Hz, 2H), 7.25 (s, 2H), 7.21 (d, *J* = 8.0 Hz, 8H), 7.12 (d, *J* = 8.0 Hz, 8H), 4.13 - 3.97 (m, 8H), 2.60 (t, *J* = 7.5 Hz, 8H), 1.98 - 1.86 (br, 4H), 1.67 - 1.54 (m, 13H), 1.47 - 1.25 (m, 54H), 0.99 - 0.83 (m, 36H); (MALDI) m/z :M$^+$, calculated for $C_{134}H_{154}N_4O_6S_8$; 2173.21 found 2171.8; Elemental analysis (%): calc. for $C_{134}H_{154}N_4O_6S_8$: C, 74.06; H, 7.14; N, 2.58, S, 11.80. Found: C, 73.71; H, 7.17; N, 2.45, S, 11.44.

6.2.46 Synthesis of IDT-DPP-INIC (46)

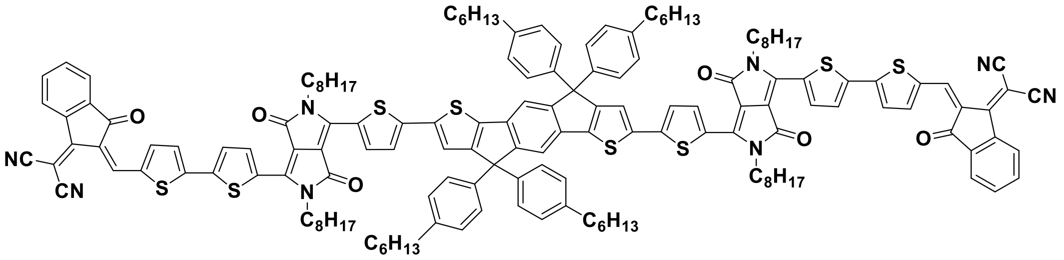

In a dry 100 mL two-necked round-bottom flask under an argon atmosphere, a mixture **IDT-DPP-CHO compound (45)** (150 mg, 0.069 mmol) and 2-(3-oxo-2,3dihydroinden-1-ylidene)malononitrile **compound (20)** (201 mg, 1.035 mmol) were placed and degassed for 5 min following the addition dry $CHCl_3$ (50 mL) and pyridine (1 mL) at room temperature. The reaction mixture was then refluxed overnight. The reaction was cooled to room temperature and extracted with $CHCl_3$ (5× 150 mL). The combined layers were then dried over $MgSO_4$, and the solvent was evaporated under reduced pressure. The crude product was washed with methanol and filtered through a Buchner funnel. Subsequently, the product of compound **IDT-DPP-INIC** was obtained as a black solid (158 mg, 91%). M.P > 350 °C. ^{1}H NMR (400 MHz, $CDCl_3$) δ (ppm): 8.99 (d, *J* = 4.0 Hz, 2H), 8.95 (d, *J* = 4.0 Hz, 2H), 8.82 (s, 2H), 8.68 - 8.64 (m, 2H), 7.97 - 7.93 (m, 2H), 7.78 (d, *J* = 4.5 Hz, 2H), 7.77 - 7.71 (m, 4H), 7.59 (d, *J* = 4.11, 2H), 7.46 (s, 2H), 7.43 (d, *J* = 4.08 Hz, 2H), 7.30 (d, *J* = 4.11 Hz, 2H), 7.26 (s, 2H), 7.22 (d, *J* = 7.0 Hz, 8H), 7.13 (d, *J* = 7.0 Hz, 8H), 4.05 (br, 8H), 2.61 (t, *J* = 7.5 Hz, 8H), 1.98 - 1.85 (br, 4H), 1.68 - 1.55 (m, 10H), 1.48 - 1.20 (m, 54H), 0.99 - 0.81 (m, 36H); (MALDI) m/z: M^+, calculated for $C_{158}H_{162}N_8O_6S_8$; 2525.56 found 2524.6; Elemental analysis (%): calc. for $C_{158}H_{162}N_8O_6S_8$: C, 75.14; H, 6.47; N, 4.44, S, 10.16. Found: C, 74.61; H, 6.36; N, 4.19, S, 10.33.

6.2.47 Synthesis of IDT-DPP-CN (47)

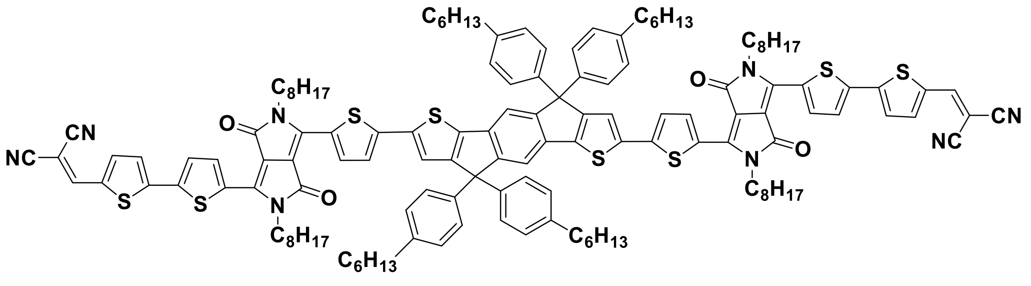

This compound was obtained following similar procedures of to those for preparing **IDTT-DPP-INIC**. **IDT-DPP-CHO compound (45)** (150 mg, 0.069 mmol), malononitrile(68.3 mg, 1.03 mmol) and pyridine(1mL) were used to synthesize the desired product as a black- solid (124 mg, 91%). M.P > 350 °C. ^{1}H NMR (400 MHz, $CDCl_3$) δ (ppm): 9.01 (d, *J* = 4.0 Hz, 2H), 8.86 (d, *J* = 4.0 Hz, 2H), 7.74 (s, 2H), 7.69 (d, *J* = 4.0 Hz, 2H), 7.54 (d, *J* = 4.0 Hz, 2H), 7.45 (s, 2H), 7.40 (d, *J* = 4.0 Hz, 2H), 7.32 (d, *J* = 4.0 Hz, 2H), 7.25 (s, 2H), 7.21 (d, *J* = 8.0 Hz, 8H), 7.12 (d, *J* = 8.0 Hz, 8H) 4.12-3.98 (m, 8H), 2.60 (t, *J* = 8.0 Hz, 8H), 1.97 - 1.85 (m, 4H), 1.67 - 1.53 (m, 10H), 1.47 - 1.23 (m, 54H), 0.99 - 0.82 (m, 36H); (MALDI) m/z :M^+ , calculated for $C_{140}H_{154}N_8O_4S_8$; 2269.30 found 2268.1; Elemental analysis (%): calculated for $C_{140}H_{154}N_8O_4S_8$: C, 74.10; H, 6.84; N, 4.94 S, 11.30. Found: C, 72.76; H, 6.84; N, 4.62, S, 11.12.

Chapter VII: References

1. Shirakawa, H.; Louis, E. J.; MacDiarmid, A. G.; Chiang, C. K.; Heeger, A. J. Synthesis of electrically conducting organic polymers: halogen derivatives of polyacetylene,(CH) x. *Journal of the Chemical Society, Chemical Communications* **1977**, 578-580.
2. Halls, J.; Walsh, C.; Greenham, N. C.; Marseglia, E.; Friend, R. H.; Moratti, S.; Holmes, A. Efficient photodiodes from interpenetrating polymer networks. *Nature* **1995***, 376*, 498.
3. Inzelt, G.; Pineri, M.; Schultze, J.; Vorotyntsev, M. Electron and proton conducting polymers: recent developments and prospects. *Electrochim. Acta* **2000***, 45*, 2403-2421.
4. Kraft, A.; Grimsdale, A. C.; Holmes, A. B. Electroluminescent conjugated polymers—seeing polymers in a new light. *Angewandte Chemie International Edition* **1998***, 37*, 402-428.
5. Taliani, C.; Gebauer, W.; Fichou, D. Handbook of Oligo and Polythiophenes. **1999**.
6. MacDiarmid, A. G. "Synthetic metals": A novel role for organic polymers (Nobel lecture). *Angewandte Chemie International Edition* **2001***, 40*, 2581-2590.
7. Chandrasekhar, P. Basics of Conducting Polymers (CPs). In *Conducting Polymers, Fundamentals and Applications*Springer: **1999**; pp 3-22.
8. Heeger, A. J. *Semiconducting and metallic polymers: the fourth generation of polymeric materials* **2001**.
9. Sapoval, B.; Hermann, C.; Hermann, C. *Physics of semiconductors;* Springer Science & Business Media: **2003**; .
10. Skotheim, T. A.; Elsenbaumer, R. L.; Reynolds, J. R. Handbook of conducting polymers/Edited by Terje A. Skotheim, Ronald L. Elsenbaumer, John R. Reynolds.
11. Bredas, J. L.; Street, G. B. Polarons, bipolarons, and solitons in conducting polymers. *Acc. Chem. Res.* **1985***, 18*, 309-315.
12. Moliton, A.; Hiorns, R. C. Review of electronic and optical properties of semiconducting p-conjugated polymers: applications in optoelectronics. *Polym. Int.* **2004***, 53*, 1397-1412.
13. Heeger, A. J.; Kivelson, S.; Schrieffer, J.; Su, W. Solitons in conducting polymers. *Reviews of Modern Physics* **1988***, 60*, 781.
14. Brédas, J.; Beljonne, D.; Coropceanu, V.; Cornil, J. Charge-transfer and energy-transfer processes in π-conjugated oligomers and polymers: a molecular picture. *Chem. Rev.* **2004***, 104*, 4971-5004.

15. Sandman, D. Semiconducting polymers and their solid-state properties: are these materials semiconductors or large conjugated molecules. *Trends in Polymer Science* **1994**, *2*, 44-55.
16. Moliton, A. Optoelectronics of Molecules and Polymers. 2005.
17. MacDiarmid, A. G. “Synthetic metals”: A novel role for organic polymers (Nobel lecture). *Angew Chem Inter Edition* **2001**, *40*, 2581-2590.
18. Chandrasekhar, P. Conducting polymers. *Fundamentals and Applications: A Practical Approach* **1999**, 83.
19. Taliani, C.; Gebauer, W.; Fichou, D. Handbook of Oligo and Polythiophenes. **1999**.
20. Heeger, A. J. Semiconducting and metallic polymers: the fourth generation of polymeric materials (Nobel lecture). *Angewandte Chemie International Edition* **2001**, *40*, 2591-2611.
21. Harun, M. H.; Saion, E.; Kassim, A.; Yahya, N.; Mahmud, E. Conjugated conducting polymers: A brief overview. *UCSI Academic Journal: Journal for the Advancement of Science & Arts* **2007**, *2*, 63-68.
22. Pope, M.; Kallmann, H.; Magnante, P. Electroluminescence in organic crystals. *J. Chem. Phys.* **1963**, *38*, 2042-2043.
23. Burroughes, J. H.; Bradley, D. D.; Brown, A.; Marks, R.; Mackay, K.; Friend, R. H.; Burns, P.; Holmes, A. Light-emitting diodes based on conjugated polymers. *Nature* **1990**, *347*, 539.
24. Kim, D.; Cho, H.; Kim, C. Blue light emitting polymers. *Progress in Polymer Science* **2000**, *25*, 1089-1139.
25. Zhan, X.; Zhu, D. Conjugated polymers for high-efficiency organic photovoltaics. *Polymer Chemistry* **2010**, *1*, 409-419.
26. Anishetty, L. *Schottky behavior of organic solar cells with different cathode deposition methods* **2011**.
27. Bozzetti, M.; De Candia, G.; Gallo, M.; Losito, O.; Mescia, L.; Prudenzano, F. In *In Analysis and design of a solar rectenna;* 2010 IEEE International Symposium on Industrial Electronics; IEEE: **2010**; , pp 2001-2004.
28. Forrest, S. R. The limits to organic photovoltaic cell efficiency. *MRS Bull* **2005**, *30*, 28-32.
29. Brütting, W. *Physics of organic semiconductors;* John Wiley & Sons: 2006; .
30. Pal, S. K.; Kesti, T.; Maiti, M.; Zhang, F.; Inganas, O.; Hellstrom, S.; Andersson, M. R.; Oswald, F.; Langa, F.; Osterman, T. Geminate charge recombination in

polymer/fullerene bulk heterojunction films and implications for solar cell function. *J. Am. Chem. Soc.* **2010**, *132*, 12440-12451.

31. Nelson, J. *The physics of solar cells;* World Scientific: **2003**; Vol. 1.
32. Koster, L.; Mihailetchi, V.; Blom, P. Bimolecular recombination in polymer/fullerene bulk heterojunction solar cells. *Appl. Phys. Lett.* **2006**, *88*, 052104.
33. Kallmann, H.; Pope, M. Photovoltaic effect in organic crystals. *J. Chem. Phys.* **1959**, *30*, 585-586.
34. Tang, C. W. Two-layer organic photovoltaic cell. *Appl. Phys. Lett.* **1986**, *48*, 183-185.
35. Peumans, P.; Yakimov, A.; Forrest, S. R. Small molecular weight organic thin-film photodetectors and solar cells. *J. Appl. Phys.* **2003**, *93*, 3693-3723.
36. Hoppea, H.; Sariciftci, N. S. Organic solar cells: An overview. *J. Mater. Res.* **2004**, *19*, 1925.
37. Granström, M.; Petritsch, K.; Arias, A.; Lux, A.; Andersson, M.; Friend, R. Laminated fabrication of polymeric photovoltaic diodes. *Nature* **1998**, *395*, 257-260.
38. Yu, G.; Gao, J.; Hummelen, J. C.; Wudl, F.; Heeger, A. J. Polymer photovoltiac cells: Enhanced efficiencies via a network of internal donor-acceptor heterojunctions. *Science* **1995**, *270*, 1789.
39. Halls, J.; Walsh, C.; Greenham, N.; Marseglia, E.; Friend, R.; Moratti, S.; Holmes, A. Efficient photodiodes from interpenetrating polymer networks. **1995**.
40. Burke, T. M.; Sweetnam, S.; Vandewal, K.; McGehee, M. D. Beyond Langevin recombination: How equilibrium between free carriers and charge transfer states determines the open-circuit voltage of organic solar cells. *Advanced Energy Materials* **2015**, *5*, 1500123.
41. Scharber, M. C.; Mühlbacher, D.; Koppe, M.; Denk, P.; Waldauf, C.; Heeger, A. J.; Brabec, C. J. Design rules for donors in bulk-heterojunction solar cells—Towards 10% energy-conversion efficiency. *Adv Mater* **2006**, *18*, 789-794.
42. Moliton, A.; Nunzi, J. How to model the behaviour of organic photovoltaic cells. *Polym. Int.* **2006**, *55*, 583-600.
43. Rand, B. P.; Richter, H. *Organic Solar Cells: fundamentals, devices, and upscaling;* Pan Stanford: **2014**; .
44. Hoppe, H.; Sariciftci, N. S. Organic solar cells: An overview. *J. Mater. Res.* **2004**, *19*, 1924-1945.

45. Mishra, A.; Bäuerle, P. Small molecule organic semiconductors on the move: promises for future solar energy technology. *Angewandte Chemie International Edition* **2012**, *51*, 2020-2067.
46. Bartesaghi, D. I. d. C. Pérez, J. Kniepert, S. Roland, M. Turbiez, D. Neher and LJA Koster. *Nat.Commun* **2015**, *6*, 7083.
47. Schipper, D. J.; Fagnou, K. Direct arylation as a synthetic tool for the synthesis of thiophene-based organic electronic materials. *Chemistry of Materials* **2011**, *23*, 1594-1600.
48. Okamoto, K.; Zhang, J.; Housekeeper, J. B.; Marder, S. R.; Luscombe, C. K. C–H arylation reaction: atom efficient and greener syntheses of π-conjugated small molecules and macromolecules for organic electronic materials. *Macromolecules* **2013**, *46*, 8059-8078.
49. Facchetti, A.; Vaccaro, L.; Marrocchi, A. Semiconducting polymers prepared by direct arylation polycondensation. *Angewandte Chemie International Edition* **2012**, *51*, 3520-3523.
50. Wang, K.; Wang, M. Direct arylation polymerization: a green, streamlining synthetic approach to π-conjugated polymers. *Current Organic Chemistry* **2013**, *17*, 999-1012.
51. Sonar, P.; Foong, T. R. B.; Dodabalapur, A. Synthesis of diketopyrrolopyrrole based copolymers via the direct arylation method for p-channel and ambipolar OFETs. *Physical Chemistry Chemical Physics* **2014**, *16*, 4275-4283.
52. Alberico, D.; Scott, M. E.; Lautens, M. Aryl− aryl bond formation by transition-metal-catalyzed direct arylation. *Chem. Rev.* **2007**, *107*, 174-238.
53. Wakioka, M.; Ichihara, N.; Kitano, Y.; Ozawa, F. A highly efficient catalyst for the synthesis of alternating copolymers with thieno [3, 4-c] pyrrole-4, 6-dione units via direct arylation polymerization. *Macromolecules* **2014**, *47*, 626-631.
54. Lafrance, M.; Fagnou, K. Palladium-catalyzed benzene arylation: incorporation of catalytic pivalic acid as a proton shuttle and a key element in catalyst design. *J. Am. Chem. Soc.* **2006**, *128*, 16496-16497.
55. Milstein, D.; Stille, J. A general, selective, and facile method for ketone synthesis from acid chlorides and organotin compounds catalyzed by palladium. *J. Am. Chem. Soc.* **1978**, *100*, 3636-3638.
56. Azarian, D.; Dua, S. S.; Eaborn, C.; Walton, D. R. Reactions of organic halides with R 3 MMR 3 compounds (M= Si, Ge, Sn) in the presence of tetrakis (triarylphosphine) palladium. *Journal of Organometallic Chemistry* **1976**, *117*, C55-C57.

57. Kosugi, M.; Sasazawa, K.; Shimizu, Y.; Migita, T. REACTIONS OF ALLYLTIN COMPOUNDS III. ALLYLATION OF AROMATIC HALIDES WITH ALLYLTRIBUTYLTIN IN THE PRESENCE OF TETRAKIS (TRIPHENYLPHOSPHINE) PALLADIUM (O). *Chem. Lett.* **1977***, 6*, 301-302.

58. Kosugi, M.; Sasazawa, K. Y. shimizu, and T. Migita. *Chem. Lett.* **1977***, 301*.

59. Zhuang, W.; Zhen, H.; Kroon, R.; Tang, Z.; Hellström, S.; Hou, L.; Wang, E.; Gedefaw, D.; Inganäs, O.; Zhang, F. Molecular orbital energy level modulation through incorporation of selenium and fluorine into conjugated polymers for organic photovoltaic cells. *Journal of Materials Chemistry A* **2013***, 1*, 13422-13425.

60. Bolognesi, M.; Gedefaw, D.; Dang, D.; Henriksson, P.; Zhuang, W.; Tessarolo, M.; Wang, E.; Muccini, M.; Seri, M.; Andersson, M. R. 2D π-conjugated benzo [1, 2-b: 4, 5-b′] dithiophene-and quinoxaline-based copolymers for photovoltaic applications. *RSC Advances* **2013***, 3*, 24543-24552.

61. Zhuang, W.; Bolognesi, M.; Seri, M.; Henriksson, P.; Gedefaw, D.; Kroon, R.; Jarvid, M.; Lundin, A.; Wang, E.; Muccini, M. Influence of incorporating different electron-rich thiophene-based units on the photovoltaic properties of isoindigo-based conjugated polymers: an experimental and DFT study. *Macromolecules* **2013***, 46*, 8488-8499.

62. Bao, Z.; Chan, W. K.; Yu, L. Exploration of the Stille coupling reaction for the synthesis of functional polymers. *J. Am. Chem. Soc.* **1995***, 117*, 12426-12435.

63. Boyer, I. J. Toxicity of dibutyltin, tributyltin and other organotin compounds to humans and to experimental animals. *Toxicology* **1989***, 55*, 253-298.

64. Miyaura, N.; Yamada, K.; Suzuki, A. A new stereospecific cross-coupling by the palladium-catalyzed reaction of 1-alkenylboranes with 1-alkenyl or 1-alkynyl halides. *Tetrahedron Lett.* **1979***, 20*, 3437-3440.

65. Miyaura, N.; Suzuki, A. Stereoselective synthesis of arylated (E)-alkenes by the reaction of alk-1-enylboranes with aryl halides in the presence of palladium catalyst. *Journal of the Chemical Society, Chemical Communications* **1979**, 866-867.

66. Miyaura, N.; Yanagi, T.; Suzuki, A. The palladium-catalyzed cross-coupling reaction of phenylboronic acid with haloarenes in the presence of bases. *Synthetic Communications* **1981***, 11*, 513-519.

67. Suzuki, A. Recent advances in the cross-coupling reactions of organoboron derivatives with organic electrophiles, 1995–1998. *Journal of Organometallic Chemistry* **1999***, 576*, 147-168.

68. Zhuang, W.; Zhang, Y.; Hou, Q.; Wang, L.; Cao, Y. High-efficiency, electrophosphorescent polymers with porphyrin–platinum complexes in the conjugated backbone: Synthesis and device performance. *Journal of Polymer Science Part A: Polymer Chemistry* **2006**, *44*, 4174-4186.

69. Wang, E.; Li, C.; Zhuang, W.; Peng, J.; Cao, Y. High-efficiency red and green light-emitting polymers based on a novel wide bandgap poly (2, 7-silafluorene). *Journal of Materials Chemistry* **2008**, *18*, 797-801.

70. Beryozkina, T.; Boyko, K.; Khanduyeva, N.; Senkovskyy, V.; Horecha, M.; Oertel, U.; Simon, F.; Stamm, M.; Kiriy, A. Grafting of Polyfluorene by Surface-Initiated Suzuki Polycondensation. *Angewandte Chemie International Edition* **2009**, *48*, 2695-2698.

71. Schlüter, A. The tenth anniversary of Suzuki polycondensation (SPC). *Journal of Polymer Science Part A: Polymer Chemistry* **2001**, *39*, 1533-1556.

72. Ma, Z.; Wang, E.; Jarvid, M. E.; Henriksson, P.; Inganäs, O.; Zhang, F.; Andersson, M. R. Synthesis and characterization of benzodithiophene–isoindigo polymers for solar cells. *Journal of Materials Chemistry* **2012**, *22*, 2306-2314.

73. Scharber, M. C.; Mühlbacher, D.; Koppe, M.; Denk, P.; Waldauf, C.; Heeger, A. J.; Brabec, C. J. Design rules for donors in bulk-heterojunction solar cells—Towards 10% energy-conversion efficiency. *Adv Mater* **2006**, *18*, 789-794.

74. Brabec, C. J. Organic photovoltaics: technology and market. *Solar Energy Mater. Solar Cells* **2004**, *83*, 273-292.

75. Bundgaard, E.; Krebs, F. C. Low band gap polymers for organic photovoltaics. *Solar Energy Mater. Solar Cells* **2007**, *91*, 954-985.

76. Dennler, G.; Scharber, M. C.; Ameri, T.; Denk, P.; Forberich, K.; Waldauf, C.; Brabec, C. J. Design Rules for Donors in Bulk-Heterojunction Tandem Solar Cells Towards 15% Energy-Conversion Efficiency. *Adv Mater* **2008**, *20*, 579-583.

77. Veldman, D.; Meskers, S. C.; Janssen, R. A. The Energy of Charge-Transfer States in Electron Donor–Acceptor Blends: Insight into the Energy Losses in Organic Solar Cells. *Advanced Functional Materials* **2009**, *19*, 1939-1948.

78. Kippelen, B.; Brédas, J. Organic photovoltaics. *Energy & Environmental Science* **2009**, *2*, 251-261.

79. Havinga, E.; Ten Hoeve, W.; Wynberg, H. A new class of small band gap organic polymer conductors. *Polymer Bulletin* **1992**, *29*, 119-126.

80. Sendur, M.; Balan, A.; Baran, D.; Karabay, B.; Toppare, L. Combination of donor characters in a donor–acceptor–donor (DAD) type polymer containing benzothiadiazole as the acceptor unit. *Organic Electronics* **2010***, 11*, 1877-1885.

81. İçli, M.; Pamuk, M.; Algı, F.; Önal, A. M.; Cihaner, A. A new soluble neutral state black electrochromic copolymer via a donor–acceptor approach. *Organic Electronics* **2010***, 11*, 1255-1260.

82. Nie, G.; Qu, L.; Zhang, Y.; Xu, J.; Zhang, S. Electrochemical copolymerization of 3, 4-ethylenedioxythiophene and 5-methylindole and characterizations of the copolymers. *J Appl Polym Sci* **2008***, 109*, 373-381.

83. Brocks, G.; Tol, A. Small band gap semiconducting polymers made from dye molecules: polysquaraines. *J. Phys. Chem.* **1996***, 100*, 1838-1846.

84. Brocks, G.; Tol, A. A theoretical study of polysquaraines. *Synth. Met.* **1996***, 76*, 213-216.

85. Cheng, Y.; Yang, S.; Hsu, C. Synthesis of conjugated polymers for organic solar cell applications. *Chem. Rev.* **2009***, 109*, 5868-5923.

86. Bao, Z.; Lovinger, A. J. Soluble regioregular polythiophene derivatives as semiconducting materials for field-effect transistors. *Chemistry of materials* **1999***, 11*, 2607-2612.

87. Havinga, E.; Ten Hoeve, W.; Wynberg, H. Alternate donor-acceptor small-band-gap semiconducting polymers; Polysquaraines and polycroconaines. *Synth. Met.* **1993***, 55*, 299-306.

88. Brunetti, F. G.; Kumar, R.; Wudl, F. Organic electronics from perylene to organic photovoltaics: painting a brief history with a broad brush. *Journal of Materials Chemistry* **2010***, 20*, 2934-2948.

89. You, J.; Dou, L.; Yoshimura, K.; Kato, T.; Ohya, K.; Moriarty, T.; Emery, K.; Chen, C.; Gao, J.; Li, G. A polymer tandem solar cell with 10.6% power conversion efficiency. *Nature communications* **2013***, 4*, 1446.

90. Li, C.; Yip, H.; Jen, A. K. Functional fullerenes for organic photovoltaics. *Journal of Materials Chemistry* **2012***, 22*, 4161-4177.

91. Hudhomme, P. An overview of molecular acceptors for organic solar cells. *EPJ Photovoltaics* **2013***, 4*, 40401.

92. Anthony, J. E. Small-Molecule, Nonfullerene Acceptors for Polymer Bulk Heterojunction Organic Photovoltaics†. *Chemistry of Materials* **2010***, 23*, 583-590.

93. Sonar, P.; Lim, J. P. F.; Chan, K. L. Organic non-fullerene acceptors for organic photovoltaics. *Energy & Environmental Science* **2011***, 4*, 1558-1574.

94. Hummelen, J. C.; Knight, B. W.; LePeq, F.; Wudl, F.; Yao, J.; Wilkins, C. L. Preparation and characterization of fulleroid and methanofullerene derivatives. *J. Org. Chem.* **1995**, *60*, 532-538.

95. Li, C.; Yip, H.; Jen, A. K. Functional fullerenes for organic photovoltaics. *Journal of Materials Chemistry* **2012**, *22*, 4161-4177.

96. Li, Y. Fullerene-bisadduct acceptors for polymer solar cells. *Chemistry–An Asian Journal* **2013**, *8*, 2316-2328.

97. Liu, T.; Troisi, A. What makes fullerene acceptors special as electron acceptors in organic solar cells and how to replace them. *Adv Mater* **2013**, *25*, 1038-1041.

98. Ma, W.; Tumbleston, J. R.; Wang, M.; Gann, E.; Huang, F.; Ade, H. Domain purity, miscibility, and molecular orientation at donor/acceptor interfaces in high performance organic solar cells: paths to further improvement. *Advanced Energy Materials* **2013**, *3*, 864-872.

99. Jamieson, F. C.; Domingo, E. B.; McCarthy-Ward, T.; Heeney, M.; Stingelin, N.; Durrant, J. R. Fullerene crystallisation as a key driver of charge separation in polymer/fullerene bulk heterojunction solar cells. *Chemical Science* **2012**, *3*, 485-492.

100. Chen, C.; Chang, W.; Yoshimura, K.; Ohya, K.; You, J.; Gao, J.; Hong, Z.; Yang, Y. An efficient triple-junction polymer solar cell having a power conversion efficiency exceeding 11%. *Adv Mater* **2014**, *26*, 5670-5677.

101. Zhou, H.; Zhang, Y.; Mai, C.; Collins, S. D.; Bazan, G. C.; Nguyen, T.; Heeger, A. J. Polymer homo-tandem solar cells with best efficiency of 11.3%. *Adv Mater* **2015**, *27*, 1767-1773.

102. Wong, H. C.; Li, Z.; Tan, C. H.; Zhong, H.; Huang, Z.; Bronstein, H.; McCulloch, I.; Cabral, J. T.; Durrant, J. R. Morphological stability and performance of polymer–fullerene solar cells under thermal stress: the impact of photoinduced PC60BM oligomerization. *ACS nano* **2014**, *8*, 1297-1308.

103. Wong, H. C.; Li, Z.; Tan, C. H.; Zhong, H.; Huang, Z.; Bronstein, H.; McCulloch, I.; Cabral, J. T.; Durrant, J. R. Morphological stability and performance of polymer–fullerene solar cells under thermal stress: the impact of photoinduced PC60BM oligomerization. *ACS nano* **2014**, *8*, 1297-1308.

104. Lin, Y.; Li, Y.; Zhan, X. Small molecule semiconductors for high-efficiency organic photovoltaics. *Chem. Soc. Rev.* **2012**, *41*, 4245-4272.

105. Lin, Y.; Zhan, X. Non-fullerene acceptors for organic photovoltaics: an emerging horizon. *Materials Horizons* **2014**, *1*, 470-488.

106. Guo, X.; Facchetti, A.; Marks, T. J. Imide-and amide-functionalized polymer semiconductors. *Chem. Rev.* **2014**, *114*, 8943-9021.

107. Facchetti, A. Polymer donor–polymer acceptor (all-polymer) solar cells. *Materials Today* **2013**, *16*, 123-132.

108. Zhan, X.; Facchetti, A.; Barlow, S.; Marks, T. J.; Ratner, M. A.; Wasielewski, M. R.; Marder, S. R. Rylene and related diimides for organic electronics. *Adv Mater* **2011**, *23*, 268-284.

109. Peumans, P.; Bulović, V.; Forrest, S. Efficient photon harvesting at high optical intensities in ultrathin organic double-heterostructure photovoltaic diodes. *Appl. Phys. Lett.* **2000**, *76*, 2650-2652.

110. Yakimov, A.; Forrest, S. High photovoltage multiple-heterojunction organic solar cells incorporating interfacial metallic nanoclusters. *Appl. Phys. Lett.* **2002**, *80*, 1667-1669.

111. Huang, C.; Barlow, S.; Marder, S. R. Perylene-3, 4, 9, 10-tetracarboxylic acid diimides: Synthesis, physical properties, and use in organic electronics. *J. Org. Chem.* **2011**, *76*, 2386-2407.

112. Würthner, F. Perylene bisimide dyes as versatile building blocks for functional supramolecular architectures. *Chemical communications* **2004**, 1564-1579.

113. Schmidt-Mende, L.; Fechtenkotter, A.; Mullen, K.; Moons, E.; Friend, R. H.; MacKenzie, J. D. Self-organized discotic liquid crystals for high-efficiency organic photovoltaics. *Science* **2001**, *293*, 1119-1122.

114. Bijleveld, J. C.; Zoombelt, A. P.; Mathijssen, S. G.; Wienk, M. M.; Turbiez, M.; de Leeuw, D. M.; Janssen, R. A. Poly (diketopyrrolopyrrole− terthiophene) for ambipolar logic and photovoltaics. *J. Am. Chem. Soc.* **2009**, *131*, 16616-16617.

115. Sonar, P.; Ng, G.; Lin, T. T.; Dodabalapur, A.; Chen, Z. Solution processable low bandgap diketopyrrolopyrrole (DPP) based derivatives: novel acceptors for organic solar cells. *Journal of Materials Chemistry* **2010**, *20*, 3626-3636.

116. Lin, Y.; Wang, J.; Zhang, Z.; Bai, H.; Li, Y.; Zhu, D.; Zhan, X. An electron acceptor challenging fullerenes for efficient polymer solar cells. *Adv Mater* **2015**, *27*, 1170-1174.

117. Zhao, W.; Qian, D.; Zhang, S.; Li, S.; Inganäs, O.; Gao, F.; Hou, J. Fullerene-free polymer solar cells with over 11% efficiency and excellent thermal stability. *Adv Mater* **2016**, *28*, 4734-4739.

118. Zhao, W.; Li, S.; Yao, H.; Zhang, S.; Zhang, Y.; Yang, B.; Hou, J. Molecular optimization enables over 13% efficiency in organic solar cells. *J. Am. Chem. Soc.* **2017***, 139*, 7148-7151.

119. Jayawardena, K. I.; Rozanski, L. J.; Mills, C. A.; Beliatis, M. J.; Nismy, N. A.; Silva, S. R. P. 'Inorganics-in-Organics': recent developments and outlook for 4G polymer solar cells. *Nanoscale* **2013***, 5*, 8411-8427.

120. Lu, L.; Zheng, T.; Wu, Q.; Schneider, A. M.; Zhao, D.; Yu, L. Recent advances in bulk heterojunction polymer solar cells. *Chem. Rev.* **2015***, 115*, 12666-12731.

121. Thompson, B. C.; Fréchet, J. M. Polymer–fullerene composite solar cells. *Angewandte chemie international edition* **2008***, 47*, 58-77.

122. Heeger, A. J. 25th anniversary article: bulk heterojunction solar cells: understanding the mechanism of operation. *Adv Mater* **2014***, 26*, 10-28.

123. Brabec, C.; Sarici, N. S. ci and JC Hummelen. *Adv.Funct.Mater* **2001***, 11*, 15.

124. Krebs, F. C.; Gevorgyan, S. A.; Alstrup, J. A roll-to-roll process to flexible polymer solar cells: model studies, manufacture and operational stability studies. *Journal of Materials Chemistry* **2009***, 19*, 5442-5451.

125. Yu, G.; Gao, J.; Hummelen, J. C.; Wudl, F.; Heeger, A. J. Polymer photovoltaic cells: enhanced efficiencies via a network of internal donor-acceptor heterojunctions. *Science* **1995***, 270*, 1789-1791.

126. Lu, L.; Zheng, T.; Wu, Q.; Schneider, A. M.; Zhao, D.; Yu, L. Recent advances in bulk heterojunction polymer solar cells. *Chem. Rev.* **2015***, 115*, 12666-12731.

127. Liu, K.; Larsen-Olsen, T. T.; Lin, Y.; Beliatis, M.; Bundgaard, E.; Jørgensen, M.; Krebs, F. C.; Zhan, X. Roll-coating fabrication of flexible organic solar cells: comparison of fullerene and fullerene-free systems. *Journal of Materials Chemistry A* **2016***, 4*, 1044-1051.

128. Heeger, A. J. 25th anniversary article: bulk heterojunction solar cells: understanding the mechanism of operation. *Adv Mater* **2014***, 26*, 10-28.

129. Yao, H.; Ye, L.; Zhang, H.; Li, S.; Zhang, S.; Hou, J. Molecular design of benzodithiophene-based organic photovoltaic materials. *Chem. Rev.* **2016***, 116*, 7397-7457.

130. Cai, Y.; Huo, L.; Sun, Y. Recent Advances in Wide-Bandgap Photovoltaic Polymers. *Adv Mater* **2017***, 29*, 1605437.

131. Brabec, C. J.; Gowrisanker, S.; Halls, J. J.; Laird, D.; Jia, S.; Williams, S. P. Polymer–fullerene bulk-heterojunction solar cells. *Adv Mater* **2010***, 22*, 3839-3856.

132. He, Y.; Li, Y. Fullerene derivative acceptors for high performance polymer solar cells. *Physical chemistry chemical physics* **2011***, 13*, 1970-1983.

133. Huang, Y.; Kramer, E. J.; Heeger, A. J.; Bazan, G. C. Bulk heterojunction solar cells: morphology and performance relationships. *Chem. Rev.* **2014***, 114*, 7006-7043.

134. Chen, J.; Cui, C.; Li, Y.; Zhou, L.; Ou, Q.; Li, C.; Li, Y.; Tang, J. Single-junction polymer solar cells exceeding 10% power conversion efficiency. *Adv Mater* **2015***, 27*, 1035-1041.

135. Liu, T.; Pan, X.; Meng, X.; Liu, Y.; Wei, D.; Ma, W.; Huo, L.; Sun, X.; Lee, T. H.; Huang, M. Alkyl Side-Chain Engineering in Wide-Bandgap Copolymers Leading to Power Conversion Efficiencies over 10%. *Adv Mater* **2017***, 29*, 1604251.

136. Deng, D.; Zhang, Y.; Zhang, J.; Wang, Z.; Zhu, L.; Fang, J.; Xia, B.; Wang, Z.; Lu, K.; Ma, W. Fluorination-enabled optimal morphology leads to over 11% efficiency for inverted small-molecule organic solar cells. *Nature communications* **2016***, 7*, 13740.

137. Zhao, J.; Li, Y.; Yang, G.; Jiang, K.; Lin, H.; Ade, H.; Ma, W.; Yan, H. Efficient organic solar cells processed from hydrocarbon solvents. *Nature Energy* **2016***, 1*, 15027.

138. Jin, Y.; Chen, Z.; Dong, S.; Zheng, N.; Ying, L.; Jiang, X.; Liu, F.; Huang, F.; Cao, Y. A Novel Naphtho [1, 2-c: 5, 6-c′] Bis ([1, 2, 5] Thiadiazole)-Based Narrow-Bandgap π-Conjugated Polymer with Power Conversion Efficiency Over 10%. *Adv Mater* **2016***, 28*, 9811-9818.

139. He, Z.; Xiao, B.; Liu, F.; Wu, H.; Yang, Y.; Xiao, S.; Wang, C.; Russell, T. P.; Cao, Y. Single-junction polymer solar cells with high efficiency and photovoltage. *Nature Photonics* **2015***, 9*, 174.

140. Yan, C.; Barlow, S.; Wang, Z.; Yan, H.; Jen, A. K.; Marder, S. R.; Zhan, X. Non-fullerene acceptors for organic solar cells. *Nature Reviews Materials* **2018***, 3*, 18003.

141. Nielsen, C. B.; Holliday, S.; Chen, H.; Cryer, S. J.; McCulloch, I. Non-fullerene electron acceptors for use in organic solar cells. *Acc. Chem. Res.* **2015***, 48*, 2803-2812.

142. Lin, Y.; Zhan, X. Oligomer molecules for efficient organic photovoltaics. *Acc. Chem. Res.* **2015***, 49*, 175-183.

143. Krueger, K. B.; Schwenn, P. E.; Gui, K.; Pivrikas, A.; Meredith, P.; Burn, P. L. Morphology dependent electron transport in an n-type electron accepting small molecule for solar cell applications. *Appl. Phys. Lett.* **2011***, 98*, 41.

144. Fang, Y.; Pandey, A. K.; Nardes, A. M.; Kopidakis, N.; Burn, P. L.; Meredith, P. A narrow optical gap small molecule acceptor for organic solar cells. *Advanced Energy Materials* **2013***, 3*, 54-59.

145. Holliday, S.; Ashraf, R. S.; Nielsen, C. B.; Kirkus, M.; Röhr, J. A.; Tan, C.; Collado-Fregoso, E.; Knall, A.; Durrant, J. R.; Nelson, J. A rhodanine flanked nonfullerene acceptor for solution-processed organic photovoltaics. *J. Am. Chem. Soc.* **2015***, 137*, 898-904.

146. Schwenn, P. E.; Gui, K.; Nardes, A. M.; Krueger, K. B.; Lee, K. H.; Mutkins, K.; Rubinstein-Dunlop, H.; Shaw, P. E.; Kopidakis, N.; Burn, P. L. A Small Molecule Non-fullerene Electron Acceptor for Organic Solar Cells. *Advanced Energy Materials* **2011***, 1*, 73-81.

147. Lin, Y.; Li, Y.; Zhan, X. A Solution-Processable Electron Acceptor Based on Dibenzosilole and Diketopyrrolopyrrole for Organic Solar Cells. *Advanced Energy Materials* **2013***, 3*, 724-728.

148. Li, W.; Roelofs, W. C.; Turbiez, M.; Wienk, M. M.; Janssen, R. A. Polymer solar cells with diketopyrrolopyrrole conjugated polymers as the electron donor and electron acceptor. *Adv Mater* **2014***, 26*, 3304-3309.

149. Lin, Y.; Cheng, P.; Li, Y.; Zhan, X. A 3D star-shaped non-fullerene acceptor for solution-processed organic solar cells with a high open-circuit voltage of 1.18 V. *Chemical Communications* **2012***, 48*, 4773-4775.

150. Bai, H.; Cheng, P.; Wang, Y.; Ma, L.; Li, Y.; Zhu, D.; Zhan, X. A bipolar small molecule based on indacenodithiophene and diketopyrrolopyrrole for solution processed organic solar cells. *Journal of Materials Chemistry A* **2014***, 2*, 778-784.

151. Zhan, X.; Tan, Z.; Domercq, B.; An, Z.; Zhang, X.; Barlow, S.; Li, Y.; Zhu, D.; Kippelen, B.; Marder, S. R. A high-mobility electron-transport polymer with broad absorption and its use in field-effect transistors and all-polymer solar cells. *J. Am. Chem. Soc.* **2007***, 129*, 7246-7247.

152. Lin, Y.; Wang, Y.; Wang, J.; Hou, J.; Li, Y.; Zhu, D.; Zhan, X. A Star-Shaped Perylene Diimide Electron Acceptor for High-Performance Organic Solar Cells. *Adv Mater* **2014***, 26*, 5137-5142.

153. Ye, L.; Jiang, W.; Zhao, W.; Zhang, S.; Qian, D.; Wang, Z.; Hou, J. Selecting a Donor Polymer for Realizing Favorable Morphology in Efficient Non-fullerene Acceptor-based Solar Cells. *Small* **2014***, 10*, 4658-4663.

154. Zang, Y.; Li, C.; Chueh, C.; Williams, S. T.; Jiang, W.; Wang, Z.; Yu, J.; Jen, A. K. Integrated Molecular, Interfacial, and Device Engineering towards High-Performance Non-Fullerene Based Organic Solar Cells. *Adv Mater* **2014**, *26*, 5708-5714.

155. Liu, Y.; Mu, C.; Jiang, K.; Zhao, J.; Li, Y.; Zhang, L.; Li, Z.; Lai, J. Y. L.; Hu, H.; Ma, T. A Tetraphenylethylene Core-Based 3D Structure Small Molecular Acceptor Enabling Efficient Non-Fullerene Organic Solar Cells. *Adv Mater* **2015**, *27*, 1015-1020.

156. Zhang, X.; Zhan, C.; Yao, J. Non-fullerene organic solar cells with 6.1% efficiency through fine-tuning parameters of the film-forming process. *Chemistry of Materials* **2014**, *27*, 166-173.

157. Zhan, X.; Facchetti, A.; Barlow, S.; Marks, T. J.; Ratner, M. A.; Wasielewski, M. R.; Marder, S. R. Rylene and related diimides for organic electronics. *Adv Mater* **2011**, *23*, 268-284.

158. Kwon, O. K.; Park, J.; Kim, D. W.; Park, S. K.; Park, S. Y. An All-Small-Molecule Organic Solar Cell with High Efficiency Nonfullerene Acceptor. *Adv Mater* **2015**, *27*, 1951-1956.

159. Hwang, Y.; Earmme, T.; Courtright, B. A.; Eberle, F. N.; Jenekhe, S. A. n-Type semiconducting naphthalene diimide-perylene diimide copolymers: controlling crystallinity, blend morphology, and compatibility toward high-performance all-polymer solar cells. *J. Am. Chem. Soc.* **2015**, *137*, 4424-4434.

160. Brunetti, F. G.; Gong, X.; Tong, M.; Heeger, A.; Wudl, F. Strain and Hückel aromaticity: driving forces for a promising new generation of electron acceptors in organic electronics. *Angewandte Chemie International Edition* **2010**, *49*, 532-536.

161. Winzenberg, K. N.; Kemppinen, P.; Scholes, F. H.; Collis, G. E.; Shu, Y.; Singh, T. B.; Bilic, A.; Forsyth, C. M.; Watkins, S. E. Indan-1, 3-dione electron-acceptor small molecules for solution-processable solar cells: a structure–property correlation. *Chemical Communications* **2013**, *49*, 6307-6309.

162. Lin, Y.; Zhang, Z.; Bai, H.; Wang, J.; Yao, Y.; Li, Y.; Zhu, D.; Zhan, X. High-performance fullerene-free polymer solar cells with 6.31% efficiency. *Energy & Environmental Science* **2015**, *8*, 610-616.

163. Bai, H.; Wang, Y.; Cheng, P.; Wang, J.; Wu, Y.; Hou, J.; Zhan, X. An electron acceptor based on indacenodithiophene and 1, 1-dicyanomethylene-3-indanone for fullerene-free organic solar cells. *Journal of Materials Chemistry A* **2015**, *3*, 1910-1914.

164. Zhou, T.; Jia, T.; Kang, B.; Li, F.; Fahlman, M.; Wang, Y. Nitrile-Substituted QA Derivatives: New Acceptor Materials for Solution-Processable Organic Bulk Heterojunction Solar Cells. *Advanced Energy Materials* **2011***, 1*, 431-439.

165. Lin, Y.; Wang, J.; Zhang, Z.; Bai, H.; Li, Y.; Zhu, D.; Zhan, X. An electron acceptor challenging fullerenes for efficient polymer solar cells. *Adv Mater* **2015***, 27*, 1170-1174.

166. Guo, X.; Zhang, M.; Tan, J.; Zhang, S.; Huo, L.; Hu, W.; Li, Y.; Hou, J. Influence of D/A ratio on photovoltaic performance of a highly efficient polymer solar cell system. *Adv Mater* **2012***, 24*, 6536-6541.

167. Xu, Y.; Chueh, C.; Yip, H.; Ding, F.; Li, Y.; Li, C.; Li, X.; Chen, W.; Jen, A. K. Improved Charge Transport and Absorption Coefficient in Indacenodithieno [3, 2-b] thiophene-based Ladder-Type Polymer Leading to Highly Efficient Polymer Solar Cells. *Adv Mater* **2012***, 24*, 6356-6361.

168. Intemann, J. J.; Yao, K.; Li, Y.; Yip, H.; Xu, Y.; Liang, P.; Chueh, C.; Ding, F.; Yang, X.; Li, X. Highly Efficient Inverted Organic Solar Cells Through Material and Interfacial Engineering of Indacenodithieno [3, 2-b] thiophene-Based Polymers and Devices. *Advanced Functional Materials* **2014***, 24*, 1465-1473.

169. Zhang, M.; Guo, X.; Wang, X.; Wang, H.; Li, Y. Synthesis and photovoltaic properties of D–A copolymers based on alkyl-substituted indacenodithiophene donor unit. *Chemistry of Materials* **2011***, 23*, 4264-4270.

170. Zou, Y.; Najari, A.; Berrouard, P.; Beaupré, S.; Réda Aïch, B.; Tao, Y.; Leclerc, M. A thieno [3, 4-c] pyrrole-4, 6-dione-based copolymer for efficient solar cells. *J. Am. Chem. Soc.* **2010***, 132*, 5330-5331.

171. Fu, L.; Pan, H.; Larsen-Olsen, T. T.; Andersen, T. R.; Bundgaard, E.; Krebs, F. C.; Chen, H. Synthesis and characterization of new electron-withdrawing moiety thieno [2, 3-c] pyrrole-4, 6-dione-based molecules for small molecule solar cells. *Dyes and Pigments* **2013***, 97*, 141-147.

172. Small, C. E.; Chen, S.; Subbiah, J.; Amb, C. M.; Tsang, S.; Lai, T.; Reynolds, J. R.; So, F. High-efficiency inverted dithienogermole–thienopyrrolodione-based polymer solar cells. *Nature Photonics* **2012***, 6*, 115.

173. Stalder, R.; Mei, J.; Graham, K. R.; Estrada, L. A.; Reynolds, J. R. Isoindigo, a versatile electron-deficient unit for high-performance organic electronics. *Chemistry of Materials* **2013***, 26*, 664-678.

174. Lee, O. P.; Yiu, A. T.; Beaujuge, P. M.; Woo, C. H.; Holcombe, T. W.; Millstone, J. E.; Douglas, J. D.; Chen, M. S.; Fréchet, J. M. Efficient Small Molecule Bulk Heterojunction Solar Cells with High Fill Factors via Pyrene-Directed Molecular Self-Assembly. *Adv Mater* **2011**, *23*, 5359-5363.

175. Lin, Y.; Cheng, P.; Liu, Y.; Zhao, X.; Li, D.; Tan, J.; Hu, W.; Li, Y.; Zhan, X. Solution-processable small molecules based on thieno [3, 4-c] pyrrole-4, 6-dione for high-performance solar cells. *Solar Energy Mater. Solar Cells* **2012**, *99*, 301-307.

176. Berrouard, P.; Grenier, F.; Pouliot, J.; Gagnon, E.; Tessier, C.; Leclerc, M. Synthesis and characterization of 5-octylthieno [3, 4-c] pyrrole-4, 6-dione derivatives as new monomers for conjugated copolymers. *Org. Lett.* **2010**, *13*, 38-41.

177. Sabnis, R.; Rangnekar, D.; Sonawane, N. 2-Aminothiophenes by the Gewald reaction. *J. Heterocycl. Chem.* **1999**, *36*, 333-345.

178. Li, Y.; Yao, K.; Yip, H.; Ding, F.; Xu, Y.; Li, X.; Chen, Y.; Jen, A. K. Eleven-Membered Fused-Ring Low Band-Gap Polymer with Enhanced Charge Carrier Mobility and Photovoltaic Performance. *Advanced Functional Materials* **2014**, *24*, 3631-3638.

179. Yu, G.; Gao, J.; Hummelen, J. C.; Wudl, F.; Heeger, A. J. Polymer photovoltaic cells: enhanced efficiencies via a network of internal donor-acceptor heterojunctions. *Science* **1995**, *270*, 1789-1791.

180. Lu, L.; Zheng, T.; Wu, Q.; Schneider, A. M.; Zhao, D.; Yu, L. Recent advances in bulk heterojunction polymer solar cells. *Chem. Rev.* **2015**, *115*, 12666-12731.

181. Li, Y. Molecular design of photovoltaic materials for polymer solar cells: toward suitable electronic energy levels and broad absorption. *Acc. Chem. Res.* **2012**, *45*, 723-733.

182. Chen, Y.; Wan, X.; Long, G. High performance photovoltaic applications using solution-processed small molecules. *Acc. Chem. Res.* **2013**, *46*, 2645-2655.

183. Su, Y.; Lan, S.; Wei, K. Organic photovoltaics. *Materials Today* **2012**, *15*, 554-562.

184. Dou, L.; Liu, Y.; Hong, Z.; Li, G.; Yang, Y. Low-bandgap near-IR conjugated polymers/molecules for organic electronics. *Chem. Rev.* **2015**, *115*, 12633-12665.

185. Wu, J.; Cheng, S.; Cheng, Y.; Hsu, C. Donor–acceptor conjugated polymers based on multifused ladder-type arenes for organic solar cells. *Chem. Soc. Rev.* **2015**, *44*, 1113-1154.

186. Huang, Y.; Kramer, E. J.; Heeger, A. J.; Bazan, G. C. Bulk heterojunction solar cells: morphology and performance relationships. *Chem. Rev.* **2014**, *114*, 7006-7043.

187. Zhang, S.; Qin, Y.; Zhu, J.; Hou, J. Over 14% efficiency in polymer solar cells enabled by a chlorinated polymer donor. *Adv Mater* **2018**, *30*, 1800868.

188. Zhan, C.; Zhang, X.; Yao, J. New advances in non-fullerene acceptor based organic solar cells. *RSC Advances* **2015**, *5*, 93002-93026.

189. Liu, T.; Troisi, A. What makes fullerene acceptors special as electron acceptors in organic solar cells and how to replace them. *Adv Mater* **2013**, *25*, 1038-1041.

190. Lin, Y.; Zhan, X. Designing Efficient Non-Fullerene Acceptors by Tailoring Extended Fused-Rings with Electron-Deficient Groups. *Advanced Energy Materials* **2015**, *5*, 1501063.

191. Yan, C.; Barlow, S.; Wang, Z.; Yan, H.; Jen, A. K.; Marder, S. R.; Zhan, X. Non-fullerene acceptors for organic solar cells. *Nature Reviews Materials* **2018**, *3*, 18003.

192. Li, S.; Liu, W.; Li, C.; Shi, M.; Chen, H. Efficient Organic Solar Cells with Non-Fullerene Acceptors. *Small* **2017**, *13*, 1701120.

193. Hou, J.; Inganäs, O.; Friend, R. H.; Gao, F. Organic solar cells based on non-fullerene acceptors. *Nature materials* **2018**, *17*, 119.

194. Eastham, N. D.; Logsdon, J. L.; Manley, E. F.; Aldrich, T. J.; Leonardi, M. J.; Wang, G.; Powers-Riggs, N. E.; Young, R. M.; Chen, L. X.; Wasielewski, M. R. Hole-Transfer Dependence on Blend Morphology and Energy Level Alignment in Polymer: ITIC Photovoltaic Materials. *Adv Mater* **2018**, *30*, 1704263.

195. Zhou, N.; Lin, H.; Lou, S. J.; Yu, X.; Guo, P.; Manley, E. F.; Loser, S.; Hartnett, P.; Huang, H.; Wasielewski, M. R. Morphology-Performance Relationships in High-Efficiency All-Polymer Solar Cells. *Advanced Energy Materials* **2014**, *4*, 1300785.

196. Chen, S.; Liu, Y.; Zhang, L.; Chow, P. C.; Wang, Z.; Zhang, G.; Ma, W.; Yan, H. A wide-bandgap donor polymer for highly efficient non-fullerene organic solar cells with a small voltage loss. *J. Am. Chem. Soc.* **2017**, *139*, 6298-6301.

197. Wu, Y.; Bai, H.; Wang, Z.; Cheng, P.; Zhu, S.; Wang, Y.; Ma, W.; Zhan, X. A planar electron acceptor for efficient polymer solar cells. *Energy & Environmental Science* **2015**, *8*, 3215-3221.

198. Swick, S. M.; Zhu, W.; Matta, M.; Aldrich, T. J.; Harbuzaru, A.; Lopez Navarrete, J. T.; Ponce Ortiz, R.; Kohlstedt, K. L.; Schatz, G. C.; Facchetti, A.; Melkonyan, F. S.; Marks, T. J. Closely packed, low reorganization energy pi-extended postfullerene acceptors for efficient polymer solar cells. *Proc. Natl. Acad. Sci. U. S. A.* **2018**, *115*, E8341-E8348.

199. Holliday, S.; Ashraf, R. S.; Wadsworth, A.; Baran, D.; Yousaf, S. A.; Nielsen, C. B.; Tan, C.; Dimitrov, S. D.; Shang, Z.; Gasparini, N. High-efficiency and air-stable P3HT-based polymer solar cells with a new non-fullerene acceptor. *Nature communications* **2016***, 7*, 11585.

200. Li, S.; Liu, W.; Li, C.; Lau, T.; Lu, X.; Shi, M.; Chen, H. A non-fullerene acceptor with a fully fused backbone for efficient polymer solar cells with a high open-circuit voltage. *Journal of Materials Chemistry A* **2016***, 4*, 14983-14987.

201. Li, Y.; Gu, M.; Pan, Z.; Zhang, B.; Yang, X.; Gu, J.; Chen, Y. Indacenodithiophene: a promising building block for high performance polymer solar cells. *Journal of Materials Chemistry A* **2017***, 5*, 10798-10814.

202. Zheng, Z.; Awartani, O. M.; Gautam, B.; Liu, D.; Qin, Y.; Li, W.; Bataller, A.; Gundogdu, K.; Ade, H.; Hou, J. Efficient charge transfer and fine-tuned energy level alignment in a THF-processed fullerene-free organic solar cell with 11.3% efficiency. *Adv Mater* **2017***, 29*, 1604241.

203. Zhao, W.; Qian, D.; Zhang, S.; Li, S.; Inganäs, O.; Gao, F.; Hou, J. Fullerene-free polymer solar cells with over 11% efficiency and excellent thermal stability. *Adv Mater* **2016***, 28*, 4734-4739.

204. Lin, Y.; Wang, J.; Zhang, Z.; Bai, H.; Li, Y.; Zhu, D.; Zhan, X. An electron acceptor challenging fullerenes for efficient polymer solar cells. *Adv Mater* **2015***, 27*, 1170-1174.

205. An, M.; Xie, F.; Geng, X.; Zhang, J.; Jiang, J.; Lei, Z.; He, D.; Xiao, Z.; Ding, L. A High-Performance D–A Copolymer Based on Dithieno [3, 2-b: 2′, 3′-d] Pyridin-5 (4H)-One Unit Compatible with Fullerene and Nonfullerene Acceptors in Solar Cells. *Advanced Energy Materials* **2017***, 7*, 1602509.

206. Zhao, W.; Qian, D.; Zhang, S.; Li, S.; Inganäs, O.; Gao, F.; Hou, J. Fullerene-free polymer solar cells with over 11% efficiency and excellent thermal stability. *Adv Mater* **2016***, 28*, 4734-4739.

207. Dai, S.; Zhao, F.; Zhang, Q.; Lau, T.; Li, T.; Liu, K.; Ling, Q.; Wang, C.; Lu, X.; You, W. Fused nonacyclic electron acceptors for efficient polymer solar cells. *J. Am. Chem. Soc.* **2017***, 139*, 1336-1343.

208. Feng, H.; Chang, M.; Zhang, H.; Wan, X.; Li, C.; Chen, Y. New small-molecule acceptors based on hexacyclic naphthalene (cyclopentadithiophene) for efficient non-fullerene organic solar cells. *Journal of Materials Chemistry A* **2017***, 5*, 17204-17210.

209. Shi, X.; Zuo, L.; Jo, S. B.; Gao, K.; Lin, F.; Liu, F.; Jen, A. K. Design of a highly crystalline low-band gap fused-ring electron acceptor for high-efficiency solar cells with low energy loss. *Chemistry of Materials* **2017**, *29*, 8369-8376.

210. Gao, W.; An, Q.; Ming, R.; Xie, D.; Wu, K.; Luo, Z.; Zou, Y.; Zhang, F.; Yang, C. Side Group Engineering of Small Molecular Acceptors for High-Performance Fullerene-Free Polymer Solar Cells: Thiophene Being Superior to Selenophene. *Advanced Functional Materials* **2017**, *27*, 1702194.

211. Yang, Y.; Zhang, Z.; Bin, H.; Chen, S.; Gao, L.; Xue, L.; Yang, C.; Li, Y. Side-chain isomerization on an n-type organic semiconductor ITIC acceptor makes 11.77% high efficiency polymer solar cells. *J. Am. Chem. Soc.* **2016**, *138*, 15011-15018.

212. Aldrich, T. J.; Swick, S. M.; Melkonyan, F. S.; Marks, T. J. Enhancing indacenodithiophene acceptor crystallinity via substituent manipulation increases organic solar cell efficiency. *Chemistry of Materials* **2017**, *29*, 10294-10298.

213. Lin, Y.; Zhao, F.; He, Q.; Huo, L.; Wu, Y.; Parker, T. C.; Ma, W.; Sun, Y.; Wang, C.; Zhu, D. High-performance electron acceptor with thienyl side chains for organic photovoltaics. *J. Am. Chem. Soc.* **2016**, *138*, 4955-4961.

214. Yao, H.; Ye, L.; Hou, J.; Jang, B.; Han, G.; Cui, Y.; Su, G. M.; Wang, C.; Gao, B.; Yu, R. Achieving Highly Efficient Nonfullerene Organic Solar Cells with Improved Intermolecular Interaction and Open-Circuit Voltage. *Adv Mater* **2017**, *29*, 1700254.

215. Zhao, W.; Li, S.; Yao, H.; Zhang, S.; Zhang, Y.; Yang, B.; Hou, J. Molecular optimization enables over 13% efficiency in organic solar cells. *J. Am. Chem. Soc.* **2017**, *139*, 7148-7151.

216. Zhang, Z.; Feng, L.; Xu, S.; Yuan, J.; Zhang, Z.; Peng, H.; Li, Y.; Zou, Y. Achieving over 10% efficiency in a new acceptor ITTC and its blends with hexafluoroquinoxaline based polymers. *Journal of Materials Chemistry A* **2017**, *5*, 11286-11293.

217. Bai, H.; Wu, Y.; Wang, Y.; Wu, Y.; Li, R.; Cheng, P.; Zhang, M.; Wang, J.; Ma, W.; Zhan, X. Nonfullerene acceptors based on extended fused rings flanked with benzothiadiazolylmethylenemalononitrile for polymer solar cells. *Journal of Materials Chemistry A* **2015**, *3*, 20758-20766.

218. Tamayo, A. B.; Walker, B.; Nguyen*, T. A low band gap, solution processable oligothiophene with a diketopyrrolopyrrole core for use in organic solar cells. *The Journal of Physical Chemistry C* **2008**, *112*, 11545-11551.

219. Walker, B.; Tamayo, A. B.; Dang, X.; Zalar, P.; Seo, J. H.; Garcia, A.; Tantiwiwat, M.; Nguyen, T. Nanoscale phase separation and high photovoltaic efficiency in solution-processed, small-molecule bulk heterojunction solar cells. *Advanced Functional Materials* **2009**, *19*, 3063-3069.

220. Mazzio, K. A.; Yuan, M.; Okamoto, K.; Luscombe, C. K. Oligoselenophene derivatives functionalized with a diketopyrrolopyrrole core for molecular bulk heterojunction solar cells. *ACS applied materials & interfaces* **2011**, *3*, 271-278.

221. Tamayo, A. B.; Dang, X.; Walker, B.; Seo, J.; Kent, T.; Nguyen, T. A low band gap, solution processable oligothiophene with a dialkylated diketopyrrolopyrrole chromophore for use in bulk heterojunction solar cells. *Appl. Phys. Lett.* **2009**, *94*, 73.

222. Lee, O. P.; Yiu, A. T.; Beaujuge, P. M.; Woo, C. H.; Holcombe, T. W.; Millstone, J. E.; Douglas, J. D.; Chen, M. S.; Fréchet, J. M. Efficient Small Molecule Bulk Heterojunction Solar Cells with High Fill Factors via Pyrene-Directed Molecular Self-Assembly. *Adv Mater* **2011**, *23*, 5359-5363.

223. Wallquist, O.; Lenz, R. In *In 20 years of DPP pigments–future perspectives;* Macromolecular Symposia; Wiley Online Library: 2002; Vol. 187, pp 617-630.

224. Loser, S.; Bruns, C.; Miyauchi, H. R. o. P. Ortiz, A. Facchetti, SI Stupp and TJ Marks. *J. Am. Chem. Soc.* **2011**, *133*, 8142.

225. Farnum, D. G.; Mehta, G.; Moore, G. G.; Siegal, F. P. Attempted reformatskii reaction of benzonitrile, 1, 4-diketo-3, 6-diphenylpyrrolo [3, 4-C] pyrrole. A lactam analogue of pentalene. *Tetrahedron Lett.* **1974**, *15*, 2549-2552.

226. Rochat, A. C.; Cassar, L.; Iqbal, A. *Preparation of pyrrolo [3, 4-c] pyrroles* **1986**.

227. Qu, Y.; Wu, Y.; Gao, Y.; Qu, S.; Yang, L.; Hua, J. Diketopyrrolopyrrole-based fluorescent conjugated polymer for application of sensing fluoride ion and bioimaging. *Sensors Actuators B: Chem.* **2014**, *197*, 13-19.

228. Cheng, Y.; Yang, S.; Hsu, C. Synthesis of conjugated polymers for organic solar cell applications. *Chem. Rev.* **2009**, *109*, 5868-5923.

229. Li, G.; Zhu, R.; Yang, Y. Polymer solar cells. *Nature photonics* **2012**, *6*, 153.

230. Ye, L.; Zhang, S.; Huo, L.; Zhang, M.; Hou, J. Molecular design toward highly efficient photovoltaic polymers based on two-dimensional conjugated benzodithiophene. *Acc. Chem. Res.* **2014**, *47*, 1595-1603.

231. Li, Y. Molecular design of photovoltaic materials for polymer solar cells: toward suitable electronic energy levels and broad absorption. *Acc. Chem. Res.* **2012***, 45*, 723-733.

232. Chen, Y.; Wan, X.; Long, G. High performance photovoltaic applications using solution-processed small molecules. *Acc. Chem. Res.* **2013***, 46*, 2645-2655.

233. Anthony, J. E.; Facchetti, A.; Heeney, M.; Marder, S. R.; Zhan, X. n-Type organic semiconductors in organic electronics. *Adv Mater* **2010***, 22*, 3876-3892.

234. Chen, C.; Chang, W.; Yoshimura, K.; Ohya, K.; You, J.; Gao, J.; Hong, Z.; Yang, Y. An efficient triple-junction polymer solar cell having a power conversion efficiency exceeding 11%. *Adv Mater* **2014***, 26*, 5670-5677.

235. Shaheen, S. E.; Brabec, C. J.; Sariciftci, N. S.; Padinger, F.; Fromherz, T.; Hummelen, J. C. 2.5% efficient organic plastic solar cells. *Appl. Phys. Lett.* **2001***, 78*, 841-843.

236. Zhou, H.; Zhang, Y.; Mai, C.; Collins, S. D.; Bazan, G. C.; Nguyen, T.; Heeger, A. J. Polymer homo-tandem solar cells with best efficiency of 11.3%. *Adv Mater* **2015***, 27*, 1767-1773.

237. Liu, Y.; Zhao, J.; Li, Z.; Mu, C.; Ma, W.; Hu, H.; Jiang, K.; Lin, H.; Ade, H.; Yan, H. Aggregation and morphology control enables multiple cases of high-efficiency polymer solar cells. *Nature communications* **2014***, 5*, 5293.

238. He, Y.; Li, Y. Fullerene derivative acceptors for high performance polymer solar cells. *Physical chemistry chemical physics* **2011***, 13*, 1970-1983.

239. Liu, T.; Troisi, A. What makes fullerene acceptors special as electron acceptors in organic solar cells and how to replace them. *Adv Mater* **2013***, 25*, 1038-1041.

240. Yu, G.; Gao, J.; Hummelen, J. C.; Wudl, F.; Heeger, A. J. Polymer photovoltaic cells: enhanced efficiencies via a network of internal donor-acceptor heterojunctions. *Science* **1995***, 270*, 1789-1791.

241. Tournebize, A.; Bussiere, P.; Rivaton, A.; Gardette, J.; Medlej, H.; Hiorns, R. C.; Dagron-Lartigau, C.; Krebs, F. C.; Norrman, K. New insights into the mechanisms of photodegradation/stabilization of P3HT: PCBM active layers using poly (3-hexyl-d 13-thiophene). *Chemistry of Materials* **2013***, 25*, 4522-4528.

242. Lin, Y.; Li, Y.; Zhan, X. Small molecule semiconductors for high-efficiency organic photovoltaics. *Chem. Soc. Rev.* **2012***, 41*, 4245-4272.

243. Sonar, P.; Lim, J. P. F.; Chan, K. L. Organic non-fullerene acceptors for organic photovoltaics. *Energy & Environmental Science* **2011***, 4*, 1558-1574.

244. Anthony, J. E. Small-molecule, nonfullerene acceptors for polymer bulk heterojunction organic photovoltaics. *Chemistry of Materials* **2010**, *23*, 583-590.

245. Lin, Y.; Zhan, X. Non-fullerene acceptors for organic photovoltaics: an emerging horizon. *Materials Horizons* **2014**, *1*, 470-488.

246. Zhao, X.; Zhan, X. Electron transporting semiconducting polymers in organic electronics. *Chem. Soc. Rev.* **2011**, *40*, 3728-3743.

247. Facchetti, A. Polymer donor–polymer acceptor (all-polymer) solar cells. *Materials Today* **2013**, *16*, 123-132.

248. Zhan, X.; Facchetti, A.; Barlow, S.; Marks, T. J.; Ratner, M. A.; Wasielewski, M. R.; Marder, S. R. Rylene and related diimides for organic electronics. *Adv Mater* **2011**, *23*, 268-284.

249. Zhang, X.; Lu, Z.; Ye, L.; Zhan, C.; Hou, J.; Zhang, S.; Jiang, B.; Zhao, Y.; Huang, J.; Zhang, S. A potential perylene diimide dimer-based acceptor material for highly efficient solution-processed non-fullerene organic solar cells with 4.03% efficiency. *Adv Mater* **2013**, *25*, 5791-5797.

250. Mori, D.; Benten, H.; Okada, I.; Ohkita, H.; Ito, S. Highly efficient charge-carrier generation and collection in polymer/polymer blend solar cells with a power conversion efficiency of 5.7%. *Energy & Environmental Science* **2014**, *7*, 2939-2943.

251. Zhao, J.; Li, Y.; Lin, H.; Liu, Y.; Jiang, K.; Mu, C.; Ma, T.; Lai, J. Y. L.; Hu, H.; Yu, D. High-efficiency non-fullerene organic solar cells enabled by a difluorobenzothiadiazole-based donor polymer combined with a properly matched small molecule acceptor. *Energy & Environmental Science* **2015**, *8*, 520-525.

252. Liu, Y.; Mu, C.; Jiang, K.; Zhao, J.; Li, Y.; Zhang, L.; Li, Z.; Lai, J. Y. L.; Hu, H.; Ma, T. A Tetraphenylethylene Core-Based 3D Structure Small Molecular Acceptor Enabling Efficient Non-Fullerene Organic Solar Cells. *Adv Mater* **2015**, *27*, 1015-1020.

253. Lin, Y.; Zhang, Z.; Bai, H.; Wang, J.; Yao, Y.; Li, Y.; Zhu, D.; Zhan, X. High-performance fullerene-free polymer solar cells with 6.31% efficiency. *Energy & Environmental Science* **2015**, *8*, 610-616.

254. Jung, J. W.; Jo, J. W.; Chueh, C.; Liu, F.; Jo, W. H.; Russell, T. P.; Jen, A. K. Fluoro-Substituted n-Type Conjugated Polymers for Additive-Free All-Polymer Bulk Heterojunction Solar Cells with High Power Conversion Efficiency of 6.71%. *Adv Mater* **2015**, *27*, 3310-3317.

255. Zhao, W.; Li, S.; Yao, H.; Zhang, S.; Zhang, Y.; Yang, B.; Hou, J. Molecular optimization enables over 13% efficiency in organic solar cells. *J. Am. Chem. Soc.* **2017**, *139*, 7148-7151.

256. Lin, Y.; Wang, J.; Zhang, Z.; Bai, H.; Li, Y.; Zhu, D.; Zhan, X. An electron acceptor challenging fullerenes for efficient polymer solar cells. *Adv Mater* **2015**, *27*, 1170-1174.

257. Bai, H.; Wang, Y.; Cheng, P.; Wang, J.; Wu, Y.; Hou, J.; Zhan, X. An electron acceptor based on indacenodithiophene and 1, 1-dicyanomethylene-3-indanone for fullerene-free organic solar cells. *Journal of Materials Chemistry A* **2015**, *3*, 1910-1914.

258. Lin, Y.; Wang, J.; Dai, S.; Li, Y.; Zhu, D.; Zhan, X. A twisted dimeric perylene diimide electron acceptor for efficient organic solar cells. *Advanced Energy Materials* **2014**, *4*, 1400420.

259. Bai, H.; Cheng, P.; Wang, Y.; Ma, L.; Li, Y.; Zhu, D.; Zhan, X. A bipolar small molecule based on indacenodithiophene and diketopyrrolopyrrole for solution processed organic solar cells. *Journal of Materials Chemistry A* **2014**, *2*, 778-784.

260. Li, Y.; Yao, K.; Yip, H.; Ding, F.; Xu, Y.; Li, X.; Chen, Y.; Jen, A. K. Eleven-Membered Fused-Ring Low Band-Gap Polymer with Enhanced Charge Carrier Mobility and Photovoltaic Performance. *Advanced Functional Materials* **2014**, *24*, 3631-3638.

261. Bai, H.; Wang, Y.; Cheng, P.; Li, Y.; Zhu, D.; Zhan, X. Acceptor–donor–acceptor small molecules based on indacenodithiophene for efficient organic solar cells. *ACS applied materials & interfaces* **2014**, *6*, 8426-8433.

262. Lee, H.; Lee, J. S.; Cho, S.; Kim, H.; Kwak, K.; Yoon, Y.; Son, S. K.; Kim, H.; Ko, M. J.; Lee, D. Crystallinity-controlled naphthalene-alt-diketopyrrolopyrrole copolymers for high-performance ambipolar field effect transistors. *The Journal of Physical Chemistry C* **2012**, *116*, 26204-26213.

263. Li, W.; Lee, T.; Oh, S. J.; Kagan, C. R. Diketopyrrolopyrrole-based π-bridged donor–acceptor polymer for photovoltaic applications. *ACS applied materials & interfaces* **2011**, *3*, 3874-3883.

264. Sonar, P.; Singh, S. P.; Williams, E. L.; Li, Y.; Soh, M. S.; Dodabalapur, A. Furan containing diketopyrrolopyrrole copolymers: synthesis, characterization, organic field effect transistor performance and photovoltaic properties. *Journal of Materials Chemistry* **2012**, *22*, 4425-4435.

265. Choi, Y. S.; Jo, W. H. A strategy to enhance both VOC and JSC of A–D–A type small molecules based on diketopyrrolopyrrole for high efficient organic solar cells. *Organic Electronics* **2013**, *14*, 1621-1628.

266. Jung, J. W.; Jo, W. H. A low band-gap copolymer composed of thienyl substituted anthracene and diketopyrrolopyrrole compatible with multiple electron acceptors for high efficiency polymer solar cells. *Polymer Chemistry* **2015**, *6*, 4013-4019.

267. Sonar, P.; Singh, S. P.; Li, Y.; Ooi, Z.; Ha, T.; Wong, I.; Soh, M. S.; Dodabalapur, A. High mobility organic thin film transistor and efficient photovoltaic devices using versatile donor–acceptor polymer semiconductor by molecular design. *Energy & Environmental Science* **2011**, *4*, 2288-2296.

268. Bijleveld, J. C.; Gevaerts, V. S.; Di Nuzzo, D.; Turbiez, M.; Mathijssen, S. G.; de Leeuw, D. M.; Wienk, M. M.; Janssen, R. A. Efficient solar cells based on an easily accessible diketopyrrolopyrrole polymer. *Adv Mater* **2010**, *22*, E242-E246.

269. Palai, A. K.; Lee, J.; Jea, M.; Na, H.; Shin, T. J.; Jang, S.; Park, S.; Pyo, S. Symmetrically functionalized diketopyrrolopyrrole with alkylated thiophene moiety: from synthesis to electronic devices applications. *J. Mater. Sci.* **2014**, *49*, 4215-4224.

270. Qu, S.; Tian, H. Diketopyrrolopyrrole (DPP)-based materials for organic photovoltaics. *Chemical Communications* **2012**, *48*, 3039-3051.

271. Lai, Y.; Yeh, J.; Tsai, C.; Cheng, Y. Synthesis, Molecular and Photovoltaic Properties of an Indolo [3, 2-b] indole-Based Acceptor–Donor–Acceptor Small Molecule. *European Journal of Organic Chemistry* **2013**, *2013*, 5076-5084.

272. Yiu, A. T.; Beaujuge, P. M.; Lee, O. P.; Woo, C. H.; Toney, M. F.; Fréchet, J. M. Side-chain tunability of furan-containing low-band-gap polymers provides control of structural order in efficient solar cells. *J. Am. Chem. Soc.* **2012**, *134*, 2180-2185.

273. Bronstein, H.; Chen, Z.; Ashraf, R. S.; Zhang, W.; Du, J.; Durrant, J. R.; Shakya Tuladhar, P.; Song, K.; Watkins, S. E.; Geerts, Y. Thieno [3, 2-b] thiophene−diketopyrrolopyrrole-containing polymers for high-performance organic field-effect transistors and organic photovoltaic devices. *J. Am. Chem. Soc.* **2011**, *133*, 3272-3275.

274. Chen, H.; Guo, Y.; Yu, G.; Zhao, Y.; Zhang, J.; Gao, D.; Liu, H.; Liu, Y. Highly π-Extended Copolymers with Diketopyrrolopyrrole Moieties for High-Performance Field-Effect Transistors. *Adv Mater* **2012**, *24*, 4618-4622.

275. Dou, L.; Gao, J.; Richard, E.; You, J.; Chen, C.; Cha, K. C.; He, Y.; Li, G.; Yang, Y. Systematic investigation of benzodithiophene-and diketopyrrolopyrrole-based low-bandgap polymers designed for single junction and tandem polymer solar cells. *J. Am. Chem. Soc.* **2012**, *134*, 10071-10079.

276. Lin, Y.; Ma, L.; Li, Y.; Liu, Y.; Zhu, D.; Zhan, X. A Solution-Processable Small Molecule Based on Benzodithiophene and Diketopyrrolopyrrole for High-Performance Organic Solar Cells. *Advanced Energy Materials* **2013***, 3*, 1166-1170.

277. Lin, Y.; Li, Y.; Zhan, X. A Solution-Processable Electron Acceptor Based on Dibenzosilole and Diketopyrrolopyrrole for Organic Solar Cells. *Advanced Energy Materials* **2013***, 3*, 724-728.

278. Lin, Y.; Cheng, P.; Li, Y.; Zhan, X. A 3D star-shaped non-fullerene acceptor for solution-processed organic solar cells with a high open-circuit voltage of 1.18 V. *Chemical Communications* **2012***, 48*, 4773-4775.

279. Park, S. H.; Park, G. E.; Choi, S.; Kim, Y. U.; Park, S. Y.; Park, C. G.; Cho, M. J.; Choi, D. H. Effect of a methyl thiophene-3-carboxylate bridge in an indacenodithiophene-based acceptor–donor–acceptor-type molecule on the performance of non-fullerene polymer solar cells. *Journal of Materials Chemistry C* **2018***, 6*, 7549-7556.

280. Henssler, J. T.; Matzger, A. J. Facile and scalable synthesis of the fused-ring heterocycles thieno [3, 2-b] thiophene and thieno [3, 2-b] furan. *Org. Lett.* **2009***, 11*, 3144-3147.

281. Henssler, J. T.; Matzger, A. J. Facile and scalable synthesis of the fused-ring heterocycles thieno [3, 2-b] thiophene and thieno [3, 2-b] furan. *Org. Lett.* **2009***, 11*, 3144-3147.

282. Liu, S.; Bao, X.; Li, W.; Wu, K.; Xie, G.; Yang, R.; Yang, C. Benzo [1, 2-b: 4, 5-b′] dithiophene and thieno [3, 4-c] pyrrole-4, 6-dione based donor-π-acceptor conjugated polymers for high performance solar cells by rational structure modulation. *Macromolecules* **2015***, 48*, 2948-2957.

283. Luo, M.; Zhang, Z.; Feng, L.; Peng, H.; Jiang, L.; Xu, S.; Li, H.; Cai, F.; Li, Y.; Zou, Y. Synthesis and photovoltaic properties of a non-fullerene acceptor with F-phenylalkoxy as a side chain. *New Journal of Chemistry* **2018***, 42*, 19279-19284.

284. Dai, S.; Zhao, F.; Zhang, Q.; Lau, T.; Li, T.; Liu, K.; Ling, Q.; Wang, C.; Lu, X.; You, W. Fused nonacyclic electron acceptors for efficient polymer solar cells. *J. Am. Chem. Soc.* **2017***, 139*, 1336-1343.

285. Xu, X.; Cai, P.; Lu, Y.; Choon, N. S.; Chen, J.; Ong, B. S.; Hu, X. Synthesis of a Novel Low-Bandgap Polymer Based on a Ladder-Type Heptacyclic Arene Consisting of Outer Thieno [3, 2-b] thiophene Units for Efficient Photovoltaic Application. *Macromolecular rapid communications* **2013***, 34*, 681-688.

286. Matsueda, Y.; Xu, S.; Negishi, E. A novel highly enantio-and diastereoselective synthesis of vitamin E side-chain. *Tetrahedron Lett.* **2015***, 56*, 3346-3348.

287. Thomson, A.; O'Connor, S.; Knuckley, B.; Causey, C. P. Design, synthesis, and in vitro evaluation of an activity-based protein profiling (ABPP) probe targeting agmatine deiminases. *Bioorg. Med. Chem.* **2014***, 22*, 4602-4608.

288. Yue, W.; Zhao, Y.; Shao, S.; Tian, H.; Xie, Z.; Geng, Y.; Wang, F. Novel NIR-absorbing conjugated polymers for efficient polymer solar cells: effect of alkyl chain length on device performance. *Journal of Materials Chemistry* **2009***, 19*, 2199-2206.

289. Warnan, J.; El Labban, A.; Cabanetos, C.; Hoke, E. T.; Shukla, P. K.; Risko, C.; Brédas, J.; McGehee, M. D.; Beaujuge, P. M. Ring substituents mediate the morphology of PBDTTPD-PCBM bulk-heterojunction solar cells. *Chemistry of Materials* **2014***, 26*, 2299-2306.

290. Aytun, T.; Barreda, L.; Ruiz-Carretero, A.; Lehrman, J. A.; Stupp, S. I. Improving solar cell efficiency through hydrogen bonding: a method for tuning active layer morphology. *Chemistry of Materials* **2015***, 27*, 1201-1209.

291. Pielak, K.; Bondu, F.; Sanguinet, L.; Rodriguez, V.; Champagne, B.; Castet, F. Second-order nonlinear optical properties of multiaddressable indolinooxazolidine derivatives: joint computational and hyper-Rayleigh scattering investigations. *The Journal of Physical Chemistry C* **2017***, 121*, 1851-1860.

292. Cui, Y.; Ren, H.; Yu, J.; Wang, Z.; Qian, G. An indanone-based alkoxysilane dye with second order nonlinear optical properties. *Dyes and Pigments* **2009***, 81*, 53-57.

293. Xu, Y.; Chueh, C.; Yip, H.; Ding, F.; Li, Y.; Li, C.; Li, X.; Chen, W.; Jen, A. K. Improved Charge Transport and Absorption Coefficient in Indacenodithieno [3, 2-b] thiophene-based Ladder-Type Polymer Leading to Highly Efficient Polymer Solar Cells. *Adv Mater* **2012***, 24*, 6356-6361.

294. Li, Y.; Tatum, W. K.; Onorato, J. W.; Barajas, S. D.; Yang, Y. Y.; Luscombe, C. K. An indacenodithiophene-based semiconducting polymer with high ductility for stretchable organic electronics. *Polymer Chemistry* **2017***, 8*, 5185-5193.

295. Sun, Y.; Chien, S.; Yip, H.; Zhang, Y.; Chen, K.; Zeigler, D. F.; Chen, F.; Lin, B.; Jen, A. K. High-mobility low-bandgap conjugated copolymers based on indacenodithiophene and thiadiazolo [3, 4-c] pyridine units for thin film transistor and photovoltaic applications. *Journal of Materials Chemistry* **2011***, 21*, 13247-13255.

296. Rochat, A. C.; Cassar, L.; Iqbal, A. *Preparation of pyrrolo [3, 4-c] pyrroles* **1986**.

297. Huo, L.; Hou, J.; Chen, H.; Zhang, S.; Jiang, Y.; Chen, T. L.; Yang, Y. Bandgap and molecular level control of the low-bandgap polymers based on 3, 6-dithiophen-2-yl-2, 5-dihydropyrrolo [3, 4-c] pyrrole-1, 4-dione toward highly efficient polymer solar cells. *Macromolecules* **2009**, *42*, 6564-6571.

298. Sahu, D.; Tsai, C.; Wei, H.; Ho, K.; Chang, F.; Chu, C. Synthesis and applications of novel low bandgap star-burst molecules containing a triphenylamine core and dialkylated diketopyrrolopyrrole arms for organic photovoltaics. *Journal of Materials Chemistry* **2012**, *22*, 7945-7953.

Chapter IIV: Supplementary information

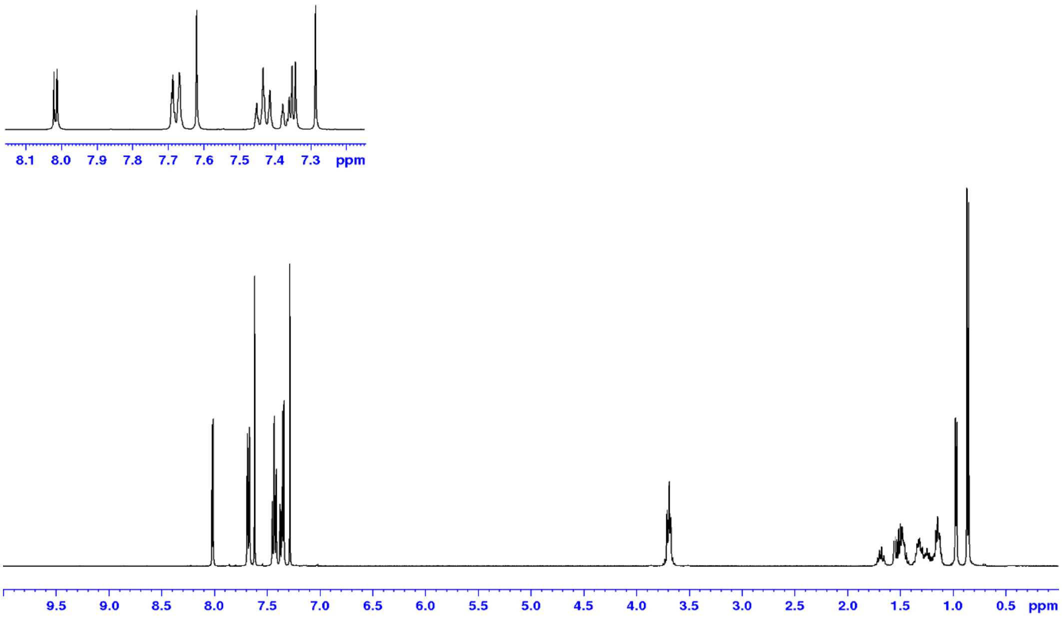

Figure 7. 1: ^{1}H NMR spectrum of **TPD-PHT (M2).**

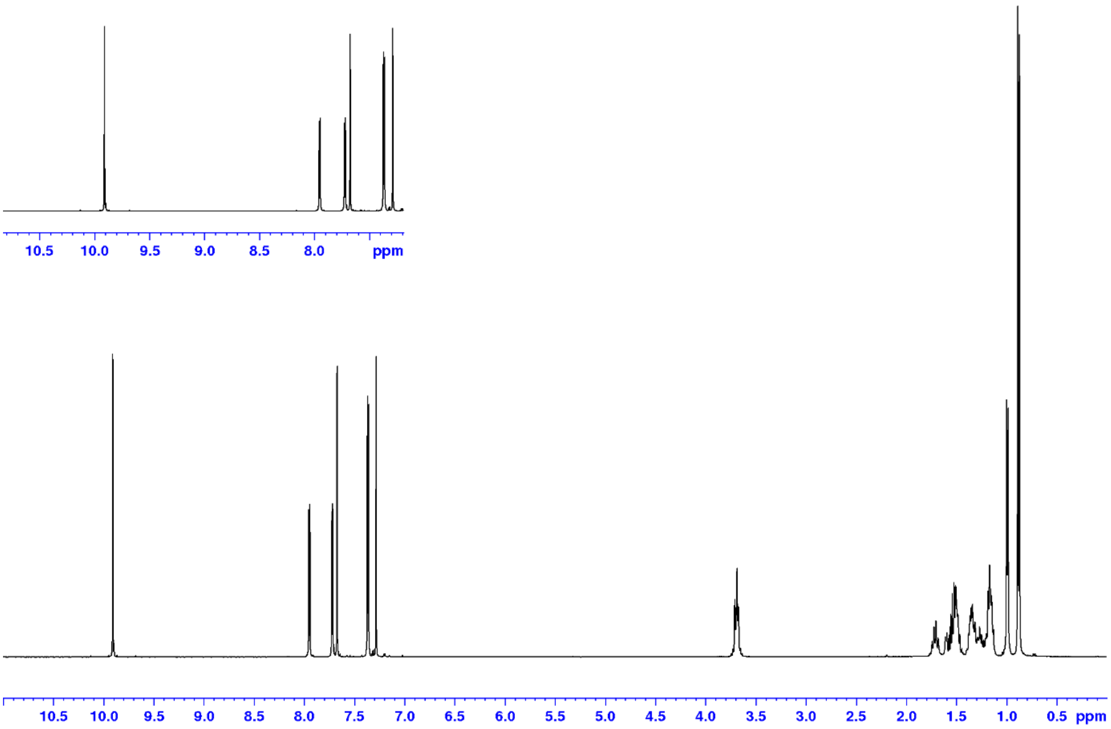

Figure 7. 2: ^{1}H NMR spectrum of **TPD-PHT (M3).**

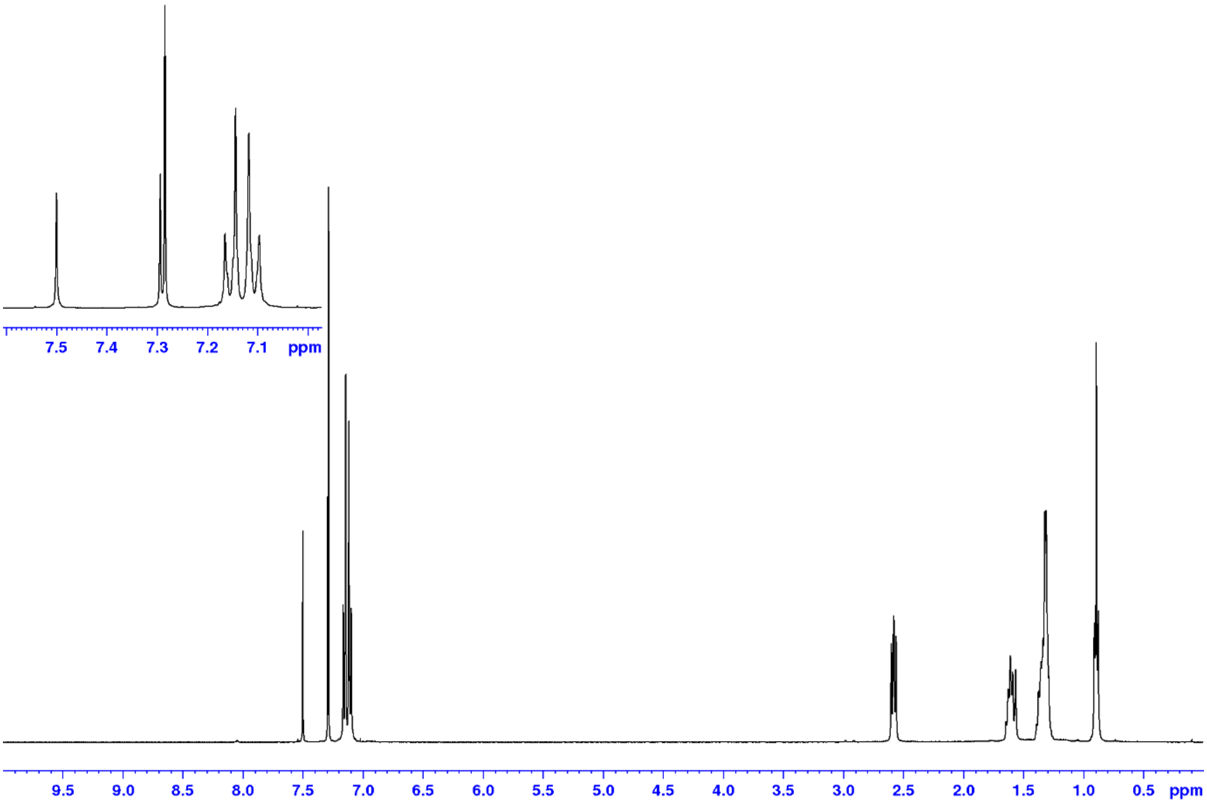

Figure 7. 3: ^{1}H NMR spectrum of **IDTT-Br2 (M4)** in **$CDCl_3$.**

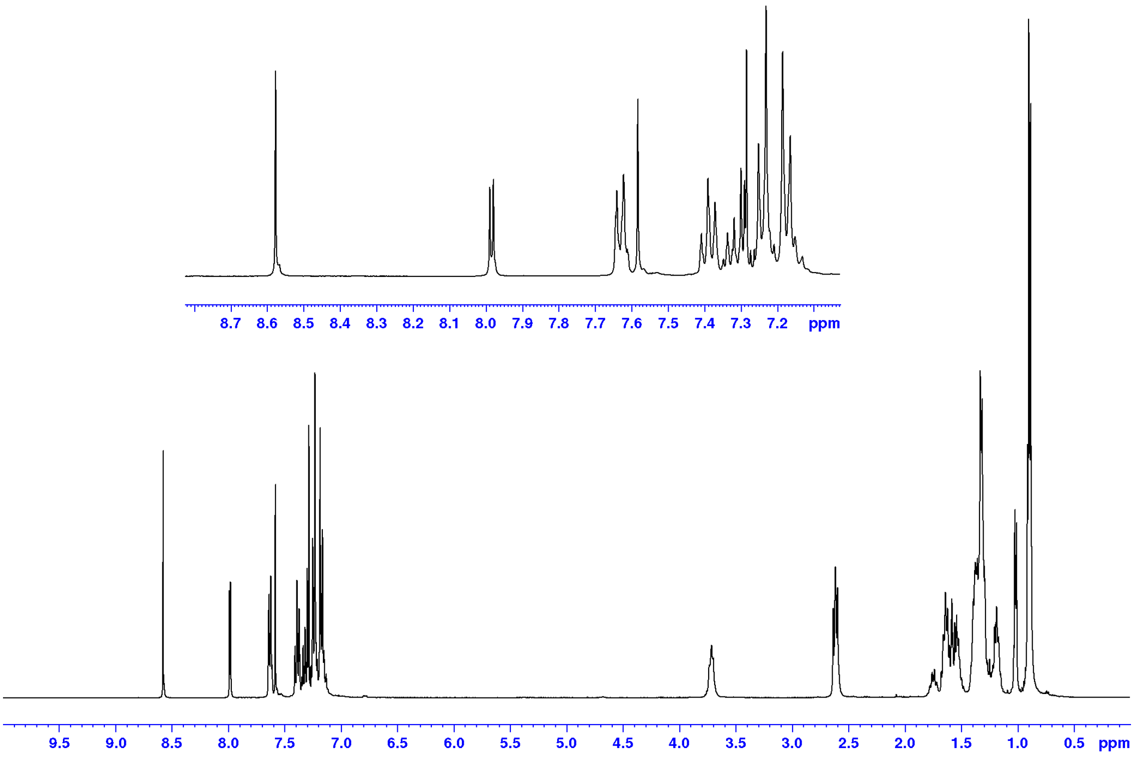

Figure 7. 4: The ^{1}H NMR spectrum of **IDTT-TPD-PHT** in **CDCl$_3$.**

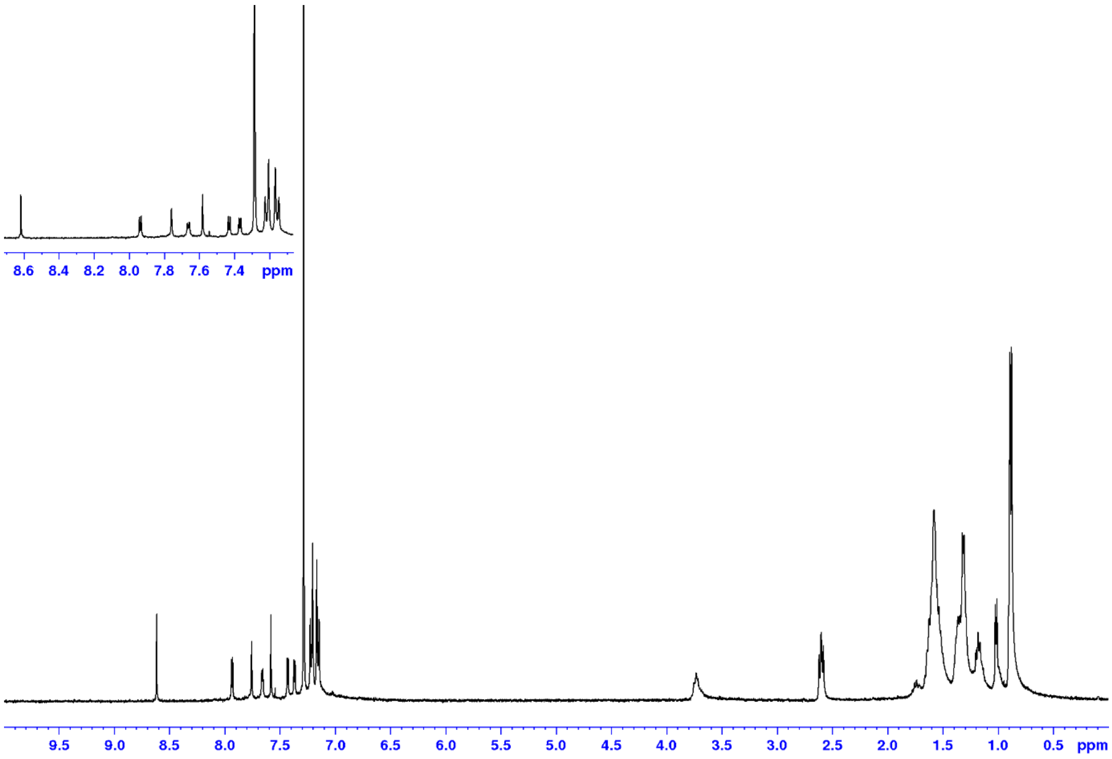

Figure 7. 5: The ^{1}H NMR spectrum of **IDTT-TPD-CN** in **CDCl$_3$.**

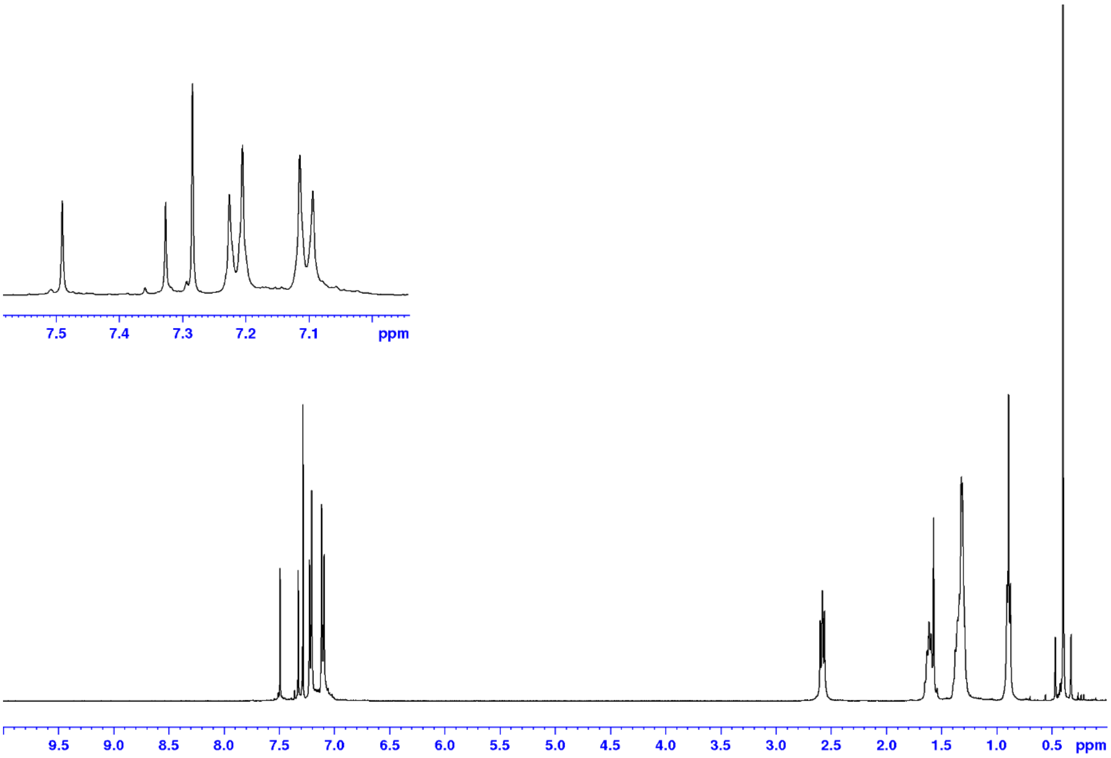

Figure 7. 6: ^{1}H NMR spectrum of **IDTT-Sn2** in **CDCl$_3$.**

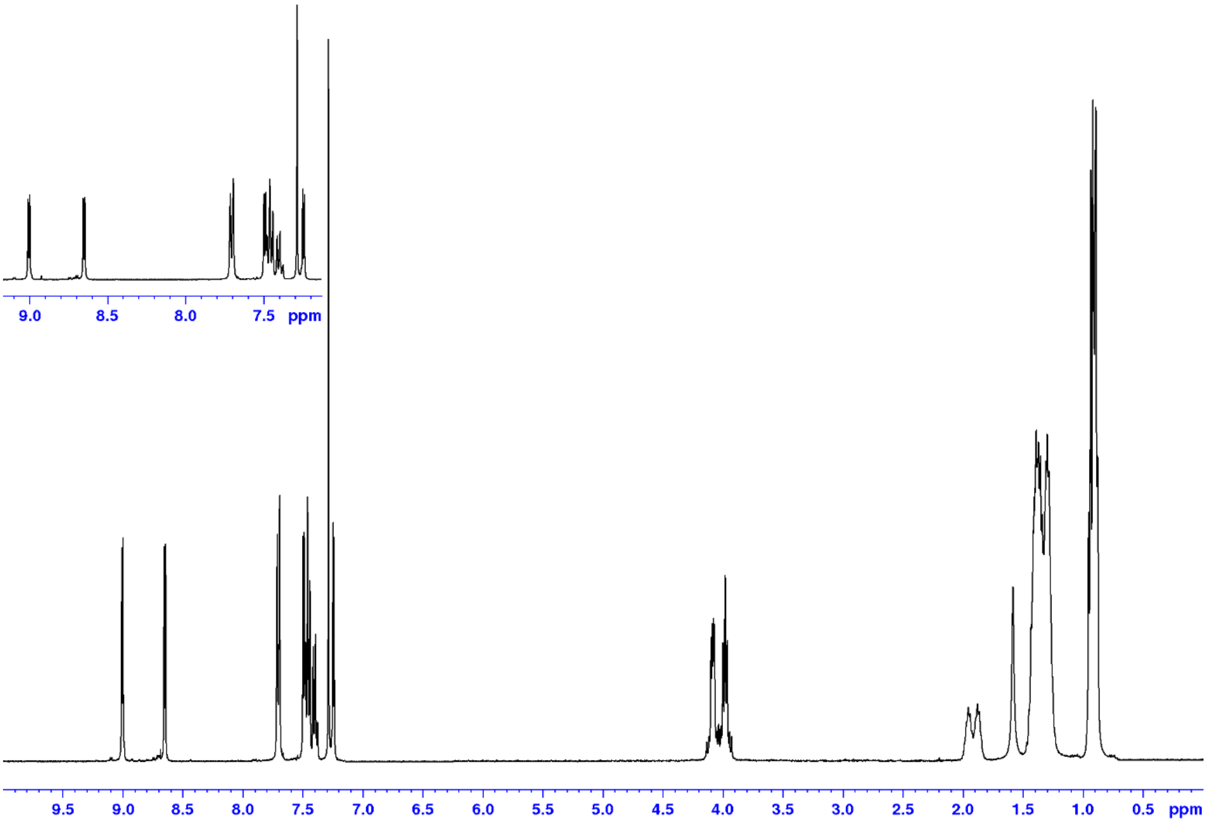

Figure 7. 7: ^{1}H NMR spectrum of **DPP-PH-Br** in **CDCl$_3$.**

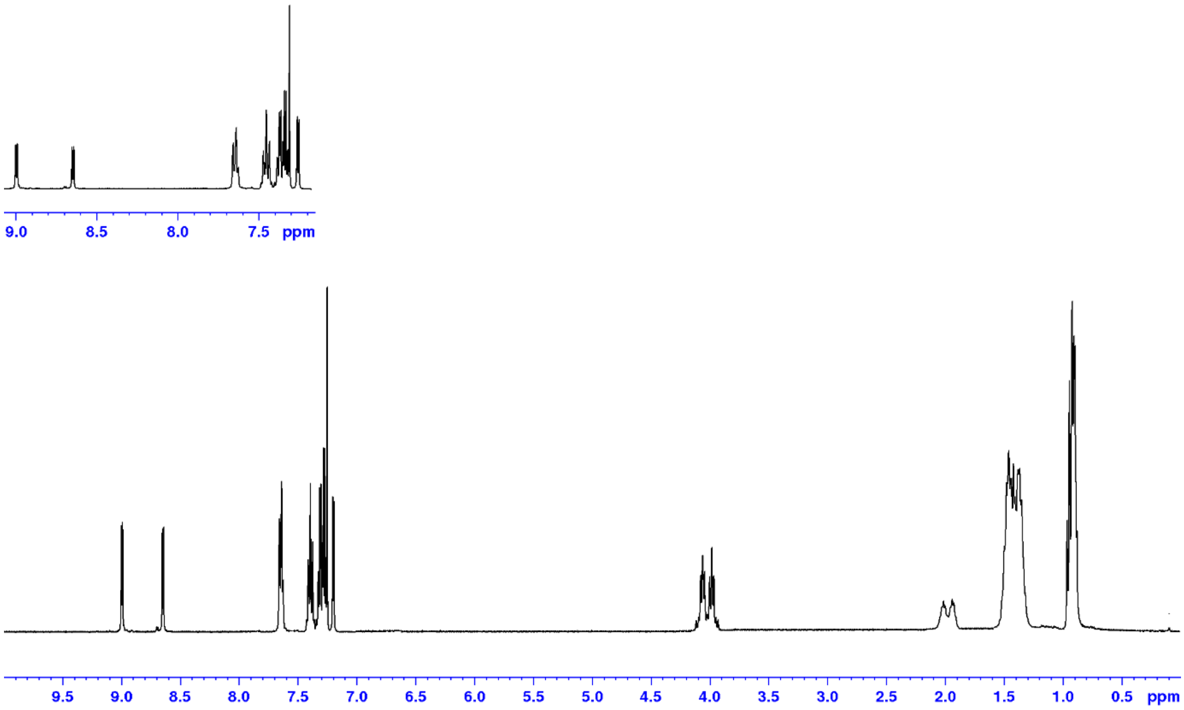

Figure 7. 8: ^{1}H NMR spectrum of **DPP-PHT-Br** in **CDCl$_3$.**

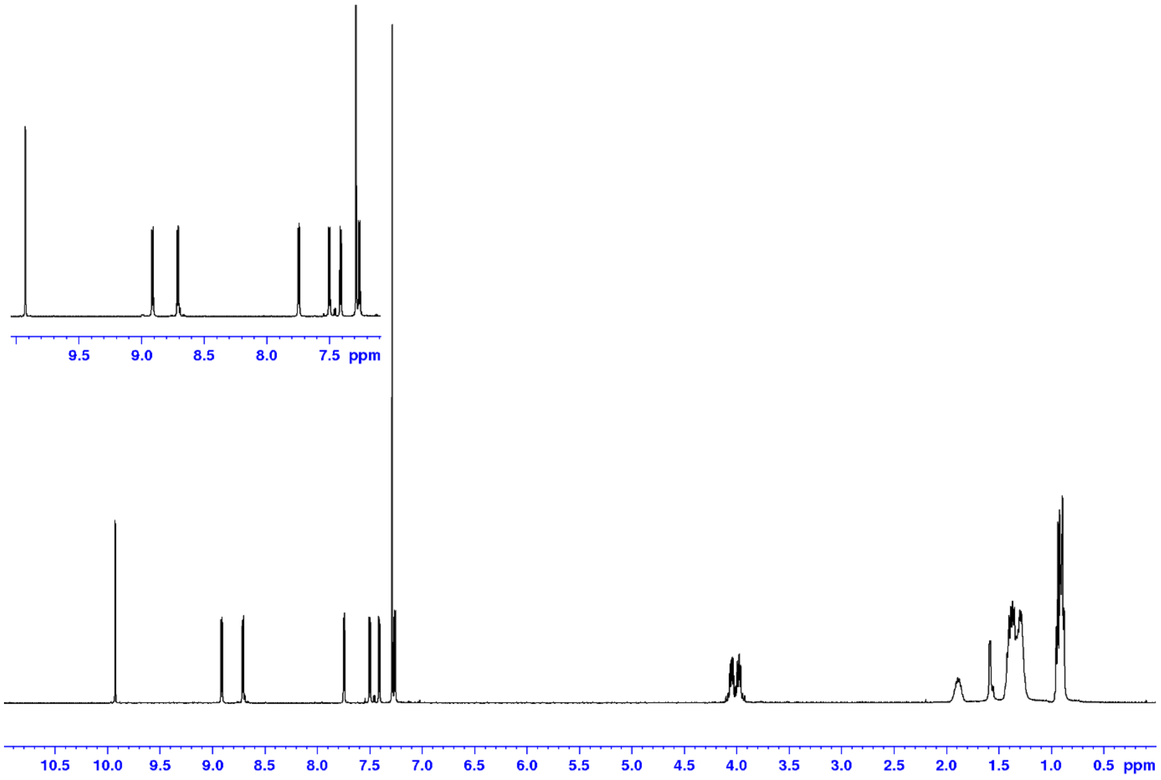

Figure 7. 9: ^{1}H NMR spectrum of **DPP-CHO-Br** in **CDCl$_3$.**

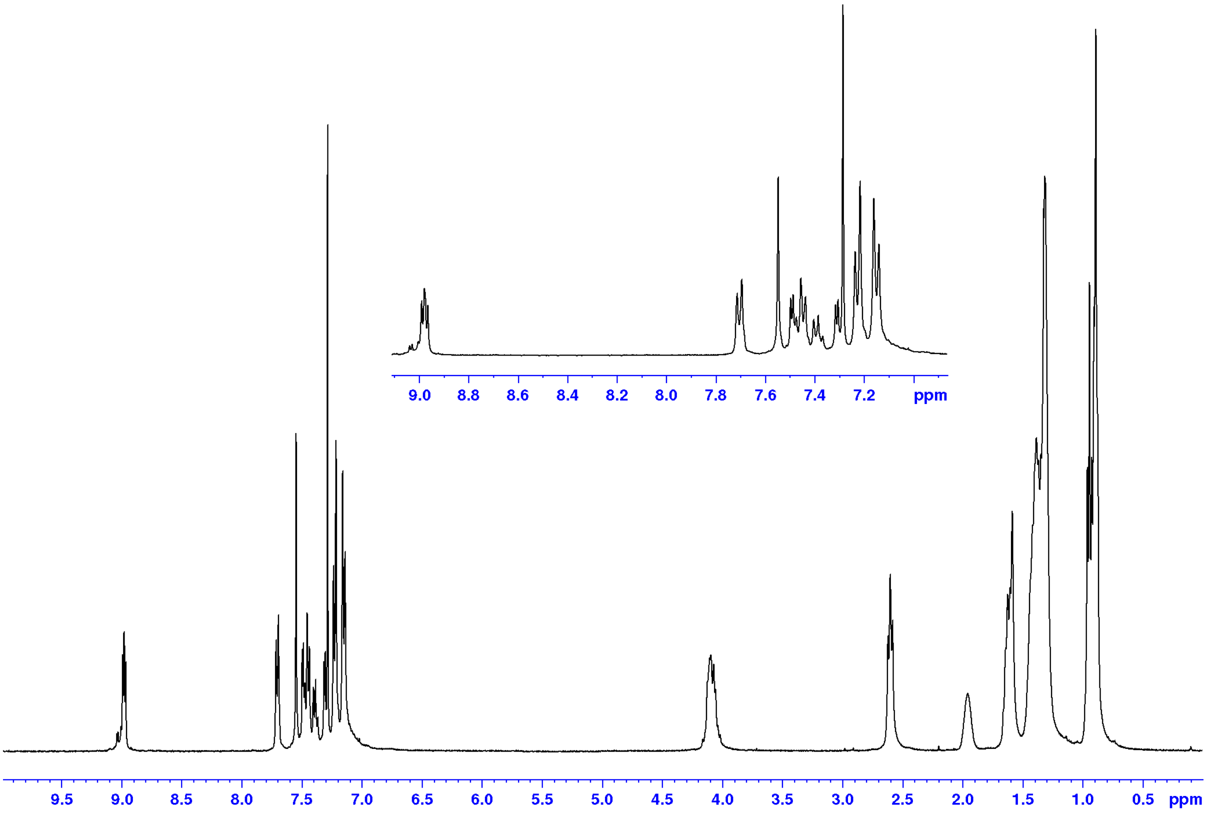

Figure 7. 10: ^{1}H NMR spectrum of **IDTT-DPP-PH** in **CDCl$_3$.**

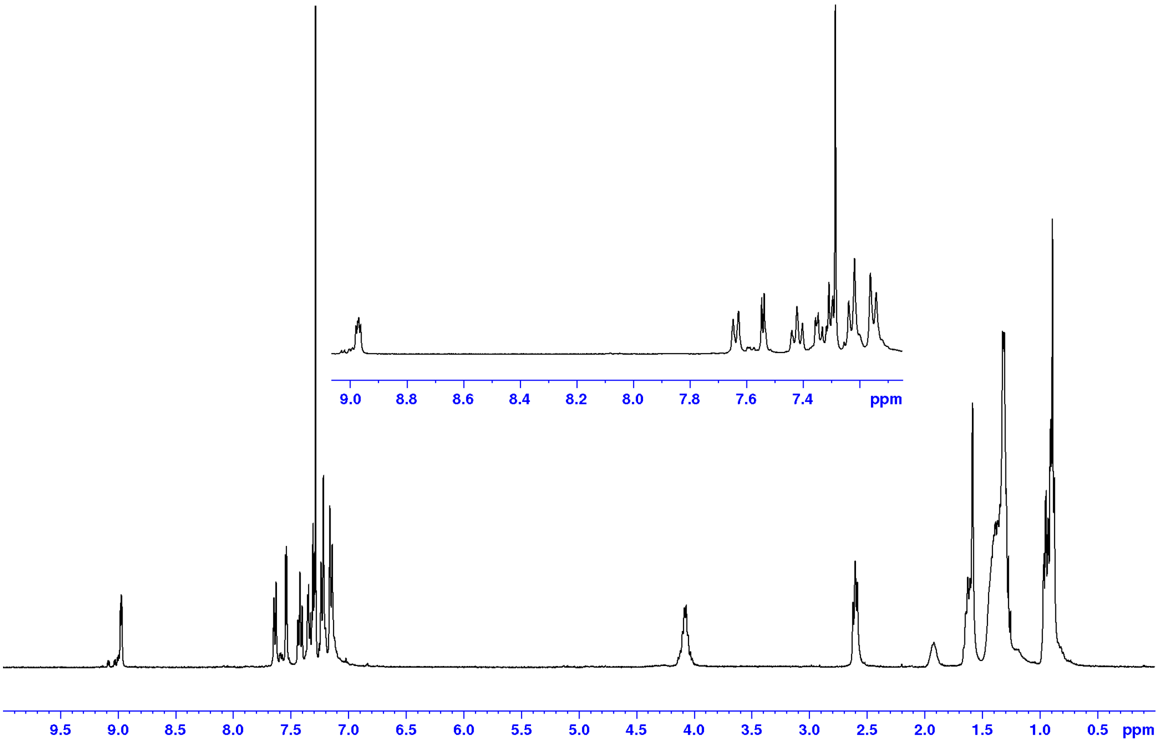

Figure 7. 11: ^{1}H NMR spectrum of **IDTT-DPP-PH** in **CDCl$_3$.**

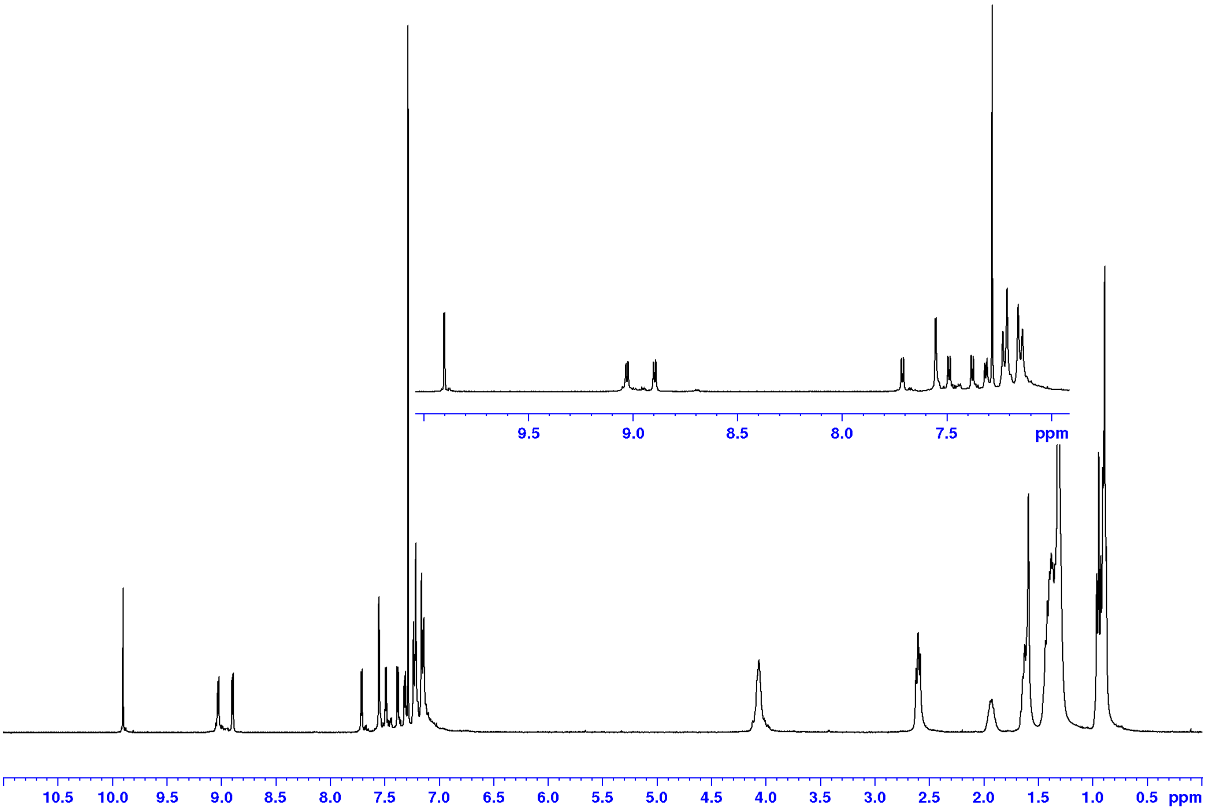

Figure 7. 12: ^{1}H NMR spectrum of **IDTT-DPP-CHO** in **CDCl$_3$.**

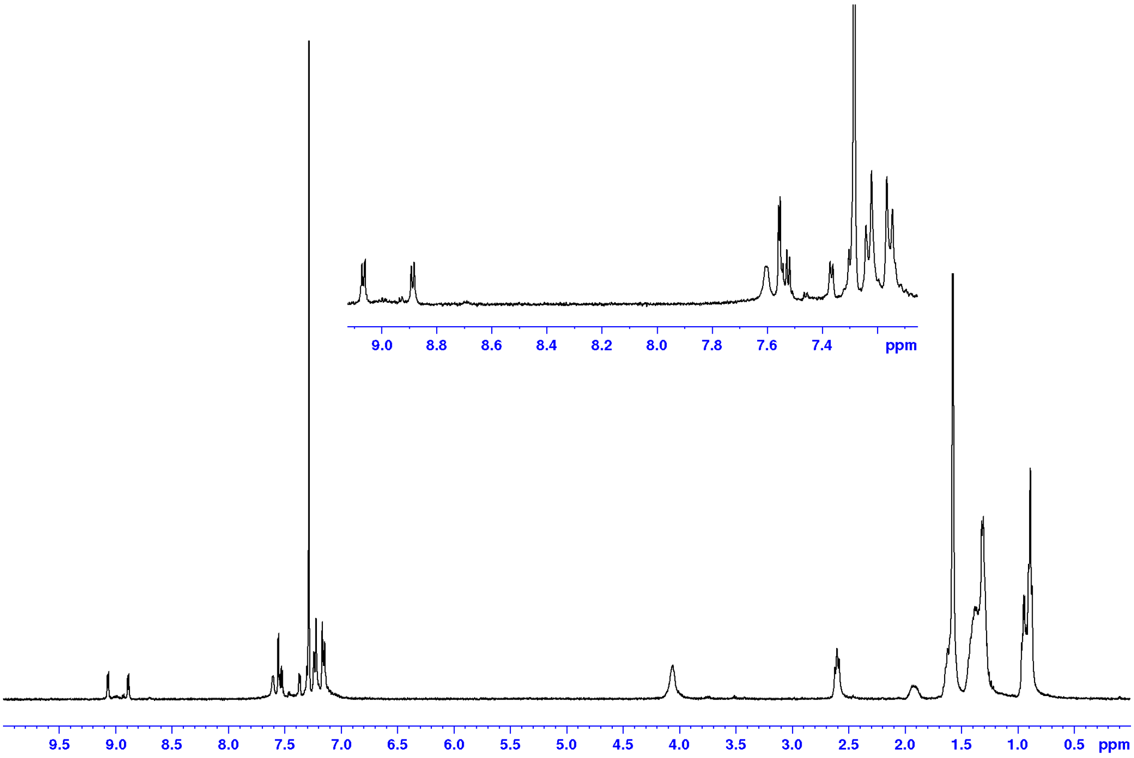

Figure 7. 13: The ^{1}H NMR spectrum of **IDTT-DPP-CN** in **CDCl$_3$.**

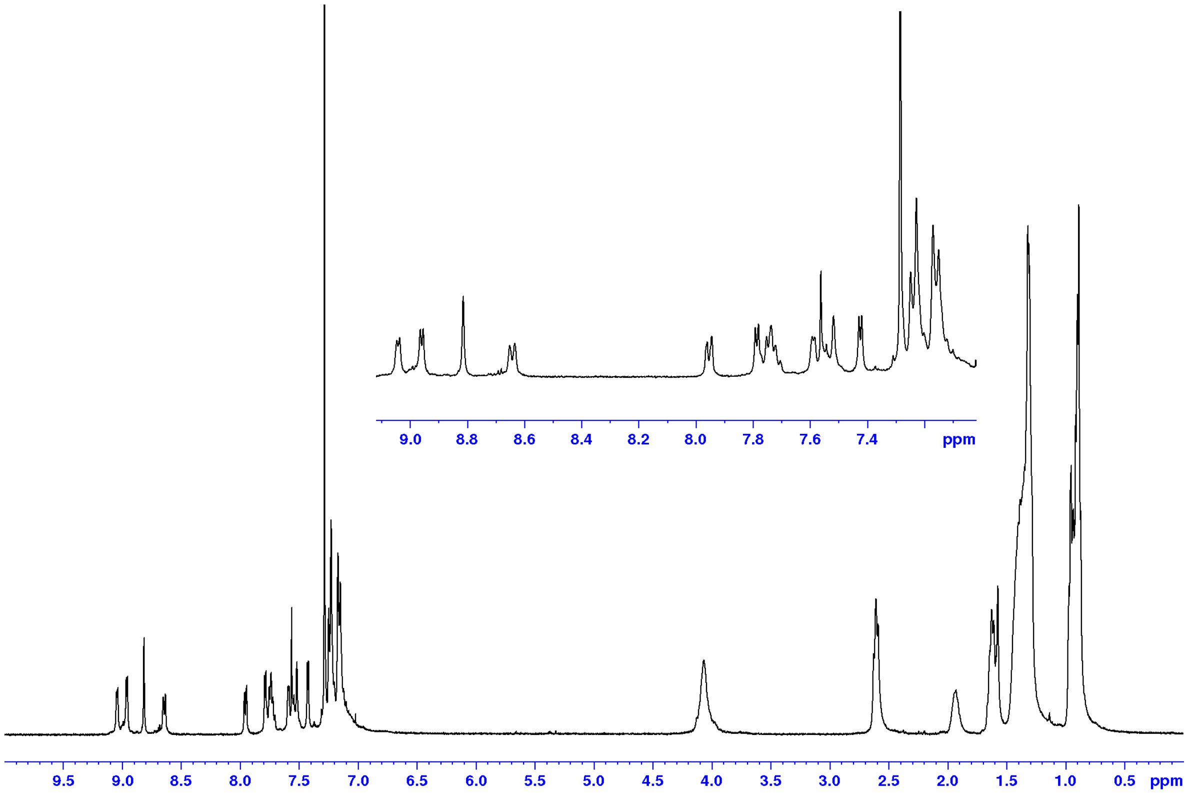

Figure 7. 14: The ^{1}H NMR spectrum of **IDTT-DPP-INIC** in **CDCl$_3$.**

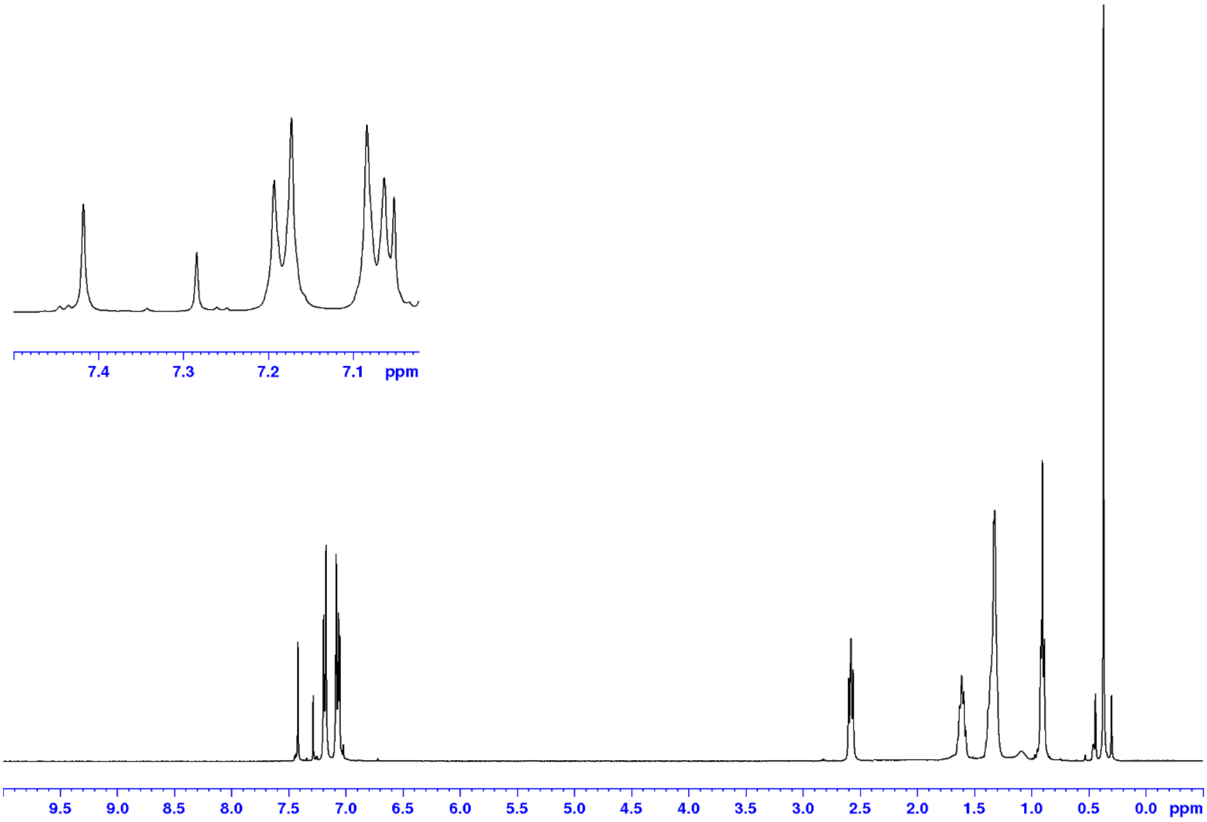

Figure 7. 15: The ^{1}H NMR spectrum of **IDT-Sn2** in **CDCl$_3$.**

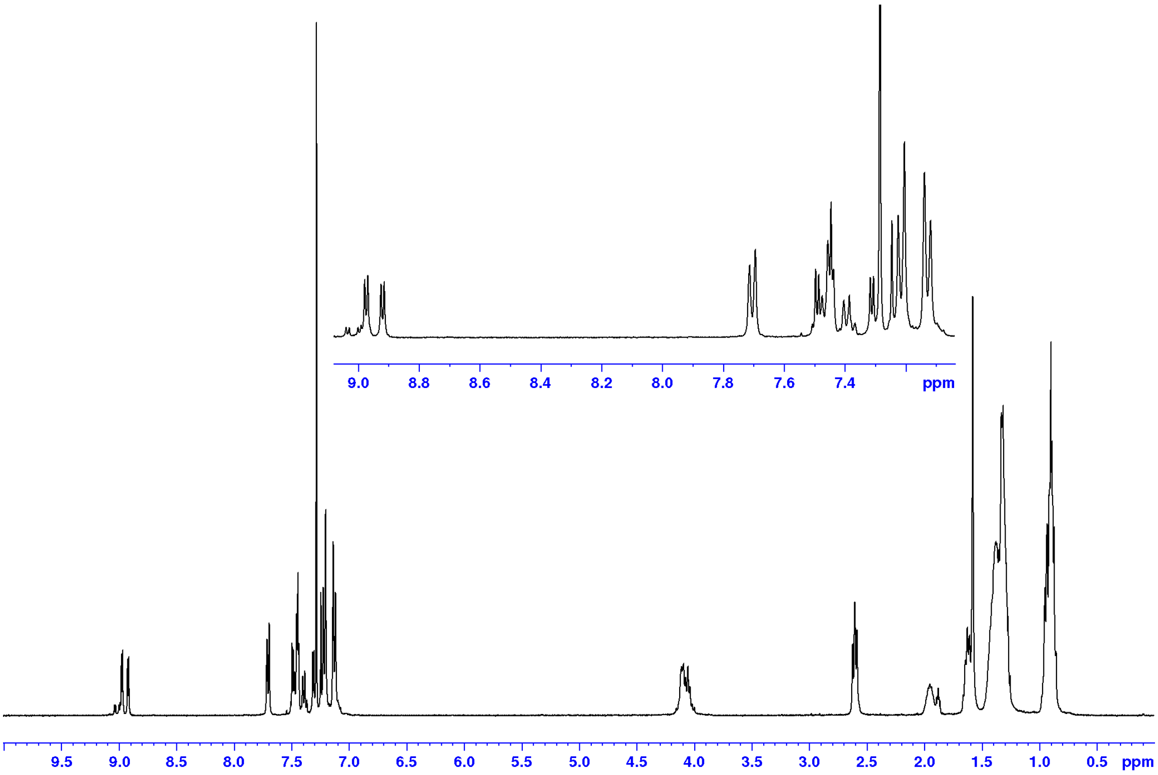

Figure 7. 16: The ^{1}H NMR spectrum of **IDT-DPP-PH** in **CDCl$_3$.**

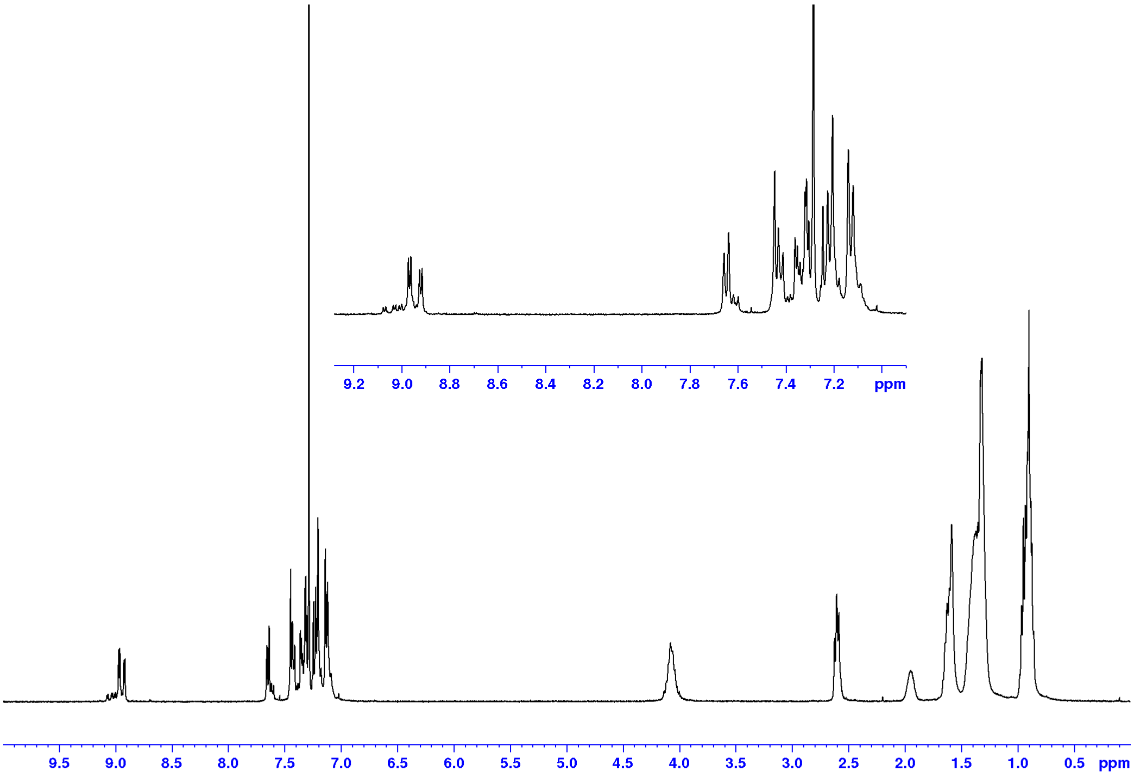

Figure 7. 17: The ^{1}H NMR spectrum of **IDT-DPP-PHT** in **CDCl$_3$.**

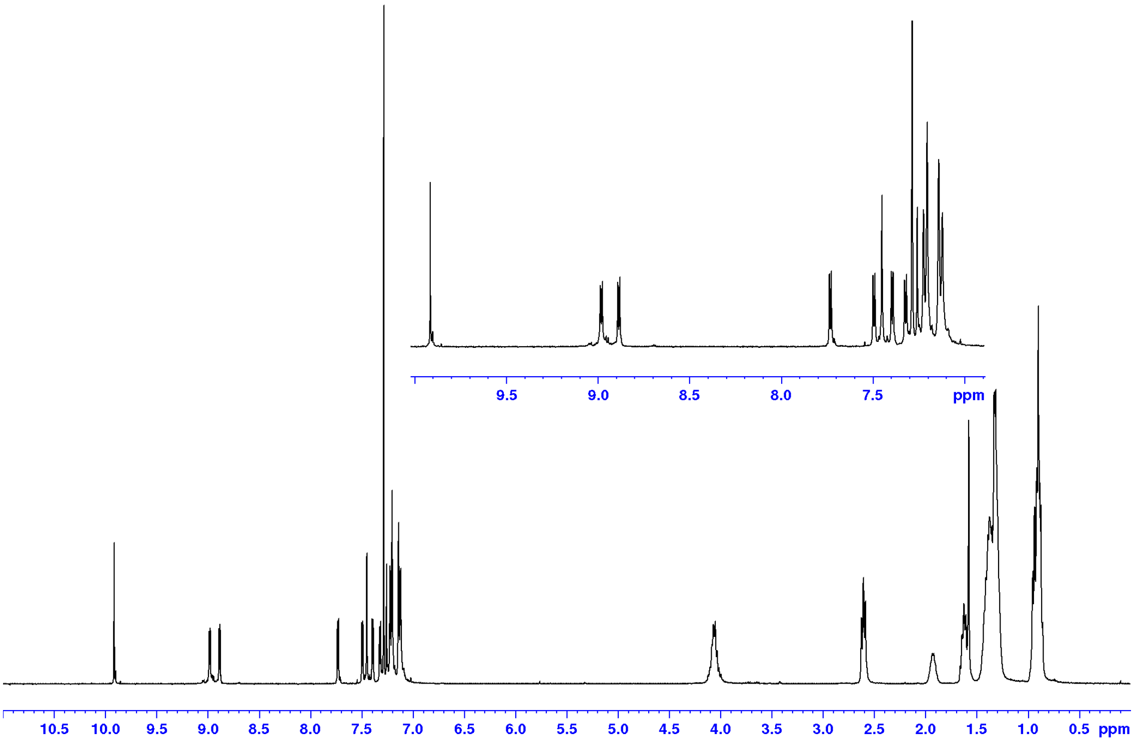

Figure 7. 18: The ^{1}H NMR spectrum of **IDT-DPP-CHO** in **CDCl$_3$.**

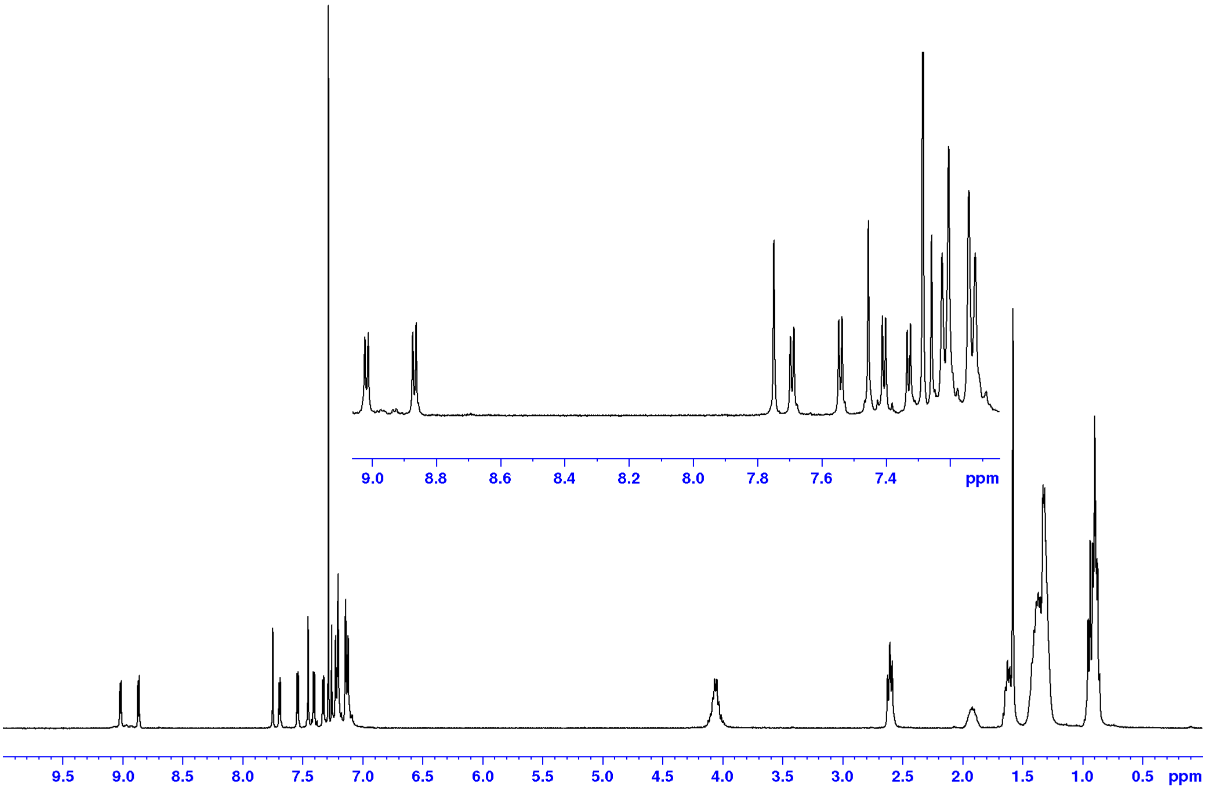

Figure 7. 19: The ^{1}H NMR spectrum of **IDT-DPP-CN** in **CDCl$_3$.**

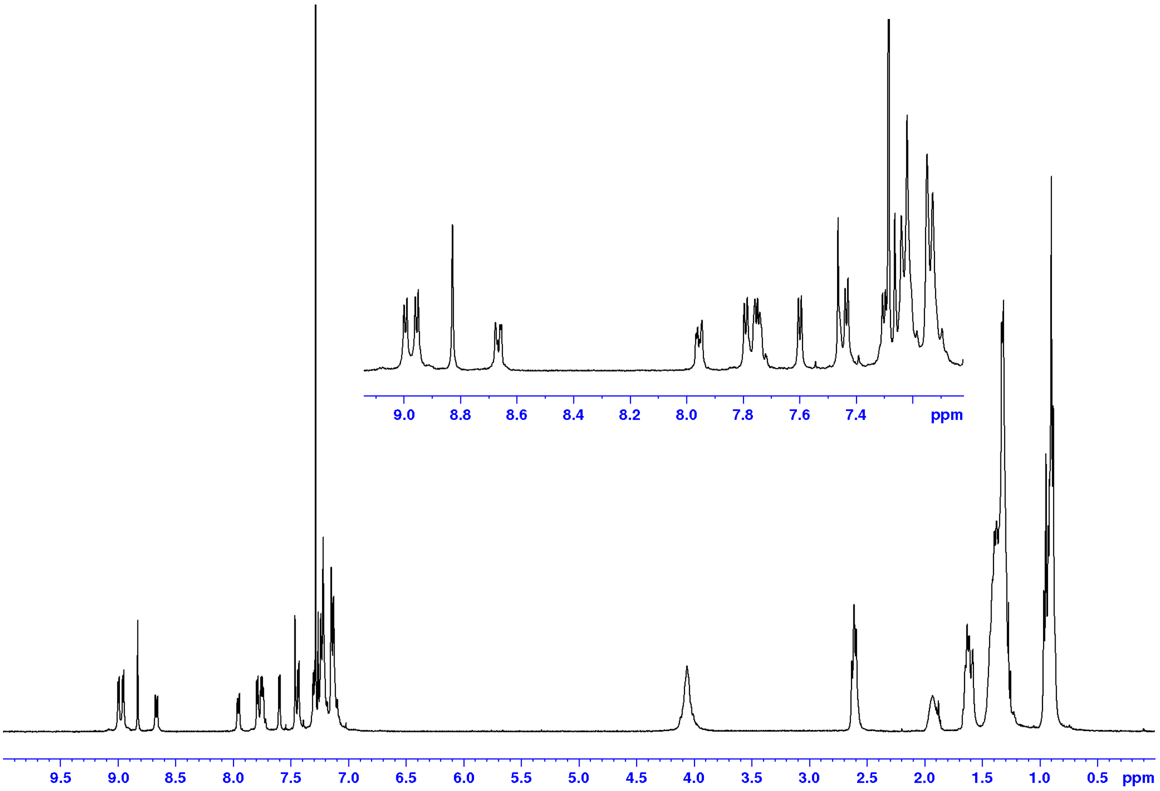

Figure 7. 20: The ^{1}H NMR spectrum of **IDT-DPP-INIC** in **CDCl$_3$.**